Pharmacological and pathological modulation at presynaptic terminals of small central synapses

Submitted for the degree of Doctor of Philosophy

Kate Fennell

University of Sussex

December 2018

Declaration

I declare that this thesis has not been and will not be submitted in whole or in part to another University for the award of any other degree.

Signature:

Kate Fennell

Acknowledgements

My first big ‘thank you’ is to Kevin Staras for his guidance, support and patience throughout the course of my PhD. You have nurtured my love of experimental neuroscience and have provided just the right proportions of encouragement and tough-love that have shaped the independent scientist that I am today; I feel very lucky to have had you as my principal supervisor. I would also like to thank my second supervisor, John Atack for seeing my potential and for reminding me to believe in myself in times of self-doubt. Our chats over coffee have got me through some of my most difficult moments and I hope that I have made you proud and proved you right. Also to my industrial supervisor, Hilde Lavreysen for all of your help with my project, especially during my time at Janssen Pharamceutica, and to Louise Serpell for all of the support with the tau chapter, for being generally lovely and for including me in your group: lab meetings, Christmas outings, karaoke and all!

To my ‘lab mum’, Stephanie Rey, for being my mentor and for sharing with me all of your expertise and to Milena Wagner for teaching me everything that you know about fluorescence imaging; the skills that I have learnt from both of you have been invaluable. Karen Marshall, for reminding me that the sun will come up tomorrow, even if everything has failed and Devkee Vadukul for always being there for me, whatever or whenever; we are not only colleagues but have become firm friends and I couldn’t have wished to share an office with a better group of girls. Also to Mahmoud Maina, who does a remarkable job at putting up with us all, and for all of his help with molecular biology. To Luca Biasetti, Saskia Pollock, Youssra Al-Hilaly and Ana Raulin for being wonderful friends and colleagues; it’s been a privilege to share a lab space with you.

I would also like to thank Tom Baden, Paul Pichler and Tristan Heintz for being my coding gurus and for their patience in answering my many questions.

I was fortunate enough on my first day at Sussex to meet the person who was to become my best friend and partner-in-crime, Molly O'Reilly. Sharing the PhD journey with you has meant more to me than I could ever describe; we have laughed, we have cried, and have been each other's greatest asset and greatest downfall in equal measure. I love you very much and I know that no matter how many miles there are between us we will continue to inspire each other to become the best scientists that we can be, and I will always be there for 'one more drink'.

A massive thank you to Luke Young for being one of those amazing friends that gives unwavering emotional support and endless help with life in general. Your generosity and kindness knows no bounds.

To my number one cheerleader, Paul Murphy, without whom I wouldn't have eaten whilst writing this thesis! Not only have you made excellent dinners but you have been incredibly patient and supportive throughout this time; your love means the world to me. I'm excited to see what the future has in store for us – I hope for many more adventures!

My final thank you is to my family, especially my grandparents, Simon and Tricia Pettit, for providing me with the foundations and ambition to strive for all of my goals; my love to both of you.

Abstract

Many neuropharmacological interventions target presynaptic substrates but the mechanisms of functional modulation at the level of individual terminals are still poorly defined. Addressing this knowledge deficit is fundamental for revealing broader principles of pharmacological action in circuits, and for informing drug research and development. Here, using electrophysiology and genetically-encoded optical reporters of synaptic function - in particular, assays of synaptic vesicle recycling kinetics and transmitter release - we have characterized key mechanisms of modulation in rat hippocampal terminals. Specifically, we demonstrated that the actions of novel synaptic vesicle protein 2A (SV2A) modulators are driven by stimulus intensity and frequency, indicative of a use-dependent mode of action. We also examined the consequences of positive and negative allosteric modulators of metabotropic glutamate receptor 2 (mGluR2) and demonstrated that a concurrent modulation of SV2A and mGluR2 has a synergistic effect, with potentially wide-reaching clinical benefits. In addition, we characterized the role of tau protein in neurotransmission properties and the consequences of expressing pathological tau associated with FTDP-17. We describe the ramifications of FTDP-17 pathology on presynaptic transmission using various models of differential tau expression including tau knockdown and expression of pathological tau carrying the P301L *MAPT* mutation, Tau(P301L). We show that the presence of Tau(P301L) limits synaptic vesicle recycling pool size and accelerates synaptic vesicle endocytosis but these effects are ameliorated in the presence of Tau(P301L)^{K18} fibrils, favouring the idea that alterations in synaptic vesicle recycling are largely mediated by pathological tau in its soluble form. Overall, knockdown of tau has a more subtle effect, but also decreases the number of vesicles available for release. Taken together, this data suggests a role of endogenous tau in regulating synaptic vesicle release and retrieval. Neurons expressing Tau(P301L) also exhibit excessive glutamate release, which is again recovered by the addition of Tau(P301L)^{K18} fibrils. Finally, we show that glutamate clearance in neurons expressing Tau(P301L) is impaired to a similar degree, independent of the presence of Tau(P301L)^{K18} fibrils. We conclude that it is likely that enhanced glutamate release and slowed reuptake contribute to the synaptotoxicity observed in models of tau pathology.

Table of Contents

List of figures

Abbreviations

AD	Alzheimer's disease
AED	Anti-epileptic drug
ANOVA	Analysis of variance
AP	Action Potential
AP-V	D-(-)-2-amino-5-phosphonopentanoic acid
Ara – C	Cytosine – β – D – arabinofuranoside
AZ	Active zone
Baf	Bafilomycin A1
CME	Clathrin mediated endocytoisis
CNQX	6-cyano-7-nitroquinoxaline-2,3-dione
CNS	Central nervous system
DCG-IV	2S,2'R,3'R)-2-(2,3-dicarboxycyclopropyl) glycine
DIC	Differential interference contrast
DMSO	Dimethyl sulphoxide
EBS	External bath solution
EPSC	Excitatory postsynaptic current
FCS	Foetal calf serum
FTDP – 17	Familial frontal temporal lobe dementia
GECI	Genetically coded calcium indicator
HBSS	Hank's balanced salt solution
HEPES	4-(2-hydroxyethyl) piperazine-1-ethanesulfonic acid
ICC	Immunocytochemistry
iGluSnFR	intensity based glutamate-sensing fluorescence receptor

IPSC	Inhibitory postsynaptic current
LEV	Levetiracetam
LTD	Long term depression
MAPT	Microtubule-associated protein tau
mEPP	Miniature end-plate potential
mGluR	Metabotropic glutamate receptor
NFT	Neurofibrillary tangle
NAM	Negative allosteric modulator
P0/P1	Postnatal day 0 or 1
PAM	Positive allosteric modulator
PBS	Phosphate Buffered Saline
PDL	Poly-D-lysine
PFA	Paraformaldehyde
p_r	probability of release
ROI	region of interest
RRP	Readily releasable pool
RtP	Resting pool
SNARE	Soluble NSF attachment receptor
SV2A	Synaptic vesicle protein 2A
TEM	Transmission electron microscopy
TP	total pool
TRP	total recycling pool
v-ATPase	vacuolar proton-ATPase
VGAT1-pH	VGAT1-pHluorin
VGLUT	vesicular glutamate transporter
VGLUT1-pH	VGLUT1-pHluorin

Chapter 1: Introduction

1.1 Neurons and synapses

In 1877, using Golgi stained sections of brain tissue, Santiago Ramón y Cajal produced the iconic illustrations that came to form the basis of the neuron doctrine. This states that, rather than consisting of a diffuse network of continuous tissue, neurons are anatomically distinct structures that communicate with each other via synapses; highly specialized junctions where signals are rapidly passed from one neuron to the next or to a target tissue. In addition to conveying information, synapses can also be finely tuned according to their activity history and network demands, and have the ability to adjust their structure and function accordingly; a phenomenon termed synaptic plasticity (Hopf et al., 2002, O'Rourke et al., 2012, Regehr, 2012). Therefore, synapses are crucial sites in the maintenance of a healthy nervous system, allowing flexibility and adaptation in response to functional demands.

Synapses can be of two types, electrical or chemical. In the central nervous system (CNS), the majority of interneuronal communication occurs via chemical synapses, on which this work focuses. The pioneering discoveries about the nature of chemical transmission at presynaptic terminals were made by Bernard Katz who, in collaboration with Paul Fatt and José del Castillo, conducted a series of electrophysiological experiments at the frog neuromuscular junction (NMJ). They observed that amplitudes of spontaneous miniature end-plate potentials (mEPPs) were distributed in such a way that suggested synapses responded in a unitary manner, leading to the proposal that neurotransmitter molecules are released as discrete packets: the quantal theory of neurotransmitter release (Fatt and Katz, 1952, Del Castillo and Katz, 1954). Concurrently, the first electron micrographs (EM) of the synapse were being developed, displaying the existence of spherical organelles residing in the presynaptic terminal (Sjostrand, 1953); these EM images, alongside Katz's theory, gave rise to the vesicular hypothesis of neurotransmission, namely that neurotransmitter is packaged in the spherical organelles observed in the presynaptic terminal, synaptic vesicles, and that its release from these vesicles forms the basis of quantal neurotransmission.

1.2 Structure of the synapse

Although the functional properties of chemical synapses are varied (O'Rourke et al., 2012), they share similar structural characteristics: a presynaptic compartment and a postsynaptic compartment separated by a gap measuring approximately 15-20nm, termed the synaptic cleft (Fig 1.1) (De Robertis and Bennett, 1955). Under EM, presynaptic terminals can be easily identified by the presence of synaptic vesicles, some of which are clustered in the terminal and others which appear docked at the active zone (AZ) ready for release (Sudhof, 2012). Located directly opposite to the AZ is an electron-dense structure composed of numerous proteins and neurotransmitter receptors termed the postsynaptic density (PSD). Organization of synapses in this way allows efficient transfer of information from pre- to postsynaptic terminals.

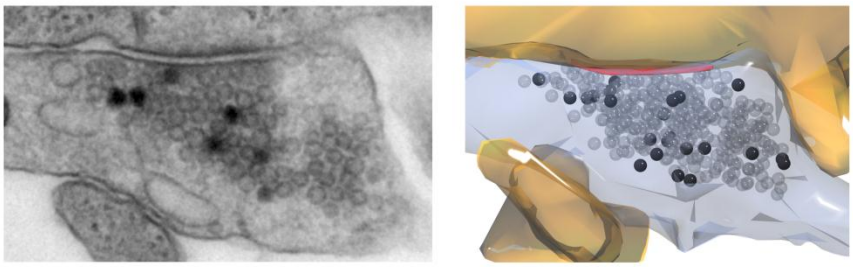

Fig 1.1. Structure of the synapse. Electron micrograph (left) and 3D reconstruction (right) of a presynaptic terminal showing vesicle clusters. Darkened vesicles have been labelled with FM1-43 and photoconverted.

1.2.1 Structure and organization of the presynaptic terminal

Synaptic vesicles, which appear on electron micrographs as small, spherical, membranous structures, are the most prominent ultrastructural feature of presynaptic terminals (Fig 1.1). In rat hippocampal neurons, diameters of synaptic vesicles range between 20 and 66nm, with ~40nm across being average (Harata et al., 2001, Schikorski and Stevens, 1997, Harris and Sultan, 1995). Fluctuation in vesicle size is thought to be determined by current functional demands, for example vesicles that are filled with glutamate appear morphologically bigger than those that are not (Budzinski et al., 2009).

Cryo-electron tomography of presynaptic compartments has shown that synaptic vesicles are arranged into distinct clusters, ranging in size from 2-50 vesicles and tethered by filamentous connectors (Fernandez-Busnadiego et al., 2010). More recently, three-dimensional renderings of presynaptic terminals have been produced using high pressure freezing and freeze substitution in combination with EM tomography (Cole et al., 2016). Reconstructions reveal that three filament types dominate the cytoplasmic structure of presynaptic terminals; docking filaments, bridge filaments and cluster filaments. The complex connectivity of vesicles with the different filament types produces an organized network extending out from the active zone, with many vesicles connected to all three filament types (Fig 1.2). Docked vesicles are typically connected to the AZ by 3 or more docking filaments (teal). Cluster filaments are longer and either extend from the AZ (white) or are free within the vesicle cloud (gold), Vesicles are paired throughout the cloud via small bridge filaments (purple). The extent of connectivity between vesicles has been linked to the activity-status of the terminal, with resting synapses exhibiting a greater degree of clustering (Fernandez-Busnadiego et al., 2010)

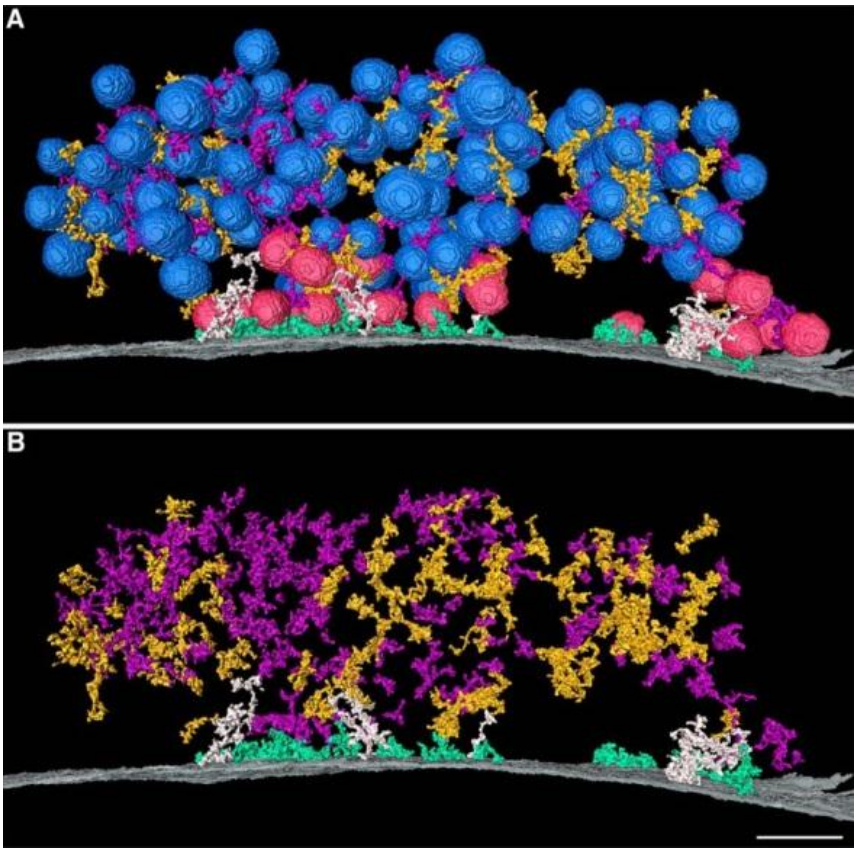

Fig 1.2. Three types of filaments connect to synaptic vesicles. *A*) All synaptic vesicles (blue, or red if directly connected to filaments extending from the active zone membrane) are interlinked

or linked to the active zone by filaments, forming the vesicle cloud. Four small docking filaments (teal) extend from the active zone and surround each docked vesicle. Longer cluster filaments are found either extending from the active zone (white) or free throughout the vesicle cloud (gold). Small bridge filaments (purple) are distributed throughout the cloud and pair vesicles. *B*) Same view and colour code as in *A*, but vesicles are removed to expose the underlying filamentous network. Scale bar, 50 nm. Taken from Cole et. al., 2016.

Currently, precise identification of filaments in the presynaptic terminal is uncertain, however their size, shape and distribution allows for some speculation. Vesicles connected to the AZ are most likely to be released following simulation (Fernandez-Busnadiego et al., 2010, Watanabe et al., 2013). As docking filaments are the only filament type to surround docked vesicles, Cole et. al. propose that they most likely correspond to SNAREpin complexes, which have been shown to surround docked vesicles (Rickman et al., 2005). Bridge filaments are likely to correspond to synapsin, with knockout of synapsin resulting in more diffuse vesicle clouds (Siksou et al., 2007, Gitler et al., 2008). The features of cluster filaments are yet to be matched to known molecules (Cole et al., 2016).

Correlative transmission electron microscopy (TEM) has allowed detailed analysis of structure-function relationships. The probability of release *(ρr)* describes the likelihood of a vesicle to release following a single action potential, and is an important determinant in presynaptic strength (Branco and Staras, 2009, Murthy et al., 1997). In hippocampal synapses, the number of docked vesicles is strongly correlated with *ρr* (Branco et al., 2010) and has also been shown to scale linearly with the area of the AZ (Holderith et al., 2012). Small boutons on thin spines with a total pool of >200 vesicles have, on average, 6-8 docked vesicles, whereas medium sized boutons on medium mushroom-shaped dendritic spines have 13-16 docked vesicles from a total vesicle pool of >450 vesicles (Harris and Sultan, 1995). Logically, this translates as larger synapses with larger vesicle pools having a higher *ρr* than smaller synapses. However, this interpretation has been shown to be too simplistic, with wide variation in *ρr* across synapses of all sizes, which is, in-part, attributed to the high variability in the size of recycling fractions at individual synapses (Branco et al., 2010). It is worth noting that despite drawing correlations between various presynaptic parameters, the authors of these studies comment on the heterogeneity of structural and functional properties within homogenous synapse populations, underpinning the complex nature between synaptic function and the architecture of presynaptic terminals.

1.3. The synaptic vesicle cycle

The recycling of synaptic vesicles was first shown using a combination of electrophysiology and TEM at the frog neuromuscular junction (Ceccarelli et al., 1973). Following stimulation, synaptic vesicles fuse with the plasma membrane and release their neurotransmitter content in a process known as exocytosis. Subsequently, vesicles undergo endocytosis; reformation via fission of the presynaptic membrane and re-entry into the presynaptic terminal (Fig 1.3).

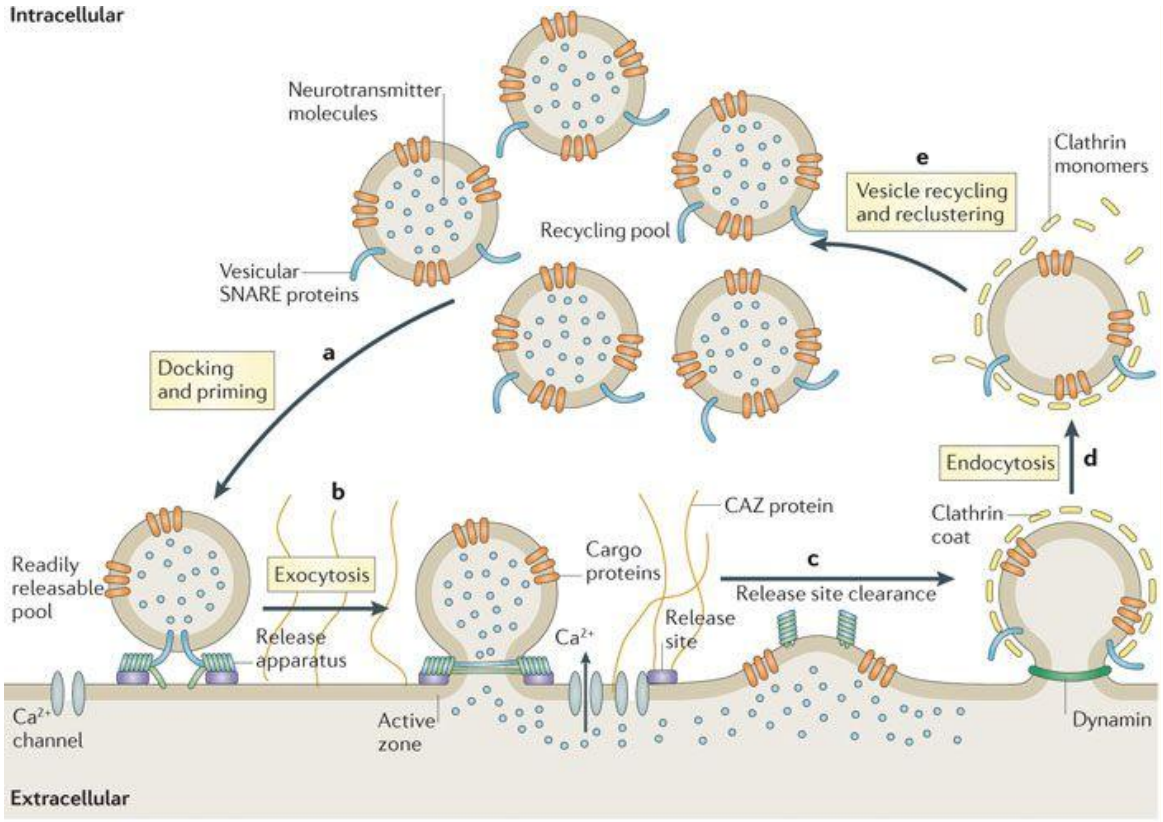

Fig 1.3. The synaptic vesicle cycle. Vesicles are primed and docked (a) constituting the readily releasable pool (RRP). Upon Ca^{2+}- influx, they undergo exocytosis (b), releasing their neurotransmitter content into the synaptic cleft. The release site is cleared (c) to avoid expansion and swelling of the AZ. Endocytosis (d) is predominantly mediated by a clathrin and dynamin-dependent pathway. Following clathrin uncoating and neurotransmitter reuptake, vesicles are returned to the recycling pool where they undergo clustering (e). Modified from Haucke et. al., 2011.

1.3.1 Exocytosis

Exocytosis is a highly regulated process and is controlled by protein-machinery that remains highly conserved from yeast through to mammals (Bennett and Scheller, 1993, Ferro-Novick and Jahn, 1994). Soluble N-ethylmaleimide-sensitive factor attachment receptor (SNARE) proteins and Sec1/Munc18-like proteins (SM) are essential in mediating a number of protein interactions between synaptic vesicle membranes and the active zone (Sudhof, 2013), culminating in the fusion of the two membranes (Rothman, 1994, Bajjalieh and Scheller, 1995, Sudhof, 1995). In order to become fusion-competent, synaptic vesicles must first undergo priming and docking (Fig 1.4), regulated by the AZ proteins RIM, RIM-BP and Munc13 (Kaeser et al., 2012, Sudhof, 2013). RIM and RIM-BP are also crucial in the localization of N- and P/Q-type Ca^{2+}- channels in close proximity to docked vesicles at the AZ, making them important contributors in the organization of vesicle release sites (Kaeser et al., 2011).

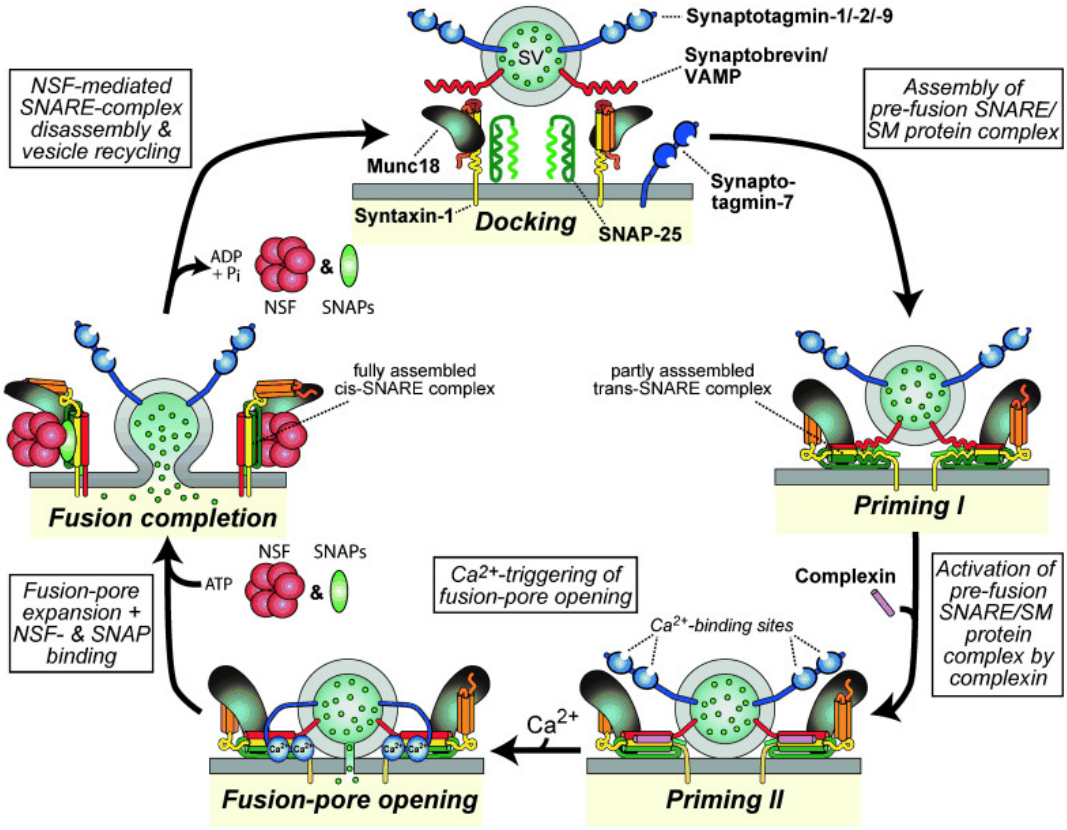

Fig 1.4. Synaptic vesicle exocytosis: schematic of SNARE/SM protein cycle leading to synaptic vesicle release. Prior to SNARE complex assembly *(Docking)*, syntaxin -1 is present in a closed

conformation and it must first open to initiate SNARE complex assembly; in this closed conformation, syntaxin – 1 is associated with Munc18. As syntaxin -1 opens during SNARE complex assembly, Munc18 alters the way in which it is bound to syntaxin -1, via interactions with the syntaxin – 1 N peptide, causing it to bind to assembling trans – SNARE complexes. Once SNARE complexes are partially assembled *(Priming I)*, complexin binds to further increase priming. The 'superprimed' SNARE/SM protein complexes *(Priming II)* are now substrates for Ca^{2+} - triggered fusion- pore opening, caused by Ca^{2+} binding to synaptotagmin – 1, which in turn causes interactions between synaptotagmin – 1, SNARES and phospholipids *(Fusion-pore opening)*. After fusion-pore opening, the resulting cis – SNARE complexes *(Fusion completion)* are disassembled by NSF/SNAP ATPases and vesicles are recycled, refilled with neurotransmitter and reused for release. Modified from Südhof, 2014.

During exocytosis, the vesicular SNARE protein, synaptobrevin forms a helical *trans*-SNARE complex with syntaxin - 1 and SNAP-25, bringing the AZ and vesicle into close proximity (Fig 1.4). Finally, Ca^{2+}- influx via N- and P/Q –type Ca^{2+} channels, generated from the arrival of the action potential at the terminal, triggers an electrostatic or chemical change in the Ca^{2+-} sensor, synaptotagmin - 1, which completes the fusion reaction (Sudhof, 1995, Sudhof, 2013). It is thought that subsequent interaction of SM proteins with the *trans*-SNARE complex leads to the opening of the fusion pore and release of neurotransmitter (Sudhof and Rizo, 2011). Disassembly of the SNARE complex is mediated by α/β-SNAPs (Burgalossi et al., 2010, Haucke et al., 2011).

1.3.1.1 Variation in quantal size

Although morphologically similar under EM, synaptic vesicles display considerable variability in their quantal output, a phenomenon that occurs not only in the comparison across different boutons (Karunanithi et al., 2002) but even within individual terminals (Liu and Tsien, 1995). Differences in quantal transmission can be attributed to pre- and postsynaptic elements, namely i) vesicle size; ii) glutamate content; iii) neurotransmitter concentration in the synaptic cleft; iv) the release site of vesicles, and v) number of postsynaptic receptors present at the postsynaptic membrane.

Synaptic vesicles in the hippocampus differ in size from 20nm to 66nm in diameter (Harris and Sultan, 1995), which the authors associated with fluctuations in glutamate concentration, estimated to be between 0.24 and 11mM, although these values were calculated based upon the size of synaptic vesicles from reconstructed images of synaptic terminals from the hippocampus, and therefore are of limited accuracy. An alternative study has estimated that glutamate concentration in individual vesicles is at least 60mM (Burger et al., 1989). More recently, it has

been shown that synaptic vesicles undergo an increase in diameter of ~25% following glutamate loading, dependent on the presence of synaptic vesicle protein 2A (SV2A) (Budzinski et al., 2009). It has been hypothesized that changes in neurotransmitter concentration drive changes in osmotic pressure, and that it is this that affects the size of synaptic vesicles, but this has since been shown to be untrue (Qu et al., 2009).

Variability in glutamate concentration may also arise from differential expression of vesicular glutamate transporters (VGLUTs). There are three known VGLUT isoforms (VGLUT1-3) that display nearly identical uptake characteristics but have distinct patterns of expression in adulthood, with VGLUT1 being the predominant isoform expressed in excitatory neurons in the cerebral and cerebellar cortices, as well as the hippocampus and thalamus (Herzog et al., 2006). VGLUT1 expression in cultures from mouse hippocampal neurons is correlated with quantal size, which is decreased in VGLUT knockout models but increased in models of VGLUT1 overexpression (Wojcik et al., 2004). This data also suggests that under regular physiological conditions, synaptic vesicles are not filled to full capacity allowing for dynamic regulation of quantal size. Notably, increased expression of VGLUT1 has been associated with synaptic excitotoxicity and neurodegeneration in the P301L model of tauopathy (Hunsberger et al., 2015), and increased glutamate transmission is a hallmark of many neuropathological disorders (Sheldon and Robinson, 2007).

1.3.2. Endocytosis

Following exocytosis, clearance of excess membrane from the presynaptic terminal is necessary to maintain membrane tension and for the recycling of vesicular proteins. The exact mechanism by which vesicular proteins are sorted from the plasma membrane of the terminal and into reformed vesicles is still a matter of debate, but it is considered to be one of the major rate-limiting steps in the synaptic vesicle cycle (Haucke et al., 2011). Today, there are four different forms of endocytosis that have been identified in hippocampal neurons, namely clathrin-mediated endocytosis (CME), kiss-and-run endocytosis, ultrafast endocytosis and bulk endocytosis. Following endocytosis, vesicles are re-acidified by vacuolar-ATPase (v-ATPase), which generates the proton gradient necessary for neurotransmitter filling (Sudhof, 2004). The identity of the vesicular transporter is dependent on the neurotransmitter being transported, with the VGLUT family of transporters specified for the transport of glutamate, and VGAT for the transport of GABA (Zander et al., 2010).

1.3.2.1. Clathrin-mediated endocytosis

First identified in the 1970s (Heuser and Reese, 1973), clathrin-mediated endocytosis (CME) is thought to be the predominant form of endocytosis at presynaptic terminals. CME has been described as five sequential steps; nucleation, cargo-selection, coat assembly, scission and uncoating (McMahon and Boucrot, 2011, Schuske et al., 2003). Initially, the presence of vesicular proteins at the plasma membrane form a nucleation site that initiates recruitment of endocytic factors. Enrichment of the membrane with phosphatidylinositol-4,5-biphosphate ($PI(4,5)P_2$) marks the binding site for early endocytic proteins such as FCH01/2 (Fer/Cip4 homology domain only proteins 1 and 2), AP2 (assembly peptide 2) and AP180 (assembly protein 180) . Subsequently, AP2 recruits further endocytic adaptors and a clathrin coat formed of clathrin triskelia is established (Rizzoli, 2014). These clathrin-coated pits mature, gradually invaginating in a process mediated by BAR-domain proteins such as endophillin and amphiphysin (Frost et al., 2009). These BAR-domain proteins then recruit the GTPase, dynamin (Frost et al., 2009, Milosevic et al., 2011), that upon hydrolysis induces the fission of a new synaptic vesicle, formed from the presynaptic membrane (Roux et al., 2006). The final step of the CME process is uncoating, where synaptojanin 1, Hsc70 and auxillin/GAK facilitate the disassembly of the clathrin coat from the newly formed synaptic vesicle (Rizzoli, 2014).

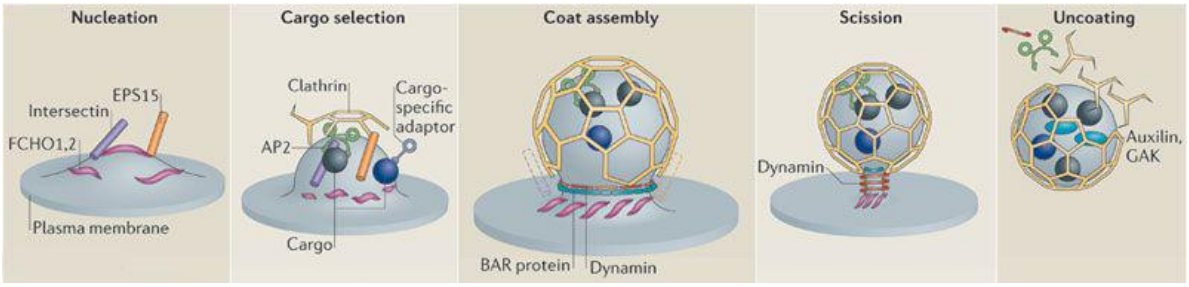

Fig 1.5. The proposed five steps of clathrin-coated vesicle endocytosis. Nucleation: FCH domain only (FCHO) proteins bind phosphatidylinositol-4,5-bisphosphate ($PtdIns(4,5)P_2$)-rich zones of the plasma membrane and recruit EPS15–EPS15R (EGFR pathway substrate 15–EPS15-related) and intersectins to initiate clathrin-coated pit formation by recruiting adaptor protein 2 (AP2). Cargo selection: AP2 recruits several classes of receptors directly through its μ-subunit and σ-subunit. Cargo-specific adaptors bind to AP2 appendage domains and recruit specific receptors to the AP2 hub. Coat assembly: clathrin triskelia are recruited by the AP2 hub and polymerize in hexagons and pentagons to form the clathrin coat around the nascent pit. Scission: the GTPase dynamin is recruited at the neck of the forming vesicle by BAR domain-containing proteins, where it self-

polymerizes and, upon GTP hydrolysis, induces membrane scission. Uncoating: auxilin or cyclin G-associated kinase (GAK) recruit the ATPase heat shock cognate 70 (HSC70) to disassemble the clathrin coat and produce an endocytic vesicle containing the cargo molecules. Synaptojanin probably facilitates this by releasing adaptor proteins from the vesicle membrane through its PtdIns lipid phosphatase activity. The components of the clathrin machinery are then freed and become available for another round of clathrin-coated vesicle formation. Modified from McMahon and Boucrot, 2011.

F-actin also appears to play a variety of roles in CME, although its precise point of action is a matter of debate (Engqvist-Goldstein and Drubin, 2003). In one study, f-actin was shown to influence the various stages of endocytosis, including formation of the pit, the splitting of clathrin-coated structures, merging and coalescing, and also constriction and internalization (Yarar et al., 2005). When actin dynamics were challenged with either Jasplakinilide or Latrunculin, these authors observed the accumulation of deeply invaginated clathrin-coated structures, suggesting a potential role of f-actin at the later stages of CME. Furthermore, f-actin accumulation at endocytic sites was mainly observed immediately preceding scission events (Yarar et al., 2005). In a contrasting study conducted in Swiss 3T3 cells, internalization of clathrin-coated pits, labelled using clathrin-dsRed, was accompanied by the recruitment of f-actin. Maximal f-actin signal was observed shortly following scission, hinting that the major role of f-actin occurs post-scission (Merrifield et al., 2005).

1.3.2.2 Kiss and run endocytosis

Kiss-and-run endocytosis, which is independent of clathrin, was first observed in 1973 at the frog NMJ (Ceccarelli et al., 1973), although the term was not coined until the 1990s (Fesce et al., 1994). In this mode, vesicles retain their identity throughout the recycling process (Harata et al., 2006), merely undergoing transient fusion with the presynaptic membrane and releasing neurotransmitter via a fusion pore, which is almost instantaneously closed (Alabi and Tsien, 2013). Kiss-and-run has been observed using a range of optical techniques, including FM-dye destaining (Richards, 2010), pHluorin-based probes (Zhang et al., 2009b), quantum dots (Zhang et al., 2009a) and capacitance recordings (Xu et al., 2008). The reason as to why vesicles do not undergo full collapse following fusion is still unknown; however it is suggested that, in some instances, the fusion-force generated by the zippering of SNARE complexes is not enough to lead to full fusion (Alabi and Tsien, 2013). In addition, it is possible that tethers linking individual vesicles may restrain vesicles from full collapse into the plasma membrane (Alabi and Tsien, 2013).

1.3.2.3 Ultrafast endocytosis

The recent development of 'flash-and-freeze' electron microscopy has led to the identification of an ultrafast form of endocytosis (Watanabe et al., 2013). Using this method, neurons can be optogenetically stimulated with a single action potential and fixed within as little as ~15ms of stimulation. By fixing cells at various points following stimulus, a picture can be formed of the endocytic process. Full-fusion of vesicles with the plasma membrane occurs within ~30ms post-stimulation and large endocytic inclusions can be seen forming within ~100ms in portions of the membrane flanking the AZ (Watanabe et al., 2013). Further experimentation revealed that, like CME, ultrafast endocytosis also has an actin component, with membrane retrieval dependent on actin polymerization. In the final stages, individual synaptic vesicles are formed from the endosome in a clathrin-dependent process, occurring approximately 5 seconds after stimulation (Watanabe et al., 2014).

1.3.2.4. Bulk endocytosis

In some aspects, bulk endocytosis can be considered similar to ultrafast endocytosis in that a large section of the membrane invaginates at sites flanking the AZ and that new vesicles are formed from endosomes in a clathrin-dependent manner (Kasprowicz et al., 2008, Watanabe et al., 2014) However, the major difference between the two processes is that ultrafast endocytosis occurs following a single AP whereas bulk endocytosis is only induced by intense stimulation (Clayton and Cousin, 2009). Both CME and bulk endocytosis can be inhibited by synaptotagmin-11, a non-Ca^{2+}-binding synaptotagmin implicated in schizophrenia and Parkinson's disease, suggesting overlap between these two endocytic modes (Wang et al., 2016).

1.3.2.5 Endocytosis at hippocampal synapses

Different modes of endocytosis have been observed within the same synapses (Richards, 2010, Zhang et al., 2009a), and there is still question over whether it is CME or kiss-and-run that is favoured at hippocampal terminals (Granseth et al., 2006, Smith et al., 2008, Zhang et al., 2009b), although it is possible that discrepancies in observations arise from alterations in experimental conditions or from sampling errors. At room temperature, Watanabe et. al. demonstrate that CME is the mode of endocytosis favoured by hippocampal synapses (Watanabe et al., 2014), occurring ~14-20 seconds following single AP stimulation (Balaji and Ryan, 2007, Granseth et al., 2006). When the temperature is increased to 34°C, ultrafast endocytosis becomes the

predominant mode, which occurs within a matter of milliseconds, although budding off of the newly formed vesicle from the endosome takes at least 3 seconds and recovery of all vesicles does not occur until 10-30 seconds post-stimulation (Watanabe et al., 2014).

Intrinsic neuronal properties are also thought to contribute to the mode of endocytosis favoured by a given synapse. At hippocampal terminals, kiss-and-run has been shown to take place within a timeframe of a few seconds (Harata et al., 2006, Zhang et al., 2009a). Ghandi and Stevens show that synapses with low release probability *(ρr)* preferentially recycle vesicles via kiss-and-run, whereas those with higher *ρr* tend towards CME as their preferred endocytic route (Gandhi and Stevens, 2003). Synapse activity has also been implicated in the prediction of endocytic mode (Kononenko et al., 2014). The variability in experimental findings gives a wide scope in interpretation as to how hippocampal synapses operate under physiological conditions, and underpins the complexity of synaptic vesicle recycling.

1.4 Synaptic vesicle pools

Despite appearing morphologically similar under EM, synaptic vesicles in presynaptic terminals are classified into sub-populations or 'pools', with distinctions founded upon differences in structural and functional characteristics (Alabi and Tsien, Denker and Rizzoli, Fowler and Staras, 2015). Ultrastructural readouts of presynaptic architecture reveal clear spatial variation in the localization of vesicles within the terminal, with a few vesicles clustered near to the protein-rich active zone (AZ), whilst others reside in the wider bouton area (Schikorski and Stevens, 1997). Therefore, in terms of spatial arrangement, apart from the relatively small number of vesicles that are docked at the AZ, the vast majority seem to constitute a single homogenous population (Rizzoli and Betz, 2005). However, further investigation has uncovered substantial heterogeneity within the structure and operation of vesicle sub-classes, allowing an array of different pool types to be identified throughout a variety of systems; some of these groups are discrete, whilst others form subsets, and some are comprised of several pools. This has resulted in a somewhat diverse number of names and descriptions of vesicle pool types. For clarity, we will abide by the nomenclature and classification proposed by Alabi and Tsien (Alabi and Tsien, 2012).

In simple terms, synaptic vesicles within the presynaptic terminal can be systematically designated into one of three pools: the total pool (TP), the recycling pool (TRP) and the resting (often termed

'reserve') pool (RtP) (Alabi and Tsien, 2012). In this model, the total number of vesicles in the presynaptic terminal can be determined by summation of the TRP and the RtP (Fig 1.6); at hippocampal synapses, the total pool numbers approximately 200 vesicles (Harris and Sultan, 1995, Schikorski and Stevens, 1997). Estimates of the size of the recycling fraction at individual boutons are highly variable, with values ranging from 15-20% to over 70% (Harata et al., 2001, Ikeda and Bekkers, 2009). It has also been reported that a recycling fraction of as little as 1-5% is adequate to sustain neurotransmission (Denker et al., 2011). Given this, it is somewhat puzzling as to why a large resting population of vesicles is maintained at the presynaptic terminal; nevertheless the RtP is a highly conserved characteristic of synapses across evolutionary distinct species, suggesting that it has a vital physiological role (Denker et al., 2011). A possible explanation is that the RtP acts as a buffer for soluble accessory proteins required for synaptic vesicle recycling, preventing their loss into the axon (Denker et al., 2011).

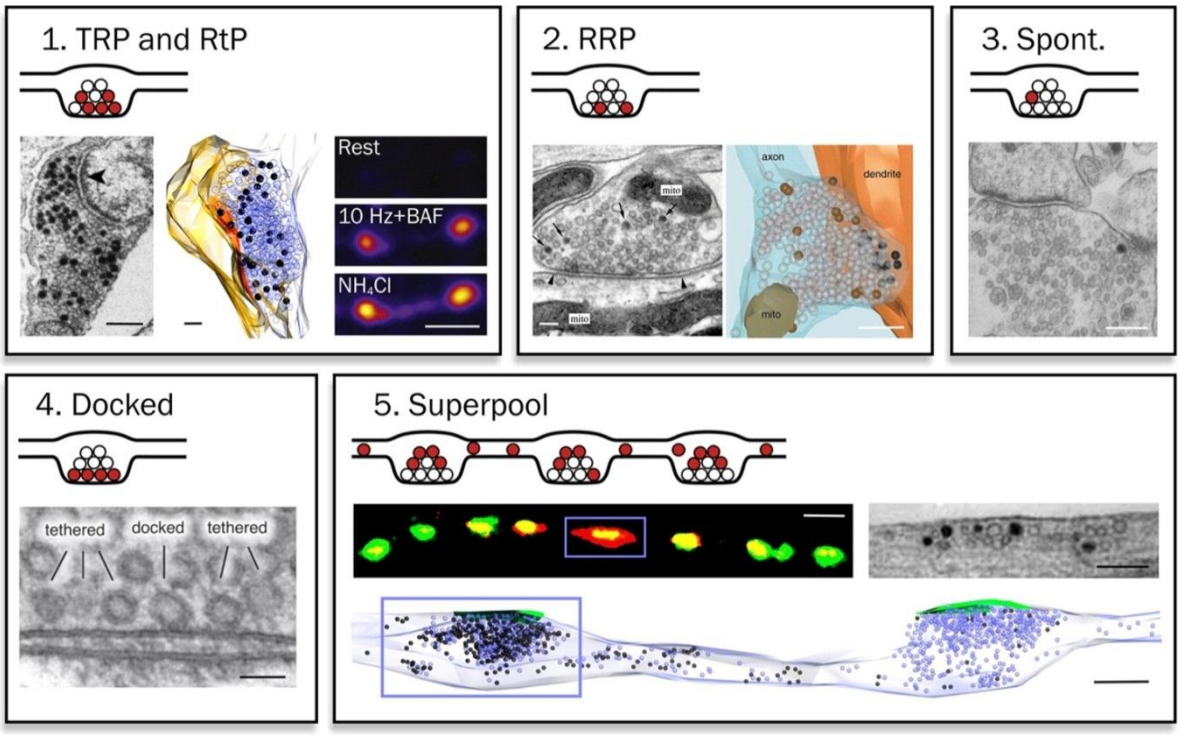

Figure 1.6 Synaptic vesicle pools 1). Recycling pool (TRP) and Resting Pool (RtP); electron micrograph (left) from cultured hippocampal neurons depicts the total recycling fraction (TRP) (labelled with FM1-43 and photoconverted, resulting in a darkened lumen) and RtP, which appears as clear vesicles. 3D reconstruction of the synapse (middle). Fluorescence panels (right) show functional readout of vesicle pools sizes using the v-ATPase, bafilomycin. 2). Electron

micrograph of the RRP obtained with same technique as in (1) with 3D reconstruction. 3). Electron micrograph of spontaneous pool labelled using HRP (dark vesicles). 4). Electron micrograph showing the presence of docked vesicles at the presynaptic membrane 5). The superpool of vesicles is not confined to a single terminal but is shared between neighbouring synapses. Taken from Staras et. al. 2010.

Within the recycling fraction exists a subset of vesicles that preferentially engage in fusion following synaptic activity, referred to as the readily releasable pool (RRP) (Rosenmund and Stevens, 1996). Estimations of RRP size range from 5 – 15 vesicles, with fluctuations in these values likely driven by the different stimulation paradigms used across experiments (Dobrunz and Stevens, 1997, Murthy and Stevens, 1998). One possible experimental approach for inducing RRP release is the application of a hypertonic solution (typically sucrose), which elicits Ca^{2+}-independent exocytosis (Rosenmund and Stevens, 1996). Another approach, such as the one we will use in this research, evokes RRP release using action potential stimulation (typically 10-50APS, 10-20Hz), which results in conventional, Ca^{2+} -dependent fusion (Murthy and Stevens, 1998, Park et al., 2012). There is increasing evidence in the literature to support the idea that the size of the RRP positively correlates with release probability (Dobrunz, 2002, Dobrunz and Stevens, 1997, Matz et al., 2010, Murthy et al., 2001). Consequently, modulation of RRP size may have implications for long term potentiation (LTP), and its pharmacological manipulation could provide a useful strategy in targeting neurodegenerative disorders.

Relatively new findings have described the existence of several alternative vesicle pools at the synapse. One such pool, the spontaneous pool, comprises synaptic vesicles that are released in the absence of stimulation (Kavalali, 2015, Truckenbrodt and Rizzoli, 2014). The precise identity of these vesicles is still under debate, with some groups claiming that they form a subset of the RtP (Fredj and Burrone, 2009, Sara et al., 2005), others that they originate from the TRP (Groemer and Klingauf, 2007, Herzog et al., 2011, Wilhelm et al., 2010), or are derived from both (Kavalali, 2015). Another pool, the 'superpool' defines a vesicle population that is not confined to a single synapse but is instead shared across multiple terminals at a reasonably high dynamic rate (~4% of the total pool per minute) (Staras et al., 2010).

1.5. Synaptic vesicles as potential therapeutic targets

Presynaptic machinery is an attractive target for pharmacological intervention as it permits dynamic modulation of neurotransmission. Manipulation of synaptic vesicles can subtly and

selectively alter neurotransmitter release, with nonsynchronous forms of release implicated in the regulation of synaptic plasticity, memory processing and anti-depressant action (Li and Kavalali, 2017). Nevertheless, synaptic vesicle machinery remains a relatively underexplored drug target. In this work, we focus our attention on the modulation of synaptic vesicle protein 2A (SV2A), target of the anti-epileptic drug (AED), levetiracetam

1.5.1. Synaptic vesicle (SV) protein 2 A – Background

SV2A is a member of the synaptic vesicle (SV) protein 2 (SV2) family - large membrane-spanning glycoproteins that belong to the major facilitator superfamily (MFS) of transporters, and are specific to neurons and endocrine cells in vertebrates (Bajjalieh et al., 1992). Three paralogs of SV2 exist, namely SV2A, B and C, of which SV2A is the only isoform that is expressed ubiquitously in the adult brain, and in both excitatory and inhibitory neurons (Buckley and Kelly, 1985, Bajjalieh et al., 1994, Dong et al., 2006). Expression of SV2B follows much the same pattern of expression as SV2A, however it is absent from the dentate gyrus (DG), globus pallidus (GP), and the reticular part of the substantia nigra, and seems to be confined to glutamatergic synapses (Bajjalieh et al., 1994, Crevecoeur et al., 2013). The expression of SV2C is much more varied; it is present in high levels in the central neuraxis, including the striatum, midbrain (especially the substantia nigra), and the hindbrain. Low levels of SV2C have been observed in the cerebrum, the olfactory bulb, the hippocampus and the cerebellum. SV2C is found in certain GABAergic cell types, such as Purkinje cells, dopaminergic neurons and a fraction of cholinergic neurons (Dardou et al., 2011). In addition, the respective specificity of SV2B and SV2C for glutamatergic and GABAergic synapses has been observed by proteomic analysis and co -localization studies in immune-isolated vesicles (Gronborg et al., 2010, Bragina et al., 2011). Structurally, SV2A consists of a highly N-glycosylated backbone of ~ 80kDa, with 2 transmembrane (TM) domains and three extramembranous domains – shown in Figure 1.7 (Janz et al., 1999).

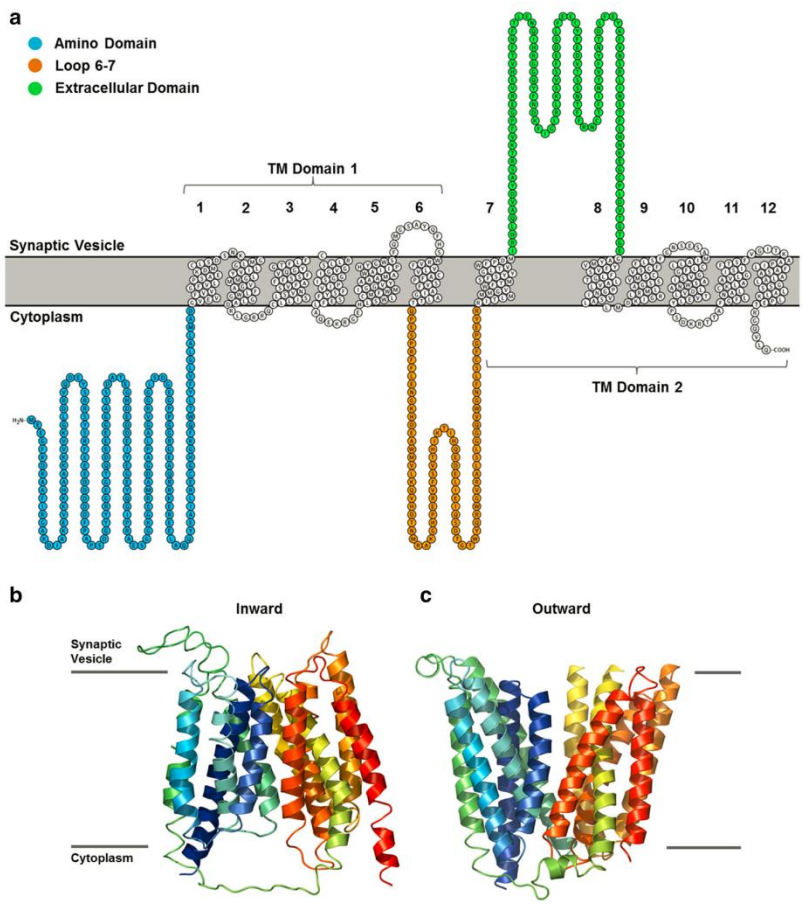

Fig 1.7. The structure of SV2A. Schematic representation (a) shows 2 TM domains, each comprised of 6 TM helices and three extramembranous domains: the amino domain (blue), a long loop spanning the region between TM helices 6 and 7 (orange) and an extracellular domain between TM helices 7 and 8 (green). 2D protein topology generated using Protter reveal inward-open (b) and outward-open (c) conformations of the SV2A protein. Modified from Löscher, 2016.

1.5.2. Possible functions of SV2A

The exact role of SV2A in synaptic vesicle function is yet to be fully understood (Mendoza-Torreblanca et al., 2013), although knockout mice develop a severe seizure phenotype and fail to thrive beyond 21 days, emphasizing its necessity in normal synaptic behaviour (Crowder et al., 1999, Janz et al., 1999). Brain architecture is preserved in SV2A knockout (KO) mice, with no changes observed in either synapse density or morphology, making a role in development unlikely (Crowder et al., 1999, Janz et al., 1999).

In terms of electrophysiology, the frequency of miniature excitatory (mESPC) and inhibitory currents (mISPC) is unchanged in SV2A KO mice, indicating that the physiological machinery that partakes in vesicle fusion events is preserved in the absence of SV2A (Crowder et al., 1999, Janz et al., 1999, Chang and Sudhof, 2009, Venkatesan et al., 2012). However, spontaneous and evoked postsynaptic currents (sPSCs and ePSCs) are altered in SV2A KOs. Nonetheless, whilst all experimental data in the field concurs that IPSCs (both spontaneous and evoked) occur at a reduced amplitude and frequency (Crowder et al., 1999, Chang and Sudhof, 2009, Venkatesan et al., 2012), the effect on EPSCs is still undefined. One possibility as to the discrepancies in ESPC data could lie within the experimental system used; broad analysis of the current data reveals that the electrophysiological parameters in neurons cultured from wildtype (WT) and KO animals show reduction in amplitude of ~37% in EPSCs and ~39% in IPSCs, which could indicate that they stem from the same defect. However, in hippocampal slices, the effect on IPSCs is more pronounced than on EPSCs (Bartholome et al., 2017).

In terms of neuronal organization *in* vivo, inhibitory synapses are usually located closer to the soma than excitatory synapses (Ito et al., 1997, Gulyas et al., 1999, Kulik et al., 2003, Darstein et al., 2003), which implies that inhibitory signals are more constant, and can therefore act as a gating system to control the traffic at local excitatory networks (Jaffe and Carnevale, 1999). Overall, these observations suggest that the inhibitory system could be more sensitive to SV2A depletion: at a cellular level, the amplitude of both PSCs is reduced, but at the tissue level, the effect on the inhibitory system is overriding. Lack of inhibitory currents means that these neurons can no longer carry out their 'gating' role, which in turn unleashes excitatory currents, leading to an overload of the excitatory system and a hyperactive state (Bartholome et al., 2017).

At low frequency (2Hz), EPSCs recorded from SV2A/B double knockouts (DKOs) show facilitation in response to trains of action potentials (N.B. when normalized to the first response in the train; raw amplitudes are, in fact, decreased in comparison to WT) (Custer et al., 2006). At 2Hz, this is sustained over 25 stimuli, however at 10Hz and 20Hz, facilitation occurs briefly at the start of the train but synaptic depression is quickly induced. The authors also observe a reduction in RRP size; taken together, they conclude that these results are consistent with a model in which loss of SV2A decreases initial release probability, and therefore primarily has consequences upon low frequency neurotransmission (Custer et al., 2006). This interpretation is consistent with observations in chromaffin cells, where Ca^{2+}-induced exocytotic bursts and SDS-resistant SNARE

complexes were reduced in the absence of SV2A, resulting in a smaller RRP (Xu and Bajjalieh, 2001). The overall interpretation from these studies is that SV2A has some involvement in vesicle fusion competence.

In vesicles studied at the Torpedo electric organ, it is suggested that an intravesicular matrix is formed from proteoglycans, in a manner similar to that observed in mast cells and chromaffin granules (Reigada et al., 2003). It is suggested that the intravesicular matrix of cholinergic synaptic vesicles behaves like an ion-exchange gel, whereby ACh and ATP^{3-} are displaced by ions and the matrix size increases. In fact, in contradiction to the wider assumption that neurotransmitter exists in vesicles in solution, only ~5% of ACh content is 'free' and the rest is adsorbed into the intravesicular proteoglycan matrix, which controls its storage and release (Reigada et al., 2003). Furthermore, the cholinergic synaptic vesicle proteoglycan is a structure composed of several proteins, with the most abundant being SV2 (Scranton et al., 1993). Additional research in isolated synaptic vesicles has demonstrated that vesicles undergo an increase in diameter of ~25% following glutamate loading, but that those lacking SV2A do not present such a change (Budzinski et al., 2009). Together, these studies imply that SV2 is a necessary component of neurotransmitter filling and retention (Reigada et al., 2003).

1.5.3 Levetiracetam, an SV2A ligand in the treatment of epilepsy

Since 1937, when Putnam and Merritt first described the use of an electroshock seizure model to evaluate the efficacy of potential AEDs, preclinical trials in animal seizure models have remained the cornerstone in the discovery of novel seizure therapeutics (Putnam and Merritt, 1937). Simple models of acute seizure, such as the maximal (tonic hindlimb extension) electroshock seizure (MES) test and subcutaneous administration of the $GABA_A$ antagonist, pentylenetetrazol (PTZ) gave rise to the discovery of many of the early AEDs in clinical usage; compounds such as phenytoin, carbamazepine and valproate (Loscher and Schmidt, 2011). Indeed, the success of the MES and PTZ animal models in identifying the differential properties of novel AEDs was such that it was proposed that these two tests in combination should form the 'gold standard' in the prediction of anticonvulsant activity, and thus be responsible for the selection of all potential AEDs taken forward into human clinical trials (Swinyard, 1949, Swinyard et al., 1952).

For many decades, screening compounds based on efficacy in the MES and PTZ seizure models remained the basis of AED identification. However, in the late 1980s pharmacologist Alma Gower

noted that the (S)-enantiomer of the ethyl analogue of the nootropic, piracetam, later to become known as levetiracetam (LEV), exhibited potent anticonvulsant properties in audiogenic seizure prone mice (Gower et al., 1992). Interestingly, Gower also reported LEV to be efficacious in both the MES and PTZ tests, however numerous attempts to replicate this data have failed (Loscher and Honack, 1993, Klitgaard et al., 1998, White et al., 2006). Nevertheless, the initial misclassification of LEV prompted a battery of other tests to be performed using alternative seizure models. LEV proved effective in attenuating seizure in chronic models of primary generalised seizures, including the kindling model of temporal lobe epilepsy (TLE), in which seizure is induced via repetitive electrical stimulation in limbic structures, most often the amygdala (Loscher and Honack, 1993); a discovery that opened the door for a reconsideration of the optimal strategy in AED screening and underpins the unique profile of LEV in the treatment of seizure. Subsequently, the binding site of levetiracetam was identified as SV2A, sparking curiosity in how modulation of this target could be harnessed for other pharmacotherapies (Lynch et al., 2004).

Clinically, LEV is currently one of the most widely prescribed AEDs, yet almost nothing is known about its mechanism of action. Through applying a novel approach that uses targeted optical reporters to monitor presynaptic function, a major aim of this work was to gain a better insight into how LEV operates at synaptic terminals.

1.6. Metabotropic glutamate receptor 2 (mGluR2) as a target for neuropharmacotherapies

1.6.1. mGluRs: G-protein coupled receptors (GPCRs) in glutamatergic neurotransmission

In the mid-1980s, research emerged supporting the existence of a new family of receptors that could modulate the action of the major excitatory neurotransmitter, glutamate, via G-protein coupled secondary messenger (GPCR) systems (Sladeczek et al., 1985, Sugiyama et al., 1987). Up until this point, actions of glutamate were thought to be exclusively mediated by the activation of glutamate-gated cation channels: ionotropic glutamate receptors (iGluRs). The discovery of metabotropic glutamate receptors (mGluRs) dramatically altered the viewpoint of glutamate transmission in the CNS as, unlike receptors for other neuromodulators, mGluRs have the ability to

modulate and fine-tune activity at the same synapses at which they invoke rapid glutamatergic responses (Conn and Pin, 1997). Today, identification of mGluR-related cDNA has led to the isolation of seven other genes and splice variants that encode eight different mGluRs, named mGluR1 through mGluR8 (Tanabe et al., 1992, Pin et al., 1992, Abe et al., 1992, Nakajima et al., 1993, Okamoto et al., 1994, Saugstad et al., 1994, Joly et al., 1995, Minakami et al., 1994, Duvoisin et al., 1995, Iversen et al., 1994, Laurie et al., 1996). Based on their sequence homology, pharmacological properties and intracellular transduction pathways, these eight mGluRs can be further classified into three groups; group I includes mGluR1 and mGluR5; group II, mGluR2 and mGluR3, and group III, all others (Nakanishi, 1992).

Group II mGluRs are negatively coupled to adenylate cyclase (AC) through G proteins of the G_i/G_0 type (Conn and Pin, 1997) and act as both autoreceptors and presynaptic heteroreceptors in order to inhibit glutamate release (Xi et al., 2002). Autoreceptors are located presynaptically and are sensitive to the neurotransmitter released from the neuron on which they are located, whereas heteroreceptors regulate the synthesis and/or release of mediators other than their own ligands. Therefore, as an autoreceptor, mGluR2 responds to the glutamate released by the neuron on which it is situated. Alternatively, mGluR2 can interact with 2AR (a member of an unrelated GPCR family) via specific transmembrane helix domains which results in functional 2AR/mGluR2 complexes that are able integrate serotonin and glutamate transmission (Gonzalez-Maeso et al., 2008). Both mGluR2 and mGluR3 are widely expressed in the hippocampus, cortex, nucleus accumbens, striatum and amygdala (Ferraguti and Shigemoto, 2006). Despite their widespread distribution, there is currently limited knowledge as to how mGluRs modulate release of glutamate (Pinheiro and Mulle, 2008). The cellular role of adenylate cyclase is to catalyze the conversion of cytosolic adenosine trisphosphate (ATP) to its monophosphate form (cAMP). Therefore, inhibition of AC results in decreased cAMP production Presynaptically, alterations in cAMP can have direct implications on ion channel activity, as well as on members of the serine/threonine-specific protein kinase A (PKA) family (Anwyl, 1999, Cartmell and Schoepp, 2000, Moghaddam, 2004, Schoepp et al., 1999). Interestingly, Xi et al. have illustrated that Group II mGluRs regulate glutamate release via non-vesicular and vesicular mechanisms (Xi et al., 2002), and alterations in synaptic vesicle release have been shown to exist in mGluR2-dependent long term depression (LTD) (Zakharenko et al., 2002). mGlu2 receptors have a prominent effect upon synaptic plasticity (Anwyl, 1999), with mGluR2 influencing both the suppression of LTP and induction of LTD in the mossy fibers of the hippocampus (Nicholls et al., 2006). Notably, the Group

II mGluRs (particularly mGluR2) are also implicated in a range of neurological disorders, including Parkinson's disease, schizophrenia and Alzheimer's disease (AD) (Conn and Jones, 2009, Lee et al., 2009b), thus hinting that they may provide desirable targets for pharmacological interventions.

1.6.2 Development of GPCR allosteric modulators and their pharmacological implications

GPCRs, such as mGluR2, are the most widespread class of cell-surface receptors and play vital roles in almost every cellular system. As stated above, mGluR2 is linked to a number of neurological disorders, and generalized GPCR dysfunction is implicated in a myriad of human disorders and diseases. Therefore, it is obvious as to why they make desirable drug targets. In fact, it has been estimated that nearly half of therapeutic agents in current use modulate GPCR activity in some way (reviewed in (George et al., 2002)). Nevertheless, there are a number of issues that have contributed to the limitation of selective, orthosteric ligands that can be used therapeutically. One major problem is that the orthosteric binding site across GPCRs of the same sub-family is highly conserved, making it almost impossible to develop ligands that have high selectivity for a particular receptor subtype (Conn et al., 2009). For example, (2S,2'R,3'R)-2-(2,3-dicarboxycyclopropyl) glycine (DCG-IV) acts as an agonist at both mGlu2 and mGlu3 receptor subtypes (Hayashi et al., 1992).

More recently, pharmaceutical research has turned its attention to the development of ligands that do not bind orthosterically, but instead act at an alternatively located binding site, termed an allosteric binding site. These sites are distinct from the orthosteric site and their modulation can either potentiate or inhibit the actions of the endogenous ligand, making them sensitive to the demands of the immediate physiological environment, a desirable property in therapeutic design. Moreover, allosteric binding sites tend to be more specific for individual GPCR subtypes, making it easier to generate selective ligands (Conn et al., 2009). Our industrial partner, Janssen Pharmaceutica, has played a pivotal role in the research and development of highly selective positive and negative allosteric modulators (PAMs and NAMs) of mGluR2 (Farinha et al., 2015, Lavreysen et al., 2015a, Doornbos et al., 2016, Metcalf et al., 2017) and has uncovered a synergistic effect *in vivo* between PAMs of mGluR2 and levetiracetam. Consequently, another major aim of this work was to exploit optical techniques to characterize the actions of novel allosteric modulators of mGluR2 at the presynaptic terminal, and to further investigate the synergistic interaction between LEV and mGluR2 PAMs using an *in vitro* model system.

1.7. Synaptic dysfunction in tauopathy

1.7.1 Background

Tau is a microtubule-associated-protein (MAP) that is widely implicated in a number of neurodegenerative diseases (tauopathies), the most notable of which is Alzheimer's disease (AD). According to the 2015 annual report released by Alzheimer's Disease International, 46.8 million people globally are currently living with AD and other related dementias and, given that statistical forecasting predicts that this number will double every 20 years, the outlook appears grim (Prince et al., 2015). Pathologically, AD, the most prevalent of the dementias, yields atrophy of the transentorhinal, hippocampal and neocortical regions of the brain, arising as a result of neuronal degradation and synapse loss. The disease is also hallmarked by two definitive proteineous lesions: Aβ plaques and neurofibrillary tangles (NFT), which are formed through the deposition of amyloid beta and hyperphosphorylated tau protein respectively (Gomez-Isla et al., 2008). Interestingly, despite elevated Aβ being closely associated with AD onset through genetic mutation e.g.) familial AD and trisomy 21, which triplicates the Aβ-precursor protein (Bertram et al., 2008), amyloid pathology is not a robust indicator of disease progression in terms of cognitive decline and synapse loss (Hardy and Selkoe, 2002), whereas tau pathology is a much higher correlate (Giannakopoulos et al., 2003, Gomez-Isla et al., 1997) (Fig 1.8). This, coupled with the discovery that tau is an essential mediator of Aβ-toxicity (Ittner et al., 2010, Roberson et al., 2011, Yu et al., 2012), suggests that AD may have multiple phases: the primary Aβ-dependent/ tau-independent phase and the latter Aβ-independent/ tau-dependent phase (Hyman, 2011).

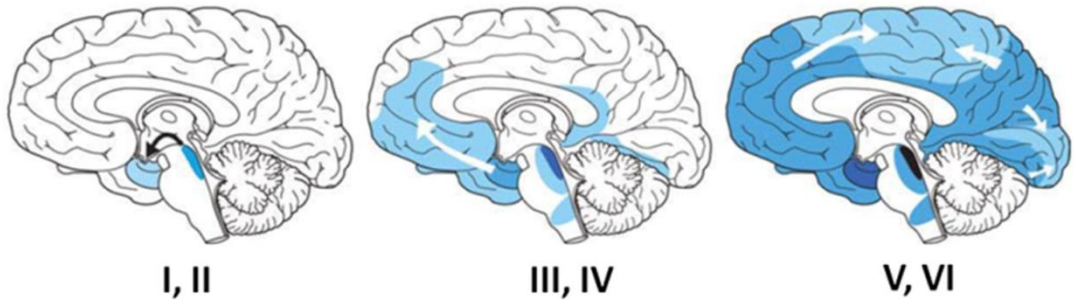

Fig 1.8. Braak staging in tauopathy. Pathology begins in lower brainstem and olfactory system (I and II) and spreads upwards through the substantia nigra and mesocortex (III and IV) until it reaches the temporal, parietal and locus ceruleus until fully invading the neocortex (V and IV). Figure modified from Jouanne et. al., 2017.

1.7.2. Tau isoforms

Under normal physiological circumstances, six common isoforms of human tau exist as highly soluble and natively unfolded proteins that are predominantly located in the neuronal axons of the CNS, where they associate with tubulin, promoting its assembly into microtubules and hence stabilizing its structure (Bunker et al., 2004). Isoforms can differ both at the N and C terminals, where alternative splicing of exons 2 and 3 can generate proteins with 0 (0N), 1 (1N) or 2 (2N) inserts at the N-terminus, and the presence or absence of exon 10 can yield protein variants with either 3 (3R) or 4 (4R) microtubule-binding domains at the C-terminus; 4R binding to microtubules more tightly than its 3R counterpart (Panda et al., 2003). Normally, both 3R and 4R tau are expressed in the adult human brain at a ratio of 1:1, yet in a number of tauopathies, this ratio switches. For instance, in variations of FTDP-17 dementia, mutations at exon 10 cause overexpression of the 4R isoform, resulting in an increased interaction of tau with microtubules (Hutton et al., 1998).

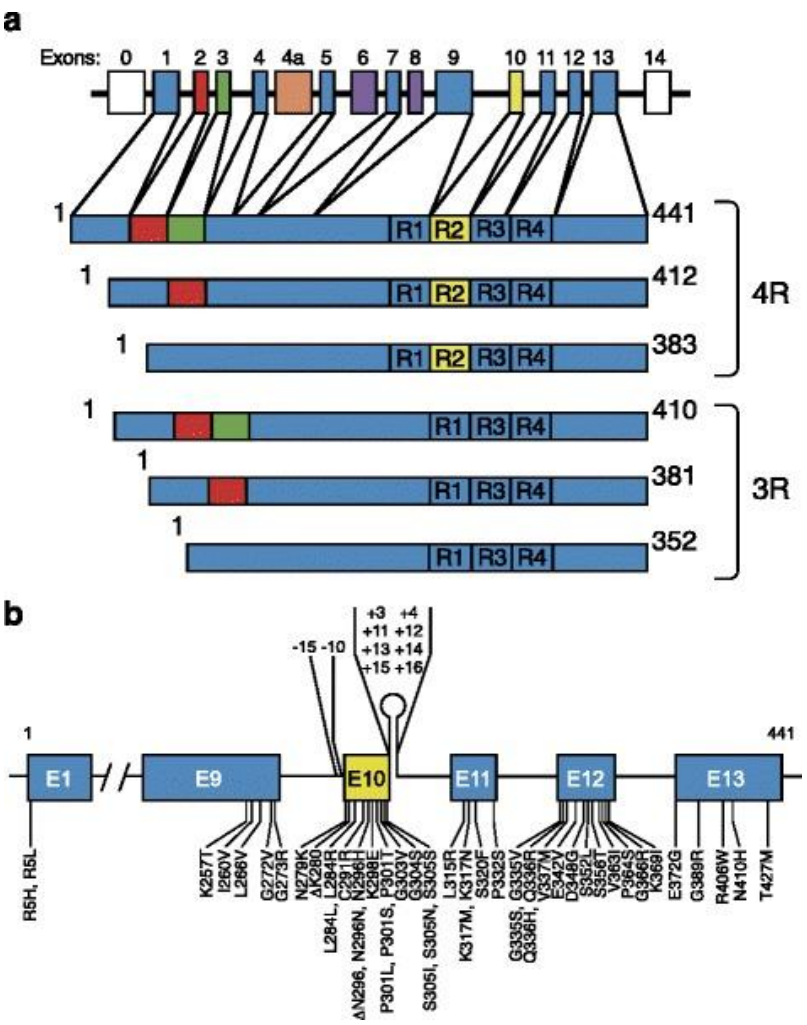

Fig 1.9. Six identified isoforms of tau exist in humans (a) that have either 3 or 4 repeats of the microtubule- binding domain. (b) Mutations in the *MAPT* gene in frontal-temporal lobe dementia linked to chromosome 17. Taken from Goedert et. al., 2012

1.7.3. Post-translational modifications

In both homeostatic and stress-induced biological states, tau is regulated by an array of post-translational processes, of which phosphorylation has been the most intensively studied. Due to its unfolded structure, a large proportion of Tau's 85 phosphorylatable residues can serve as phosphorylation sites, of which approximately 45 have been identified experimentally (Hanger et al., 2009). In contrast to the healthy brain, where phosphorylation typically occurs in 2-3 residues, the brains of patients suffering from AD and other tauopathies exhibit rates of phosphorylation that are, at the least, three-fold this (Wang et al., 2013). Tau hyperphosphorylation results in a lowered affinity for microtubules, which in turn results in structural disorganization; tau is miss-

sorted from axons to the somatodendritic compartments. Hyperphosphorylated tau also displays an increased resistance to degradation via the ubiquitin-proteosome pathway and subsequently tau begins to self-aggregate into insoluble helical fragments, which combine to form NFTs (Iqbal et al., 2009). Recently, reversible acetylation of lysine residues has been identified as a post-translational modification of tau, with notable cross-talk evident between acetylation and phosphorylation; in hTau KI mutant *Drosophila melanogaster,* pseudo-acetylation of residues K163, K280, K281 and K368 results in increased phosphorylation at S262 but severe dephosphorylation at other phosphorylation sites (Gorsky et al., 2017). This finding highlights the importance of the interplay between post-translational modifications, which ultimately has potential consequences in terms of regulating the bioavailability of tau for microtubules.

Interestingly, animals in hibernation also display hyperphosphorylation of tau, whereby its polar distribution is lost and it is instead found ubiquitously within the neuron, mirroring that which occurs in patients with tauopathy (Arendt et al., 2003). Hibernation also induces differential expression of the presynaptic proteins synaptophysin and piccolo, which acts as a mediator between the dynamic actin cytoskeleton and the endo- and exocytosis of synaptic vesicles (Fenster et al., 2003). Whether the two phenomena are linked remains to be seen, however a set of experiments carried out in *Drosophila melanogaster* utilising fluorescence imaging and immunohistochemistry provides initial evidence that tau may be intrinsically linked to proteins of the synaptic vesicle cycle (Zhou et al., 2017). These experiments establish the co-localization of pathogenic mutant tau and cysteine string protein (CSP), a co-chaperone protein belonging to the DNAJ/Hsp40 family that is localized to synaptic vesicles and is essential for neurotransmitter release in Drosophila, as well as being implicated in neurodegenerative processes in both Drosophila and mice (Chamberlain and Burgoyne, 1998, Fernandez-Chacon et al., 2004). Additional research from Begcervic et.al conducting proteomic analysis of hippocampal tissues from AD patients also revealed significant alterations in hippocampal proteins responsible for synaptic vesicle trafficking and LTD in the brains of AD sufferers (Begcevic et al., 2013).

1.7.4. Tau aggregation and synaptic impairment

Tangle deposition, arising from self-aggregation, occurs in a distinct pattern (Fig 1.8), emerging in the entorhinal cortex in the early stages of AD and steadily spreading through the hippocampus, association cortices and lastly, the primary sensory cortex (Braak and Braak, 1991); this

progression is well correlated with cognitive decline (Gomez-Isla et al., 1997, Giannakopoulos et al., 2003). However, in terms of synaptic dysfunction, relevance of tangle load is a hotly debated topic. Some studies postulate that aggregates are the primary factors in synaptotoxicity, for example a reduction in the number and size of synaptic boutons has been observed in tangle-baring neurons in the spinal cord of P301L mice when compared with neurons from a wild type (Katsuse et al., 2006). Furthermore, the expression of the synaptic vesicle associated protein, synaptophysin, was shown to be diminished in tangle bearing vs adjacent non-tangle bearing neurons in post mortem examinations of the brains from AD patients (Callahan and Coleman, 1995, Callahan et al., 1999).

The association between NFTs and synapse and neuronal loss has resulted in the assumption that tangle load is a key player in tau-driven synaptotoxicity. However, the concept of NFT toxicity is increasingly being challenged (Lee et al., 2005, Smith et al., 2002), and evidence from a number of models implies that NFTs are not required for tau-induced neuronal dysfunction and toxicity, with neuronal cell loss and synaptotoxicity occurring in the absence of NFT pathology (Gomez-Isla et al., 1997, Fox et al., 2011, Andorfer et al., 2005, Polydoro et al., 2009). One example of this is the rTg4510 mouse model, which repressively expresses the P301L human tau mutation, where the data shows that neuronal loss can be halted by suppression of the tau transgene even though NFTs persist (Santacruz et al., 2005). Additional data recorded from P301L transgenic animals has ascertained that, when a comparison is made between tangle bearing and non-tangle bearing neurons, no significant differences are apparent in spine density, electrophysiology (Rocher et al., 2010) or the ability to respond appropriately to stimuli (Fox et al., 2011). In fact, a potential neuroprotective effect of NFTs has been put forward, the rationale being that NFT formation is preceded by caspase activation, and that tangle-bearing cells have an enhanced tolerance to apoptotic cascades (Santacruz et al., 2005). The mechanism by which this occurs is unclear, yet it has been hypothesized that NFTs absorb some of the toxic soluble tau species, hence defending against cell death and conserving the neuron for a greater length of time (Spires-Jones et al., 2009, de Calignon et al., 2012).

Soluble tau, or oligomeric tau, is a poorly defined species in which tau can be in a variety of pre-tangle states; these include hyperphosphorylated, mislocalized and conformationally altered tau, which in turn can result in a loss of dendritic spines, dysregulation of calcium homeostasis, impaired trafficking of organelles and apoptosis (Hoover et al., 2010b, Spires-Jones et al., 2009, Yu

et al., 2009, Ebneth et al., 1998, Takashima, 2008, Mandelkow et al., 2001, Baas and Qiang, 2005, Dubey et al., 2008, Thies and Mandelkow, 2007). These processes appear independent of NFT formation, often occurring in the primary stages of AD, demarcating soluble tau as the probable cause. Additionally, it has been demonstrated that injection of oligomers, but not monomers or fibrils, into the hippocampi of wildtype mice induces memory impairment as well as synaptic and mitochondrial dysfunction (Lasagna-Reeves et al., 2011). The propagation of a soluble species of tau from one synapse to the next has been effectively shown, suggesting it may be the soluble form that is responsible for the spread of the disease and the ensuing cognitive decline (Calafate et al., 2015a). There are several potential molecular mechanisms by which soluble or aggregated tau can lead to synaptotoxicity, and these can be broadly sorted into either of two categories: tau-induced interruption of microtubule-based transport and calcium dysregulation.

1.7.5 Mechanisms of tau toxicity

Given the elongated structure of a neuron, an effective transportation system must be in place to deliver vital components and organelles from the cell body to the synapse. The microtubule network is such a system: the microtubules serve as 'tracks', the organelles, vesicles and other components as 'cargoes', the motor proteins as 'engines' and the MAPs as stabilization, so as to maintain the tracks (Mandelkow et al., 2003). MAP tau is located in the axon, and thus the toxicity of aberrant tau is frequently linked to disruptions in the axonal component of the microtubule transportation network which, in turn, upsets the trafficking of various organelles and other vital components for synapse function (Ebneth et al., 1998). The process by which this occurs is debatable, with some suggesting that tau acts as a 'roadblock', with soluble tau forcing anterograde-moving kinesins to detach from microtubules, resulting in the accumulation of cargoes in the cell body (Dixit et al., 2008). Another hypothesis suggests that tau either directly competes with the cargoes for binding sites upon the microtubule framework or that it impedes signal transduction (Morfini et al., 2009, Mietelska-Porowska et al., 2014). Nevertheless, the final outcome is an impairment in neuronal transport that results in abnormal distribution of organelles and prevention of necessary proteins reaching the synapse, which in turn leads to synapse starvation and loss, abnormal cell function, and finally cell death (Morfini et al., 2009).

The organelles which appear most susceptible to disturbances in tau localization are mitochondria, with tau-overexpression in cell culture leading to mitochondrial perinuclear clumping (Kopeikina et

al., 2011). Due to their elongated shape, neurons harbour unique metabolic demands and thus mitochondria cluster in the areas with most need, such as at the synapse. A number of cellular functions are reliant upon mitochondrial ATP production, including synaptic vesicle recycling and mobilization, construction of the presynaptic actin cytoskeleton, and the generation of action potentials (Verstreken et al., 2005, Lee and Peng, 2008, Attwell and Laughlin, 2001, Sun et al., 2013). Hence, mitochondrial dysfunction can have widespread ramifications for synaptic transmission. Several studies have documented the role of mitochondria in sustained synaptic transmission, showing that mitochondria are crucial to maintain vesicle release over an extended period of time (Sun et al., 2013, Verstreken et al., 2005, Heidelberger et al., 2002, Ivannikov et al., 2013). Experiments conducted in *Drosophila drp1* mutants, which display abnormal mitochondrial disorganization similar to that in AD, concluded that intracellular Ca^{2+} is two-fold higher in mutants than in controls but that this does not impact upon basal neurotransmitter release. However, release does decline during prolonged stimulation, which might suggest that recycling from the reserve to the recycling pool is disrupted. This is further backed by the failure of standard FM1-43 loading protocols to load the RtP in *drp1* mutants (Verstreken et al., 2005). Interestingly, in his more recent work in *Drosophila*, Verstreken established that TRP cycling was also reduced in pathogenic tau mutants (Zhou et al., 2017). Note that vesicle pool dynamics at the *Drosophila* NMJ differ considerably to those at small central terminals; vesicles are designated into one of three pools: the RRP, the TRP and the reserve pool, however unlike the resting pool at mammalian hippocampal synapses, the reserve pool in the *Drosophila* can be fully depleted following prolonged stimulation.

Since Khachaturian, Landfield and Gibson first hypothesized that intracellular calcium dyshomeostasis plays a role in aging and neurodegeneration (Khachaturian, 1987, Landfield, 1987, Gibson and Peterson, 1987), calcium disturbances have been well documented within multiple neurodegenerative disorders and nowadays it is well established that calcium dysregulation is evident within both the Aβ and tau pathogenic pathways in AD, perhaps even providing a link between the two (Huang and Mucke, 2012). Many receptors are implicated in dysfunctional Ca^{2+} signalling associated with taopathy, including (but not limited to) the NMDA receptor, calcium-sensing receptors, inositol triphosphate receptor, metabotropic glutamate receptors and the ryanodine receptor (Chakroborty and Stutzmann, 2014, Armato et al., 2013, LaFerla, 2002, Popugaeva and Bezprozvanny, 2013, Um et al., 2013, Stutzmann et al., 2006). To date, the major body of research concerning calcium dynamics in AD has concentrated upon the Aβ-pathway,

however more studies that attest that elevated Ca^{2+} levels are apparent in models of tau pathology are coming to the forefront (Rocher et al., 2010, Crimins et al., 2011). In terms of synaptic dysfunction, the major consequence of elevated calcium at the synapse is an alteration in synaptic plasticity. As the basis of learning and memory, it is unsurprising that effects on synaptic plasticity are seen within AD and, although there is some research suggesting that mutations in presenilin-1 (the predominant cause of familial AD) lead to a ryanodine-receptor mediated decrease in synaptic vesicle release and plasticity (Wu et al., 2013, Zhang et al., 2010), there is a scarcity in research that focuses on the tau-related presynaptic plasticity, with most focusing on the postsynaptic side (Ittner et al., 2010, Hoover et al., 2010b, Van der Jeugd et al., 2011). This said, a recent publication by the Mandelkow laboratory found a reduction in both basal synaptic transmission and plasticity in pro-aggregant $tau^{RD\Delta}$ mice, which particularly show mis-conformational tau in the mossy fibre presynapse due to co-aggregation of human and endogenous tau, and further ultrastructural analysis revealed severe reduction in vesicle density (Decker et al., 2015).

In this work, we hope to further elucidate the actions of pathogenic tau at the presynaptic terminal by using targeted optical reporters of presynaptic function. We focus on tau(P301L), a mutation in the *MAPT* gene associated with FTDP-17 in which the proline residue at position 301 is changed to lysine. The mutation occurs in a highly conserved region within exon 10 and therefore only affects the 4-repeat (4R) tau isoforms. It was originally identified in a Dutch kindred (HFTD1), a U.S. kindred (FTD003) (Hutton et al., 1998), and in six French families diagnosed with frontotemporal dementia and parkinsonism (Dumanchin et al., 1998). We also hope to gain further insight into the endogenous role of tau in terms of synaptic function by examining the ramifications of tau knockdown in primary hippocampal cultures.

1.8. Research Objectives

The small size of the presynaptic terminal and the rapid timescale at which processes accompanying synaptic vesicle release and retrieval occur present technical challenges for monitoring dynamic changes at the presynaptic terminal. In this work, we exploit targeted optical reporters of presynaptic function (reviewed and validated in Chapter 3) to provide a unique and novel insight into pharmacological and pathological modulation at presynaptic terminals in small central synapses. By using these fluorescent readouts of synaptic function in primary hippocampal

cultures, we aim to characterize the mechanistic actions of the AED, levetiracetam, which at present are still somewhat enigmatic, despite it being in wide clinical circulation. We also aim to characterize the actions of novel allosteric modulators of mGluR2, developed by our industrial partner, Janssen Pharamceutica, and to explore the potential synergistic relationship between mGluR2 PAMs and LEV. A final focus of the research programme is to exploit the same optical approaches targeted at single synapses to directly examine the role of tau pathology on neurotransmission.

Chapter 2: Methods and Materials

2.1. Preparation of primary hippocampal cultures

2.1.1 Animal Handling

Experimental and animal handling procedures were in accordance with the Animals (Scientific Procedures) Act 1986 and approved by a local ethics committee. Pregnant Sprague Dawley dams were purchased from Charles River Ltd, UK and housed in compliance with Home Office guidelines. Dams littered on site and pups were sacrificed at P0/P1 using cervical dislocation.

2.1.2 Cell Culture

Following confirmation of death, brains were removed and transferred to ice-cold Hank's Buffered Saline Solution (HBSS) containing 0.1M HEPES. The hippocampus was isolated and washed three times with pre-warmed/pre-buffered 1x Minimal Essential Media (MEM) (Gibco Life Technologies) containing 10% FCS, 3% glucose and 1% pen/strep (Gibco Life Technologies). Using a 1ml pipette, the tissue was triturated until fully dissociated and diluted further with supplemented MEM. Neurons were seeded at a density of $6x10^4$ cells/well on 12mm glass coverslips (Fisher) pre-coated with poly-D-lysine ($20\mu g.ml^{-1}$) and laminin ($20\mu g.ml^{-1}$) (Sigma Aldrich). 3-4 hours later plating media was exchanged to Neurobasal medium without phenol red (Gibco Life Technologies), supplemented with 2% B27, 1% Glutamax (Gibco Life Technologies) and 1% pen/strep, in which cultures were maintained until experimentation at DIV 14-21. Phenol red in culture medium has been shown to increase levels of background fluorescence in imaging experiments (Stadtfeld et al., 2005), hence the use of phenol red free media. After 4-5 days incubation, cells were treated with 3.25µM cytosine arabinoside (Sigma-Aldrich) to stop astrocyte proliferation. Cultures were kept in conditions of 5% CO_2/95% air at 37^oC and fed every 3-4 days via exchange of half the media volume.

2.1.3 Transfection

Neurons were transfected at DIV 6/7 using a calcium phosphate transfection protocol. Quantities cited are for one well of a 24-well plate with a total volume of 800µl/well. 1-4µg DNA (stock in TE

buffer and stored at -20°C) was dissolved in Nuclease Free Water (Invitrogen) containing 250mM $CaCl_2$ and vortexed gently for 2-3 seconds. This was added dropwise to an equal volume of HEPES 2X (Invitrogen) and again vortexed for 2-3 seconds. The precipitate was shielded from light and kept at room temperature for 20 minutes. It was vortexed every 5 minutes for 2-3 seconds.

285µl conditioned media was removed from each well of the plate to be transfected (plate A) and transferred to the corresponding well of a fresh 24-well plate (plate B). 20mM kynurenic acid stock (powder dissolved in 5mM HEPES with 10mM $MgCl_2$, aliquoted and stored at -20°C) was added to each well of plate B to give a final concentration of 1mM. Kynurenic acid, an inhibitor of ionotropic glutamate receptors, reduces the excitotoxicity associated with transfection (Xia et al., 1996). Coverslips were transferred from plate A to plate B and 25-100µl DNA precipitate shared per coverslip dependent on the desired amount of DNA. Neurons were incubated with the precipitate for 1-3 hours at 37°C, 5% CO_2 (optimization required for each construct). Plate A was also returned to the incubator.

Following incubation, the precipitate was removed via application of pre-warmed acidic wash solution, containing 1mM kynurenic acid and 250µM HCl in unsupplemented Neurobasal medium without phenol red (Gibco Life Technologies). For this, neurons were transferred to a fresh 24-well plate (plate C) and incubated in the acidic wash solution for 15-20 minutes after which each coverslip was transferred back to the original plate (plate A). The volume of media in each well was topped up to 800µl with fresh Neurobasal medium supplemented with 2% B27, 1% glutamax and 1% pen/strep.

2.1.4 DNA plasmid amplification and purification

To amplify DNA plasmids, DH5α competent cells (Invitrogen) were transformed with 1-3µg of the desired DNA. Following addition of DNA, DH5α competent cells were incubated on ice for 30 minutes, transferred to a pre-heated waterbath at 42°C for 30 seconds and returned to the ice for another 2 minutes, a process known as heat-shock transformation. SOC media was added to the transformed cells and the mixture incubated for 1 hour in an orbital shaker (225 rpm, 37°C). Luria-Bertani (LB) agar plates (composition g/l: 10 tryptone, 5 yeast, 10 NaCl, 15 Agar) containing the appropriate antibiotic for plasmid selection (100µg.ml^{-1} ampicillin or 50µg.ml^{-1} kanamycin, Sigma Aldrich) were inoculated with 50-100µl of transformed cells and left to incubate overnight at 37°C. The next day, single colonies were picked using a sterile pipette tip, transferred to 250ml LB broth

and incubated in an orbital shaker overnight (225 rpm, 37°C). Finally, DNA from the liquid colonies was isolated using the PureLink® HighPure Plasmid FP Maxiprep Kit, resuspended in 750µl TE buffer (10 mM Tris-HCl, pH 8.0, 0.1 mM EDTA) and stored at -20°C.

2.1.5 Viral infection

Table 2.1.

Viral constructs used within this body of work					
Insert	**Viral type**	**Vector**	**MOI / volume used**	**DIV Infection**	**Supplier**
hSyn1:SypHy1x	AAV	AAV6	200	6/7	University of Helsinki
hSyn1:syGCamP6f	AAV	AAV6	100	6/7	University of Helsinki
pCAG: iGluSnFR	AAV	AAV9	1µl x 1 in 10 dilution of stock. (Titre unavailable)	6/7	Penn Vector
hSyn1:Tau(P301L)	AAV	AAV6	100	1	University of Göttingen, Germany
hSyn1:Tau(WT)	AAV	AAV6	100	1	University of Göttingen, Germany
TRC0000091298 (shRNA for Tau kockdown)	Lentivirus	plKO.1	10µl (Titre unavailable)	1	Sigma Aldrich

2.1.4.1. Adeno-associated viruses

Adeno-associated viruses are an alternative method for gene delivery into post-mitotic cells, including primary hippocampal neurons. There are numerous AAV serotypes which display species

and tissue tropism and therefore the selection of the capsid derived from the appropriate serotype is crucial for successful transduction (Watakabe et al., 2015). Of all the serotypes, AAV6 has been shown to be the most neuron specific and thus, when possible, this was selected as our preferred vector. Alternatively, AAV9 was used, which has a comparable infection rate in primary hippocampal cultures (Royo et al., 2008). AAV constructs were stored at -80°C.

Calculating the Multiplicity of Infection (MOI)

In microbiology, the multiplicity of infection (MOI) refers to the ratio of viral particles to infectious targets, in our case the number of primary hippocampal neurons. The probability of the number of viral particles effectively infecting cells can be described using a Poisson distribution; this is used as the basis for MOI calculation (Ellis and Delbruck, 1939). The use of a standardized MOI controls consistency of viral expression across experiments. The MOI is calculated using the formula below:

$$\textit{Multiplicity of Expression (MOI)} = \frac{\textit{Viral Titre} \times \mathcal{X}}{\#\ \textit{Cells}}$$

Where $\mathcal{X}$ = volume of virus to be added.

2.1.4.2 Lentiviruses

Lentiviruses were produced in-house at Janssen Pharmaceutica via a co-transfection system in which two vectors (packaging plasmid ps.PAX2 and VSV-G expressing plasmid pMD2.G) and the shRNA of interest were co-transfected (TranstIT-LT1:*Minus*) into the packaging cell line (HEK-293T) and the lentiviral supernatant harvested. All shRNA sequences were cloned into a pLKO.1. lentiviral vector and the plasmids amplified using a STBL3 *Escherichia coli* cell line *(Invitrogen)* to ensure careful maintenance of the hairpin structure. Lentiviral DNA was extracted using a PureLink® HighPure Plasmid FP Maxiprep Kit. The relative titre of each lentivirus (~ 3.47×10^7) was determined via puromycin selection in an A549 cell line, in which selection for transduced cells was compared with a standard curve produced by a control virus (TRCN0000072201- *Sigma Aldrich*). As the relative titre was calculated in an unrelated cell line, an MOI could not be calculated for the infection of hippocampal neurons. Therefore, the final volumes of lentivirus used were selected based upon optimization. See section 6.2.1. Lentiviral constructs were stored at -80°C.

2.1.6 Synthesis of $K18^{P301L}$ fibrils

Truncated human tau fragments containing the four microtubule repeat binding domains ($K18^{P301L}$; residues Q244-E372 of the 1N4R human tau isoform) with a P301L mutation and C-terminal myc-tag were introduced to the cultures at DIV 3 ($K18^{P301L}$-Myc; *custom produced by Tebu Bio*). For *in vitro* fibril production, a solution comprising 40µM $K18^{P301L}$, 40µM low-molecular weight heparin (MW=3,000) and 2mM DTT in 100mM sodium acetate buffer (pH 7.0) was incubated at 37^{o}C for seven days. This was subsequently centrifuged at 100,000 x g for 1 hour at 4^{o}C and the pellet resuspended in the same volume of 100mM sodium acetate buffer. The $K18^{P301L}$ fibrils were sonicated with 10x 1s pulses at 20% amplitude and stored in aliquots at -80^{o}C. Upon thawing, fibrils were further diluted in 100mM sodium acetate buffer (1:4) and re-sonicated, this solution was further diluted in culture medium (Neurobasal, B27 and Glutamax) and delivered to the cells at a final concentration of 2.5nmol.

2.2 Fluorescence imaging

2.2.1. Imaging System

Table 2.2.

Optimized EMCCD camera settings				
Construct	**Stimulation**	**Exposure (ms)**	**EM Gain**	**Acquisition Frequency (Hz)**
AAV6_sypHy1x	4APS	40	15	12.5
	40APS	40	10	12.5
	1200APS	40	10	12.5
AAV6_syGCaMP6f	40APS	40	10	20
AAV9_IGluSnFr	40APS	40	20	20
vGLUT1-pHluorin	20APS	40	40	12.5
VGAT-pHluorin	20APS	60	30	12.5
Remaining camera settings were kept constant: binning 4 x 4, readout speed 13,000 MHz, pre-amplification gain 3.8, cooling temperature -77°C.				

Images were acquired using an Olympus BX61W1 microscope equipped with an electron multiplying charge-coupled device (EMCCD) camera (Andor Ixon+) using a mercury light source with 480/20 nm excitation and 520/35 emission filters and an FF493/574-Di01-25x36 dichroic. Cells were imaged via a 60X 1.0 NA dipping objective. Camera settings were optimized for each experimental protocol and optical probe (Table 2.2). Experiments were performed in a darkened room and a blackout curtain was mounted around the stage to minimize extraneous light. Room temperature was maintained at 23°C.

2.2.2 Field Stimulation

Experiments were performed in a custom-built chamber consisting of a plastic O-ring with a gridded glass coverslip on the base (Fig 2.1). Field stimulation was applied through a pair of parallel platinum wires (0.5mm diameter), positioned either side of the chamber, 1.2mm apart. (Edelstein et al.). Stimulation was delivered via a Grass SD9 Stimulator (Astro-Med Inc, USA), and action potentials evoked using a 22.5V stimulus of 1ms duration - calibration shown in Figure 2.2. Stimulation protocols were controlled using customized protocols written using Micro-Manager (NIH). Unless otherwise stated, all experiments were carried out in pre-warmed Extracellular Bath Solution, pH 7.35, composition (mM): 136 NaCl, 2.5 KCl, 10 HEPES, 1.3 $MgCl_2$, 10 D-Glucose, 2 $CaCl_3$, supplemented with 20µM CNQX and 50µM APV for the blockage of AMPA and NMDA receptors. Ionic concentrations of EBS mimic the normal extracellular environment whilst the addition of blockers prevents propagation of spontaneously generated signals and recurrent stimulation activity.

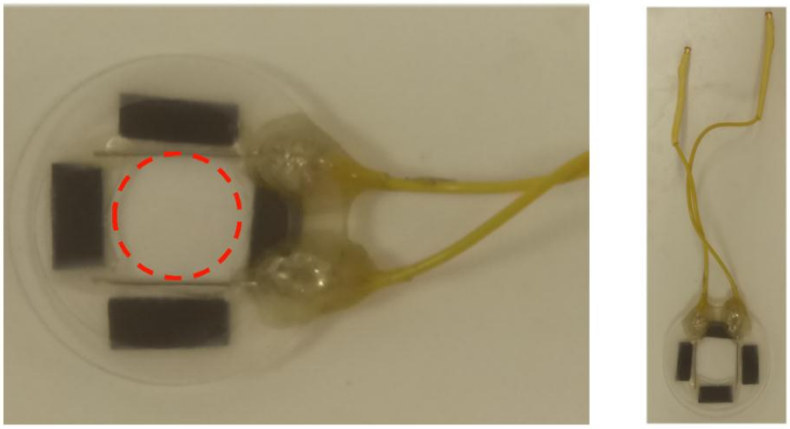

Figure 2.1. Customized Imaging Chamber Custom designed imaging chamber with magnetic strips to aid stability during imaging. Dashed red line indicates positioning of coverslip.

2.2.3 Calibration of stimulation intensity

A first priority of this work was to establish that observed synaptic responses arose as a result of the applied stimulation and to calibrate the stimulus intensity, ensuring that it was sufficient to reliably elicit synaptic responses. To calibrate the stimulus, we used the membrane-permeable Ca^{2+} indicator, Fluo4-AM (Molecular Probes), which displays an increase in fluorescence intensity upon binding Ca^{2+} (Gee et al., 2000). Cultures were incubated with 1µM Fluo-4AM for 30 minutes (5% CO_2, 37°C), added directly to the culture media. Coverslips were washed x3 with EBS supplemented with CNQX and APV to remove any free dye and transferred to the imaging chamber. Fluo-4 is not eliminated from the cells during stimulation which allowed for multiple imaging of the same region. Time-lapse images were collected (12.5 Hz, 0.08 secs per frame) whilst a 10AP stimulus was delivered at increasing voltages (5-25V). Igor Pro (version.6.37, Wavemetrics) was used for image analysis and ROIs identified using the SARFIA plugin. Stimulation at 5V produced no detectable changes in fluorescence ($p > 0.999$ when compared with 0V; one-way ANOVA with Tukey's post-hoc comparisons). However, stimulation at 10V produced a rise in fluorescence intensity followed by a decay in signal (Fig 2.2.C) ($p<0.001$ when compared with 0V and 5V, one-way ANOVA with Tukey's post-hoc comparisons), demonstrating an obvious stimulus-response relationship at this voltage. Response amplitude reached saturation between 20-22.5 V, and further increases in voltage did not result in statistically larger response amplitudes. Therefore, the optimal voltage selected for this chamber was 22.5V.

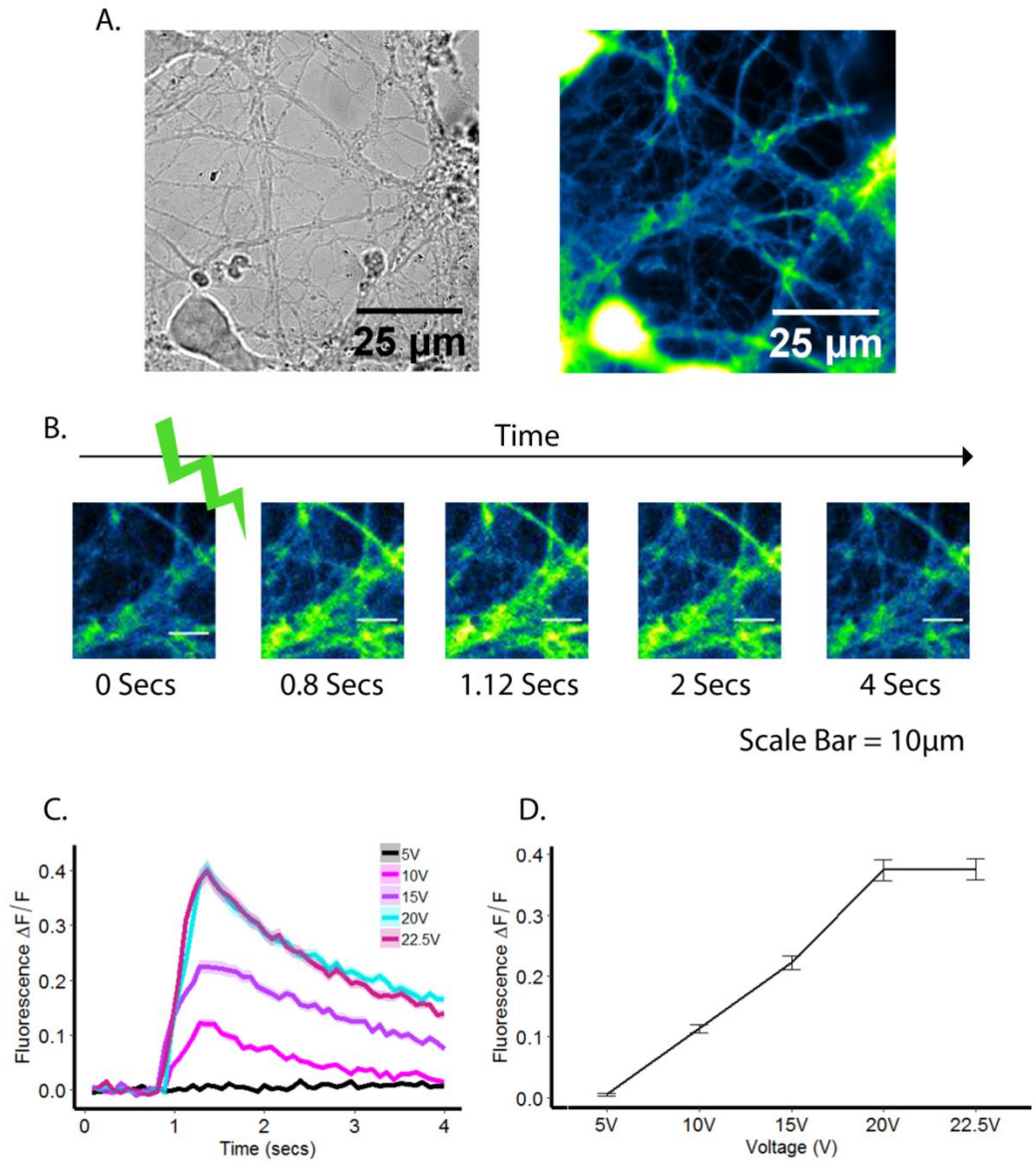

Figure 2.2.Calibration of stimulation intensity using Fluo-4AM. Representative image of primary hippocampal cultures (left) incubated with Fluo4-AM (right) (60X objective, 1x1 binning, scale bar = 25µm). B) Time-lapse images demonstrating change in Fluo4 fluorescence as it binds Ca^{2+} in a stimulation-dependent manner. C) Mean responses of 327 synapses (3 coverslips) in response to stimuli of increasing voltage. D) Quantification of Ca_{2+} influx evoked by different voltages measured as a difference between the peak fluorescence and the baseline prior to the stimulation. Significant increases were seen between 5-10V, 10-15V, 15-20V ($p<0.0001$ in all instances, one-way ANOVA with Tukey's post-hoc comparisons). Further increases in voltage did not result in any significant changes in peak amplitudes of responses.

2.2.4 Pharmacology

Table 2.3

Pharmacological compounds used in this body of work				
Compound	**Solvent**	**Storage**	**Preparation**	**Supplier**
Levetiracetam	EBS	4°C	6mM stock prepared and used within 14 days	Janssen Pharmaceutica
DCG-IV	EBS	-20°C	6mM stock prepared and frozen.	Tocris
JNJ-46281222	DMSO	-20°C	6mM stock prepared and frozen. Further diluted to 100µM stock in EBS (stored at 4°C) and used fresh on day of experiment.	Janssen Pharmaceutica
JNJ-56140864	DMSO	-20°C	6mM stock prepared and frozen. Further diluted to 150µM stock in EBS (stored at 4°C) and used fresh on day of experiment.	Janssen Pharmaceutica
Compounds X and Y	DMSO	-20°C	10mM stock prepared and frozen. Further diluted to 100µM	Syndesi Therapeutics

			in EBS (stored at 4°C) and used fresh on day of experiment	

All compounds were prepared as detailed in Table 2.3 and further diluted to the required concentrations in EBS supplemented with CNQX and APV and introduced into the experimental system via exchange of half the buffer volume in the imaging chamber; total volume 600µl.

2.2.5 Measuring synaptic vesicle pool sizes

For readouts of functional vesicle pool sizes, alkaline trapping experiments (Sankaranarayanan and Ryan, 2001) were performed using bafilomycin A1 (baf), a potent inhibitor of v-ATPase that prevents reacidification of newly formed vesicles (Fernandez-Alfonso and Ryan, 2004). Neurons, infected with AAV6_sypHy1x, were transferred to the imaging chamber and a functional region identified using a 40AP, 20Hz stimulus. Following 2 minutes recovery, neurons were again stimulated with 40AP, 20Hz to generate a readout of RRP size, after which pharmacological compounds were introduced where desired. Stimulation protocols after addition of compound and pre-addition of baf were compound specific and therefore are described separately in the appropriate results sections. 2 minutes after the prior round of stimulation, the total volume of EBS in the imaging chamber (600µl) was replaced with EBS containing 1µM bafilomycin (Sigma Aldrich) and the neurons allowed to incubate for 30 seconds before a 600AP, 20Hz stimulation was applied to release the recycling pool, which became locked in the alkaline state due to the presence of baf (Fernandez-Alfonso and Ryan, 2004, Rey et al., 2015). The total vesicle pool population was visualized by replacement of the EBS-baf with NH_4Cl solution, composition (mM) 50 NH_4Cl, 86 NaCl, 2.5 KCl, 10 HEPES, 1.3 $MgCl_2$, 10 D-Glucose, 2 $CaCl_3$.

2.2.6 Image analysis of fluorescent z-stacks

Image stacks were imported into Igor Pro (version 6.37, Wavemetrics) via the SARFIA plugin (Dorostkar et al., 2010) and stored as single-precision floating-point arrays (which are termed “waves” in Igor Pro). Recordings taken from the same region were imported in sequential order and corrected for x-y drift using the built in image registration function, based on an algorithm

described by Thévenaz et.al. (Thevenaz et al., 1998). A schematic of image processing is shown in Fig 2.3.A.

2.2.6.1. ROI detection for sypHy, syGCaMP6f, vGLUT1-pHluorin and VGAT-pHluorin

Following correction for motion artefacts, images were transformed using the Laplace operator, which is commonly used for edge sharpening in images (Burger and Burge, 2008) and improves detection of units of lower contrast. Segmentation was carried out using a threshold calculated as a multiple of the standard deviation (SD) of all pixel values in the Laplace operator (Fig 2.3.C). A threshold value of (-3) x SD was shown to be optimal for our experiments. The ROIs were numbered and stored in a matrix, referred to as the 'ROI mask', which had the same *x* and *y* dimensions as the original image stack. A small section of the image background was selected and averaged, and this number was subtracted from the average intensity to correct for differing levels of background fluorescence. The average intensity over each ROI at each time point was measured and stored in a 2D matrix, indexed by the ROI number. To allow comparisons between ROIs of different baseline intensities, ΔF/F values were calculated using the 10 frames prior to stimulation as baseline. Using a customized script, ROIs were examined to see if they had exceeded a threshold change in fluorescence post-stimulation. The threshold used to determine robust responses was dependent on the signal:noise ratio and the stimulus strength, therefore these experiment-specific details are reported in the respective results sections. ROIs that failed to reach threshold were scrubbed from the ROI mask. For sequential images, ROI recognition was based upon the first z-stack and the mask computed from this was used to analyse all other images in the sequence. Finally, poor traces were removed from the dataset. To avoid bias, a strict set of exclusion criteria were adhered to (Figure 2.3.D) that included removal of synapses that failed to respond to the second control stimulus (2.3.Di), synapses with 'double' responses and unusual baseline artefacts (2.3.D.ii and iv), traces that reached saturation (2.3.D.iii) and ROIs that shifted from the field of view (2.3.D.v),

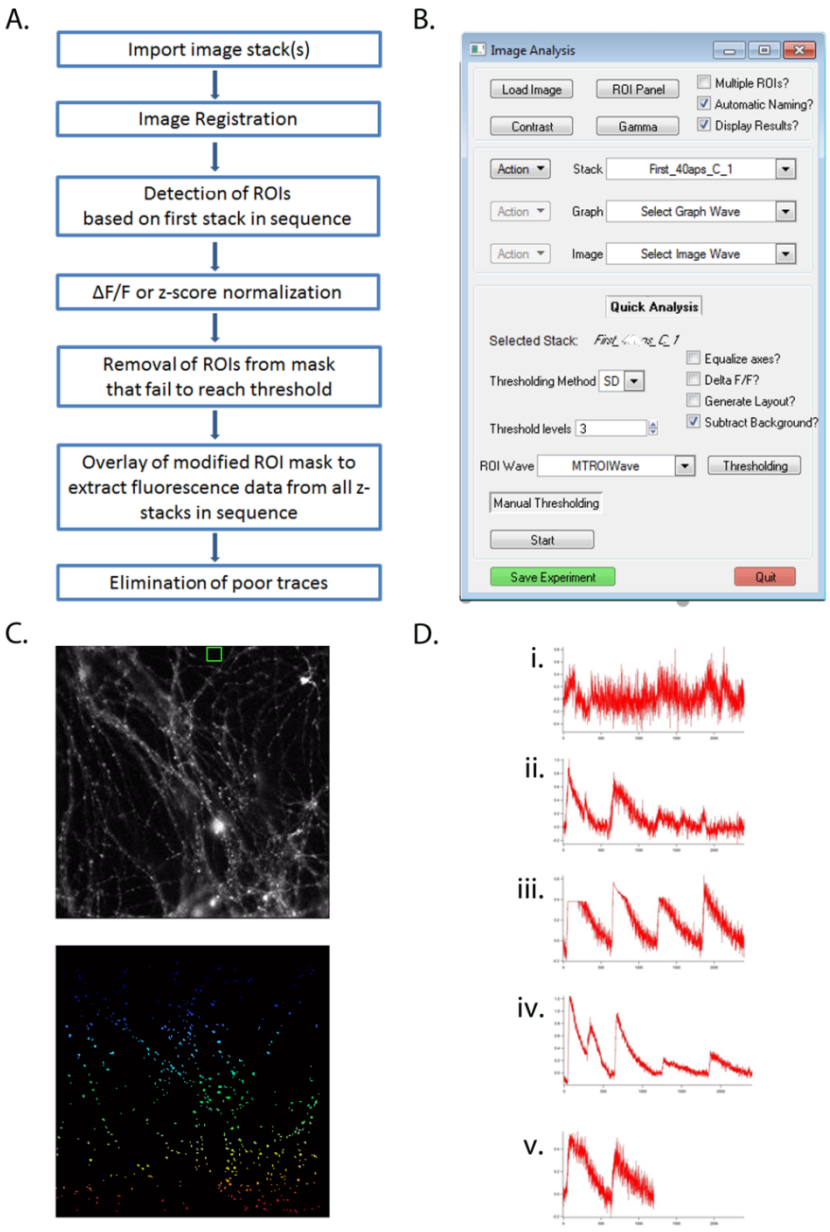

Figure 2.3. Processing of image stacks. A. Workflow showing stages of analysis of optical recordings. B) Example of SARFIA graphical user interface (GUI) with correct parameters selected C) Primary hippocampal neurons expressing AAV6_sypHy1x (top) and Laplace transformation with ROI detection (bottom) D) Examples of traces meeting the exclusion criteria for elimination i) failure to respond to the second control stimulus, ii) Artefact in baseline and 'double-response' – bouton responds a second time during endocytosis iii) Responses reach saturation iv) Large 'double-response' – bouton responds a second time during endocytosis v) ROI drifted from field of view.

2.2.6.2. ROI detection for iGluSnFR

As iGluSnFR is a membrane bound construct, as opposed to sypHy or sy-GCaMP6f where expression is localized to presynaptic terminals, detection of ROIs based upon pixel standard deviation was unsuitable. Therefore, we used a customized correlation algorithm in Igor Pro (version 6.37, Wavemetrics), written by Professor Tom Baden (Franke et al., 2017). Firstly, the image was smoothed and the traces of all pixels in the field of view (FOV) were linearly correlated to the traces of every other pixel in the FOV. Neighbouring pixels with correlation coefficients (*ρ)* exceeding threshold correlation, $\rho_{Threshold}$ were then grouped into single ROIs. ROIs were grown until $\rho < \rho_{Threshold}$ in all neighbouring pixels, or the area of the ROI exceeded a specified number of pixels. Following ROI detection, image processing was identical to that described in 2.2.6.1.

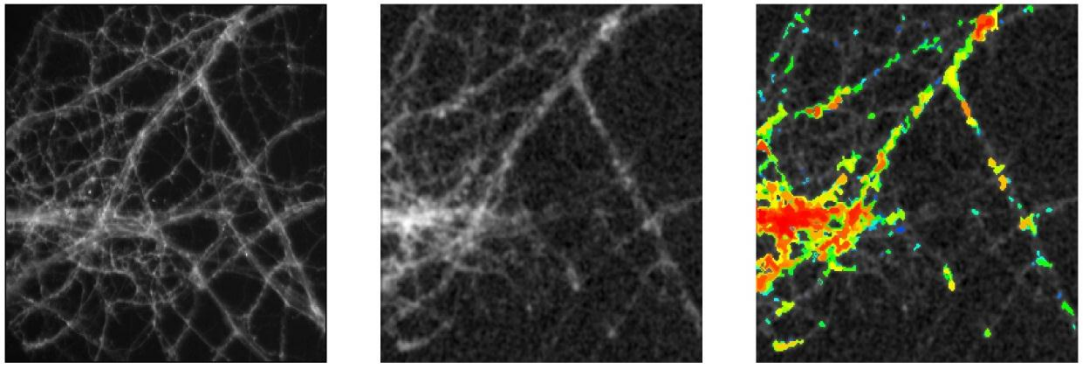

Figure 2.4. Identification of ROIs in neurons expressing iGluSnFR. Average projected image stack of primary hippocampal neurons expressing AAV9_iGluSnFR (left), smoothed (centre) and ROIs detected based on smoothed correlation map (right).

2.3 Protein Detection Techniques

Table 2.4

Antibodies used in this work			
Antibody	**Dilution**	**Target**	**Supplier**
Anti-mGluR2	ICC 1:100	mGluR2	Alomone Labs
Anti-SV2A	IP 1µg/ml	SV2A	Santa Cruz Biotech
Anti-SV2A	WB 1:500	SV2A	AbCam
Anti-synaptotagmin1	WB: 1:1000	Synaptotagmin - 1	Alomone Labs
mTau5	WB 1:1000	Murine Tau	Janssen Pharmaceutica
TAU-5	ICC 1:200	Murine Tau	Invitrogen
AT-8	WB 1:1000 ICC: 1:500	Phospho-tau Ser202-Thr205	Janssen Pharmaceutica/ Invitrogen
HT-7	WB 1:2000	Human Tau	Janssen Pharmaceutica
BA3R	WB: 1:10,000	ß-actin	Invitrogen
Anti-Mouse-HRP Conjugated	WB: 1:10,000	Mouse IgG	G.E. Healthcare/ Invitrogen
Anti-rabbit HRP conjugated	WB: 1:10,000	Rabbit IgG	Invitrogen
Anti-mouse AlexaFLuor-488 conjugated	ICC: 1:500	Mouse IgG	Invitrogen
Anti-rabbit AlexaFluor-555 conjugated	ICC 1:500	Rabbit IgG	Invitrogen

WB- Western Blot, IP- Immunoprecipitation, ICC- Immunocytochemistry

2.3.1. Western Blotting

10 µg of protein sample was loaded on NuPage Novex Bis-Tris 4-12% gels (Life Technologies) and run in 1X running buffer at 180V (diluted from 20X NuPage® MOPS SDS, ThermoFisher). Gels were transferred to 0.45µm nitrocellulose membranes using the trans-blot turbo transfer system (Bio-Rad). Membranes were blocked in 5% milk for 1 hour at room temperature and probed with primary antibody in 5% milk overnight at 4°C. The following day, membranes were washed x3 with 1X TBS-T, 10 minutes per wash. For detection, membranes were counter-probed with HRP-linked secondary antibody in 1X TBS-T for 1 hour, washed again x3 in 1x TBS-T and imaged by exposure to SuperSignal™ West Dura solution (Pierce) using a digital Syngene imager (Syngene). Membranes were stripped by 15-25 minutes incubation in Restore™ Western Blot Stripping Buffer (ThermoFisher) and re-probed for ß-actin to allow relative protein quantification. Quantification was carried out using ImageJ.

2.3.2 Co-Immunoprecipitation

For co-immunoprecipitation, cells were lysed using NP40 lysis buffer (ThermoFisher) supplemented with phosphatase and protease inhibitors (1:100 dilution). Lysates were collected in Eppendorf tubes and centrifuged at max speed, 4°C for 15 minutes. Care was taken to keep lysates on ice between steps to prevent protein degradation. DynaBeads™ Protein G (Thermo Fisher) were incubated in SV2A antibody (1µg/ml) (mouse monoclonal) for 10 minutes at room temperature with rotation. Using a magnet, the beads were separated and the supernatant removed. Beads-Ab complex was washed x3 with 0.025% PBS-Tween and incubated with 100µg protein sample for 1-2 hours at 4°C with rotation. Beads were separated from the lysate using the magnet and the supernatant retained to verify successful antibody binding. Following this, beads were again washed three times with 0.025% PBS/Tween. For elution, beads were boiled at 70°C for 10 minutes in 20µl of 50mM glycine (in H2O) and 10µl 4x Laemelli Buffer containing 1:10 BME. For the final separation, samples were placed on to the magnet and the supernatant harvested. 5µg of protein was loaded onto NuPage Novex Bis-Tris 4-12% gels and Western blots carried out as described above using an alternative SV2A antibody (rabbit polyclonal) - raised in a different species to avoid detection of IgG bands (1:500), and anti-synaptotagmin-1 (1:1000) (also rabbit polyclonal). Signal detection was carried out with anti-rabbit HRP conjugated secondary antibody (1: 10,000).

2.3.3 Immunofluorescent labelling and confocal microscopy

Primary hippocampal neurons (DIV 14) were fixed with 2% paraformaldehyde (PFA) for 15 minutes, washed using washing buffer (25% Superblock in PBS (ThermoFisher)) and permeabilized with 0.3% Triton-X 100 for 10 minutes. Unreacted aldehydes were then blocked using 50µM glycine (in PBS) and cells blocked with undiluted Superblock for 30 minutes. Primary antibodies were diluted to the appropriate concentrations (see Table 2.3) and incubated with the cells for 1 hour at room temperature. Following this, cells were washed x3 using wash buffer (5 minutes per wash). Cells were incubated for 1 hour with AlexaFluor-555 conjugated goat anti-rabbit and AlexaFluor-488 conjugated goat anti-mouse secondary antibodies (1:500 dilution in wash buffer) and washed again x3 with wash buffer. Coverslips were mounted in ProLong Gold containing DAPI stain (Life Technologies) and cured for 24 hours before imaging. Cells were imaged using a 20x0.75 DRY objective on a Leica SP8 confocal microscope. Excitation laser lines at 405nm (DAPI), 488nm (AlexaFluor-488) and 561nm (AlexaFluor-555) generated emissions at 410-480nm, collected using a PMT detector; 500-560mn, collected using a HyD detector, and 555-650nm, also collected using a HyD detector.

2.3.4. mRNA extraction and cDNA synthesis

Total RNA was extracted using TRIzol Plus RNA Purification Kit (12183555, Lifetechnologies, UK). Primary hippocampal cultures were lysed with 250µl/well TRIzol reagent for 5 min at room temperature to allow complete dissociation of nucleoprotein complexes. Lysates were transferred to separate 1.5 ml Eppendorf tubes, mixed with 50 µl chloroform, agitated by hand vigorously for 15 sec, and incubated for 2-3 min at room temperature. Samples were centrifuged at 12,000 x g for 15 min, 4^{o}C for separation into a lower red phenol-chloroform phase and an upper colourless phase, containing the RNA. Approximately 400 µL of the top aqueous phase from each sample was transferred to new RNase-free tubes and vortexed with an equal volume of 70% ethanol (~5 seconds) This mixture was transferred to separate spin cartridges (with collection tubes), centrifuged at 12,000 × g for 15 seconds at room temperature and the flow through discarded. The cartridges were washed with Wash Buffer I, centrifuged at 12,000 × g, for 15 seconds at room temperature and washed twice with Wash Buffer II, spinning each time for 15 seconds at 12,000 × g, room temperature. The cartridges containing the RNA were dried by an additional spin at 12,000 × g for 1 min at room temperature. Using recovery tubes, the RNA from

the different cartridges was eluted after 5 minutes incubation in 30 µl RNase-free water and centrifuged for 2 min at 16,000 x g. The RNA extracts were stored on ice and used for cDNA synthesis using the High Capacity cDNA Reverse Transcription Kit (Lifetechnologies, UK). In PCR tubes on ice, a 20 µl cDNA reaction was prepared for each sample containing 10 µl total RNA and 10 µl 2x Reverse Transcription master mix supplemented with RiboLock RNase inhibitor at a concentration of 1 U/µl (Lifetechnologies). All tubes were spun briefly to eliminate bubbles and loaded into the thermal cycler (Biometra), programmed to run at 25°C for 10 minutes, 37°C for 120 minutes and 85°C for 5 minutes. The cDNA collected was used for RT-PCR.

For a single 25µl RT-PCR reaction, 0.5µl cDNA was combined with 200µM dNTPs, 0.4µM sense/antisense primers, 1X GC buffer and 2000 U/ml Phusion High-Fidelity DNA polymerase (NEB). cDNA was added last and the final volume topped to 25µl with ddH_2O. Samples were loaded into the thermal cycler (Biometra), cycle conditions: 95º, 3mins; 28 x (95ºC, 30 secs: 66ºC, 30secs: 72ºC, 20 Secs), 72ºC, 1 minute for final extrusion. Primers for RT-PCR were designed using Ensembl sequences of mGluR2 and GAPDH, from which potential intron sequences were selected. http://tmcalculator.neb.com was used to verify that primers had similar annealing temperatures. G-C content was assessed using http://biotools.nubic.northwestern.edu/OligoCalc.html to avoid excessive secondary structure.

2.4 Biophysical methods for characterization of amyloid proteins

2.4.1 TEM

Samples from aliquots of 10µM Tau(P301L)^{K18}, prepared as described in section 2.1.6, were taken pre- and post-sonication to verify the morphology of K18^{P301L} fibres when added to the primary cultures. 4µl of peptide was applied to the surface of Formvar/Carbon film coated 400 mesh copper grids (Agar Scientific) and allowed to absorb for 2 minutes before blotting dry. The grid was washed once with 4µl of milliQ-filtered water and again blotted dry. The grid was negatively stained using 2% (w/v) uranyl acetate, incubated for 2 minutes, blotted and dried. This step was repeated once more, and the grid was left to air dry before imaging. Grids were examined and imaged using a JEOL JEM1400-Plus TEM at 120 kV and images were acquired using a Gatan OneView 4K camera (Abingdon, UK). ImageJ software was used for image processing.

2.4.2. Circular Dichroism

40µM peptide samples (prepared in 100mM sodium acetate buffer, pH 7.0) were placed in a 1mm path length quartz cuvette (Hellma). Scans were taken between 180-280nm on a JASCO J715 Spectropolarimeter at 20°C. Three spectra were averaged for each measurement. Spectral data were converted to molar ellipticity using the following equation: Mdeg x Molecular Weight / (10 x $mg \cdot ml^{-1}$ x pathlength of cuvette x number of amino acids).

2.4.3. X-ray fibre diffraction

X-Ray fibre diffraction (XRFD) patterns of partially aligned fibres formed by $K18^{P301L}$ in 100mM sodium acetate buffer were obtained with the help of Youssra Al-Halily (University of Sussex). 40µM $K18^{P301L}$ fibrils in 100mM sodium acetate buffer were centrifuged for 10 minutes at 12,000 x g. A 10µl droplet of peptide was suspended between two wax-tipped 1.2mm O.D, 0.94mm I.D borosilicate capillaries (Harvard apparatus). These were incubated for 24 hours at room temperature in a parafilm sealed petri dish. X-ray diffraction patters were obtained using a Rigaku 007HFcuKa (λ 1.5419 Å) rotating anode generator with a Saturn 944+ CCD detector. Exposure times of 10–120 seconds were used with specimen to detect distances of 50 or 100 mm. The images were displayed and examined using Mosflm.

Chapter 3: Establishing optical methods for the study of pharmacology and pathology at presynaptic terminals

3.1 Introduction

The small size, diversity and relative inaccessibility of presynaptic terminals has made a full understanding of their function, structure and regulation challenging to realize (Schweizer et al., 2012). In recent years, however, with the development and advancement of sophisticated optical reporters and sensitive, high – resolution imaging systems, powerful new strategies for interrogating presynaptic events have emerged. The key aim of this work was to exploit these optical approaches to characterize, for the first time, the actions of novel pharmacological agents and pathological tau at presynaptic terminals of hippocampal synapses. An important initial objective of this research program was to establish a robust system for conducting these assays. After some consideration, we chose to use primary dissociated hippocampal cultures for this work. Although there are some key disadvantages of this system, in particular the removal of native connectivity, cell culture is an extremely powerful approach for controlling, manipulating and monitoring cellular functions and processes. In this way, primary culture systems are a valuable compliment to *ex vivo* and *in vivo* systems for understanding how specific cellular events are regulated by external modulators. As such, primary hippocampal cultures offer a relatively easy strategy for inducing the expression of optical reporters through viral delivery or plasmid DNA transfection, as well as manipulating the expression of tau protein to generate models of tau knockdown or pathogenic overexpression. The principle aim of this chapter was to optimize the culturing of primary neurons and to validate optical tool readouts that could be applied to address our key research questions.

3.2 Culture of Primary Hippocampal Neurons

The first essential requirement of this work was to establish a robust and reproducible method of harvesting and maintaining healthy primary hippocampal cultures. This preparation is widely employed in the field due to the lack of complexity compared with tissue slices, that retain native architecture, or *in vivo* systems, allows for acute manipulation and observation of processes (Kaech and Banker, 2006). Indeed, the ability to readily control expression of DNA and hence protein expression in primary hippocampal cultures is exploited in Chapter 6, where the effects of artificially altering expression of tau protein at the synapse is examined. Additionally, the last decade has seen advancements in the design of genetically encoded fluorescent reporters that enable accurate optical readouts of voltage change, fluctuations in pre- and postsynaptic calcium, synaptic vesicle exo- and endocytosis, and neurotransmitter release and retrieval (Dreosti and Lagnado, 2011). In combining these elements, a well-conserved, accessible model system is generated, in which various elements of synaptic function can be optically encoded, studied and recorded.

The specific methodology used to prepare dissociated hippocampal cultures has been outlined in detail in Chapter 2 (Methods). For our work, we used a modified protocol developed from the seminal neuronal cell culture preparations outlined by Banker and Cowan (Banker and Cowan, 1977). In brief, hippocampi are dissected from the brains of P0/P1 rat pups, triturated to form a cell suspension and plated onto coverslips coated with both PDL and laminin, on which the neurons were cultivated for at least 14 days prior to imaging. Neurons were initially suspended and plated in Minimum Essential Medium (MEM) supplemented with 10% FCS, 3% glucose and 1% penicillin-streptomycin. 3-4 hours later, this was exchanged with Neurobasal medium, supplemented with 2% B27, 1% glutamax and 1% penicillin-streptomycin, and without either serum or phenol red, in which cultures were maintained until experimentation at DIV 14-21. On DIV 4/5, dependent upon the growth of satisfactory astrocytic islands, cultures were treated with 3.25μM of the antimitotic agent cytosine arabinoside (ara-C) to restrict astrocyte proliferation. Adherence to this protocol led to the development of strong, healthy, duplicable primary cultures, as evidenced in Figure 3.1. Although astrocyte proliferation was halted, we did so cautiously so as to generate a co-culture of neurons and astrocytes, which produces cultures with high viability and is deemed more physiologically relevant (Anderl et al., 2009).

Following synaptogenesis and maturation, which occurs in full approximately 2 weeks after plating, neurons were transferred to a custom-built imaging chamber (Fig 3.1), in which field stimulation could be applied via two parallel platinum wires positioned approximately 1.0mm apart. All experiments, unless otherwise stated, were conducted in extracellular buffering solution (EBS) at pH 7.35, with the AMPA and NMDA receptor antagonists CNQX and AP-V present in order to prevent network feedback and limit occurrence of spontaneous action potentials; these were added at concentrations of 20μM and 50μM respectively. The ionic composition of EBS was devised in such a way as to mimic the regular extracellular environment.

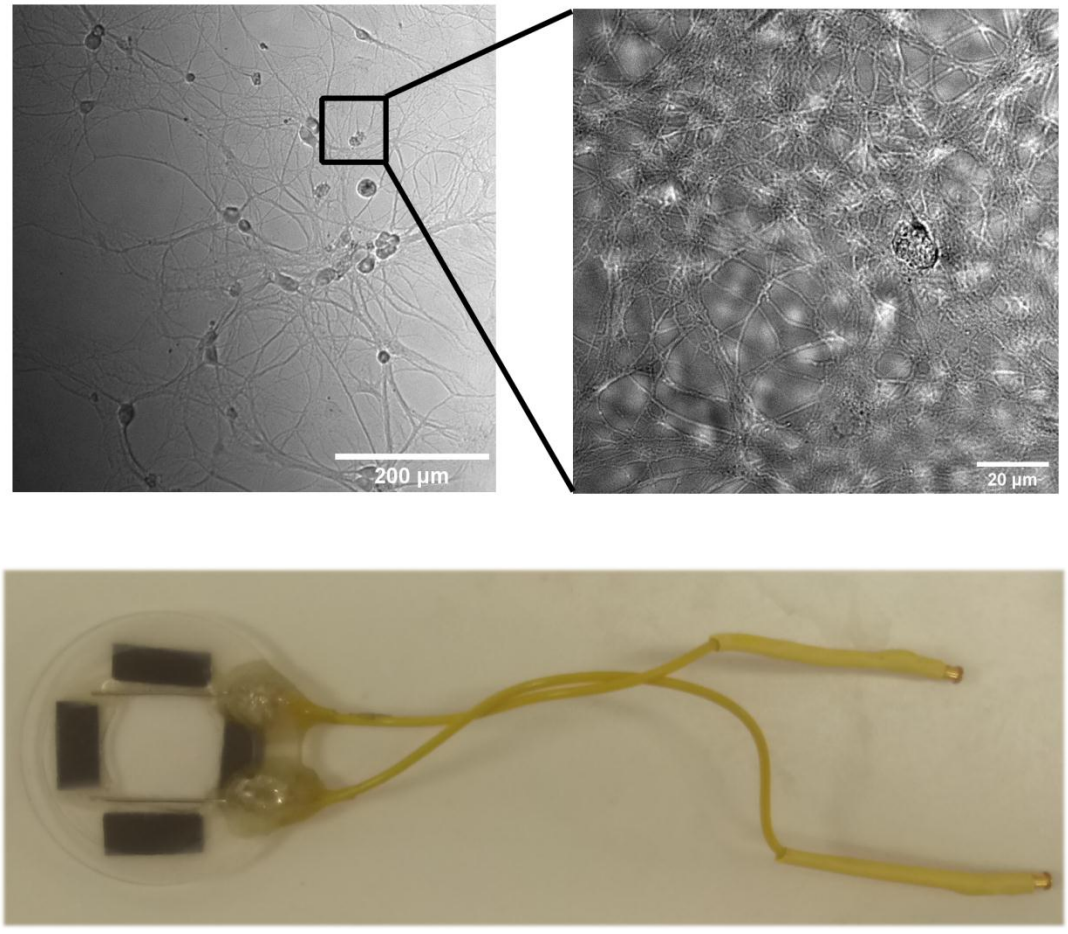

Fig 3.1. Successful culture of primary hippocampal neurons. Primary hippocampal neurons from rats (top) were grown on glass coverslips which were transferred to a customized chamber (bottom) for electrical stimulation and imaging.

3.3 Identification of functional presynaptic terminals using FM1-43

The successful labelling of presynaptic terminals with the styryl dye, FM1-43, can be used to verify the presence of functional synapses. Therefore, through using this technique, we wanted to confirm that presynaptic terminals in our hippocampal culture preparation were functional. Activity-dependent uptake of styryl dyes has been used to visualise functional synapses since their development in the early 1990s (Betz and Bewick, 1992). All styryl dyes have the same basic structure: a lipophilic tail linked to a positively charged head via one or more double bond bridges. A number of different dyes are available, which vary in tail length and the number of double bonds, although the most widely used is FM1-43 (Betz et al., 1996). Through the application of FM1-43, which utilises the endocytic phase of the synaptic vesicle cycle to fluorescently label vesicles in the presynaptic terminal, optical readouts of exo- and endocytosis can be obtained, and active synapses identified (Cochilla et al., 1999).

To label with FM1-43, neurons were incubated with EBS supplemented with 20µM AP-V and 50µM CNQX, and containing 10µM FM1-43 for 60s and stimulated with 1200APs at 20Hz to mobilize, and hence fluorescently label, all vesicles in the recycling pool (Ratnayaka et al., 2012). Following a second 60 second period of incubation to ensure completion of endocytosis, any excess dye remaining at the membrane surface was washed off using fresh EBS. Synapses effectually loaded with FM1-43, and hence active, could be recognized easily by the presence of distinct puncta along neuronal processes, as demonstrated in Figure 3.2. The successful labelling of presynaptic terminals with FM1-43 verified the presence of functional presynaptic terminals in our primary hippocampal cultures.

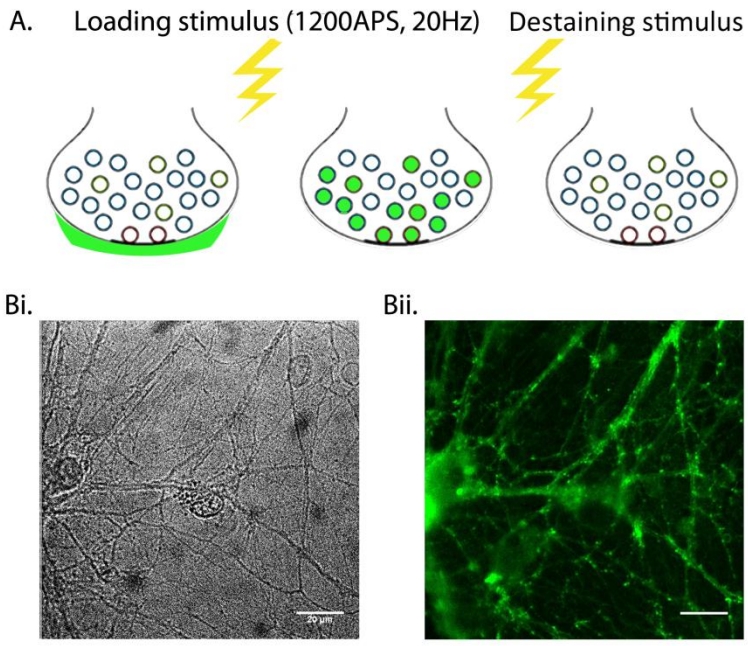

Fig 3.2. Visualization of hippocampal synapses loaded with FM1-43. A) Schematic representation of FM1-43 loading. Due to its lipophilic nature, FM1-43 binds to the outer leaflet of the presynaptic membrane. Stimulus-driven exocytosis of synaptic vesicles leads to the uptake of FM1-43. Under brightfield, neuronal cultures appeared mature and healthy (Bi), which was verified by their ability to take-up FM1-43 in an activity-dependent manner (Bii).

3.4. Genetically encoded optical reporters of synaptic function

Although fluorescent dyes have proven to be revolutionary tools in the study of neuroscience, their use in live cell imaging of synaptic processes comes with several limitations. Firstly, the majority of dyes suitable for monitoring synaptic functions are non-specific; coating all membrane surfaces that they come into contact with, so that determining a high fidelity signal from the region of interest can, at times, prove difficult. Secondly, as they are expelled from the membrane upon stimulation, their use is typically confined to a single readout or 'destaining', making recordings over sustained periods of time impossible. Third, targeted labelling of vesicle pools with these dyes often relies on prior neuronal stimulation meaning that there is an activity-history influence contributing to the results obtained. Therefore, for the main objectives of this work,

which required repeated sampling of the same cultures upon exposure to varying pharmacological conditions and concentrations, fluorescent dyes such as FM1-43 were unsuitable candidates.

The evolution of genetic constructs over the last decade has led to the development of new tools that can provide localized optical readouts of pH, calcium influx, changes in voltage, and neurotransmitter release (Dreosti and Lagnado, 2011). Through the selection of appropriate promoters, the use of genetically encoded optical reporters can provide a signal that is both targeted and sustained over multiple trials, and therefore this approach was deemed the most suitable for the majority of the imaging experiments undertaken in this work. This subchapter aims to provide thorough validation of each of the genetically encoded optical reporters used in this body of work.

3.4.1 Recording synaptic vesicle exo- and endocytosis with pHluorin-based probes

The challenges of real-time recording of synaptic vesicle exo- and endocytosis over multiple trials have, to some extent, been solved by the generation of a family of optical reporters termed the 'pHluorin-based probes'. These genetic constructs consist of a super-ecliptic pHluorin targeted to the interior of synaptic vesicles via conjugation to various proteins such as synaptobrevin (synaptopHluorin) (Miesenbock et al., 1998), synaptophysin (sypHy) (Granseth et al., 2006), synaptotagmin (Diril et al., 2006), vGLUT1 (Voglmaier et al., 2006) or VGAT (Santos et al., 2013). The term super-ecliptic pHluorin denotes a wildtype green fluorescent protein (GFP) that has been genetically altered so as to become pH-sensitive. This is achieved via amino acid substitutions that couple fluctuations in pH of the external environment with changes in the electrostatic environment of the chromophore (Miesenbock et al., 1998). The relevance of fusing a pH sensitive GFP with a vesicular protein is that the internal environment of a synaptic vesicle undergoes a shift in pH during the synaptic vesicle cycle; when the vesicle is internalized within the presynaptic terminal the pH is ~5.5 and the fluorescence of the super-ecliptic pHluorin is quenched, however upon fusion with the presynaptic membrane the lumen of the vesicle is exposed to the synaptic cleft and the pH rises to ~7, generating a fluorescent signal. The rise and decay of this signal can be interpreted as readouts of exo-and endocytosis respectively.

3.4.1.1 sypHy1x

A key objective of this work was assay synaptic vesicle release and retrieval using sypHy1x, which consists of a super-ecliptic pHluorin conjugated to the second intravesicular loop of the synaptic vesicle protein synaptophysin (Granseth et al., 2006). As a starting point for this, we first set out to establish that we could successfully express sypHy1x in our culture preparation and validate its use as a functional readout of vesicle recycling. To do this, we introduced sypHy1x into neurons by infecting with AAV6-sypHy1x, a viral form of sypHy1x generated via cloning of pAAV-sypHy1x into an AAV6 vector; carried out externally by the University of Helsinki. Neurons were infected at DIV 6-8 at a Multiplicity of Infection (MOI) of 200; these were subsequently imaged at 14-21 DIV once expression had been established. Calculation of MOI is explained in detail in section 2.1.5.

Figure 3.4 shows the successful expression of AAV6-sypHy1x in healthy primary hippocampal cultures; neurons, imaged with 480/20 nm excitation and collected on an EMCCD with 520/35 nm emission, appeared as dim punctate signals presumably corresponding to individual presynaptic terminals. Under basal conditions, this fluorescence was highly stable over time, seen in time-lapse imaging sequences. However, as expected, a field stimulation protocol corresponding to turnover of the RRP (40APS at 20Hz, (Rey et al., 2015, Li et al., 2005)) led to fast and robust rises in emission specifically at punctate sites along axons. To provide evidence to support the idea that these signals corresponded to exo- and endocytosis, we measured their kinetics by analyzing the time-lapse sequences. Timing of the rising and falling phase were 2.7 secs and 18.9 secs, which are in accordance with previous reports using the same probe (Granseth et al., 2006). Thus, we demonstrate that our cultures and expression system provides an appropriate method for readout of vesicle recycling events occurring at the level of individual synaptic terminals. ROIs were identified using correlates of standard deviation between adjoining pixels, computed via the Semi-automated routines for Fluorescent Image analysis (SARFIA) package in Igor Pro.

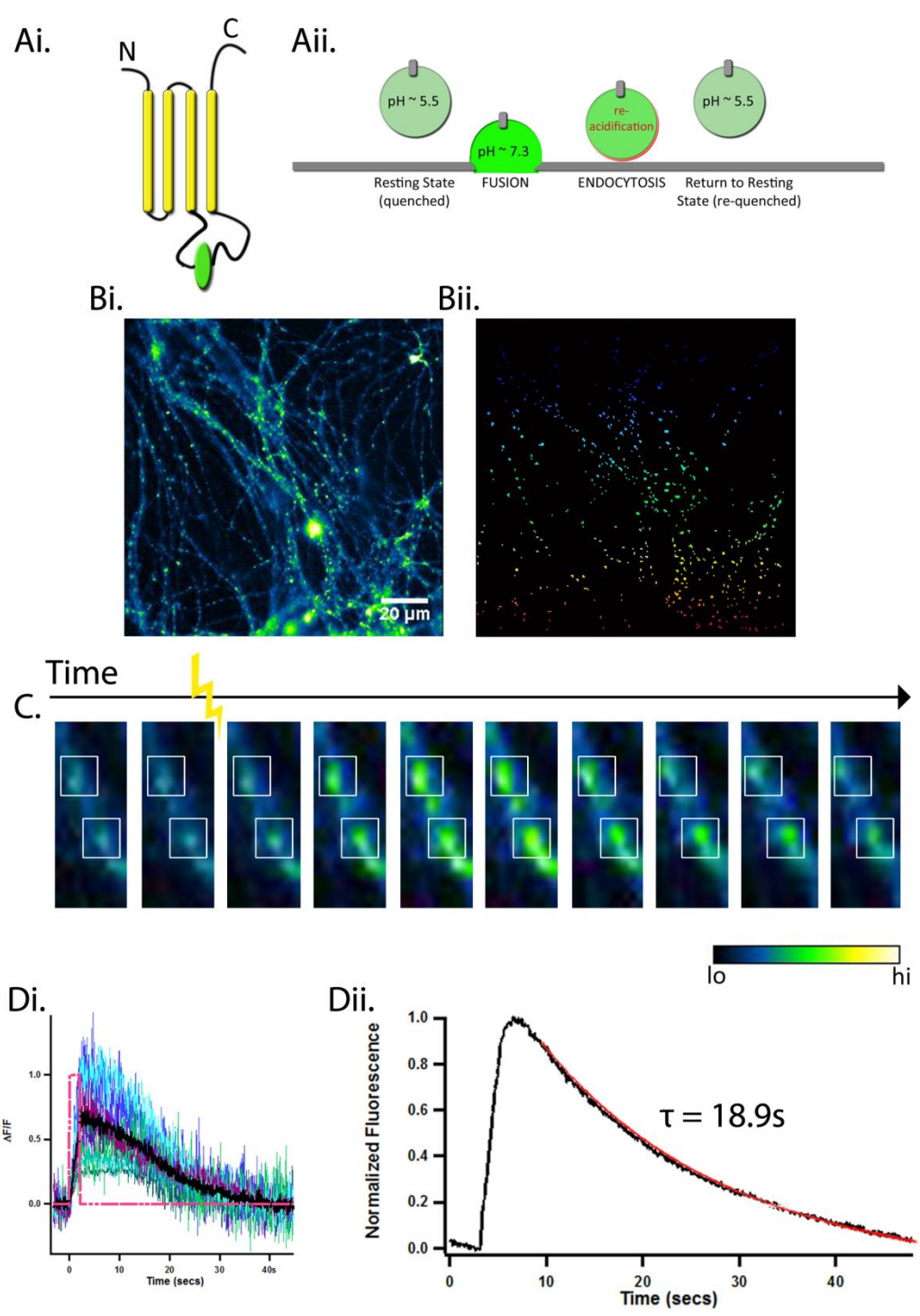

Fig. 3.4. Detection and measurement of synaptic vesicle dynamics using sypHy1x. (A) Schematic representations of sypHy1x (Ai) and its mechanism of action (ii). (B). Neurons expressing sypHy1x (i) and detection of ROIs based on a threshold calculated as a multiple of standard deviation (see Methods) (C). Timelapse showing increase and decay of fluorescent signal at

individual boutons following a 40AP, 20Hz stimulus. Di. Example traces from individual synapses following a 40AP, 20Hz stimulation, average shown in black, stimulation shown via dashed line (pink). Average peak 0.428 ± 0.118 ΔF/F. Dii. Average response from 122 synapses reveals endocytic time constant, τ = 18.9 ± 0.323 secs (3 coverslips). Single exponential fit shown in red.

3.4.1.2 VGLUT1-pHluorin

A further aim of this work was to assess the impact of compounds upon the excitatory population of neurons alone. VGLUT1-pHluorin also contains a super-ecliptic pHluorin, however in this instance it is conjugated to the first lumenal loop of vesicular glutamate transporter type 1 (VGLUT1). Vesicular glutamate transporters play an essential role in the synaptic uptake and storage of the amino acid, L-glutamate (Bellocchio et al., 1998, Takamori et al., 2000). Three known VGLUT isoforms exist in mammalian systems (Bellocchio et al., 1998, Aihara et al., 2000, Bellocchio et al., 2000, Takamori et al., 2000, Takamori et al., 2001, Takamori et al., 2002, Schafer et al., 2002, Varoqui et al., 2002), of which VGLUT1 is the form predominantly expressed in mature hippocampal neurons of the rat (Fremeau et al., 2004). Whereas the vesicular protein synaptophysin is ubiquitously expressed in the synapses of the CNS, VGLUTs are phenotypic of glutamatergic terminals, and thus can be used as markers of excitatory neurons (Takamori et al., 2000). Via the fusion of VGLUT1 to a super-ecliptic pHluorin, an optical reporter is generated that is able to isolate vesicle recycling at glutamatergic synapses, and thus can be used to evaluate the differential effects of compounds upon the excitatory neuronal sub-population.

VGLUT1-pHluorin was expressed in neurons using transfection with calcium phosphate at DIV6-8. Cultures were imaged at DIV 14-21 (Fig 3.5). The time lapse in Figure 3.5.B shows the response of individual boutons; as with sypHy, actively responding boutons can easily be discerned via the rise in fluorescence post stimulation (40APS, 20Hz), which is followed by a slow decline marking the reacidification of vesicles during endocytosis. In comparison with sypHy, VGLUT1-pH shows reduced surface expression (First panel in timelapse Fig 3.4.C cf. first panel in timelapse Fig 3.5.B); whilst advantageous in conferring signal fidelity, this proved challenging in the detection of functional VGLUT1-pH expressing terminals, which could often only be seen upon stimulation. It also proved difficult to maintain focus during sequential imaging over multiple trials as bleaching eradicated any residual surface fluorescence, making it increasingly harder to identify the correct focal plane when repeatedly imaging the same region. Finally, as VGLUT1-pH expression was

induced using calcium phosphate transfection of plasmid DNA as opposed to AAV infection, the expression efficiency was far lower than observed with sypHy. Therefore, despite the obvious advantages in using neuroexcitatory – specific optical reporters, the probe of choice for the majority of the imaging in this study remained AAV6_sypHy1x.

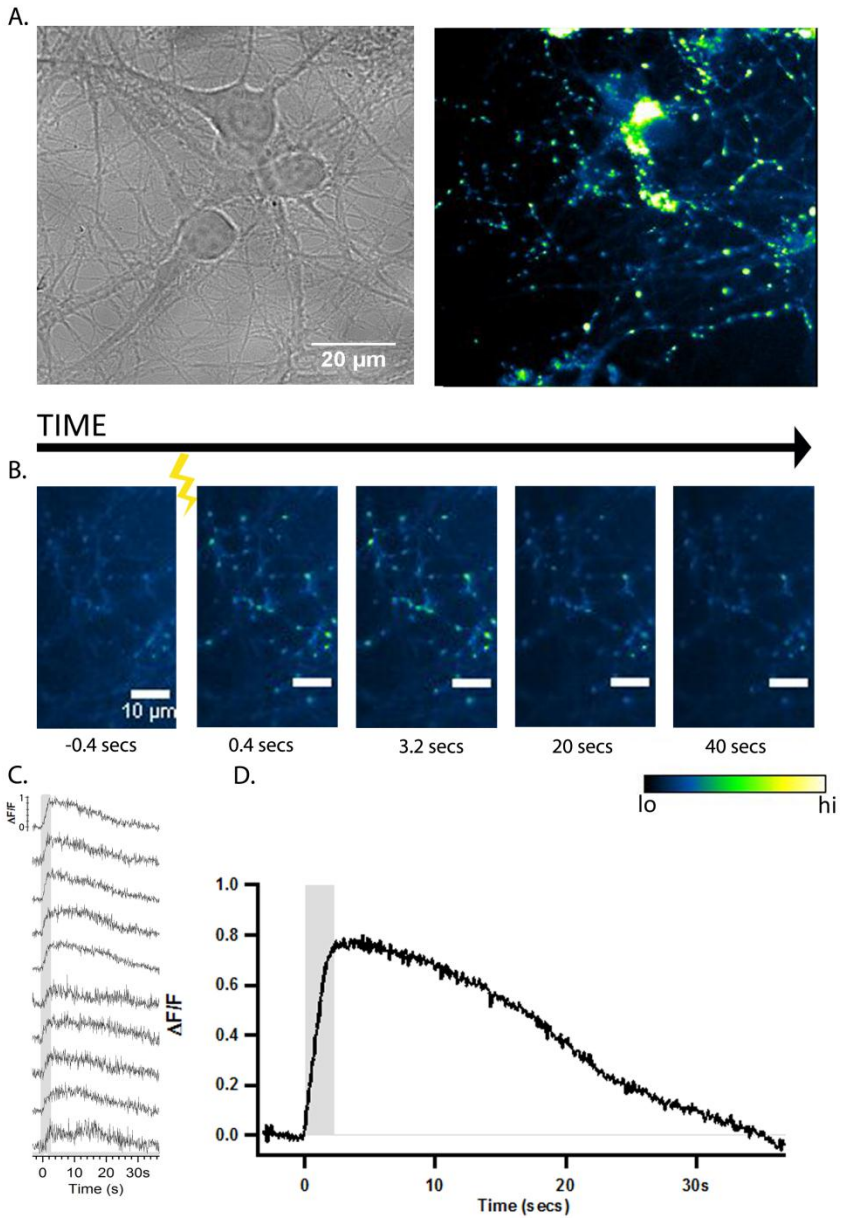

Fig 3.5. Detection and measurement of synaptic vesicle dynamics using VGLUT1-pHluorin. (A) Successful expression of VGLUT1-pH in healthy hippocampal synapses. B) Timelapse imaging shows response of individual boutons following stimulation. Panel 1 shows the limited surface

expression of VGLUT1-pH. (C). Example traces from 10 individual boutons (D). Fluorescent profile reflecting response of 164 synapses to 40AP, 20 Hz stimulus. Average peak 0.770 ± 0.031 ΔF/F.

3.4.1.3. VGAT-pHluorin

In some instances, it was desirable to isolate and record signals from inhibitory synapses to build a clearer picture of whether differences could be observed between modulation of the excitatory and inhibitory population. Just as excitatory neurons have vesicular transporters specifically evolved for glutamatergic transmission, inhibitory neurons possess a specific vesicular transporter (VGAT) that mediates the uptake and storage of the inhibitory amino acids GABA and glycine (Chaudhry et al., 1998, McIntire et al., 1997, Sagne et al., 1997). As its name suggests, VGAT-pHluorin consists of a super-ecliptic pHluorin conjugated to VGAT, and can be used to monitor synaptic vesicle recycling at inhibitory terminals (Santos et al., 2013).

VGAT-pHluorin was expressed in neurons using transfection with calcium phosphate at DIV6-8. Cultures were imaged at DIV 14-21.

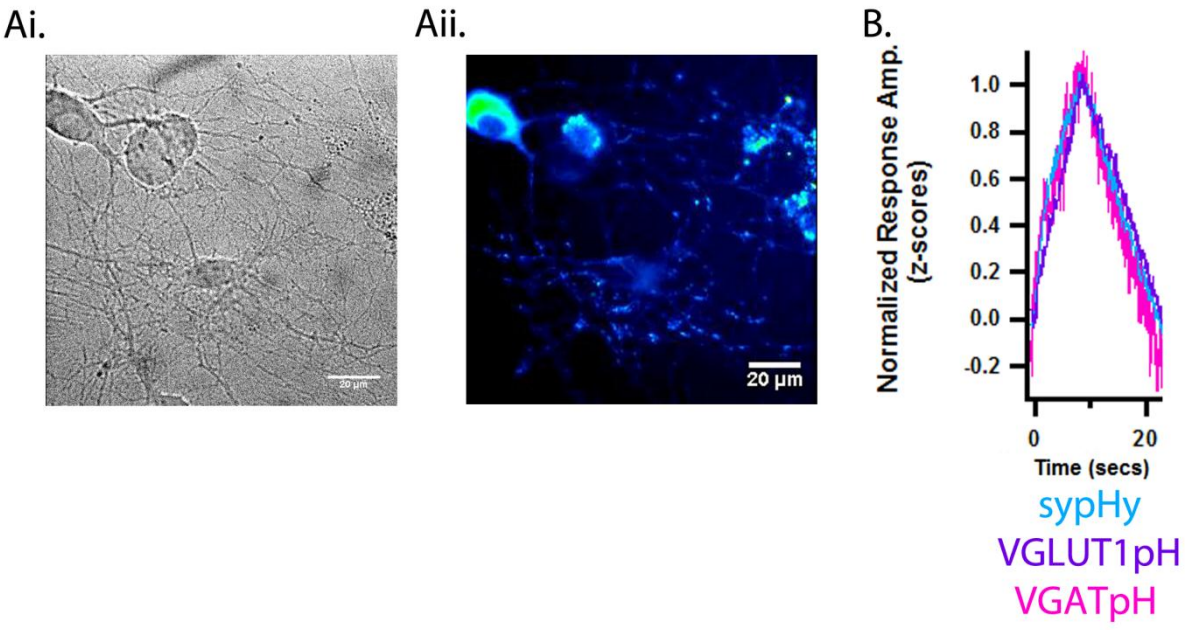

Fig. 3.6. Recording from inhibitory terminals with VGAT-pHluorin. (A) Healthy hippocampal cultures (i) were successfully transfected with VGAT-pH. (B) Kinetics of VGAT-pH, VGLUT-pH and sypHy were virtually identical following a 20AP, 2Hz stimulus.

3.4.2 Monitoring presynaptic calcium dynamics with syGCaMP6f

In addition to directly studying vesicle release and retrieval with pHluorin-based probes, one of the key aims of this work was to monitor disruptions in calcium dynamics to gain insight into the potential mechanisms and molecular pathways of agents modulating the vesicle cycle. The arrival of an action potential at the presynaptic terminal triggers the opening of Ca^{2+} channels and a transient rise in intracellular Ca^{2+} at the active zone. In terms of vesicle recycling, Ca^{2+} plays an essential role in initiating vesicle exocytosis (Katz and Miledi, 1967), it has been shown to determine the number of vesicles undergoing fusion (Li et al., 2011), and exo-endocytic coupling is thought to be regulated by stimulus-evoked Ca^{2+} influx (Hosoi et al., 2009). Therefore, through studying Ca^{2+} dynamics, we could ascertain if our modulators were affecting vesicle release via upstream modulation of Ca^{2+} or at an alternative part of the cycle, for example the release machinery itself.

There are a wide variety of genetically encoded calcium indicators (GECIs) available, but for the purpose of these experiments we selected syGCaMP6f as the most appropriate. The GCaMP reporter, developed by Junichi Nakai, consists of a circularly permutated EGFP (cpEGFP) connected at the C-terminus to calmodulin and, at the N-terminus, to the M13 domain of myosin light chain kinase; the target sequence of calmodulin (CaM). Upon binding of Ca^{2+}, Ca^{2+}-CaM-M13 interactions induce conformational changes in the cpEGFP, resulting in an increase in fluorescence (Nakai et al., 2001). The affinity of GCaMP for Ca^{2+} is determined by the equilibrium of the Ca^{2+}.CaM.RS20 peptide complex and faster variants of GCaMP can be generated by mutation of the tryptophan residue to tyrosine and the disabling of individual EF – hand Ca^{2+} binding sites of CaM by single point mutations, which together serve to weaken the Ca^{2+}.CaM.RS20 interactions and generates a faster Ca^{2+} response rate (Helassa et al., 2015, Chen et al., 2013). For our experiments, we use a fast variant of GCaMP6 (GCaMP6f) fused to synaptophysin, which generates syGCaMP6f, a GECI specifically adapted for measuring fluctuations in Ca^{2+} at the presynaptic terminal (Dreosti et al., 2009).

Neurons were infected with AAV6_syGCaMP6f (University of Helsinki) at DIV 6/7, using an MOI of 100. Cultures were subsequently imaged at DIV14-21, once satisfactory expression had been established. As with the pHluorin-based probes, ROIs were defined using the correlates of standard deviation between neighbouring pixels, computed using the SARFIA plugin for Igor Pro. Robust signals were sustained over multiple trials (Fig 4.6), therefore indicating that syGCaMP6f is

a suitable candidate for repeated imaging of individual presynaptic terminals under varying pharmacological conditions. Nevertheless, it should be highlighted that syGCaMP6f is a high affinity Ca^{2+} probe with a Kd of 0.22µM ± 0.01 at 20°C (Helassa et al., 2016), and whilst validation work carried out by our industrial partner shows that the dynamic range of syGCaMP6f increases linearly up to 40APs, 20Hz stimulation (Borges, 2017), it should be noted that signals recorded at this amplitude (such as those in Figures 3.7 and 4.2.3) are at the upper limits of the sensor's detection capability. Therefore, whilst relative comparisons can be made between conditions at this stimulus intensity, extrapolating robust data regarding Ca^{2+} concentration at the presynaptic terminal is not possible due to the risk of probe saturation.

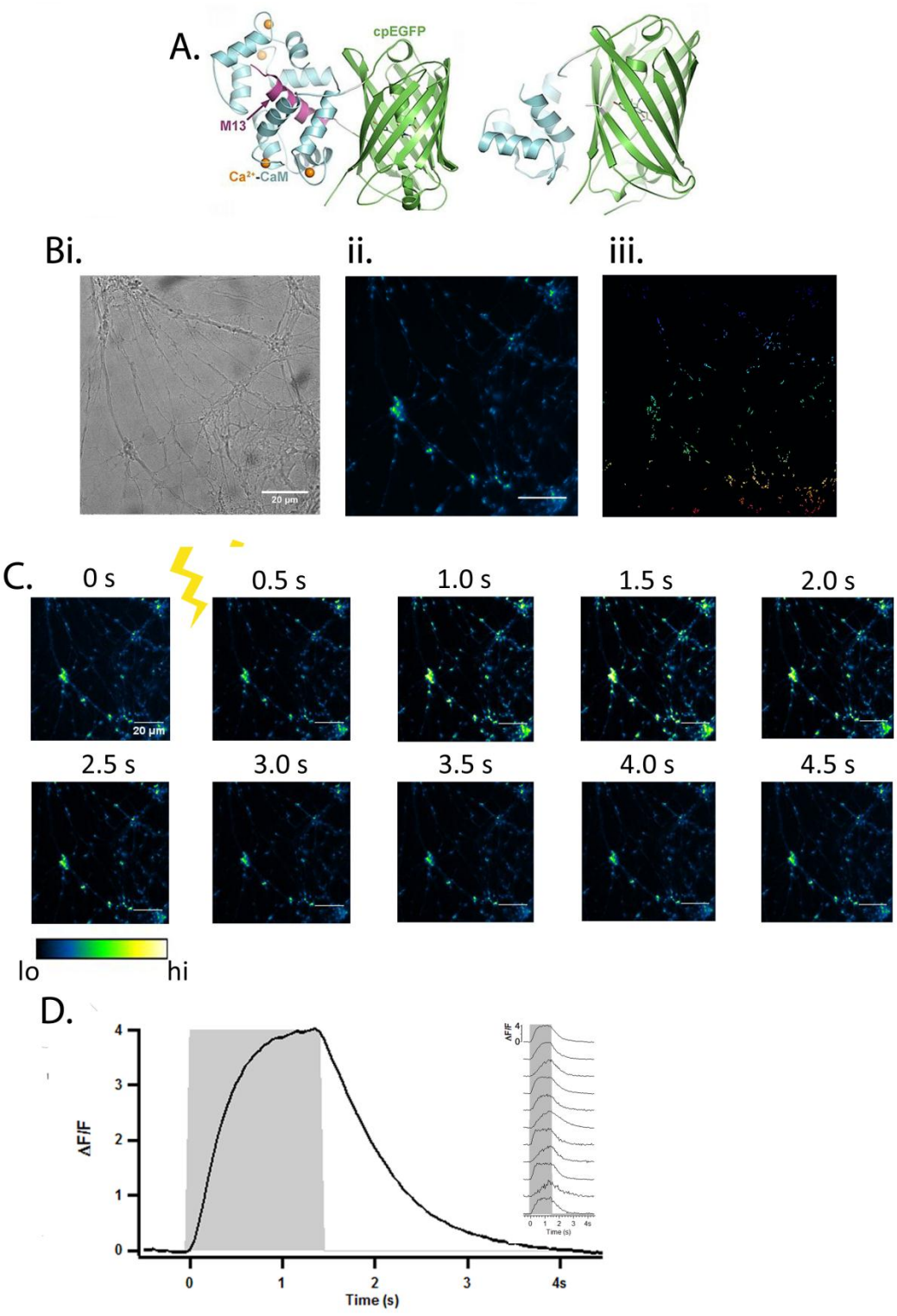

Fig 3.7. Monitoring changes in presynaptic Ca2+ with syGCaMP6f. (A) Schematic of GCaMP sensor (taken from Akerboom et. al., 2008) (B) Healthy neuronal cultures (i) were successfully infected with syGCaMP6f (ii) and ROIs detected based on a threshold calculated as a multiple of

standard deviation (see Methods) (C) Timelapse images show response of individual boutons following 40AP, 20Hz stimulation (D). Representative trace averaged from 345 synapses, grey indicates stimulation period. Average peak amplitude 3.98 ± 0.049 ΔF/F.

3.4.3 Detecting glutamate release and reuptake with iGluSnFR

Glutamate release and reuptake are key indicators of synaptic performance and alterations in glutamate transmission are implicated in a wide range of neurological disorders, including tauopathies such as Huntingdon's disease, FTDP-17 and Pick's disease (Lewerenz and Maher, 2015). Therefore in Chapter 6, we wanted to monitor changes in the release and reuptake of glutamate arising from the knockdown or overexpression of pathogenic P301L tau protein. To do so, we used iGluSnFR; a relatively new probe that gives a direct readout of glutamate release and clearance kinetics (Marvin et al., 2013, Parsons et al., 2016). Figure 3.8. D shows a representative trace averaged from 112 synapses in response to a 40AP, 20Hz stimulus, where glutamate release can be quantified by calculating the area under the curve (AUC). However it should be said that, as with syGCaMP6f, quantification at this stimulus intensity permits only relative comparisons to be drawn between conditions. This is because, whilst iGluSnFR has a high glutamate affinity and dynamic range (Marvin et al., 2013), it does not dissociate fast enough to faithfully resolve individual glutamate release events at frequencies >10Hz (Helassa et al., 2018, Taschenberger et al., 2016) .

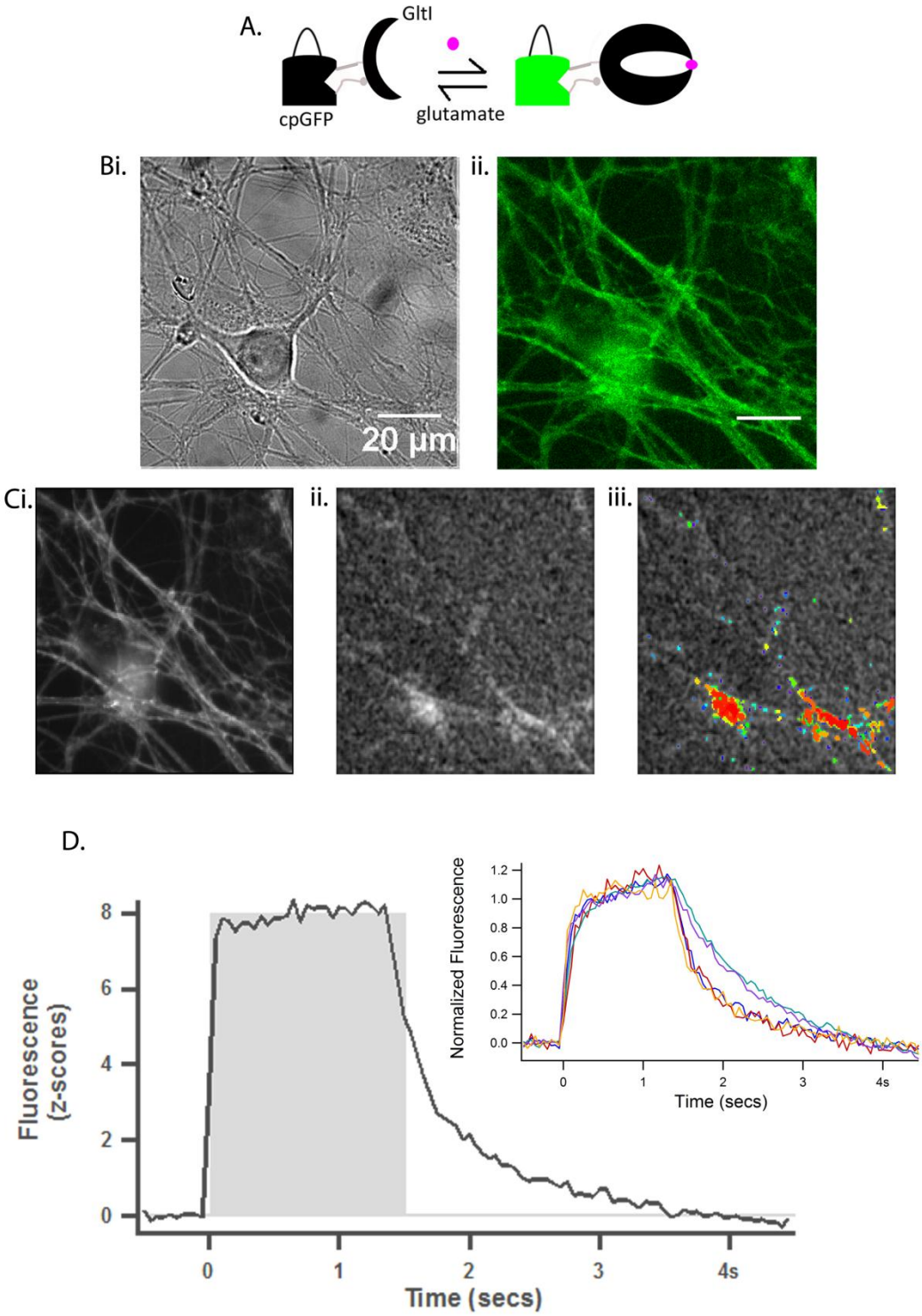

Fig 3.8. Detection of glutamate release and reuptake using iGluSnFR. (A) Schematic of iGluSnFR mechanism of action (B). Healthy neuronal cultures (i) infected with iGluSnFR (ii) show good expression. (C). Detection of ROIs. Average projected image (i) is smoothed (ii) and ROIs detected via smooth correlation map (iii). (D). Representative trace averaged from 118 synapses following stimulation at 40APs, 20Hz; grey shading indicates stimulation. Glutamate release can be quantified using area under the curve. Average peak amplitude 8.14 ± 0.316 (z-scores). Peak-normalized traces (insert) demonstrate that iGluSnFR can monitor differences in reuptake – shown normalized to peak to aid visualization of kinetics.

3.5 Discussion

The purpose of this chapter was to establish the methodology for the readout of synaptic function and to optimize the relevant approaches needed to address the aims of our central research questions. Of fundamental importance was the reliable culture of healthy, robust primary hippocampal neurons. Fig 3.2. shows the successful loading of presynaptic terminals with FM1-43 in an activity-dependent manner, verifying that our cultures contained mature and functional synapses.

Although FM1-43 can provide information about the localization of presynaptic terminals and readouts of some fundamental presynaptic properties, it has several significant limitations. The first is that it relies upon a large loading stimulus to label the recycling pool (1200APs, 20Hz), and therefore this could dramatically influence the behaviour of synapses prior to assaying any sort of modulation. The second reason is that FM1-43 is confined to a single readout because functional analysis relies on the destaining of the terminals. For the majority of our research aims it was essential to record from the same terminals pre- and post- addition of compounds, and therefore FM1-43 was an unsuitable candidate. On the other hand, genetically encoded reporters of synaptic function do not need to be loaded in an activity-dependant fashion, nor are they limited to a single readout meaning that pharmacological modulation can be studied at the same terminals before and after the addition of compound.

In this chapter we evaluated three different pHluorin-based probes for the monitoring of synaptic vesicle release and retrieval; sypHy, for recording at all terminals; VGLUT1-pHluorin, for isolating responses at excitatory terminals, and VGAT-pHluorin, for isolating responses at inhibitory terminals. In our experimental system, each of the three pHluorins demonstrated excellent localization to presynaptic terminals. Fig 3.5.B demonstrates the similar kinetics of the pHluorin-based probes following a 20AP, 2Hz stimulus. Despite the obvious advantages of being able to separate excitatory and inhibitory signals, the major advantages of using sypHy were improved neuronal health, increased expression efficiency and reduced surface bleaching. The improved neuronal health and increased level of expression were most likely due to the fact that sypHy was delivered via an AAV vehicle, whereas VGLUT1-pHluorin and VGAT-pHluorin were transfected using calcium phosphate. In addition, VGLUT1-pHluorin was particularly challenging to work with due to its reduced surface expression In comparison with sypHy (First panel in timelapse Fig 3.2.C

cf. first panel in timelapse Fig 3.4.B). Although this is a desirable property in terms of conferring signal fidelity, VGLUT1-pH expressing terminals could often only be detected after stimulation, meaning that they were difficult to localize and that the neurons often had to undergo repeated rounds of stimulation before a suitable region was discovered. In terms of sequential imaging, the lack of residual surface expression coupled with signal bleaching made locating the correct focal plane increasingly more difficult. The majority of the experiments in this work required a probe that was suitable for reliably imaging the same terminals over multiple trials for up to twenty minutes; therefore, for this reason, sypHy1x was selected as our probe of choice for monitoring vesicle dynamics.

Using sypHy1x, the average fluorescence recovery following an RRP mobilizing stimulus (40APs, 20Hz) was τ = 18.8 secs (Fig 3.4.D). This is in excellent agreement with other groups carrying out real-time imaging with pHluorin-based probes, who report the average time constant of endocytosis to be in the range of 15-20 seconds (Granseth et al., 2006, Balaji and Ryan, 2007, Kim and Ryan, 2009). As the kinetics of exo- and endocytosis are extremely sensitive to temperature (Granseth and Lagnado, 2008), we ensured to keep the microclimate of the imaging room as constant as possible and were able to obtain similar kinetic readouts across experiments.

Whilst sypHy1x is an excellent indicator of vesicle release and retrieval, it does not provide a full account of events occurring at the presynaptic terminal, which is needed when trying to pinpoint at which point a pharmacological or pathological modulator is acting. For example, changes in the rate of exocytosis could be driven by an upstream modulation of Ca^{2+} - channels or via modulating the release competency of the individual vesicles. Or, in the instance of pathological tau, vesicle fusion events are not altered but the release of neurotransmitter is. Therefore, as a complement to our experiments focusing on vesicle dynamics, we wished to assay presynaptic Ca^{2+} dynamics and neurotransmitter release; to do so we used the optical probes syGCaMP6f and iGluSnFR. Experiments carried out with these probes were designed to mirror assays of RRP function carried out using sypHy, and therefore used a stimulus intensity of 40APs, 20Hz for continuity purposes. However, it must be acknowledged that due to the limitations of syGCaMP6f and iGluSnFR (discussed previously in this chapter), this is not an optimal stimulation for either of these probes and quantitative measures of Ca^{2+} influx or glutamate release are not permitted. Nevertheless, we were entitled to make relative comparisons between conditions, which was satisfactory for the purposes of this work.

Chapter 4: Characterizing the actions of Levetiracetam at the presynaptic terminal

4.1 Introduction

The discovery that synaptic vesicle protein 2A (SV2A) was the primary binding site of the antiepileptic medication, levetiracetam (LEV) (Lynch et al., 2004), has led to increased interest in its modulation for the treatment of epilepsy and other neurodegenerative disorders. Nevertheless, the role of SV2A within the maintenance of regular neurotransmission remains elusive, although its vitality is demonstrated by the severe seizure phenotype that develops in SV2A KO mice, which do not thrive beyond 3 weeks of age (Crowder et al., 1999, Janz et al., 1999).

The sensitivity of SV2A to inputs of varying frequency is evidenced by electrophysiological experiments on hippocampal neurons cultured from SV2A/B KO mice, with knockouts showing facilitation in response to trains of action potentials. At 2Hz this is sustained over 25 pulses, however at 10Hz and 20Hz facilitation occurs only briefly before the onset of synaptic depression (Custer et al., 2006). Coupling this with levetiracetam's efficacy in clinical models that utilize repetitive rounds of electrical stimulation alongside evidence from human clinical usage that indicates that LEV only exerts its maximal effect in patients when synaptic transmission shifts into an excessive hypersynchronous state i.e. during times of seizure (2006, Stafstrom, 2012), a picture begins to form in which SV2A modulation has various activity-dependent aspects. Therefore, the aim of this chapter was to exploit various paradigms of stimulus intensity and frequency to gain a better insight into the modulation of SV2A by LEV and the ramifications of such modulation on synaptic vesicle pool dynamics and presynaptic transmission. Revealing such mechanisms would provide fundamentally novel insights into the action of SV2A ligands and have potential benefits for informing the development of new compounds to treat epilepsy and other neurological dysfunctions.

4.2 Unravelling the action-dependent mechanism of levetiracetam

Given the clinical evidence that the action of LEV appears to more prominent in states of hypersynchronous neurotransmission and that it is unique amongst anti-epileptic drugs (AEDs) in having a vesicular binding site, we hypothesized that LEV may require a high level of vesicle turnover in order to generate a significant effect. In our proposed 'use-dependent' model (Fig. 4.1), during normal transmission states the majority of LEV is situated in the synaptic cleft, where it is unable to access and bind SV2A, located on the luminal side of the intracellular vesicle membrane. However, during times of intense neuronal activity, such as seizure, an increased fraction of vesicles participate in fusion with the presynaptic membrane, the uptake of LEV into synaptic vesicles is increased and, consequently, target availability is improved. This is a similar mechanism as proposed for tetanus and botulinum toxin A, yet has not been previously reported in a pharmacological compound (Lynch et al., 2009).

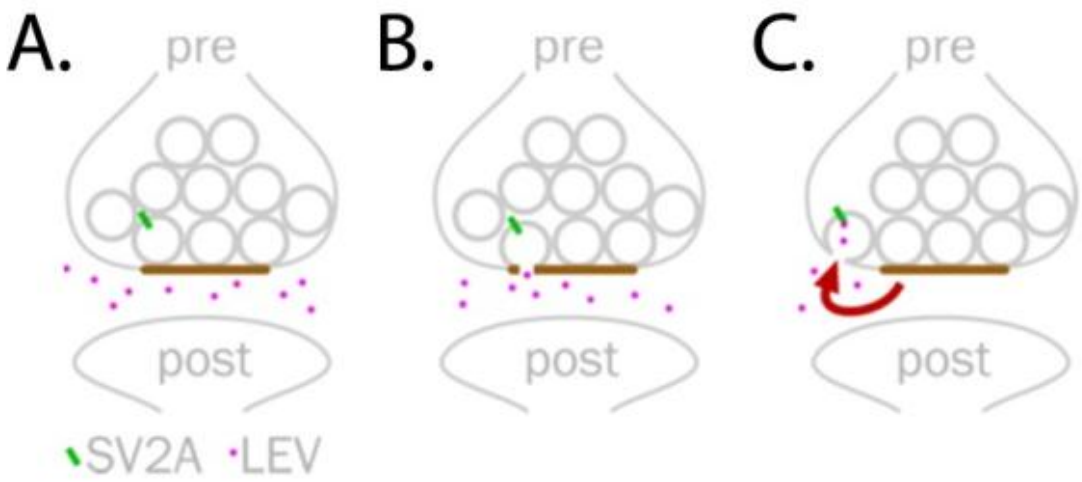

Fig. 4.1 The 'use-dependence' model of levetiracetam A) Organization of the presynaptic terminal and location of LEV (pink) as imagined under regular, synchronous neurotransmission. Note the position of SV2A on the inner luminal membrane of the SV (green). B. Under moments of extreme hypersynchronous firing, such as during ictal activity, an increased number of vesicles fuse to the presynaptic membrane and expose their lumens to the synaptic cleft. C) Presentation of vesicle lumens to the synaptic cleft provides an increased level of target exposure for LEV, leading to increased compound binding and effect.

The objective of the first section of this chapter was to test this hypothesis using optical methods that allow the monitoring of the release and retrieval of synaptic vesicles prior to and following exposure to LEV. Specifically, we assayed basal vesicle turnover using a sub-maximal activity protocol (40APs, 20 Hz via field stimulation) known to mobilize the so-called readily releasable pool (RRP) of vesicles – the population that are first to undergo fusion during synaptic activity (Fig 4.3.A) (Rosenmund and Stevens, 1996). The protocol also incorporated a single high intensity stimulation of 150APS (20Hz), which served to turn over a large portion of the recycling pool of vesicles, thus mimicking seizure. We theorized that if the action of LEV was dependent upon a large stimulus and hence, an increased level of vesicle fusion, then significant effects would only be seen in those neurons exposed to both the compound and the 150AP stimulus. Vesicle turnover was monitored using the optical reporter AAV6_sypHy1x, expressed in neurons by infection and validated in the previous chapter. Our rationale for selecting the RRP as our primary readout was two-fold; firstly, prior research has demonstrated that SV2A modulates the size of the RRP (Xu and Bajjalieh, 2001), and secondly that a 40AP stimulus recruits an adequate number of vesicles to robustly detect changes in fluorescence, with a good signal-to-noise ratio.

Preparation of cultures, infection with AAV6_sypHy1x and experimental conditions were as described in the Methods section (2.1). Prior to the first stimulus shown in the protocol, cultures were stimulated with a single round of 40APs and imaged. This ensured the selection of a responsive region and led to a pre-photo bleaching of the sample so as to remove the residual surface fluorescence (Gandhi and Stevens, 2003). It also formed part of the exclusion criteria in the final trace analysis; if a given synapse failed to respond with similar amplitude, or not at all, when comparing the response to the initial stimulus to the first stimulus of the protocol, this synapse was eliminated from the final analysis. In doing so, this assured that sampling was from robust, healthy synapses and thus any effect recorded was a true effect of the compound administered, rather than of neuronal health decline. The time-lapse images taken during the initial 40APs were also used to identify ROIs; the creation of the ROI mask from this set of images avoided bias of the mask to any of the subsequent trials used for analysis. All experiments were conducted in EBS supplemented with the NMDA and AMPA receptor blockers AP-V and CNQX (composition detailed in section 2.2.2, Methods), and unless otherwise stated, conditions labelled as ‘buffer’ in the following figures refer to this solution. 300µM LEV was dissolved in 300µl EBS (plus blockers) and introduced to the chamber via exchange of half the buffer volume (i.e. 300µl in a total volume of 600µl).

As demonstrated in Fig 4.2, the response profiles of individual boutons to 40APs, 20Hz stimulation are highly variable. Multiple factors are thought to contribute to this heterogeneity, such as the distribution of Ca^{2+} channels, ρ*r* and size of the active zone (Eggermann et al., 2011, Holderith et al., 2012, Matz et al., 2010, Marra et al., 2012). Nonetheless, this inherent variability complicates analysis when trying to first uncover a true effect of a compound. Therefore, to address this issue, responses of synapses in trials 2-4 were normalized to their responses pre-addition of LEV (Figs 4.3.B and C). Analysis was carried out on baseline (ΔF/F) and bleach corrected data; traces were baseline subtracted and subsequently divided by the exponential of the baseline fluorescence decay pre- and post- response in order to generate baseline corrected (ΔF/F) and bleach-corrected response profiles. Finally, traces from trials 2-4 were normalized to the first response, pre-addition of LEV, to establish any significant effect. Peak amplitude was calculated via subtracting the average of the baseline before the onset of the stimulus (frames 28-38) from the average of the peak (frames 75-85).

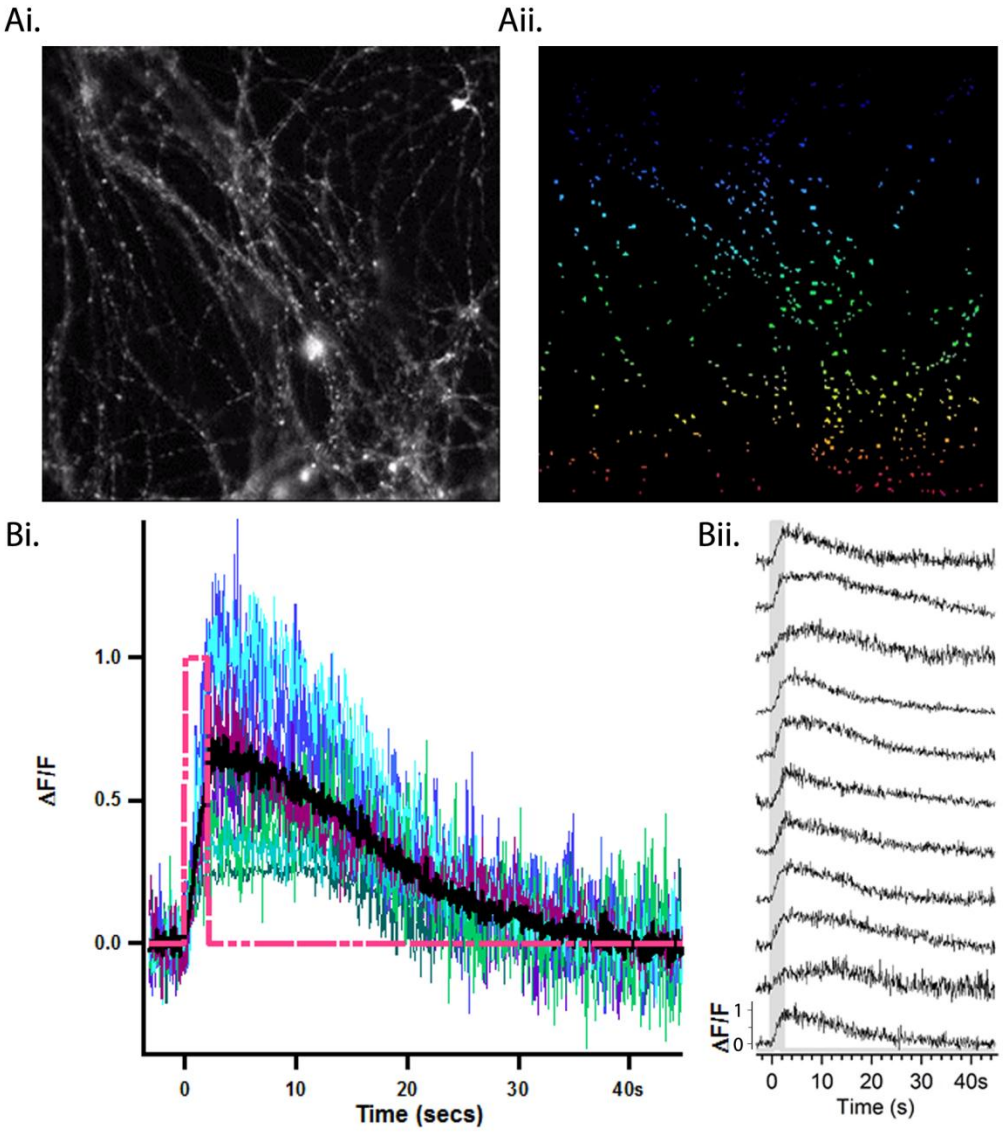

Fig.4.2 Heterogeneity in Response Profiles of individual synapses when exposed to 40APs, 20Hz stimulus Ai and ii) Example ROI and ROI mask generated using SARFIA, Igor Pro v6. Bi and ii). Individual responses to 40AP, 20Hz stimulus are highly variable, stimulation window indicated via dashed line (pink) and grey shading respectively (example traces from 11 synapses taken from same ROI). The mean trace is shown in black, average peak 0.770 ± 0.031 ΔF/F.

The traces and bar plots in Figure 4.3.C and D demonstrate the challenges of incorporating a high intensity stimulus into a protocol. In all conditions, bar the buffer time point control, the responses at the 10 and 12 minute time points are significantly different from the first 'control' stimulus i.e. pre-addition of compound/ 150AP stimulation. There are several factors that may have contributed to this. Firstly, it highly likely that even without the high intensity stimulation, some LEV would bind to the target protein and therefore a small dampening of the responses could realistically be expected. Secondly, synapses subjected to intense tetanic stimulation trains

often undergo presynaptic short-term depression (STD), whereby the response amplitude can be decreased for several minutes following stimulation (Regehr, 2012). This theory is further supported by the partial recovery of response amplitude from 10 to 12 minutes in neurons subjected to 150AP stimulation without LEV treatment (Fig.4.3.D.ii). In order to minimise the effects of STD, a 6 minute period was observed between the administration of the 150AP stimulus and the next recording, however it is clear from the results that a residual effect of this high intensity stimulus remained.

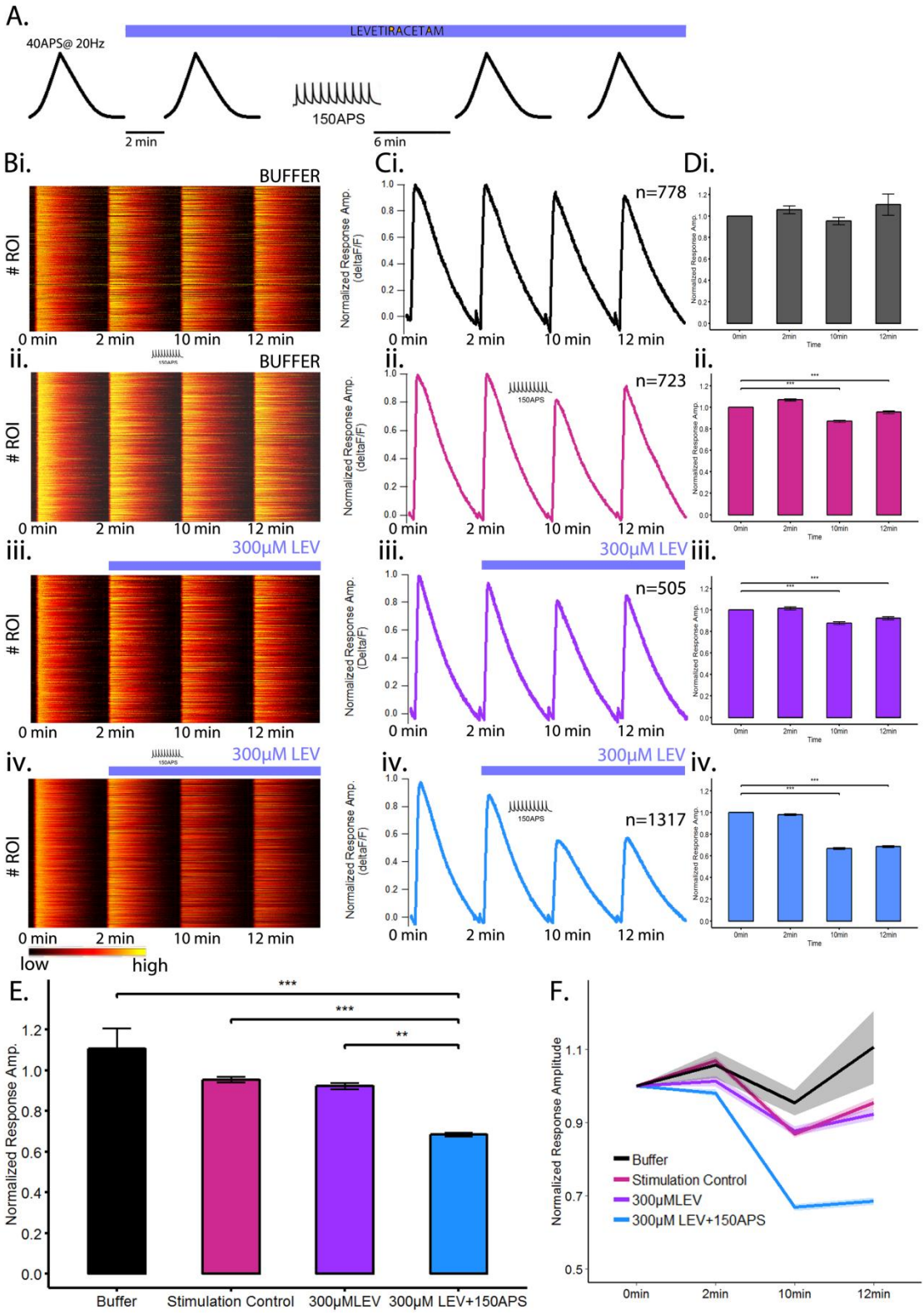

Fig. 4.3. Exposure to levetiracetam shows enhanced effect post recycling pool turnover A) Schematic of protocol. Timing of LEV addition indicated via blue bar at top edge B.(i-iv).

Heatplots illustrating intensity of responses in each trial, each point on the y-axis corresponds to an individual bouton; intensity of the response is indicated via the scale shown in the calibration bar. C(i-iv). Normalized, averaged traces from each experimental condition; traces were baseline subtracted and subsequently divided by the baseline fluorescence in order to generate baseline corrected (ΔF/F) and bleach-corrected response profiles. Traces from trials 2-4 are shown normalized to the first response, pre-addition of LEV. Numbers of synapses in the final datasets are indicated above the traces, all from a minimum of 4 coverslips. D(i-iv) . Change in response amplitude at each time point per condition. Peak amplitude was calculated via subtracting the average of the baseline before the onset of the stimulus (frames 28-38) from the average of the peak (frames 75-85). Again, amplitudes in trials 2-4 (2min, 10min and 12min time points) were normalized to the amplitude of the first response. General Linear Model of repeated measures revealed significant changes within the responses at the 10 and 12 minute time points upon exposure to 150AP stimulation, 300µM LEV or both combined, $p < 0.001$ in all instances. Values of average non-normalized peak amplitudes ± SEM (ΔF/F): Buffer (Di) 0 mins: 0.485 ± 0.008, 2mins: 0.523 ± 0.009, 10 mins: 0.498 ± 0.009, 12 mins: 0.487 ± 0.009; Buffer with 150AP stim (Dii) 0 mins: 0.650 ± 0.009, 2 mins: 0.667 ± 0.009, 10 mins: 0.538 ± 0.008, 12 mins: 0.593 ± 0.009; 300µM LEV (Diii) 0mins: 0.641 ± 0.013, 2 mins: 0.612 ± 0.011, 10 mins: 0.532 ± 0.010, 12 mins: 0.558 ± 0.011; 300µM LEV plus 150AP stim (Div) 0 mins: 0.618 ± 0.006, 2 mins: 0.580 ± 0.006, 10 mins: 0.398 ± 0.006, 12 mins: 0.404 ± 0.006. E) Comparison of response amplitudes across conditions at 12 min time point. Synapses exposed to both 150AP stimulus and 300µM LEV showed significant differences in amplitude when compared with the buffer control; $p < 0.001$, the stimulation control; $p < 0.001$, and 300µM LEV administered without 150AP stimulation; $p = 0.00176$. (One-way ANOVA with Tukey's post-hoc comparisons). F) Graphical comparison between each condition at each time point (Mean Amplitude ± SEM; standard error of measurement is indicated via shading.

Nevertheless, the necessity of the recycling pool turnover to elicit significant actions of LEV is apparent in Figure 4.3.E. At the 12 minute time point neither synapses treated with the 150AP stimulation nor 300µM LEV alone demonstrated significant deviations in responses when compared with synapses treated with the buffer (no 150AP stimulation). However, synapses exposed to a combination of LEV and the 150AP stimulus, showed significantly smaller response amplitudes at the 12 minute time point when compared with each the buffer, stimulation control and 300µM LEV administered alone. On average, responses for the 300µM LEV, 150AP stimulation condition were reduced to just 68% of their original amplitude at this time point, whereas the stimulation control and LEV conditions, although significant when analysing within-factor effects, reduced the amplitudes to 95% and 92% respectively. Figure 4.3.F clearly illustrates the greater reduction in response amplitude shown by synapses that have undergone recycling pool turnover in the presence of LEV at the 10 and 12 minute time points.

The findings of these experiments corroborate with that of other research within the field. Using hippocampal slices as model systems, exposure to levetiracetam has been shown to cause both

presynaptic depression and depression of excitatory post-synaptic currents (EPSCs) and inhibitory post-synaptic currents (IPSCs) (Yang et al., 2007, Nowack et al., 2011, Meehan et al., 2012). Interestingly, both Yang et. al. and Meehan et. al. report that an effect of LEV is only seen after prolonged exposure (>3hrs), but that no effect is seen acutely, in contradiction to our experimental system. Meehan et. al. further report that LEV fails to depress IPSCs when spontaneous activity is prevented via TTX during incubation, thus suggesting that some level of basal activity is necessary for the uptake and effect of LEV. This research, taken together with our discovery that an acute effect of LEV can only be evoked through a high level of vesicle turnover, is strongly indicative of a use-dependent mechanism, where an acute effect of LEV can be seen only upon neuronal hyperactivity, such as during seizure.

Interestingly, not all SV2A modulators exhibit use-dependent effects. In addition to our work carried out with LEV, we carried out some work on other SV2A modulators in partnership with a different industrial sponsor. The names of compounds cannot be disclosed and therefore are referred to using arbitrary names. Fig 4.3.1 shows that Compound X, a derivative of levetiracetam, has no significant effect on RRP release, even following recycling pool turnover.

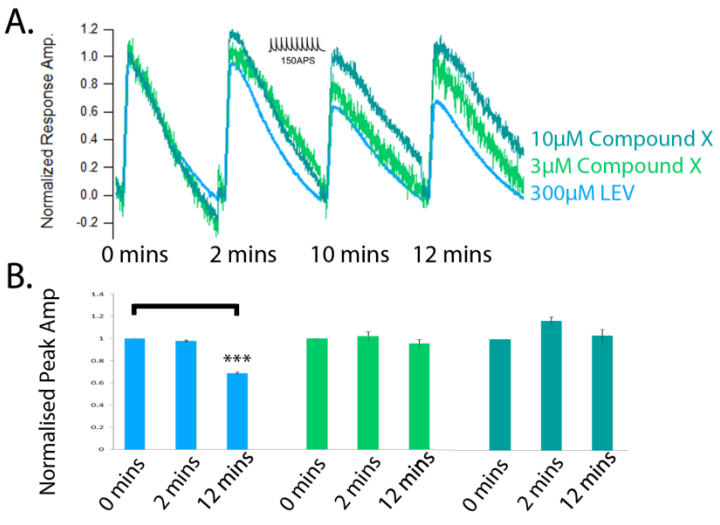

Figure 4.3.1. Some SV2A modulators do not exhibit a use-dependent mechanism of action. A) Average normalized traces show that RRP size is suppressed by LEV but not by Compound X following turnover of a large portion of the recycling pool B) Bar graphs to show mean peak amplitude ± SEM. LEV significantly reduces RRP response; $p < 0.001$, GLM – RM.

4.2.1. Levetiracetam reduces RRP release in a concentration-dependent manner

In initial experiments to determine the 'use-dependent' mechanism of LEV, we selected a starting concentration of 300μM to maximize the chances of the drug having a detectable effect in our model system at the same time as falling within a physiologically relevant range. Pharmacokinetic data recorded from the cerebrospinal fluid of rats treated with LEV shows that concentrations of >600μM can be expected following 80mg/kg intraperitoneal administration (Doheny et al., 1999). Nonetheless, having established the requirement of a high intensity stimulus in order for LEV to exert significant acute effects on RRP amplitude using a concentration closer in proximity to the maximal end of the scale, we next sought to demonstrate the effects of LEV in our model system in a concentration-dependent manner.

Based on discussions with our pharmaceutical partners, we tested the effects of 10μM and 50μM LEV upon RRP release, again using the 40AP, 20Hz stimulation and sypHy as the readout. As in the previous experiments, analysis was carried out on baseline (ΔF/F) and bleach corrected data, and traces were normalized to the peak amplitude of the pre-compound response. Apart from varying the concentration of LEV used, experimental parameters were identical to those described in Section 4.2.1.

Having justified the necessity of the recycling pool turnover to see significant effects in our system using 300μM LEV and also taking into account the significant STD effects encountered when neurons are subjected to high intensity stimulation, we concluded that the stimulation control (i.e. EBS, blockers plus 150AP stimulus) provided the most appropriate baseline control for these experiments. As no significant effects were seen at the 12 minute time point when 300μM LEV was applied without the 150AP stimulus (Fig 4.2.1.E), it was deemed unnecessary to repeat these particular experiments with 10μM and 50μM.

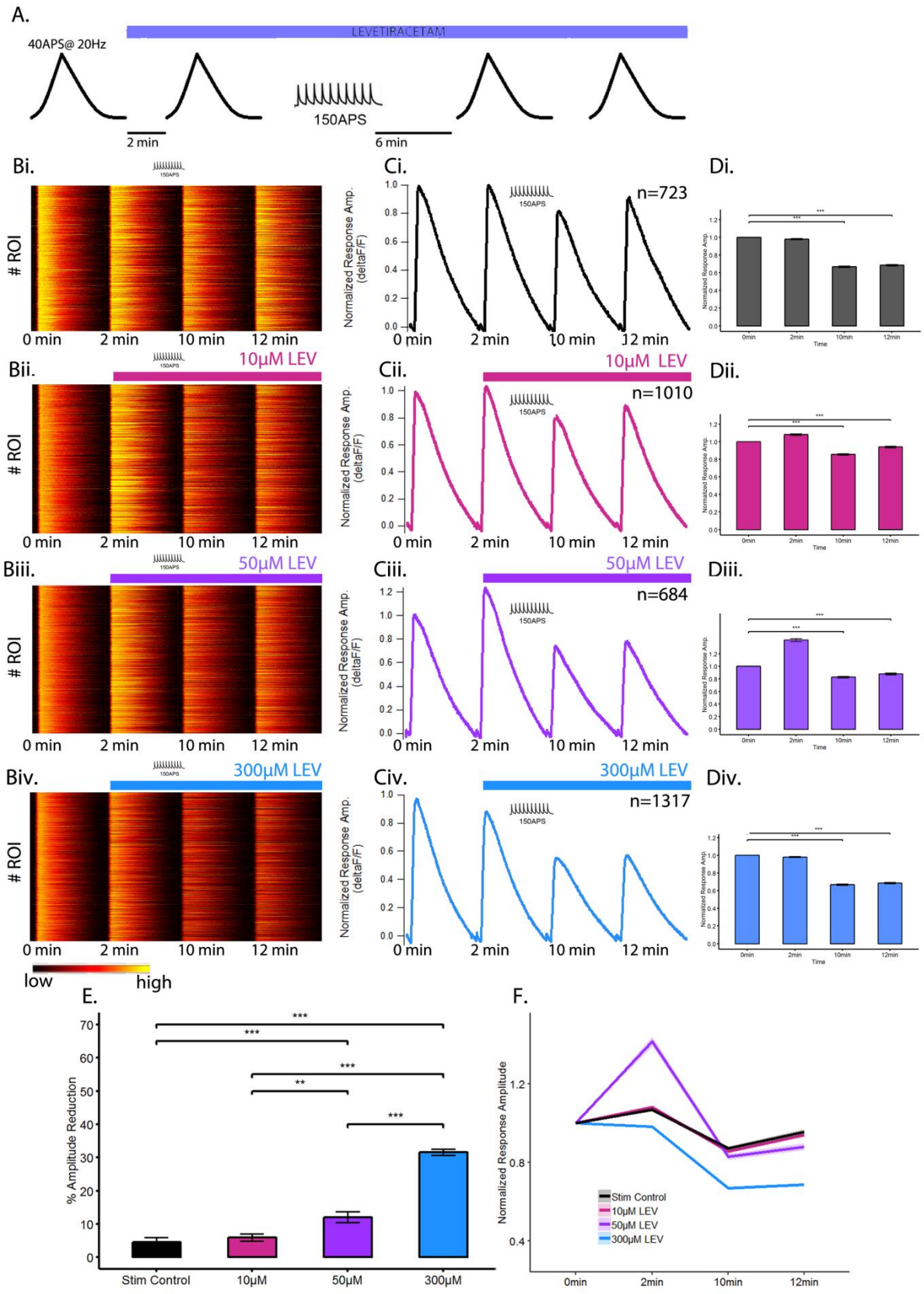

Fig 4.4. Levetiracetam reduces RRP amplitude in a concentration-dependent manner A) Schematic of protocol. Timing of LEV addition indicated via blue bar at top edge B.(i-iv).

Heatplots illustrating intensity of responses in each trial, each point on the y-axis corresponds to an individual bouton; intensity of the response is indicated via the scale shown in the calibration bar. C(i-iv). Normalized, averaged traces from each concentration assayed; traces were baseline subtracted and subsequently divided by the baseline fluorescence in order to generate baseline corrected (ΔF/F) and bleach-corrected response profiles. Traces from trials 2-4 are shown normalized to the first response, pre-addition of LEV. Numbers of synapses in the final datasets are indicated above the traces, all from a minimum of 4 coverslips. D(i-iv). Change in response amplitude at each time point per concentration assayed. Peak amplitude was calculated via subtracting the average of the baseline before the onset of the stimulus (frames 28-38) from the average of the peak (frames 75-85). Again, amplitudes in trials 2-4 (2min, 10min and 12min time points) were normalized to the amplitude of the first response. GLM-RM between Time 0 and each subsequent time point revealed significant changes within the responses at the 10 and 12 minute time points upon exposure to 150AP stimulation and all concentrations of LEV tested, $p < 0.001$ in all instances. Values of average non-normalized peak amplitudes ± SEM (ΔF/F): Buffer plus 150AP stim (Di) 0 min: 0.650 ± 0.009, 2 min: 0.667 ± 0.009, 10 min: 0.538 ± 0.008, 12 min: 0.593 ± 0.009; 10μM LEV (Dii) 0 mins: 0.691 ± 0.008, 2 mins: 0.728 ± 0.010, 10 mins: 0.574 ± 0.008, 12 mins: 0.631 ± 0.010; 50μM LEV (Diii) 0 mins: 0.538 ± 0.011, 2mins: 0.674 ± 0.010, 10 mins: 0.403 ± 0.008, 12 mins: 0.424 ± 0.008; 300μM (Div) 0 mins: 0.618 ± 0.006, 2 mins: 0.580 ± 0.006, 10 mins: 0.398 ± 0.006, 12 mins: 0.404 ± 0.006. E) Comparison of the percentage of amplitude reduction response incurred at the 12 minute time point; 300μM and 50μM LEV caused highly significant reductions in response amplitude when compared with the stimulation control; $p<0.001$ in both instances. 300μM LEV reduced response amplitude to a far greater extent than either 10μM or 50μM; $p<0.001$ in both instances. The difference in percentage reduction is less significant between the 10μM and 50μM conditions; $p= 0.00866$ (One-way ANOVA with Tukey's post-hoc comparisons) F) Graphical comparison between each condition at each time point (Mean Amplitude ± SEM; standard error of measurement is indicated via shading.

Unsurprisingly, given that all neurons used in this experiment were stimulated with 150APs to provoke a high turnover of vesicles, within-subject effects were apparent in all conditions (Fig. 4.4.D(i-iv). In the 50μM condition the response amplitude at 2 minutes is considerably greater than the response at time 0 (significance not shown, $p < 0.001$, General Linear Model of repeated measures (GLM-RM)). The response amplitudes in the other conditions at this time point also tended to be marginally bigger, perhaps indicating that this phenomena is something intrinsic to the experimental design. The fact that this effect is not concentration-dependent supports this theory, and therefore this anomaly was treated as experimental noise.

Fig 4.4.E. compares the effects of the range of concentrations after 12 minutes and clearly shows the concentration-dependent nature of the response suppression. At this timepoint, only the 50μM and 300μM concentrations significantly reduced the amplitude of the presynaptic response, $p<0.001$ in both cases (One-way ANOVA), and the depression caused by 300μM LEV was significantly greater than that caused by 50μM ($p < 0.001$, One-way ANOVA). As previously shown

in hippocampal slices, administration of 10μM LEV had no significant effect on response amplitude at 12 minutes, however it is worth noting that the reduction in amplitude incurred when using 50μM was less significant in comparison with 10μM than with the stimulation control ($p = 0.00866$ cf $p < 0.001$), suggesting a slight modulatory effect at 10μM LEV.

From the experiments discussed here and in section 4.2.1, it can be concluded that levetiracetam has the ability to acutely depress the RRP in a concentration-dependent manner, however this effect can only be elicited in acute preparations where it is administered alongside a stimulus sufficient to recruit the recycling pool. The concentration-dependent nature of the synaptic depression verifies that the effects seen in the initial use-dependence experiment were a true effect of levetiracetam. The fact that we show similar levels of synaptic depression as those seen in hippocampal slice preparations using electrophysiological measures further ratifies our experimental system as a suitable model for testing presynaptic modulators.

4.2.2. Levetiracetam slows exocytosis of the RRP

Using the same data set as generated for section 4.2.1., we wanted to ascertain the effect of LEV on the kinetics of the RRP. Note that in this instance the traces were baseline corrected (ΔF/F) but not bleach corrected, as this could potentially mask kinetic effects, particularly in endocytosis. In separate work carried out in partnership with a different industrial partner, we showed an alternative SV2A modulator, referred to as Compound X for reasons of intellectual property, significantly inhibited endocytosis following a 40AP, 20Hz stimulation. When assaying Compound X, the experimental protocol used to mobilize the RRP was identical to that used in the previous experiments i.e. sequential rounds of a 40AP, 20Hz stimulus with 2 minute intervals, plus a high intensity stimulation of 150APS at 4 minutes. However, due to the nature of its solubility it was necessary to dissolve Compound X in DMSO to a concentration of 10mM and perform serial dilutions in EBS and blockers to generate the final concentrations used. This was calculated so as to give a final maximal DMSO concentration of 0.15%.

Linear lines of best fit were used to calculate the rate of exocytosis. To compare the rates of endocytosis between varying concentrations of LEV, a single exponential fit was used to describe the signal decay. To generate readouts of kinetics in seconds, it was essential that the traces were properly scaled prior to analysis. This was achieved via a customized script written in Igor Pro. To measure exocytosis, traces were fitted so as to compute the 20-80% rise time of the fluorescent

signal (frames 45-65), a common parameter used within electrophysiology to determine the rate at which a signal rises to its peak (Fig 4.5.A - insert). Measuring the rate of decay of the signal i.e. rate of endocytosis was complicated by the fact that synapses treated with Compound X failed to complete endocytosis, thus meaning traces failed to return to baseline levels. Therefore, although we were able to use a single exponential fit to compare endocytosis across the different concentrations of LEV (Fig 4.5.C.ii), we were unable to use this methodology with Compound X. This is because fitting a curve in this manner calculates the time taken to reach the point at which the line asymptotes; if a population of vesicles fail to endocytose fully they will reach their asymptotes more quickly than vesicles undergoing complete endocytosis. The result of this is that the rate of signal decay in synapses where endocytosis has failed to complete will appear faster than those which have undergone regular endocytosis, therefore providing a misrepresentation of the data.

Therefore, to compare endocytosis between neurons treated with LEV and those treated with Compound X we used a response plateau index, which was calculated by ascertaining the average amplitude of the final 50 points of the recording (Fig 4.5.E). Prior to analysis, traces were normalized such that the peak of fluorescence following the stimulus (*Fmax)* =1, therefore through measuring plateau amplitude, this generates a readout of endocytosis success/failure that is comparable between synapses.

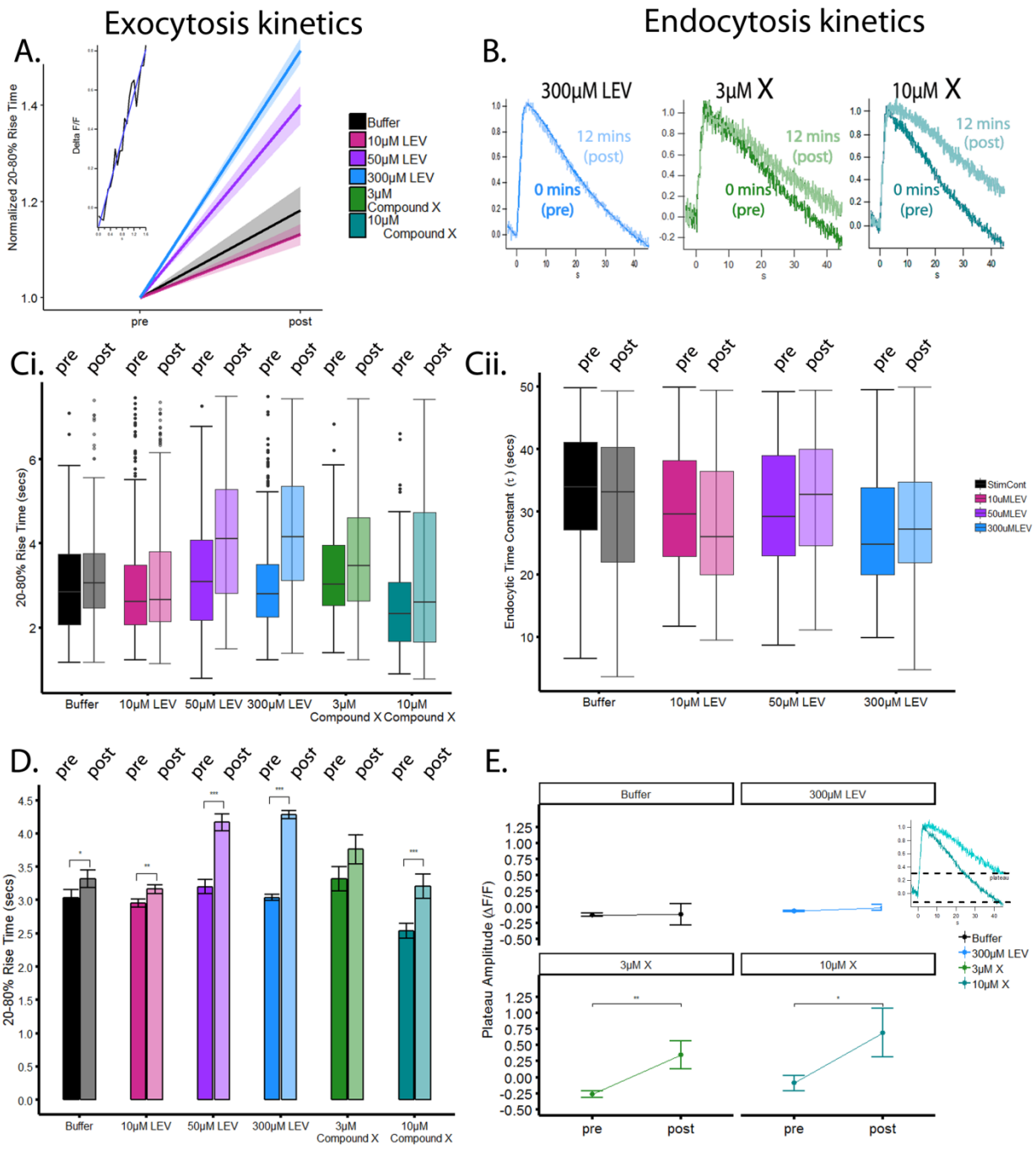

Fig 4.5 Levetiracetam slows exocytosis of the RRP in a concentration dependent manner but does not affect endocytosis A) Plotting relative change in exocytosis between 0mins and 12mins reveals a concentration-dependent slowing of RRP release in response to LEV (insert - graphic to show linear fit of 20-80% rise time *(y=ax+b,* where *a* and *b* correspond to the best-fit coefficients of a given trace). This was calculated in Igor Pro using a singular value decomposition algorithm). B. Responses to 40aps at 20 Hz pre- and post- addition of compound (N.B. pre- and post- refer to time 0 and 12 mins). Traces are shown normalized to *Fmax* to ease visualization of differences

between endocytic profiles. C(i). Boxplots showing the distribution of 20-80% rise time pre- and post- addition of compound and 150AP stimulation. Inverse values of the linear fit are plotted to give a measure of 20-80% rising time in seconds. Central divisions represent medians; shaded areas, the IQR, and whiskers extend to 1.5 x IQR. C(ii). Boxplots comparing endocytosis across different concentrations of LEV as described by a single exponential fit. Boxplot parameters are the same as Ci. D. Comparison of mean 20-80% rise times pre- and post- compound and 150AP stim (Mean ± SEM). Significant increases in exocytosis rate were seen in the buffer, p = 0.0352; 10µM LEV, p = 0.00147; 50µM LEV, p < 0.001; 300µM LEV, p < 0.001 and 10µM Compound X – compared using paired sample t-tests. E) Plot comparing plateau amplitude pre- and post-addition of compound and 150AP stim, significant increases in height of plateau were seen with 3µM and 10µM Compound X; p values = 0.0121 and 0.0478 respectively.

It is clear from the data presented in Fig 4.5 (Ai, Ci and Di) that LEV slows the rate of exocytosis in a concentration-dependent manner, with 50µM and 300µM increasing the 20-80% rise time by 0.965 and 1.25 seconds respectively (Fig 4.5.D). Addition of 10µM LEV also slowed exocytosis significantly (~0.2 seconds), however this is similar to the changes in exocytosis seen pre- and post-150AP stimulation in the buffer control. 10µM of the alternative SV2A modulator, Compound X also significantly increased 20-80% rise time, however did not have an effect at 3µM (Fig 4.5.Ciii). The initial time of exocytosis, before addition of compound or 150AP stimulation, was similar across the different treatment groups (Fig 4.5.Ci).

LEV did not have an impact upon endocytosis even at the relatively high concentration of 300µM (Fig 4.5.Cii). However, treatment with Compound X impacted on the ability of the vesicles to complete endocytosis at 3µM and 10µM (Fig 4.5.Diii), and neurons treated with 3µM and 10µM of Compound X experienced rises in final plateau amplitude of approximately 0.5 (3µM) and 0.75 (10µM) when compared to their baseline readouts. Therefore, the degree at which Compound X contributes to failure of endocytosis appears concentration-dependent. This, coupled with the lack of variation in plateau amplitude in both the control and LEV conditions, gives confidence that this is a true effect of the compound. It is worth noting that, unlike LEV, Compound X had no significant impact on the size of the RRP (40APS, 20Hz), despite the presence of a high intensity stimulation (Fig 4.3.1).

Overall, our data suggests that SV2A is a modulator of exocytosis. Therefore, given that SV2A has been shown to co-traffic with the calcium-sensor, synaptotagmin – 1, we decided to carry out co-immunoprecipitation in order to see if the presence of LEV affected this. To do so, we incubated the cells in 300µM LEV in EBS and blockers. However, because LEV appears to have an activity – dependent component, we increased the concentration of the K^+ in the EBS to 70mM (adjusting

NaCl content accordingly) to induce neuronal activity. Following 10 minutes incubation, cell lysis and co-immunoprecipitation were performed as described in section 2.3.2. Briefly, Dynamin-G beads were coated in SV2A primary antibody and incubated with lysates. Presence of SV2A and synaptotagmin – 1 was confirmed using western blot.

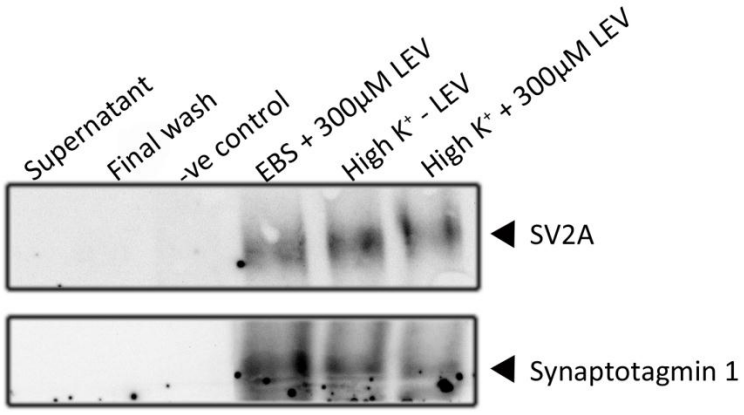

Fig 4.5.1 Co-immunoprecipitation of SV2A and synaptotagmin – 1: 100µg of protein was loaded into each well. Supernatant and final wash samples demonstrate the high binding efficiency of SV2A primary antibody and lack of band in –ve control (no primary antibody) suggests that binding is specific. SV2A successfully co-traffics with synaptotagmin – 1 in the presence of LEV in high (high K^+) and low activity states (regular EBS), although quantification was not possible as from a single experiment.

4.2.3. The effect of LEV on presynaptic Ca^{2+}

Although SV2A has been identified as the major binding site for levetiracetam (Lynch et al., 2009) and it has been demonstrated that seizures in SV2A KO mice are insensitive to treatment with LEV, indicating that this is most likely to be the primary method by which it exerts its anticonvulsant effect (Kaminski et al., 2009), other research in the field has implicated the involvement of N-type and P/Q-type high voltage-dependent Ca^{2+} channels (VDCC) (Lukyanetz et al., 2002, Pisani et al., 2004, Costa et al., 2006, Lee et al., 2009a), and also release of Ca^{2+} from intracellular stores **(**Nagarkatti et al., 2008**).** Expression and functionality of VDCCs is intrinsically linked to neurotransmitter release at the presynaptic terminal (Catterall, 1998, Neher and Sakaba, 2008, Wadel et al., 2007). At small, central synapses, P/Q-type channels are the more abundant and their dysfunction has widely been acknowledged to be a contributing factor in some epileptic phenotypes (Rajakulendran et al., 2010, Jun et al., 1999).

Taking this information into account, we wanted to determine the impact of LEV upon presynaptic Ca^{2+} dynamics in our model system. This was especially relevant as VDCCs are activated during times of high neuronal activity and thus could theoretically account for the use-dependence seen in section 4.2.1. To test this, we exploited AAV6_syGCaMP6f (reviewed in Chapter 3, section 3.3.2), a fluorescent reporter that provides an optical readout of presynaptic calcium. The protocol used was effectively identical to that described in Section 4.2.1 (Fig 4.3.A).

Preparation of cultures, infection with AAV6_syGCaMP6f and experimental conditions were as described in the Methods section (2.1). Prior to the first stimulus shown in the protocol, cultures were stimulated with a single round of 40APs and imaged. As in the sypHy assay discussed in 4.2.1., this ensured the selection of a responsive region, pre-bleached the sample so as to remove the residual surface fluorescence, and the image stack was later used to create an unbiased ROI mask using Igor Pro. All experiments were conducted in EBS supplemented with the NMDA and AMPA receptor blockers AP-V and CNQX. LEV was dissolved in 300µl EBS (plus blockers) and introduced to the chamber via exchange of half the buffer volume (i.e. 300µl in a total volume of 600µl).

Analysis was carried out on baseline (ΔF/F) and bleach corrected data. Traces from trials 2-4 were normalized to the first response, pre-addition of LEV, to establish any significant effect. Peak amplitude was calculated via subtracting the average of the baseline before the onset of the stimulus (frames 1-8) from the average of the peak (frames 30-35).

Our experiments revealed that concentrations of 10 µM and 50µM LEV levetiracetam did not significantly affect levels of presynaptic Ca^{2+} in our experimental system (Fig 4.6.Cii. and ii.) At the highest concentration, 300µM, significant within-subject effects can be seen after 10 and 12 minutes (Fig 4.6.C.iv), suggesting that perhaps at higher concentrations LEV can have an impact on Ca^{2+} dynamics. However, one-way ANOVAS with Tukey's post-hoc comparisons conducted at each time point revealed no significant impact to presynaptic Ca^{2+} activity at of any of the concentrations assayed (Fig 4.6.E). This is in contrary to our observations on vesicle recycling (4.2.1), where significant, concentration-dependent effects can be seen at 12 minutes (Fig 4.4.E). Although non-significant, it is clear that 300µM LEV depresses presynaptic Ca^{2+} to some extent (Figs 4.6.D and E), however, given the lack of concentration-dependent modulation, it is unlikely that this is the primary mechanism through which it modulates presynaptic release and is more likely to be an off-target effect seen at higher concentrations.

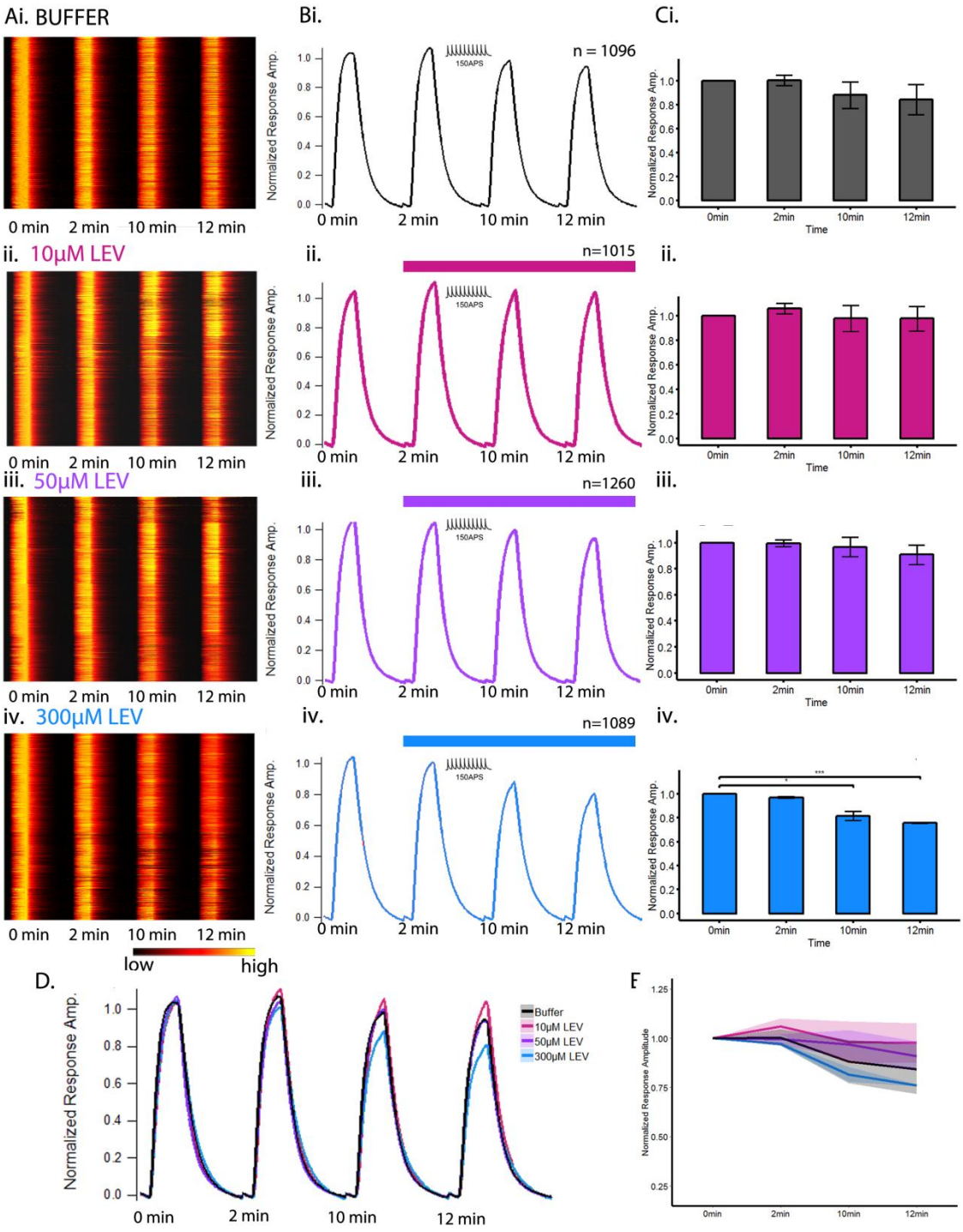

Fig 4.6 Presynaptic Ca^{2+} levels are not significantly influenced by levetiracetam A(i-iv). Heatplots illustrating intensity of responses in each trial B(i-iv). Normalized, averaged traces from each concentration assayed; traces were baseline subtracted and subsequently divided by the

baseline fluorescence in order to generate baseline corrected (ΔF/F) and bleach-corrected response profiles. Traces from trials 2-4 are shown normalized to the first response, pre-addition of LEV. Numbers of synapses in the final datasets are indicated above the traces, all from 3 separate experiments. C(i-iv). Change in response amplitude at each time point per concentration assayed. Peak amplitude was calculated via subtracting the average of the baseline before the onset of the stimulus (frames 1-8) from the average of the peak (frames 30-35). Amplitude in trials 2-4 was normalized to the amplitude of the first response. 300µM LEV significantly impacted at 10 min (p=0.0379) and 12 min (p < 0.001), (Student's paired t-tests). Values of average non-normalized peak amplitudes ± SEM (ΔF/F): Buffer (Ci) 0 mins: 2.90 ± 0.038, 2mins: 2.96 ±0.0037, 10 mins: 2.69 ± 0.034, 12 mins: 3.61 ± 0.034; 10µM LEV (Cii) 0 mins: 3.212 ± 0.040, 2 mins: 3.31 ± 0.033, 10 mins: 2.97 ± 0.032, 12 mins: 2.96 ± 0.032; 50µM LEV (Ciii) 0mins: 3.46 ± 0.029, 2 mins: 3.34 ± 0.027, 10 mins: 3.08 ± 0.0026, 12 mins: 2.92 ± 0.024; 300µM LEV (Civ) 0 mins: 3.34 ± 0.030, 2 mins: 3.17 ± 0.029, 10 mins: 2.68 ± 0.028, 12 mins: 2.48 ± 0.026. E) Composite of traces at each concentration. F) Graphical comparison between each condition at each time point (Mean Amplitude ± SEM; standard error of measurement is indicated via shading. One-way ANOVAs with Tukey's post-hoc comparisons revealed no significant differences between conditions at any time point.

4.3 Levetiracetam modulates vesicle pool sizes at small central synapses

Once we were confident that the depression in RRP amplitude caused by levetiracetam in our model system was most likely mediated by SV2A, we wanted to investigate possible mechanisms by which this depression could be occurring. One such possibility is via alterations in vesicle pool size; for example, in chromaffin cells, knockout of SV2A has been shown to reduce the size of the RRP of secretory vesicles (Xu and Bajjalieh, 2001). Therefore, we sought to establish whether SV2A, and by extension LEV, had a significant impact on vesicle pool sizes in primary hippocampal neurons.

In order to do so, we exploited the properties of bafilomycin A1 (baf), a cell permeable, v-ATP-ase inhibitor that acts by blocking reacidification of newly endocytosed vesicles, thus trapping them in an alkaline state and preventing their reuse in subsequent rounds of stimulation (Fernandez-Alfonso and Ryan, 2008). In our experiments, cultures were prepared and infected with AAV6_sypHy1x, as described in section 2.1. Firstly, a responsive region was identified by using a 40AP, 20Hz stimulus (recorded for ROI identification and to pre-bleach surface fluorescence). A second round of 40AP stimulation was administered 2 minutes later (first round shown on protocol), after which neurons were treated with 300µM LEV and subjected to 150AP stimulation to promote compound activity (as described in 4.2.1). As in previous experiments, a 6 minute

period was allowed to elapse before further stimulation (40APS, 20Hz). By using this method, we could generate a readout of RRP size pre- and post- addition of compound. Following the second RRP-recruiting stimulus and a 2 minute recovery period, 1µM bafilomycin was added to the culture and allowed to incubate for 1 minute before the cells were stimulated with a 600AP, 20Hz stimulus to mobilize the recycling pool. Finally, cells were incubated in EBS containing NH_4Cl (+LEV when appropriate). Exposure to NH_4Cl serves to neutralize the pH of all remaining acidic synaptic vesicles within the terminal, therefore generating a functional readout of total pool size (Miesenbock et al., 1998). A schematic of the protocol is provided in Fig 4.7.A. Typical changes in fluorescence corresponding to RRP, recycling pool (TRP) and total pool (TP) size are shown in Fig 4.7.B.

When response amplitudes are normalized to the size of the total pool, 300µM LEV strikingly increases the size of the recycling fraction of vesicles when compared to the control condition (buffer); $p<0.001$, independent samples t-test (Fig.4.7.C). In the control condition, the mean size of the recycling fraction was found to be 54.0% (± 1.15) of the total pool size, a value analogous to other data recorded previously in the lab (Ratnayaka et al., 2012) and other published works in this field (Fernandez-Alfonso and Ryan, 2008, Kim and Ryan, 2010). However, acute application of 300µM LEV administered alongside a high intensity 150AP stimulus increased the size of this recycling fraction to 71.9 % (± 0.653). Unexpectedly, the fractional size of the RRP was also significantly larger in the LEV condition than in the control (Fig 4.7.F); prior to the treatment the RRP fraction was 61.7% of the final total pool size. Which decreased to 39.2% post- treatment and stimulation. In the control condition, the fractional size of the RRP remained more stable: 24.2% prior to stimulation and 15.8% after stimulation; suggesting, as in previous experiments, that there are some modulatory effects of the 150AP stimulus. Nonetheless, neurons treated with 300µM LEV underwent significantly greater changes than those subjected to stimulus alone. Perhaps most intriguing is the very large fractional size of the first RRP readout in neurons before treatment with LEV (61.7% cf 24.2% in controls); this could suggest that LEV may modulate the size of the total pool of vesicles in such a way that vesicles are lost from the synapse.

The design of this protocol allowed us to explore the absolute relationships between different vesicle pool sizes. For this analysis, raw, non-normalized, non-baseline/bleach corrected traces were used. The size of the RRP was calculated by subtracting the average baseline fluorescence from RRP_{Fmax}, and the size of the TRP calculated by subtracting the average baseline fluorescence

from TRP_{Fmax}. To account for bleaching of fluorescence over time, the baseline size of each pool was regarded as the 10 frames prior to that particular stimulation; the baseline for the total pool ($+NH_4Cl$) was regarded to be same as for the TRP. TP amplitude was calculated by subtracting the baseline from the average of the first 50 frames post addition of NH_4Cl.

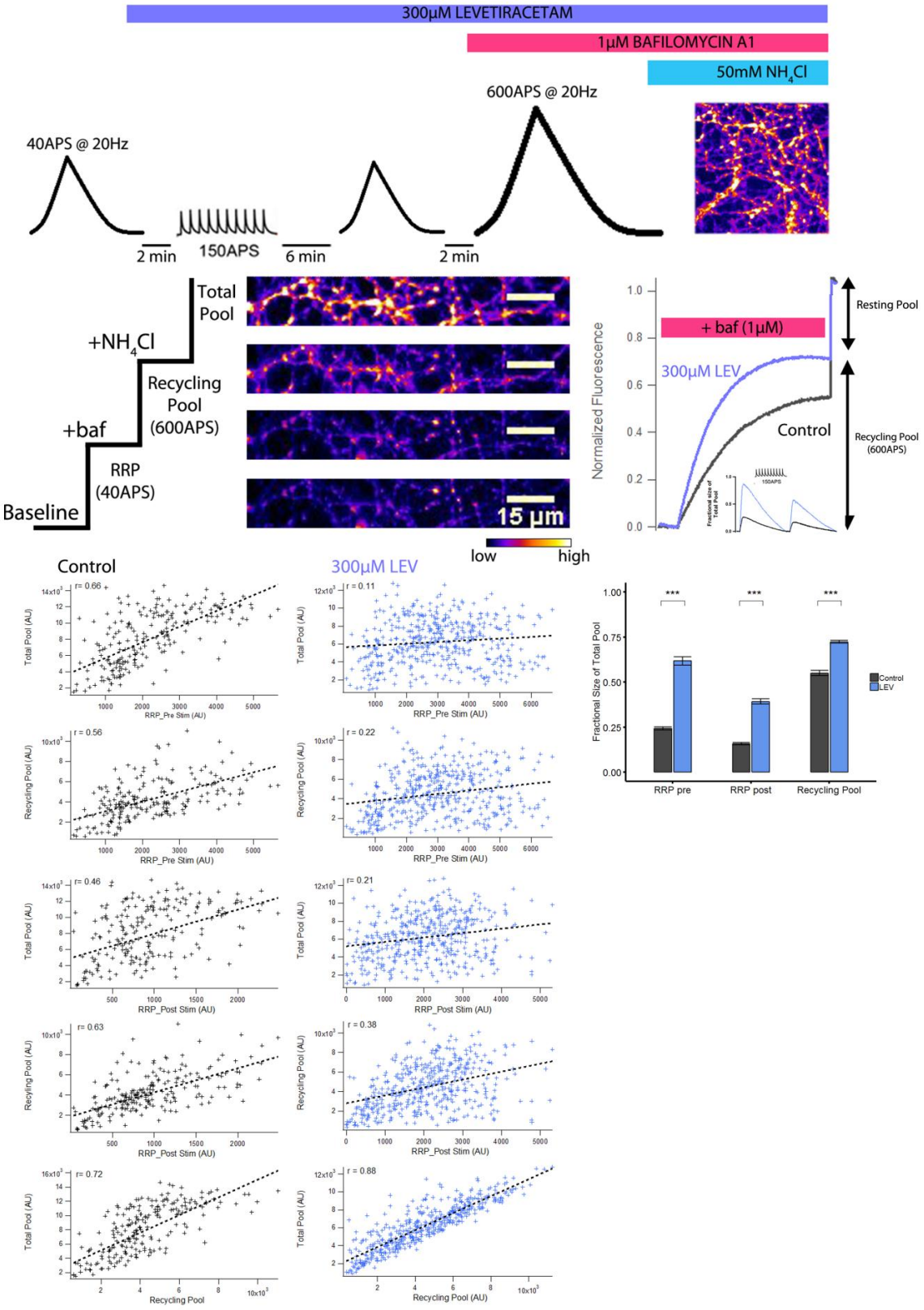

Fig 4.7 Fractional size of synaptic vesicle pools is disrupted by levetiracetam A) Schematic of protocol used B) Experimental steps taken to quantify vesicle pool size. Images represent

fluorescence intensity at each stage of the experiment C) (outer TRP, insert RRP) Measurement of the vesicle pool sizes revealed recycling and RRP fractions to be higher in LEV-treated synapses than in control; p<0.001 in both instances (Student's independent sample t-test). D(i-iv). Relationships between vesicle pool sizes in control condition (n=358 from 3 experiments), Pearson's correlation test: Total pool vs RRPpre = 0.66, RP vs RRPpre = 0.56, Total pool vs RRPpost = 0.46, RP vs RRPpost = 0.63, RP vs Total pool = 0.73). E(i-iv) Relationships between vesicle pool sizes in synapses treated with 300µM LEV (n=757 from 4 experiments, Pearson's correlation test: Total pool vs RRPpre = 0.11, RP vs RRPpre = 0.22, Total pool vs RRPpost = 0.21, RP vs RRPpost = 0.38, RP vs Total pool = 0.88). F) Significant increases in fractional pool sizes can be seen in neurons treated with LEV; p<0.001 in all instances (Student's Independent sample t-test).

In the control condition, all vesicle pools exhibited some correlation in size (Fig 4.7.D(i-iv)) Interestingly, the size of the RRP pre-stimulation with 150APS was better correlated to the size of the total pool (R=0.66) than the size of the RRP afterward (R = 0.46). The opposite was true for the scaling of the RRP with the TRP, whereby the size of the RRP measured pre-stimulation was not as well correlated with TRP size as that measured post-stimulation (R = 0.56 cf R = 0.63). One explanation for this could be that in normal synapses factors which control proportional size of the RRP to the TRP are tightly regulated; therefore the size of the TRP in this protocol, measured after the synapse has undergone high frequency stimulation, is likely to be better related to the size of the RRP measured after the high frequency stimulation. In regards to the relationship between RRP and TP size, assuming the size of the total pool remains stable throughout the experiment and that the 150AP stimulus only affects vesicles in the recycling fraction, it is logical that the initial RRP size readout would be better correlated to the total population of vesicles in the synapse.

In synapses treated with LEV, the RRP size (pre- and post- stimulation) is very weakly correlated with the TP and TRP sizes. So, the question is how does addition of LEV disrupt this finely tuned system? One possibility is revealed by Figures 4.8.C and D. These example traces, each averaged from one experiment and shown normalized to the size of the total pool, show that in the control condition the RRP, RP and TP scale as one would expect: RRP < TRP < TP. However, in synapses treated with LEV this is no longer the case. In these synapses, the fractional size of the RRP pre-addition of LEV is much larger; in Fig 4.8.Di, the size the RRP pre-LEV is virtually the same size as the size of the TRP measured post-LEV. In 4.8.Dii, the size of the RRP measured both pre- and post- LEV is larger than the size of the total pool itself; offering compelling evidence of a net loss of functional vesicles from the total pool post-addition of LEV.

Intriguingly, TRP and TP sizes scale better in the LEV-treated synapses than in the control (R=0.88 cf R=0.72) (Fig 4.8.Bi). However, if vesicles are lost from the total pool, then it is likely that a maximal stimulus such as 600AP would release a fractionally higher number of vesicles, as evident in synapses treated with LEV (Fig 4.7.F). As very little time elapsed between the end of the 600AP stimulus recording and the neutralization of the remaining vesicles, it could be possible that very few vesicles were rendered non-functional during this time. Therefore the size of the TRP still strongly correlates with the size of the TP.

To further unpick the effects of LEV on vesicle pool sizes, we decided to group the synapses by total pool size. The range of TP size was calculated and divided by 3 to give 3 subcategories of synapses: small, medium and large. As shown in Fig 4.8.E., the fractional size of the RRP in synapses with a small total pool size is much larger than those with a large total pool size, perhaps reflective of synapses that have lost a greater number of functional vesicles vs. those that have lost fewer or had larger populations to start with. In the control condition, the fractional size of the RRP does not fluctuate greatly between small, medium and large synapses suggesting that the changes in RRP fraction in the LEV-treated synapses are occurring from modulation upstream of the RRP.

Surprisingly, the fractional size of the TRP is not significantly different between control and LEV conditions in small synapses, although this may be because smaller synapses often display larger recycling fractions than larger synapses (Welzel et al., 2011). In medium and large synapses, the recycling fraction of the control remains stable at ~0.5 and the recycling fraction in synapses treated with LEV is significantly greater ($p < 0.001$ in both instances, independent t-test).

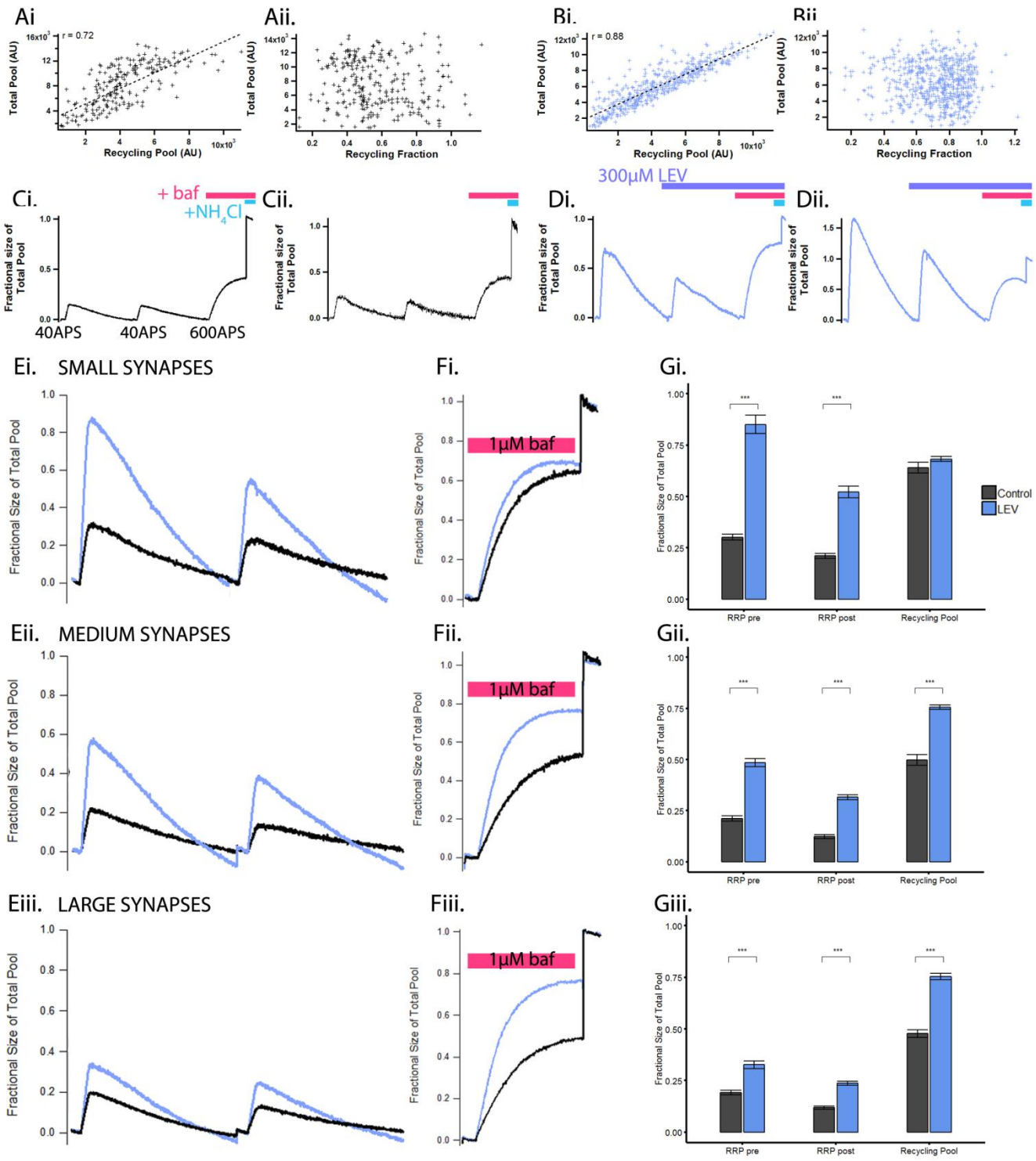

Fig 4.8 The actions of LEV on vesicle pool size in relation to total pool size (Ai and Bi) Relationships between recycling pool size and total pool fraction are correlated in both LEV and control conditions (Control: n=358 from 3 experiments, R= 0.73; 300μM LEV: n=757 from 4 experiments, R=0.88) Aii and Bii) Relationships between recycling fraction and total pool size are not correlated in either control or LEV treated groups. Example average traces taken from single experiments reveal that untreated synapses have similar RRP sizes throughout the experiment and that TRP is 0.5. D(i-ii). Functional vesicles are lost from the total pool following treatment

G(i-iv) Comparison of mean vesicle pool sizes. All comparisons shown on graph are significant at $p < 0.001$ (Students t-test).

Figure 4.9 depicts heat intensity plots generated from an average z-projection of the first 10 frames of imaging i.e. before onset of the respective round of stimulation. Prior to any stimulation or drug application, synapses in both the control and LEV conditions appear similarly punctate (LHS). However, upon addition of LEV and recycling pool turnover (150APs), boutons appear to be more diffuse and much brighter than the control (central panels). The same is true post-addition of NH_4Cl, where the unquenching of the total fluorescence reveals diffuse fluorescence patterning in cultures treated with 300µM LEV, contrary to the punctate staining still evident in the control (RHS).

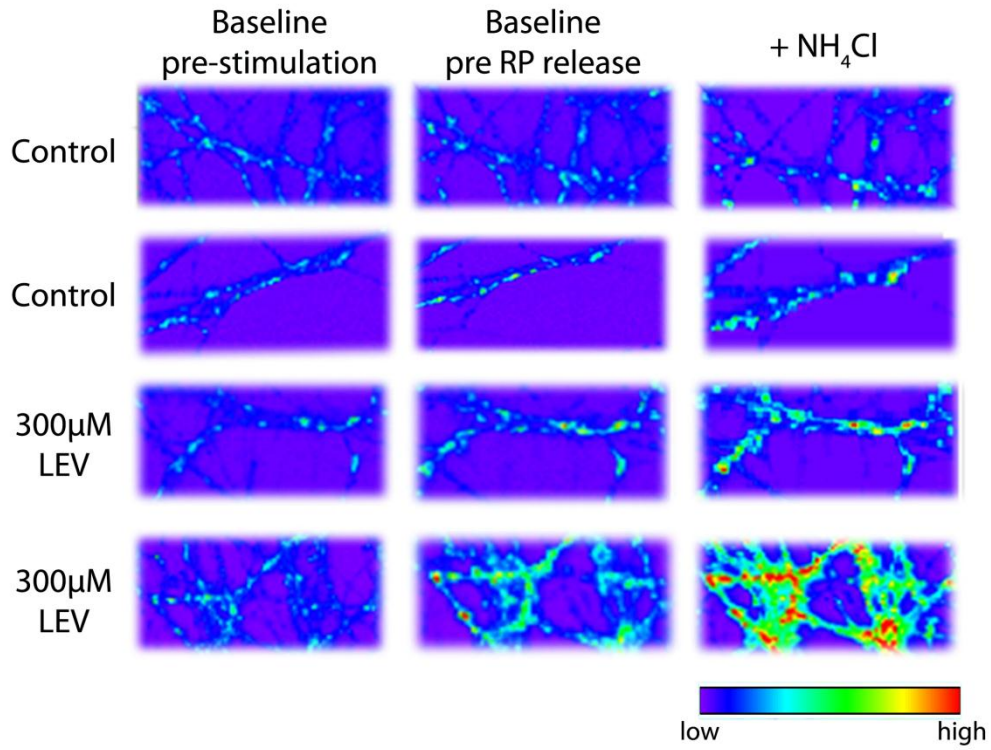

Fig 4.9 Heat intensity plots of basal fluorescence prior to RRP and TRP stimuli and after addition of NH_4Cl.

To further investigate the rise in basal fluorescence seen post-addition of LEV, we examined the raw, non-baseline corrected traces from the alkaline-trapping experiment (Fig 4.10). Although all

the cultures used in these experiments were between DIV 14-21, plated at the same density and had reporter added at DIV 7 (MOI 200), which should serve to equalize levels of reporter expression, some variation in basal fluorescence is inevitable. Therefore, when comparing raw fluorescence, a subset of the data was created whereby baseline fluorescence was within mean ± 1 St. Dev of the control group. Figure 4.10.1a depicts the average trace for this control group; between the first and second 40AP stimuli, there is a lowering of baseline fluorescence, which can be accounted for by fluorescence bleaching. However, in neurons treated with 300μM LEV, there is a significant rise in basal fluorescence between the first and second RRP-releasing stimuli, and again before the TRP-releasing stimulus (600AP) (Fig 4.10.1b- highlighted via black outline). A minor rise in basal fluorescence is also seen at this point in the control condition (4.10.1a), however this is likely due to addition of the bafilomycin, which is well documented to cause slow, spontaneous alkalization of vesicles following exposure (Li et al., 2005) . Nevertheless, the rise in baseline fluorescence after addition of bafilomycin is more dramatic in synapses exposed to LEV.

To explore whether this effect was dependent on the fusion of LEV to its target protein, presumably SV2A, we examined the raw data traces from the experiments conducted on use-dependence (Fig 4.10.2). The rationale was that if the rise in fluorescence was a result of LEV binding to SV2A and becoming pharmacologically active, as opposed to other non-specific interactions, then a rise in baseline fluorescence would be seen following the 150AP stimulus given to recruit the recycling pool but that this would be absent in neurons treated with LEV without recycling pool turnover. Figure 4.10. shows that in the presence of 300μM LEV an increase in basal fluorescence is indeed present post-TRP recruitment (a), however presence of LEV without TRP-recruitment is insufficient to raise baseline fluorescence (b). Direct comparison is made in the composite panel; Figure 4.10.2c. Therefore, this is indicative that the interaction of LEV with SV2A is essential in causing this alkalization reaction.

Finally, we examined whether this property was inherent to SV2A modulators via comparing neurons treated acutely with 300μM LEV with those treated acutely with 3μM Compound X (Fig 4.10.2d). Contrary to LEV, synapses treated with Compound X and subjected to the TRP-recruiting pool stimulus failed to alkalize vesicles. Therefore we can ascertain that this effect is not a consequence of general SV2A modulation but is a specific characteristic of levetiracetam.

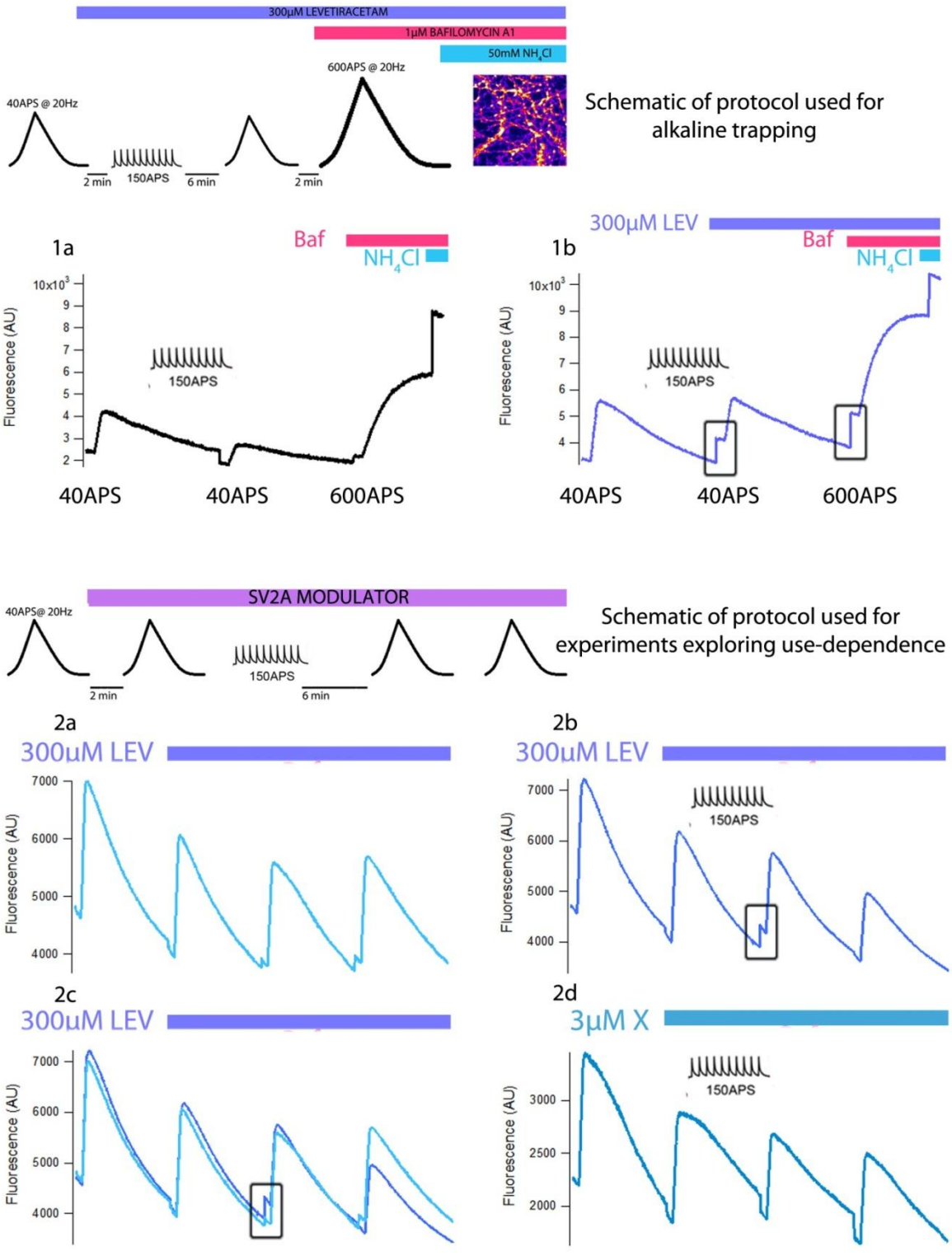

Fig 4.10. Application of LEV results in alkalization of vesicles 1) Average traces of alkaline trapping experiments (a) control, (b) 300µM LEV. 2) Average traces: 4x 40AP stimulation: (a)

300µM LEV; (b) 300µM LEV plus recycling pool turnover; (c) Composite of (a) and (b); (d) 3µM Compound X plus recycling pool turnover.

4.4. *ρr* at small central terminals is influenced by levetiracetam

Reduced synaptic depression, a form of short-term plasticity which correlates closely with release probability (Dobrunz and Stevens, 1997), is a hallmark of both SV2A KO and overexpression (Custer et al., 2006). In whole-cell patch clamp, autaptic hippocampal preparations over expressing SV2A display reduced synaptic depression following trains of 25 pulses administered at 10Hz. When cultures are subsequently incubated with 100µM LEV for 6-10hrs, regular synaptic depression is recovered (Nowack et al., 2011). Since synaptic depression and *ρr* are intrinsically linked, this is interpreted by the authors as having LEV restoring a normal *ρr* phenotype to neurons overexpressing SV2A (Nowack et al., 2011).

Several fluorescent dyes and genetic constructs have been used previously to capture single vesicle release events: FM1-43 (Aravanis et al., 2003, Chen et al., 2008), synaptopHluorin (Gandhi and Stevens, 2003), sypHy (Zhu et al., 2009), and vGLUT1-pH. Since pervious work in our lab has demonstrated that our imaging system is suited for capturing single vesicle release events, we utilized this to determine whether LEV had an influential effect upon *ρr* in our model system. Before doing so, it was first necessary to establish the signal corresponding to a single release event. Cultures were infected with AAV6_sypHy1x on DIV 7 and imaged at DIV 14 21 in EBS containing 20µM CNQX and 50µM AP-V.

Once a suitable region with a robust response had been identified, cultures were subjected to 10 rounds of a 4AP, 20Hz stimulus. Although highly variable, the probability of release at hippocampal synapses has been estimated to be 0.22±0.03 (Branco et al., 2008), meaning that stimulation with a single action potential gives rise to a release event ~25% of the time. Therefore, we opted for a 4AP stimulation, which increases the likelihood of capturing a single fusion event. Following the first round of stimulation, 300µM LEV was added to the bath via exchange of half the buffer volume (300µl) and a 2 minute window observed before a 150AP (20Hz) stimulus was given to encourage TRP turnover. In our previous experiments, 150AP stimulation was significant in depressing the response of the RRP even after six minutes was allowed for recovery (Fig 4.3.Dii). Therefore, given the extremely sensitive nature of these experiments, which are likely to be more

influenced by noise than the robust RRP response, we increased the recovery time following 150AP stimulation in these experiments to 10 minutes. Cultures were then subjected to a second round of 10x 4AP stimulation. ROIs were identified using the SARFIA plugin, Igor Pro (version 6.36, Wavemetrics) and a mask created based upon the first round of 4AP stimulation.

The distribution of response amplitudes of 1100 events from 110 synapses can be well described by a multiple Gaussian fit (Fig 4.11.B). The first peak is located at an intensity of 82.5 ΔF/F and corresponds to events that have failed to result in vesicle release; one may expect this value to be located to closer to 0, however during initial image analysis a section of the background is selected in each image stack from which an average fluorescence value is generated and used as a baseline to correct the other values. Therefore, the background of the image is taken as absolute zero and synapses which have been identified by the standard deviation algorithm but do not respond will always have a fluorescence value greater than 0. The second peak, which reflects the synapses which have released a single quanta i.e. a single release event, is located at ΔF= 287.5± 37.4 AU. The width of the peak was used to determine the size of a quantum; ΔF_Q= 249.6-324.4. We then applied this value to our analysis. When the identical multiple Gaussian fit was applied to the z-scores of the same data, the average fluorescence value of a single release event was shown to correspond to an average z-score of 0.175. This value was used as the minimum threshold in determining a release event in subsequent analysis.

Figures 4.11.Ci and 4.11.Cii show the average traces generated from these experiments. Prior to the addition of 300μM LEV, 4AP stimulation elicits responses of similar amplitude (Fig 4.11.Ci), however, following addition of LEV and 150AP stimulation, facilitation of the response occurs (Fig 4.11.Cii). This data is shown graphically in Figure 4.11.D; although non-significant, LEV treated neurons have larger responses at each time point in second round of stimulation. Figures 4.11.Ei and Eii show cumulative frequency plots of the probability of a single release event, determined from the number of trials that a synapse successfully initiates vesicle release pre- and post-recycling pool turnover ± 300μM LEV. In the control (Fig 4.11.Ei), the 150AP stimulation results in a slightly left-shifted distribution (dashed line), indicative of fewer successful release events and thus reflective of a slight but significant reduction in ρr ($p<0.001$, Kolmogorov – Smirnov test). In neurons treated with 300μM LEV, the opposite holds true; the distribution following the addition of LEV and the recycling pool turnover appears right-shifted (Fig 4.11.Eii), and thus can be interpreted as an increase in ρr ($p<0.001$, Kolmogorov – Smirnov test). These results corroborate

the findings of Nowack et. al., who demonstrated that application of levetiracetam could restore the abnormally low *ρr* phenotype in neurons overexpressing SV2A to normal levels (Nowack et al., 2011).

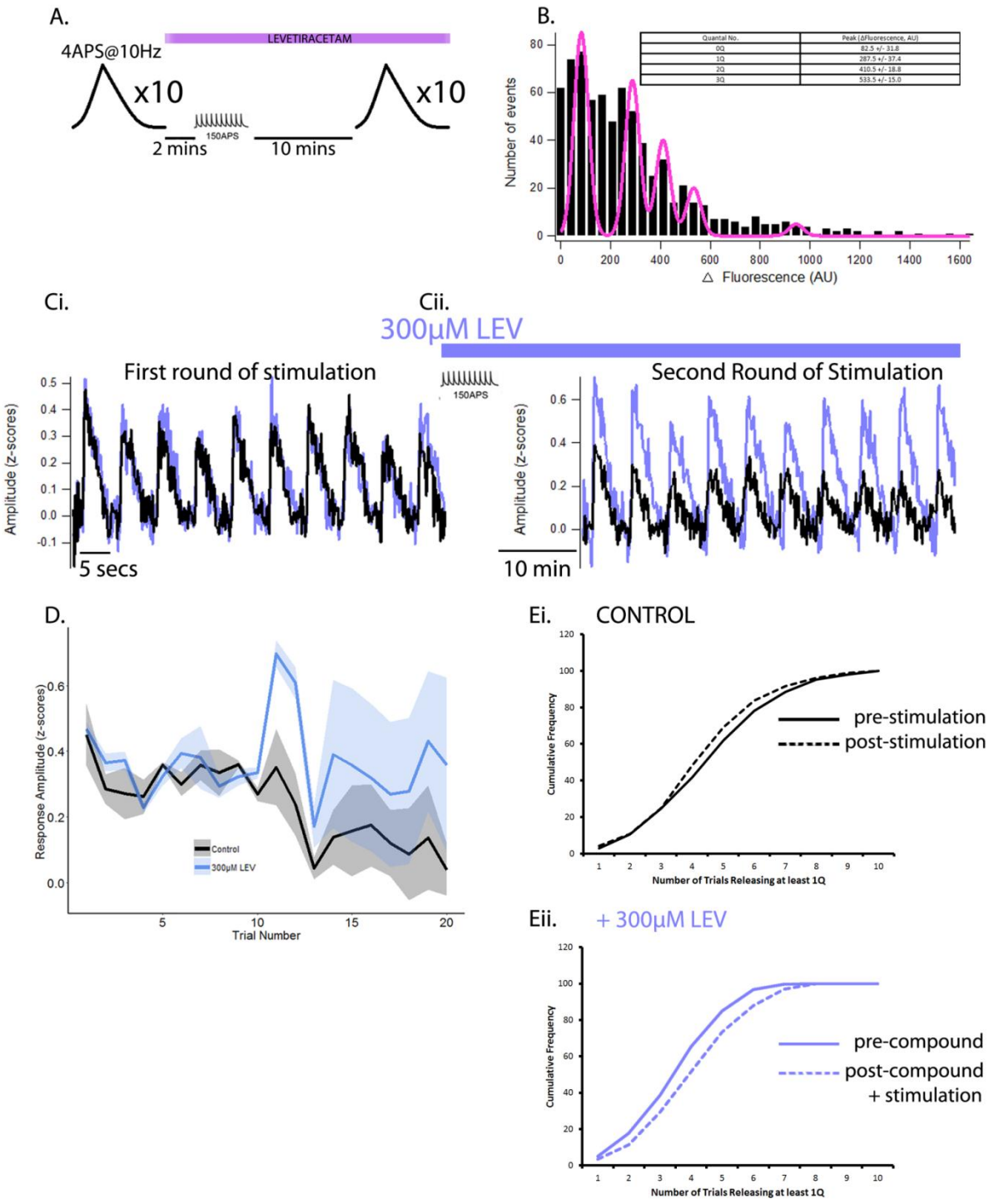

Fig 4.11. LEV inflences pr A) Schematic represents the protocol used for data collection. Synapses were imaged whilst being stimulated 10 times with a 4AP stimulus. B) Histogram of fluorescence amplitudes of 1100 events from 110 synapses, 3 experiments. Pink line represents multiple Gaussian fit revealing peaks at 81.8 ± 31.8, 287.5 ± 37.4, 410.5 ± 18.8 and 533.5 ± 15.0. C(i) Average traces in response to 10 rounds of 4AP (20Hz) stimulation, pre TRP-turnover and LEV addition; Control (black), n= 110, LEV (blue), n= 44. C(ii) Average traces in response to 10 rounds of 4AP(20Hz) stimulation, post TRP-turnover and LEV addition; Control (black), n= 110,

LEV (blue), n= 44. D. Graphical representation of data shown in Ci and Cii. Shading indicates SEM. E(i-ii). Cumulative frequency plots showing distribution of *ρr* before and after recycling pool turnover/ LEV treatment. Solid lines correspond to the first 10 rounds of stimulation, and the dashed lines the second. Kolmogorov – Smirnov tests comparing the distribution of release events pre and post the addition of LEV / high intensity stimulation revealed that the probability of release in the control condition significantly decreases post-150AP stimulation ($p<0.0001$), whereas in the LEV treated synapses *ρr* significantly increased post- addition of compound and 150AP stimulation.

4.5 Modulation of SV2A shows sensitivity to stimuli of varying frequency

As mentioned in the introduction to this chapter, previous research has indicated that SV2A may play a role in low-frequency neurotransmission. Therefore, after showing that levetiracetam had a marked effect when using a high intensity stimulus paradigm, we wanted to find out if any modulatory effect was apparent at lower frequencies. To test this, we used cultures infected with AAV6_sypHy1x, and explored vesicle release and retrieval following a 20AP, 2Hz stimulation in response to levetiracetam and other SV2A modulators. These other modulators cannot be named for purposes of intellectual property.

As the schematic in Fig 4.12.A shows, neurons were subjected to five rounds of 20AP, 2Hz stimulation, separated by an inter-stimulus interval of 1 minute. The first two rounds of stimuli were conducted in EBS (plus 20µM AP-V and 50µM CNQX), after which the respective concentration of SV2A modulator was added via exchange of half the buffer solution (300µl) and an incubation time of 15 minutes observed. As in the previous experiments, a single round of stimulation and imaging was conducted prior to the start of the experiment to identify responding boutons and for subsequent ROI detection during the analysis; 20APs was applied at 20Hz for this stimulus to aid visual detection of responses. Following this, two minutes were allowed to elapse before beginning the experiment itself.

Figure 4.12.B shows the traces of the average responses normalized to the amplitude of the first response. To minimize the impact of the higher signal-to-noise ratio experienced in experiments conducted at low-frequency stimulation, traces were corrected for the standard deviation of the baseline fluorescence (Frames 1-8), bleach corrected and expressed as z-scores. From panel 4.12.B, it is evident that 300µM LEV has no impact at low intensity stimulation. The same is true for Compound Y, however Compound X, which showed no modulatory effect on RRP amplitude

even following TRP-recruitment (Fig 4.3.1), demonstrated an approximate 31% decrease in response amplitude after 16 and 17 minutes of incubation (p-values 0.0192 and 0.00792). Taken together, our observations indicate that ligand-binding of SV2A can be influenced dramatically by the activity status of the neuron, with some SV2A modulators favouring a high intensity period of activity and others favouring the opposite. The fact that SV2A ligand efficacy can be influenced dramatically via stimulus intensity and frequency perhaps suggests a role for SV2A in the encoding of stimulus input and the ability of the presynaptic terminal to regulate vesicle release accordingly.

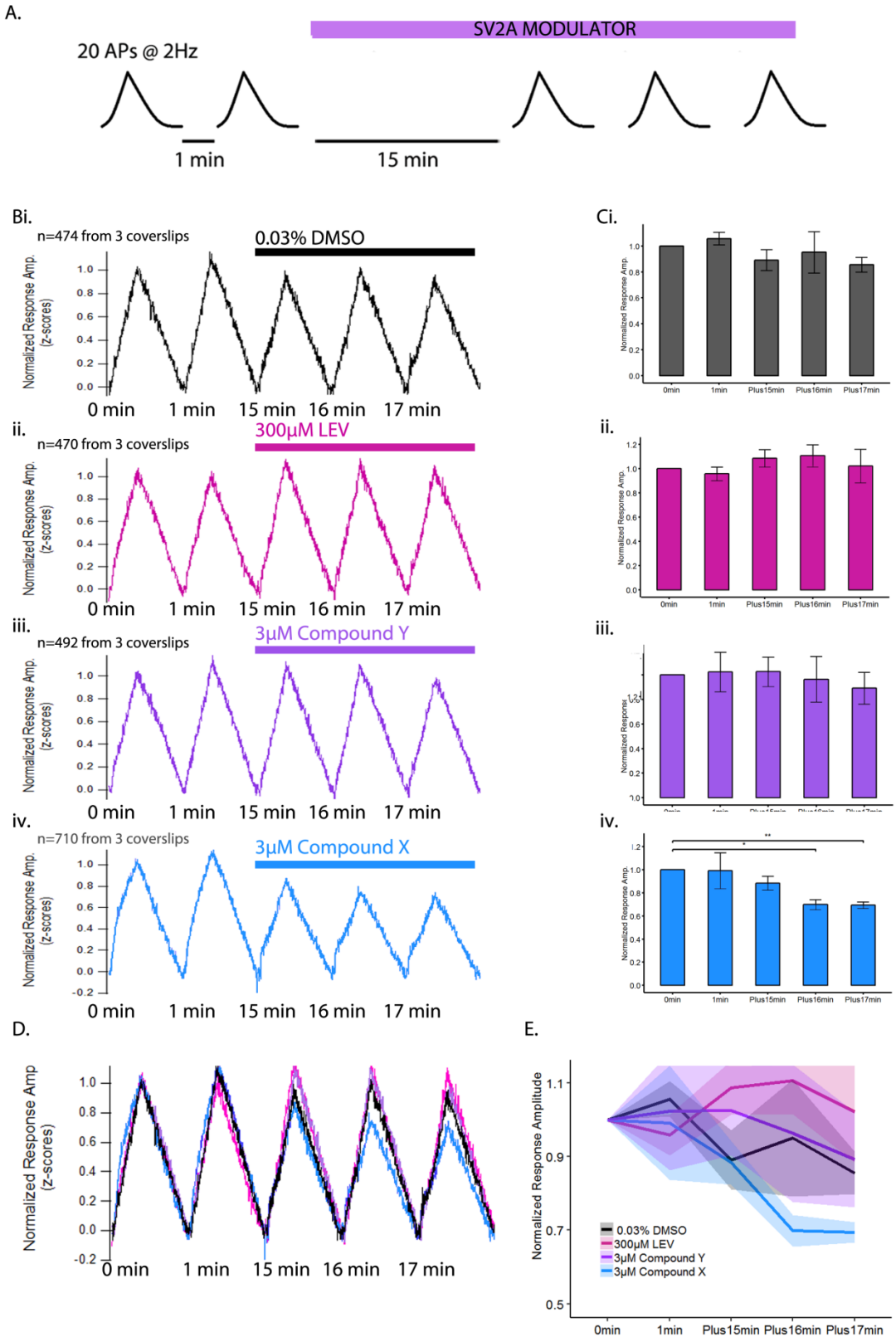

Fig 4.12. Unlike certain SV2A modulators, levetiracetam does not show activity during low-frequency stimulation A) Schematic of protocol B(i-iv). Normalized, averaged traces from each compound assayed; traces were baseline subtracted and subsequently divided by the baseline

fluorescence in order to generate baseline corrected (z-scores) and bleach-corrected response profiles. Traces from trials 2-4 are shown normalized to the first response. Numbers of synapses in the final datasets are indicated above the traces, all are generated from at least 3 separate experiments. C(i-iv) . Change in response amplitude at each time point for each compound assayed. Peak amplitude was calculated via subtracting the average of the baseline before the onset of the stimulus (frames 1-8) from the average of the peak (frames 112-116). Amplitude in trials 2-4 was normalized to the amplitude of the first response. 3µM Compound X significantly impacted at 16 min (p=0.019) and 17 min (p = 0.007), (Student's paired t-tests). Values of average non-normalized peak amplitudes ± SEM (z-scores): DMS0 (Ci) 0 mins: 2.14 ± 0.133, 1min: 2.24 ± 0.128, 15 mins: 1.98 ± 0.132, 16 mins: 2.14 ± 0.123, 17 mins: 1.88 ± 0.132 ; 300µM LEV (Cii) 0 mins: 2.01 ± 0.119, 1 min: 1.92 ± 0.110, 15 mins: 2.15 ± 0.141, 16 mins: 2.16 ± 0.117, 17 mins: 2.12 ± 0.131 ; 3µM Compound Y (Ciii) 0mins: 2.24 ± 0.152, 1 min: 2.44 ± 0.243, 15 mins: 2.38 ± 0.134, 16 mins: 2.33 ± 0.140; 3µM Compound X (Civ) 0 mins: 2.10 ± 0.087, 1 min: 2.25 ± 0.102, 15 mins: 1.74 ± 0.120, 16 mins: 1.51 ± 0.090, 17 mins: 1.37 ± 0.092. D) Composite of average traces. E) Graphical comparison between each condition at each time point (Mean Amplitude ± SEM; standard error of measurement is indicated via shading.

4.6 Discussion

In section 4.2, we showed that substantial recruitment of the recycling pool (TRP) was necessary for LEV to exert a significant depression of the RRP, and that this effect occurred in a concentration-dependent manner. This is consistent with other work in this field, which has profiled LEV as an activity-dependent modulator of neurotransmission. From our observations, a possible conclusion is that the action of LEV is dependent upon vesicular entry via endocytosis, as proposed in the model in Fig 4.1. In this model, LEV enters the vesicle upon exposure of its lumen to the synaptic cleft, whereupon it binds SV2A and gains entry into the presynaptic terminal. However, this model fails to explain the significant depression exerted by an alternative SV2A modulator, Compound X at 2Hz (section 4.5), where a TRP-recruiting stimulus is not necessary. Unsurprisingly, given its predilection for high intensity stimulation, LEV has no effect at low-frequency stimulation, at least without TRP-turnover. This data could indicate that the action of SV2A modulators is not dependent on vesicular access as we initially thought, but instead having an action which is very much determined by stimulus strength and frequency.

This interpretation of this mode of action of SV2A is corroborated by the results detailed in section 4.4, where addition of 300µM LEV significantly increases p_r as measured by the ability of synapses to release at least 1 quantum during trains of 10 x 4AP stimulation. These results mirror observations found in autapses overexpressing SV2A, where incubation with 100µM LEV for 6-10hours restores regular vesicle release (Nowack et al., 2011). Curiously, in terms of release

probability, SV2A knockout and overexpression result in similar phenotypes, whereby *pr* is decreased in both instances (Nowack et al., 2011, Custer et al., 2006). This is suggestive of a finely-tuned system in which levels of SV2A expression must be tightly regulated to sustain normal neurotransmission, and it follows that modulation of SV2A by LEV can result in a spectrum of actions upon a need-by-need basis. Similar observations have been made regarding complexin, a small cytosolic protein expressed at the presynaptic terminal that binds the SNARE complex and appears to regulate the probability of vesicles to release, with both KO and overexpression leading to a reduction of *pr* (Trimbuch and Rosenmund, 2016, Xue et al., 2007, Abderrahmani et al., 2004, Huttner et al., 1983, Itakura et al., 1999, Liu et al., 2007). Due to its small size and location, it has not yet been possible to structurally characterize SV2A by X-ray crystallography or nuclear magnetic resonance, making it difficult to underpin the precise mechanism by which LEV and other SV2A modulators exert their effects. Nevertheless, the shift in the LEV effect caused by inputs of varying intensity may suggest that SV2A undergoes conformational changes as a consequence of differing stimulation paradigms, and that this affects the ability of SV2A modulators to bind or their actions once bound.

At the synapse, proteins in the SV2 family have been shown to co-traffic with the calcium sensor, synaptotagmin - 1; a finding which we have also replicated (Fig 4.5.1). It has been shown that synapses lacking SV2 contain lower levels of synaptotagmin - 1 but display a higher proportion of synaptotagmin - 1 on the plasma membrane (Yao et al., 2010). In experiments conducted by Yao et., al, normal expression of synaptotagmin - 1 was restored via expression of either wildtype SV2A or SV2A-Y46A, a mutated form of SV2A containing an amino acid substitution in the tyrosine-based endocytosis motif . However, only wildtype SV2A restored a normal proportion of synaptotagmin on the plasma membrane. The authors interpret this as SV2 influencing the expression and trafficking of synaptotagmin via separate mechanisms and conclude that SV2 plays a major role in regulating the amount of synaptotagmin in synaptic vesicles, consistent with the observation that synapses lacking SV2 have fewer vesicles competent for calcium-induced fusion. Therefore, it may be possible that the modulation of exocytosis caused by LEV in our experiments is a consequence of the SV2A-synaptotagmin interaction. Although we started to investigate this possibility, time constraints did not allow us to make headway on this question. Therefore, further investigation of how LEV affects the molecular interactions of SV2A with synaptotagmin – 1 would be a useful future direction for this project and would provide key insights into the physiological role of SV2A and the mechanism of action of its modulators.

Intriguingly, our alkaline trapping experiments revealed that LEV appears to modulate the size of the total pool of vesicles, with synapses becoming increasingly diffuse and much brighter after LEV application. This increase in brightness of the synapse suggests that LEV may interfere with the ability of the vesicle to reacidify although, counterintuitively, LEV has no effect upon endocytic kinetics, at least in our model system. One possible theory as to why the initial reacidification remains unaffected is that the time frame needed for LEV to bind SV2A and exert an effect is longer than it takes for a vesicle to endocytose. Therefore, the vesicle undergoes reacidification as usual and it is the subsequent interactions of SV2A and LEV that disrupt the ability of the vesicle to remain in its acidified state, essentially diminishing the size of the total pool available for release.

A second theory as to why the size of the total pool is reduced upon treatment with LEV is that the vesicles disperse away from the synapse. Increased vesicle mobility leading to a reduction in size of the total pool is often associated with synapsin (Gitler et al., 2008, Orenbuch et al., 2012). Interestingly, the effects of LEV upon synaptic depression are occluded in synapsin knockouts (Garcia-Perez et al., 2015), perhaps indicative that modulation of SV2A and modulation of synapsin feeds into a common pathway. The next step in establishing whether LEV does cause diffusion of vesicles away from the synapse would be to conduct imaging experiments followed by fixation and transmission electron microscopy (TEM).

From the findings presented here it can be concluded that effects arising from the modulation of the presynaptic terminal by levetiracetam are complex. It is clear that LEV requires a certain amount of hypersynchronous activity in order to exert an effect, however whether or not this arises from the need of LEV to gain entry into the vesicle before binding SV2A, or whether neuronal activity confers some kind of conformational state of SV2A that favours the binding of certain ligands remains unclear. Furthermore, our results hint that SV2A has the ability to encode inputs of various intensity and frequency, and can alter its behaviour accordingly. We also suggest that SV2A only binds certain ligands at set intensities and frequencies, thus explaining why certain modulators have certain effects at very specific ranges of synaptic activity. The consequences of modulating SV2A with LEV are varied, however one can see disruptions in RRP size, exocytosis, ρr and vesicle pool sizes, highlighting the integral role of SV2A in the maintenance of regular neurotransmission. Finally, it must be noted that one limitation of our results is that we have not had the opportunity to test the actions of LEV or Compound X in our model system using neurons where SV2A has been knocked out or knocked down. As the effects of LEV have previously been

shown to be occluded in cultures from SV2A KO mice (Lynch et al., 2004), we have extrapolated that the results shown in our model system are mediated via SV2A, supported by the lack of evidence that LEV has a concentration dependent effect on presynaptic Ca^{2+} influx (Fig 4.6). Nevertheless, verification using a SV2A knockout/ knockdown in our primary hippocampal cultures is an important future direction of this work and the lack of an SV2A knockout/ knockdown control in this body of work limits the interpretations that can be made regarding the specific mechanism of action of SV2A modulators in our model system.

Chapter 5: Actions of metabotropic glutamate receptor 2 modulators at the presynaptic terminal alone and in combination with levetiracetam

5.1 Introduction

In recent years, metabotropic glutamate receptor 2 (mGluR2) has gained increasing interest as a potential therapeutic target for a number of neurological disorders (Niswender and Conn, 2010). Group II mGluRs, which include mGluR2 and mGluR3, are negatively coupled to adenylate cyclase (AC) through G proteins of the G_i/G_0 type (Conn and Pin, 1997). Dysfunction of mGluR2 has been linked to a number of neurological and psychiatric disorders including schizophrenia, Alzheimer's disease, Parkinson's disease, depression, anxiety and epilepsy (Niswender and Conn, 2010, Rohde et al., 2012). Despite mGluR2 being an attractive target for pharmacological intervention, the homology of the orthosteric binding site between mGluR2 and mGluR3 has hindered the development of selective orthosteric ligands (Conn et al., 2009). Therefore, in recent years, pharmaceutical research and development has concentrated its efforts on developing ligands that bind allosterically. Allosteric binding sites offer two major advantages; the first being that their modulation potentiates or inhibits the actions of the endogenous ligand, making them sensitive to the demands of the immediate physiological environment, and the second is that they tend to be specific to a receptor subtype, making it easier to develop selective ligands (Conn et al., 2009).

In this chapter we aim to use optical reporters of presynaptic function to assay the effects of novel mGluR2 allosteric modulators developed by our industrial partner, Janssen Pharmaceutica (Lavreysen et al., 2015a, Trabanco et al., 2011). In the first instance, we aim to validate primary hippocampal cultures as a suitable model system in which to assay the effects of mGluR2 modulators. Secondly, we characterize the effects of mGluR2 receptor activation in our model system using an mGluR2 orthosteric ligand. Thirdly, we characterize the effects of novel mGluR2 positive and negative allosteric modulators (PAMs and NAMs) and examine the effects of positive

allosteric modulation in combination with the anti-epileptic drug, levetiracetam, building on work carried out *in vivo* by Janssen Pharmaceutica.

5.2 Validation of primary hippocampal cultures as an appropriate model system for assaying mGluR2 modulators

The first task in this series of experiments was to validate our model system i.e. primary neuronal cultures harvested from the hippocampus of the rat at P0/P1, as a suitable system in which to assess the effects of mGluR2 modulators. The literature surrounding the expression of mGluR2 is somewhat confused, with some groups suggesting that expression in the hippocampus is higher than in the cortex (Janssens and Lesage, 2001), whilst others have reported that mGluR2 mRNA is expressed in the hippocampus and entorhinal cortex (Ohishi et al., 1993) or that expression is largely dependent upon the developmental stage (McOmish et al., 2016). To address these issues and establish the suitability of *in vitro* preparations for our purposes, here we compared expression of mGluR2 in primary hippocampal cultures with that of primary cortical cultures at DIV 14; the earliest stage at which imaging experiments could be reliably conducted.

For this, we relied on readouts of mRNA expression and immunocytochemistry (ICC), and in addition we compared the actions of (2S,2'R,3'R)-2-(2,3-dicarboxycyclopropyl) glycine (DCG-IV), a mGluR2 agonist at the presynaptic terminal, in hippocampal and cortical preparations. Figure 5.1.A shows the mRNA expression of mGluR2 in cortical and hippocampal cultures at DIV14. In brief, cultures were lysed using RIPA buffer, the mRNA extracted and the cDNA synthesized via PCR. In Figure 5.1.A, lanes 1 and 2 used self-designed forward and reverse primers; lanes 2 and 3 used identical primers to that published by Janssens and Lesage (Janssens and Lesage, 2001), and lanes 4 and 5 show the expression of the housekeeping gene GAPDH, used as a loading control (primers self-designed). In lanes 1 and 2, a clear band at ~500bp is evident in the hippocampal cultures but is absent in the cortical cultures, whereas both lanes 3 and 4 show bands at ~1000bp suggesting mGluR2 expression in both preparations.

Expression of mGluR2 in both cortical and hippocampal neurons at DIV14 is also supported by immunocytochemistry (Fig. 5.1.B). For the ICC, neurons were fixed at DIV 14 with paraformaldehyde (PFA) and glycine, and the presence of mGluR2 detected using an anti-mGluR2 antibody (Alomone labs) at a dilution of 1:100 and detected using an AlexaFluor-555 conjugated

secondary antibody (1:1000). The abundant red staining in Figures 5.1.Bi and ii indicates that mGluR2 is expressed in quantity in primary cultures of both cortical and hippocampal neurons.

Finally, we assessed the modulatory effect of increasing concentrations of the mGluR2/3 agonist, DCG-IV on presynaptic responses of hippocampal and cortical neurons using sypHy1x. Briefly, the hippocampus and a small section of cortical tissue were extracted from the brains of P0/P1 rat pups, triturated and plated on coverslips, coated with poly-D-lysine and laminin. Both preparations were plated in MEM supplemented with FCS, glucose and pen/step, which was switched ~3hours later to Neurobasal medium containing B27, glutamax and pen/strep. Neurons were cultivated in this medium until imaging at DIV14-21. Both preparations were infected with AAV6_sypHy1x at DIV7.

During imaging, the response of presynaptic boutons to a 40AP, 20Hz stimulus was assayed in response to increasing concentrations of DCG-IV. This stimulus was selected as the RRP had proven a robust readout in the assessment of the effects of levetiracetam (Chapter 4). A detailed schematic of the protocol is shown in Fig 5.2.A. A stock of DCG-IV was prepared in EBS and diluted to the appropriate concentration in EBS containing 20µM CNQX and 50µM AP-V. Following each stimulus, the whole volume of the buffer was removed, the cells washed quickly x1 with fresh EBS+ blockers, and an equal volume of the solution replaced containing a higher concentration of DCG-IV. This was repeated six times, assaying a range of concentrations from 0.5µM to 100µM. Stimuli were administered 2 minutes apart. As with the data collected for LEV, a single round of imaging and stimulation served to photo-bleach the sample and to enable the selection of an unbiased ROI mask. A second round of stimulation and imaging in the absence of compound provided a control readout to which the response amplitudes of trials 2-6, where increasing concentrations of DCG-IV were added, were normalized to counteract the heterogeneity of response profiles (Fig 4.2). Further analysis of the images was conducted using customized scripts written for Igor Pro. 6.

Figure 5.1.C. shows the normalized response amplitudes of neurons from hippocampal and cortical preparations in response to increasing concentrations of DCG-IV. Throughout the experiment, hippocampal neurons display increased sensitivity to DCG-IV than cortical neurons of the same age, with significantly more depression exhibited at each time point ($p<0.001$ in all instances, two-way ANOVA). In combination, the experimental evidence demonstrating modulation by DCG-IV and the positive identification of mGluR2 via immunocytochemistry and

mRNA detection demonstrate that primary hippocampal cultures at DIV14 are a suitable model system on which to assay the effects of mGluR2 modulators.

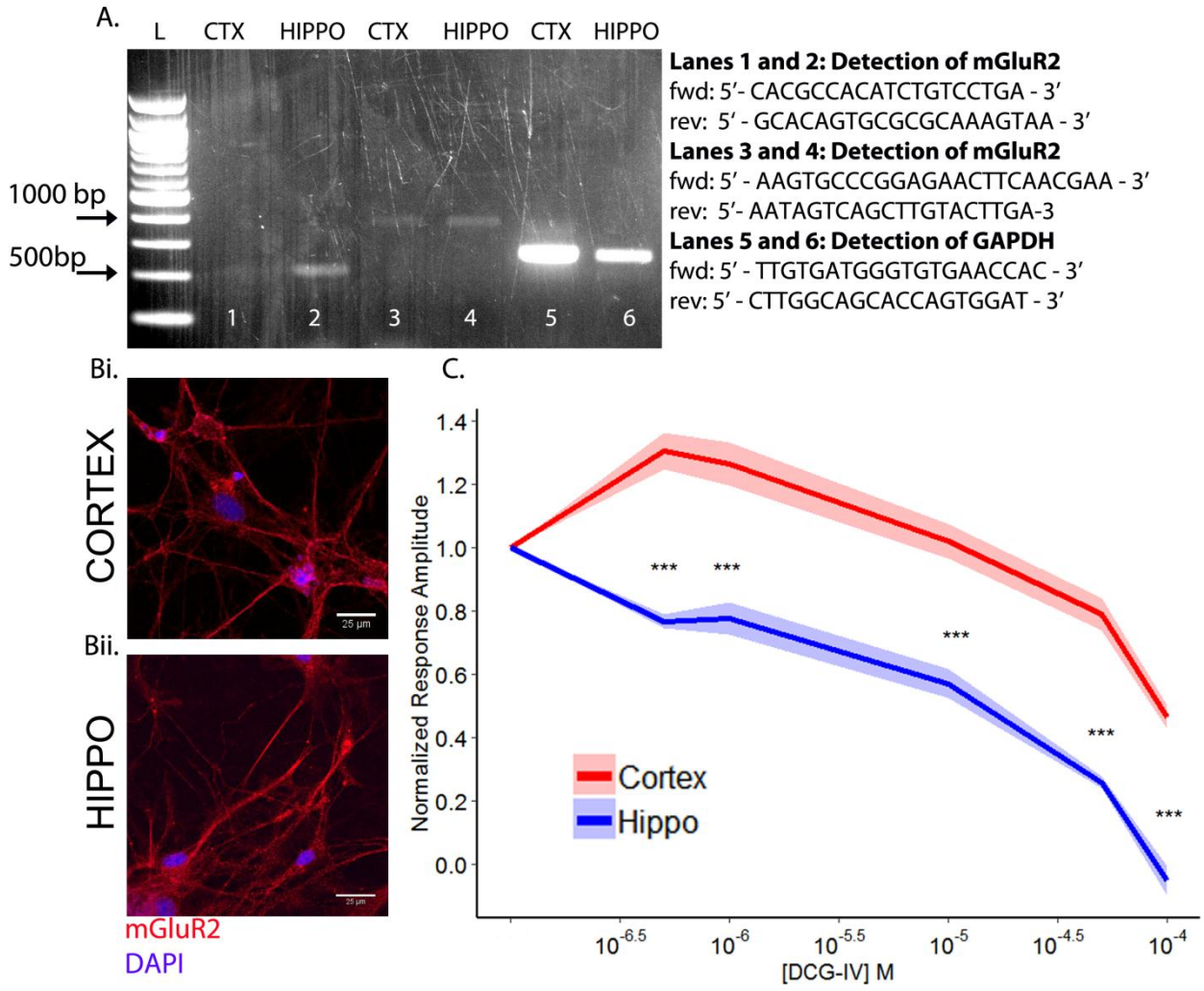

Fig 5.1 Comparison of mGluR2 expression in primary cortical and hippocampal cultures. A) mRNA extraction and cDNA synthesis. For detection of mGluR2, lanes 1 and 2 used a self-designed primer directed towards GRM2 (rat); lanes 3 and 4 used a primer directed towards GRM2 (rat) designed by Janssens and Lesage (Janssens and Lesage, 2001); lanes 5 and 6 show the detection of the housekeeping gene, GAPDH (rat) detected using self-designed primers. B) ICC reveals high expression levels of mGluR2 in cortical and hippocampal neuronal cultures C) Comparison of the sensitivity of cortical and hippocampal neuronal cultures to the mGluR2/3 agonist, DCG-IV.

5.3. Characterization of the actions of mGluR2 agonists at the presynaptic terminal

5.3.1 The effects of DCG-IV on RRP release and retrieval

As the final goal of this chapter was to characterize the actions of novel positive and negative allosteric modulators of mGluR2 receptors at the presynaptic terminal via fluorescence imaging, we first thought it pertinent to assay the effects of a known mGluR2 agonist, DCG-IV, in our model system. The data used for this characterization was the same data as collected in section 5.2, however only the data from the hippocampal cultures is examined in this subchapter. The protocol is described in detail in section 5.2 (schematic Fig 5.2.A), however the data in this section is shown in comparison with control data, in which 0.5μM DCG-IV was added to the external solution at 2 minutes and cells were incubated in this until the final time point (8mins), whilst being imaged every 2 minutes. The purpose of this was to ensure that the effects that we observed were concentration-dependent as opposed to a result of prolonged exposure. Due to the fact that treatment with 100μM DCG-IV resulted in response failure in the majority of neurons in hippocampal cultures (Fig 5.1.C), concentrations of between 0.5μM and 50μM were selected for further analysis.

As expected, DCG-IV decreased the response amplitude of the RRP in a largely concentration-dependent manner, although the depression in amplitude caused by 0.5μM and 1μM are similar (Figs 5.2.Cii and 5.2.E). In mammalian systems, activation of group II mGluRs (mGluR2, mGluR3 and the *Drosophila* homologue DmGluRA) inhibit cAMP formation via negative coupling with adenylate cyclase (AC) ((Tanabe et al., 1992, Parmentier et al., 1996, Tanabe et al., 1993), and these mGluRs can act as both autoreceptors and heteroreceptors in order to suppress glutamate release (Xi et al., 2002). Prolonged exposure to the lowest concentration of DCG-IV assayed, 0.5μM, also resulted in a continual reduction of response amplitude, although at concentrations of 10μM and 50μM the depression in the experimental group was significantly higher than in the control group ($p<0.001$ at both time points). One should also note the difference in reactions of the control group and experimental group to the initial addition of 0.5μM DCG-IV (Fig 5.2.E), where responses of the experimental group are significantly more depressed than in the control group. However, at this point the depression in the experimental group reaches a plateau, with no significant

difference between the responses at 0.5µM and 1µM, whereas the response amplitudes of the control group continue to fall until, at the 4 minute time point, the response amplitudes of the control and experimental groups do not significantly differ from one another. The most likely cause of this is slightly differing pharmacokinetics of cells across experiments.

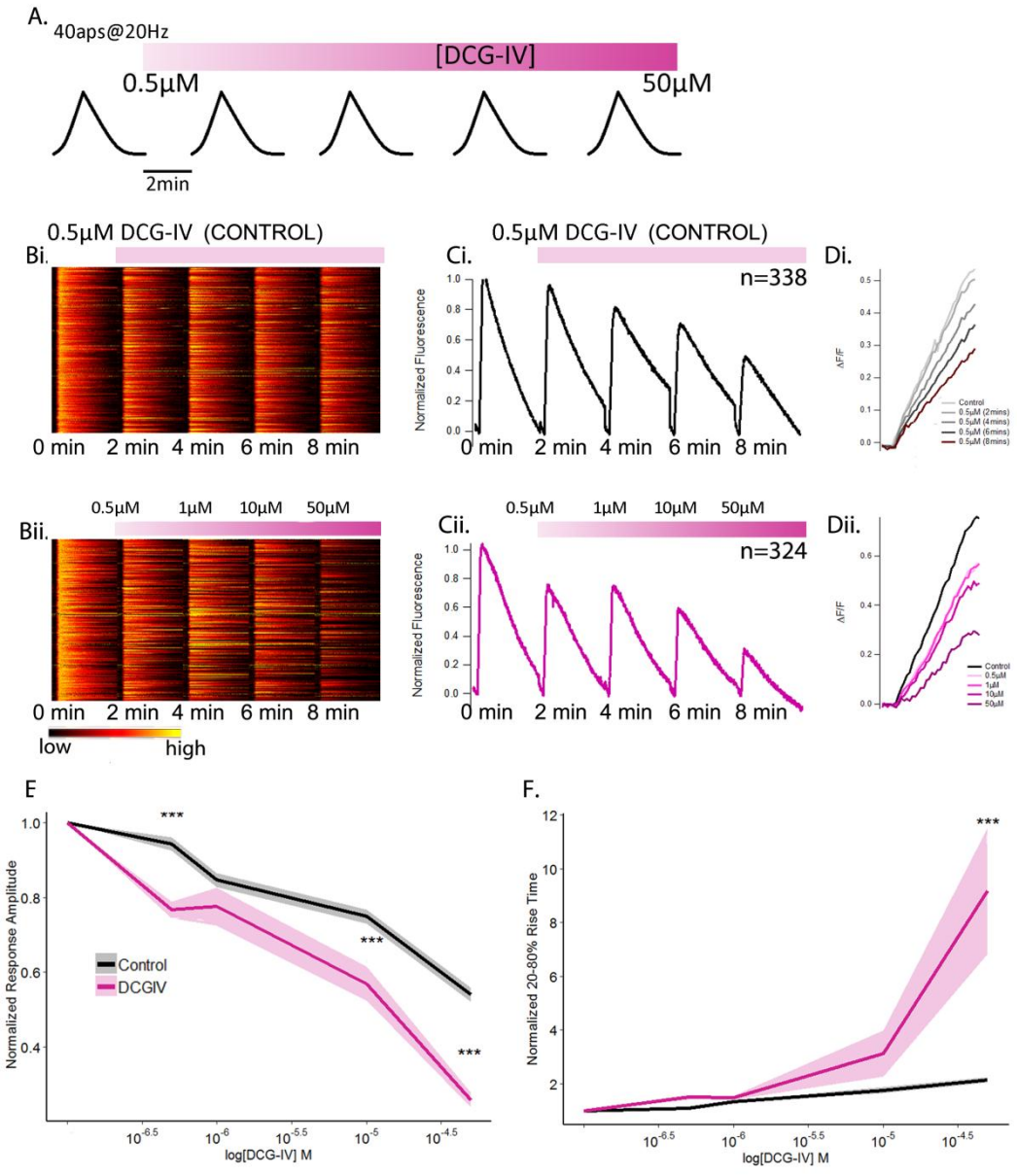

Fig 5.2. Characterizing the actions of DCG-IV upon vesicle release A) Schematic of protocol. Timing of increasing DCG-IV concentration indicated by the pink gradient bar above B(i-ii). Heatplots illustrating intensity of responses in each trial, each point on the y-axis corresponds to

an individual bouton; intensity of the response is indicated via the scale shown in the calibration bar. Control condition refers to time-matched stimulation in presence of 0.5µM DCG-IV. C(i-iv). Normalized, averaged traces; traces were baseline subtracted and subsequently divided by the baseline fluorescence in order to generate baseline corrected (ΔF/F) traces. Traces from trials 2-5 are shown normalized to the first response, pre-addition of DCG-IV. Numbers of synapses in the final datasets are indicated above the traces, from 3 and 4 coverslips respectively. Values of average non-normalized peak amplitudes ± SEM (ΔF/F): 0.5µM DCG-IV Timepoint control (Ci) 0 mins: 0.553 ± 0.016, 2 mins: 0.535 ± 0.016, 4 mins: 0.458 ± 0.012, 6 mins: 0.412 ± 0.011, 8 mins: 0.337 ± 0.009; 0 - 50µM DGG-IV (Cii) 0 mins: 0.701 ± 0.018, 2 mins: 0.502 ± 0.014, 4 mins: 0.487 ± 0.017, 6 mins: 0.377 ± 0.015, 8 mins: 0.183± 0.013. D(i-ii). Response profiles showing the slowing in exocytosis experienced post-addition of DCG-IV. E. Comparison of response amplitudes between DCG-IV and Control at each time point assayed; $p < 0.001$ in all instances; Two-way ANOVA with Tukey's post-hoc comparisons. F) Comparison of the rate of exocytosis; significance seen at 50µM DCG-IV, $p<0.001$; Two-way ANOVA with Tukey's post-hoc comparisons.

For analysis of kinetic data, a subset of the dataset was created based on certain inclusion criteria; profiles had to have positive rates of exo- and endocytosis and the rates calculated had to be less than 1000 seconds for exocytosis and 2000 seconds for endocytosis respectively. Although these values might seem high, they were selected to ensure the inclusion of traces which had become highly irregular as a consequence of the modulation, and that were not included if strict parameters were applied.

Figure 5.2.Dii displays the profiles of the response-rise across each of the DCG-IV concentrations assayed, reflective of the rate of exocytosis. Figure 5.2.Di depicts the profiles generated by prolonged exposure to 0.5µM, assayed at the corresponding time points. In both figures, there is a clear time-dependent/concentration-dependent effect upon the rate of exocytosis, with the rise becoming incrementally less steep, resulting in a right-shifted peak. Figure 5.2.F. compares the normalized 20-80% rise time in the experimental and control conditions. Prolonged exposure to a low concentration (0.5µM) of DCG-IV (control) results in a virtually linear relationship with the rate of exocytosis, with the longer the exposure time, the slower the rate of the rise. As with response amplitude, this is indicative that a low concentration of DCG-IV (0.5µM) continues to modulate the neuronal responses in a phamacokinetically stable manner over the time period assayed. The rates of 20-80% rise in the experimental and the control groups are similar until the addition of 10µM DCG-IV, where the two lines begin to diverge, although the rates do not significantly differ until the final addition of 50µM ($p<0.001$). Our results are consistent with those of Kamiya and Ozawa, who previously proposed the idea that DCG-IV is able to suppress exocytotic machinery (Kamiya and Ozawa, 1999).

The effect of DCG-IV on endocytosis was examined (data not shown); however the results were erratic and did not appear to be concentration dependent. Exocytosis-endocytosis coupling is, through necessity, a stringently regulated process, without which an excess of synaptic vesicle material would be deposited at the plasma membrane; resulting in swelling of the presynaptic terminal, change in the membrane tension and the blockage of release sites preventing the synapse from participating in future release events (Dittman and Ryan, 2009, Kononenko and Haucke, 2015, Murthy and De Camilli, 2003). Therefore, we interpret the inconsistent endocytic profiles as a secondary, 'knock-on' effect of the modulation of exocytosis, and envisage a system whereby neurons are trying to compensate for this change in the rate of exocytosis, resulting in obscure endocytosis kinetics.

To conclude, we have established two robust effects of mGluR2 modulation by DCG-IV upon the synaptic vesicle cycle in our model system, namely the depression of vesicle release and the slowing of the rate of exocytosis. Nevertheless, these results must be interpreted with caution as DCG-IV also exhibits high affinity for mGluR3 receptors; with EC50 values of $2x10^{-7}$ for mGluR3 receptors, compared with $3x10^{-7}$ for mGluR2 receptors (Hayashi et al., 1993). DCG-IV also has affinity for NMDA receptors, a value that is approximately 10-fold lower than for the group II mGluRs (Hayashi et al., 1993), however contamination of the results via NMDA receptor mediation is not likely to be a concern in our model system given the presence of AP-V in our external bath solution, which serves to block these receptors at a much higher affinity. Overall, these results give us a useful insight into the potential actions of mGluR2 agonists upon vesicle release and retrieval at the presynaptic terminal in primary hippocampal cultures, which we were able to use as a basis for testing more specific and selective modulators of the mGluR2 receptor in our later work.

5.3.2. The relationship between mGluR2 receptor activation and Ca^{2+} influx at the presynaptic terminal

It has been widely established that Ca^{2+} influx at the presynaptic terminal is intrinsically linked to the release of neurotransmitter. However, from experiments conducted by Kamiya and Ozawa, the actions of DCG-IV upon vesicle recycling at the presynaptic terminal, particularly upon the rate of exocytosis, are deemed to be most likely a result of interference with exocytotic machinery as opposed to a direct influence upon presynaptic Ca^{2+} influx (Kamiya and Ozawa, 1999). Yet as these experiments were largely carried out by examining EPSC amplitude, these authors were unable to isolate precisely those actions that were occurring presynaptically.

To address a possible role of presynaptic Ca^{2+} in the results presented in 5.3.1, we employed an identical stimulation paradigm as that described in that section (Fig 5.3.A) but this time using the reporter AAV6_syGCaMP6f. This is targeted to the vesicular protein synaptophysin and provides a direct read-out of changes in presynaptic Ca^{2+}. By using this approach, we hoped to directly assay the effects of DCG-IV on presynaptic Ca^{2+} dynamics to help underpin where in the pathway mediation occurs; if DCG-IV modulates presynaptic Ca^{2+} directly this should be reflected by a reduction in Ca^{2+} influx, whereas if DCG-IV is affecting vesicle release machinery via a target downstream of Ca^{2+}, response amplitudes should remain relatively unchanged. AAV-syGCaMP6f was introduced to the cells at DIV7 at an MOI of 100. Other than the alteration in fluorescent reporter, all other experimental parameters were kept the same.

Figures 5.3.Cii. and Dii show that the initial introduction of 0.5μM DCG-IV into the experimental system reduced Ca^{2+} by ~20%, but that this depression then remains stable throughout the experiment even when increasing concentrations of DCG-IV are applied. Due to the lack of within-subject concentration-dependent effects, even at the highest concentrations, (Fig 5.3.Dii), we did not assess the effect of prolonged exposure to 0.5μM DCG-IV upon presynaptic Ca^{2+}. Therefore, unlike in Fig 5.2.2, the control data shown here is a time point control conducted in buffer only (Fig 5.2.3.Bi, Ci and Di). When directly comparing the normalized response amplitude of DCG-IV treated neurons with the control group (Fig 5.3.E), it is clear that neurons in the experimental group underwent significant modulation by DCG-IV ($p<0.001$ at each time point, 2-way ANOVA). Nonetheless, after the initial decrease in amplitude, the modulation appears relatively stable and a concentration-dependent effect is not observed. Figure 5.3.F compares the inhibition of presynaptic Ca^{2+} influx (syGCaMP) with the inhibition of vesicle release (sypHy). From the graph, it can be seen that the relationship between vesicle release and DCG-IV concentration is almost linear, whereas this clear concentration dependent effect is not evident in regards to Ca^{2+}. As DCG-IV significantly depressed presynaptic Ca^{2+} levels, we cannot completely rule-out an effect of Ca^{2+} in mGluR2 modulation of vesicle release. However, the lack of evidence of a concentration – dependent effect on Ca^{2+} dynamics could indicate that DCG-IV most likely slows the rate of exocytosis by a mechanism located downstream of presynaptic Ca^{2+} influx, and therefore may be a consequence of targeted hindrance of exocytotic machinery.

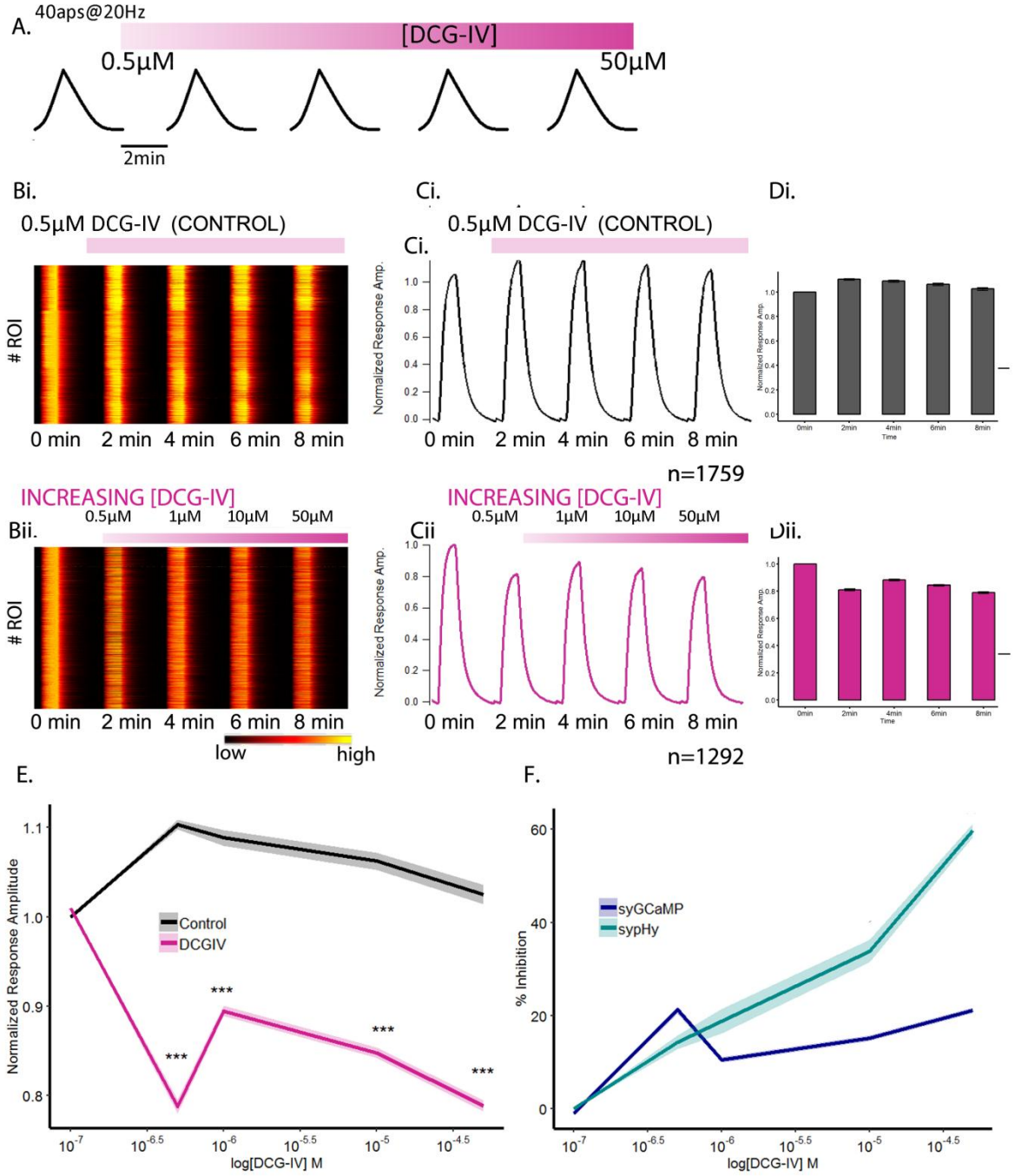

Fig 5.3. Characterizing the actions of DCG-IV upon presynaptic Ca^{2+} A) Schematic of protocol; increasing DCG-IV concentration indicated by the pink bar – darker gradient indicates higher concentration B.(i-ii). Heatplots illustrating intensity of responses in each trial, each point on the y-axis corresponds to an individual bouton; intensity of the response is indicated via the scale shown in the calibration bar. C(i-iv). Normalized, averaged traces; traces were baseline

subtracted and subsequently divided by the baseline fluorescence in order to generate baseline corrected (ΔF/F) and bleach corrected traces. Traces from trials 2-5 are shown normalized to the first response, pre-addition of DCG-IV. Numbers of synapses in the final datasets are indicated above the traces, from 3 and 4 coverslips respectively. D(i-ii) . Bar plots representing the normalized mean response amplitude ± SEM at each time point assayed. Values of average non-normalized peak amplitudes ± SEM (ΔF/F): 0.5µM DCG-IV timepoint control (Di) 0 mins: 3.18 ± 0.026, 2 mins: 3.31 ± 0.030, 4 mins: 3.29 ± 0.028, 6 mins: 3.25 ± 0.024, 8 mins: 3.21 ± 0.023; 0 - 50µM DGG-IV (Cii) 0 mins: 3.32 ± 0.024, 2 mins: 2.67 ± 0.030, 4 mins: 2.84 ± 0.021, 6 mins: 2.75 ± 0.023, 8 mins: 2.56± 0.023. E. Comparison of response amplitudes between DCG-IV and Control at each time point assayed; $p < 0.001$ in all instances; Two-way ANOVA with Tukey's post-hoc comparisons. F) Relationship between increasing concentrations of DCG-IV and presynaptic Ca^{2+} (blue – syGCaMP6f) and vesicle release (green – sypHy)).

5.4. Characterizing the effects of novel mGluR2 allosteric modulators upon synaptic vesicle recycling

Having established that DCG-IV, a direct agonist of mGluR2/3, affected the amplitude and kinetics of vesicle release in our model system, we sought to characterize the actions of highly selective mGluR2 allosteric modulators developed by our industrial partner. Therapeutically, allosteric modulators often offer a better solution than orthosteric ligands as their actions are dependent on the supply of the endogenous ligand, and therefore they act in accordance to the physiological demands of the synapse. As defective glutamate transmission is implicated in a vast number of neuropathological disorders, research and development into the actions of these modulators could provide key insights into novel strategies for the pharmacological management of conditions such as epilepsy, schizophrenia and dementia ((Niswender and Conn, 2010)). Figure 5.3 shows the location of the orthosteric binding site of mGluR2 and depicts an example of an allosteric binding site between the sixth and seventh transmembrane domains.

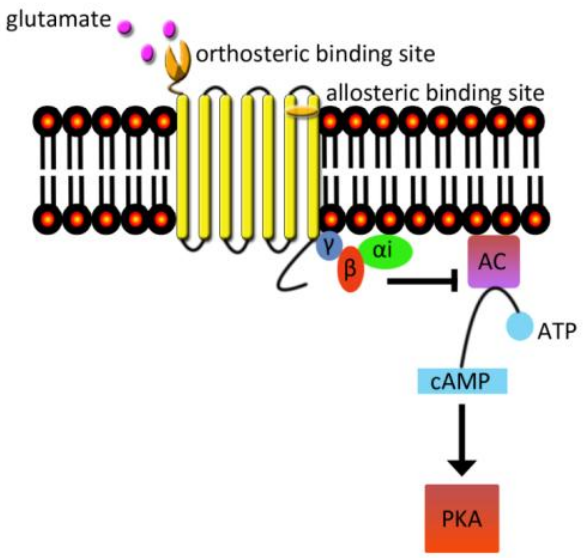

Fig 5.4.Cartoon representation of the orthosteric and allosteric binding sites of mGluR2

In this subchapter, we investigated the effects of a positive allosteric modulator (PAM), JNJ-46281222 and a negative allosteric modulator (NAM), JNJ-56140864 on vesicle release and retrieval in primary hippocampal cultures using sypHy as the optical readout. As in the previous experiments conducted with DCG-IV, we exposed the cultures to increasing concentrations of the PAM/NAM whilst assessing their effects on RRP mobility using a 40AP, 20Hz stimulus. Stimuli were administered 2 minutes apart and cultures were imaged concurrently; schematics of the protocols used are shown in Fig 5.5.Ai and 5.5.Aii. Compounds were firstly dissolved in DMSO and further diluted to the appropriate concentration in EBS containing 20μM CNQX and 50μM AP-V to ensure the blockage of AMPA and NMDA receptors. The final DMSO concentration was <0.002% at the highest concentrations assayed. Following each stimulus, cells were quickly washed with EBS + blockers before introducing the next concentration to the experimental system.

The first round of stimulation and imaging (not shown) was used to identify ROIs and served to pre-photobleach the cells. The second round of stimulation was administered in the absence of compound and served as a baseline control for the subsequent responses. As allosteric modulators require the presence of an orthosteric ligand in order to elicit their effects, a low concentration (0.5μM) DCG-IV was also introduced to the cells following the second round of stimulation. Panels Ci and Di on Fig 5.5 demonstrate the reduction in vesicle release following the introduction of

0.5μM DCG-IV, however introduction of increasing concentrations of the PAM, JNJ-46281222 exacerbates this effect. When this effect is examined within-subject, (Fig 5.5.Di) concentrations of 1μM and 10μM PAM reduce the response amplitude to a significantly greater degree than the DCG-IV alone ($p=0.00737$ and $p=0.0279$ respectively, two-way ANOVA). Panel Ei compares the normalized response amplitudes of the first five responses with the responses from the control dataset (i.e. prolonged exposure to 0.5μM DCG-IV). From this, it is clear that the positive allosteric modulation of the mGluR2 receptor by JNJ-46281222 reduces the release of vesicles to a significantly greater extent than 0.5μM DCG-IV alone, $P<0.001$ at each time point (two-way ANOVA).

To confirm that these effects were mediated via mGluR2, we used JNJ-56140864, a highly selective negative allosteric modulator (NAM) of the mGlu2 receptor. We hypothesized that if positive allosteric modulation resulted in inhibition of vesicle release, then negative allosteric modulation should result in its either its facilitation, or at the very least a lack of inhibition caused by the presence of the orthosteric ligand (DCG-IV). Therefore, we expected to see either an increase in response amplitude and the rate of exocytosis, or their failure to be modulated by the presence of DCG-IV i.e. an inhibition of depression and the slowing of exocytosis. Consistent with this, the presence of the NAM increased the response amplitudes in comparison to the control stimulus and led to complete recovery of the response following treatment with 0.5μM DCG-IV (Figs 5.5.Dii and Eii). It is clear from our results that the data collected in the presence of the NAM was subject to more experimental noise that that collected in the presence of the PAM. We believe that this is most likely due to the presence of DCG-IV, which acts on both mGluR2 and 3 receptors to depress vesicle release. Therefore, in our experimental system there is potential that we are assaying from synapses where both mGluR2 and mGluR3 have been modulated by DCG-IV, yet the addition of the NAM only has the ability to reverse these effects at mGluR2, leading to a wide variation in response profiles.

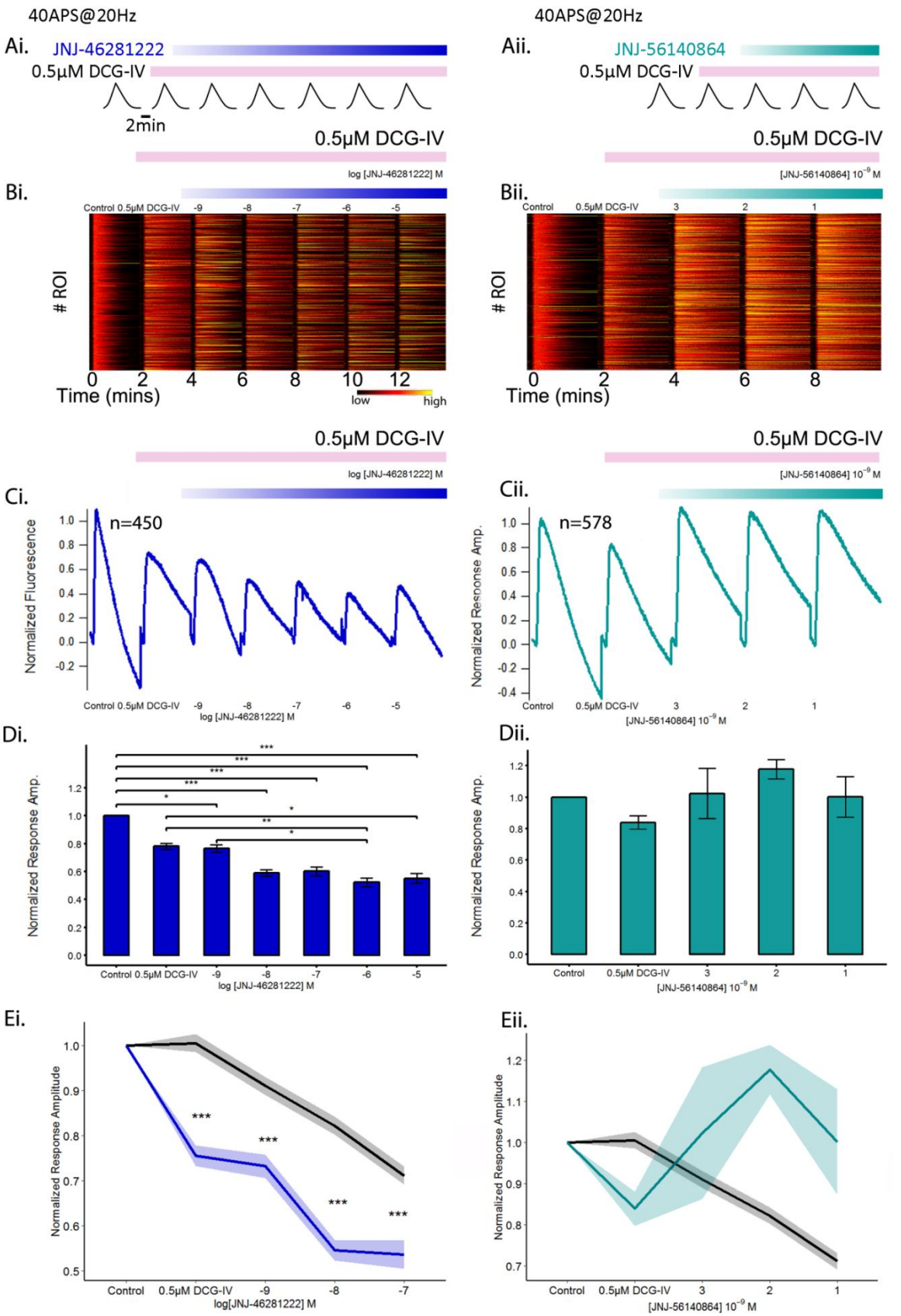

Fig 5.5. Characterizing the actions of mGluR2 allosteric modulators upon presynaptic response amplitude A) Schematic of protocol; increasing concentrations of mGluR2 modulators indicated

by the gradient above B.(i-ii). Heatplots illustrating intensity of responses in each trial; intensity of the response is indicated via the scale shown in the calibration bar. C(i-iv). Normalized, averaged traces; traces were baseline subtracted and subsequently divided by the baseline fluorescence in order to generate baseline corrected (ΔF/F) traces. Traces from trials 2 onwards are shown normalized to the first response, pre-addition of compound. Numbers of synapses in the final datasets are indicated above the traces. D(i-ii) . Bar plots representing the mean ± SEM normalized response amplitudes at each time point assayed. Values of average non-normalized peak amplitudes ± SEM (ΔF/F): JNJ- 46281222 (PAM) (Di) 0μM: 0.537 ± 0.010, 500nMol DCG-IV alone: 0.368 ± 0.010, 1 nMol JNJ- 46281222: 0.349 ± 0.011, 10nMol JNJ- 46281222: 0.271 ± 0.010, 100nMol JNJ- 46281222: 0.264 ± 0.014, 1μM JNJ- 46281222: 0.219 ± 0.014, 10μM JNJ- 46281222: 0.244 ± 0.015; JNJ-56140864 (NAM) (Dii) 0μM: 0.417 ± 0.011, 500nMol DCG-IV alone: 0.388 ± 0.009, 100nMol JNJ-56140864: 0.508 ± 0.013, 200nMol JNJ-56140864: 0.511 ± 0.012, 300nMol JNJ-56140864: 0.517± 0.015. E(i). Comparison of response amplitudes between JNJ-46281222 (mGluR2 PAM) and Control at each time point assayed; $p < 0.001$ in all instances; Two-way ANOVA with Tukey's post-hoc comparisons; E(ii) Comparison of response amplitudes between JNJ-56140864 (mGluR2 NAM) and Control at each time point assayed.

5.4.1 The effects of mGluR2 modulators on the kinetics of vesicle release

For analysis of the kinetic data, subsets of the PAM and NAM datasets were created from the dataset used in 5.3.1. These subsets included only synapses that fell within certain constraints. The constraints applied were the same as those applied for the DCG-IV kinetic dataset, namely that profiles had to have positive rates of exo- and endocytosis, and that the values computed had to be less than 1000 and 2000 seconds respectively. These values were selected to ensure the selection of some of the more obscurely mediated traces.

In terms of the release kinetics (Fig 5.6), positive allosteric modulation of the mGluR2 receptor by JNJ-46281222 resulted in a concentration-dependent slowing of the rate of exocytosis (Fig 5.6.Bi and Ci; this is evident in the right-shifted response profiles in Fig 5.6.Ai). In comparison with the DCG-IV time point control (Fig 5.6.Di), the addition of 100nMol and 1μM JNJ-46281222 slowed the rate of exocytosis to a significantly greater degree than prolonged exposure to 0.5μM DCG-IV alone ($p=0.00543$ and $p<0.001$ respectively). Similar to the effects seen on amplitude, the mGluR2 NAM, JNJ-56140864 did not have a significant impact upon release kinetics. However it is evident in Fig 5.6.Dii that the rates of exocytosis in the presence of JNJ-56140864 are more rapid than those in the control condition. It can also be seen that JNJ-56140864 rescues the slowing of exocytosis caused by the initial addition of DCG-IV, and that this is evident in the recovery of the response profiles shown in Fig 5.6.Aii, where addition of DCG-IV is marked via a right-shifted trace, which recovers post-addition of the NAM.

From this data as a whole, we can conclude that changes in the extent and rate of vesicle release are hallmarks of mGluR2 modulation at the presynaptic terminal.

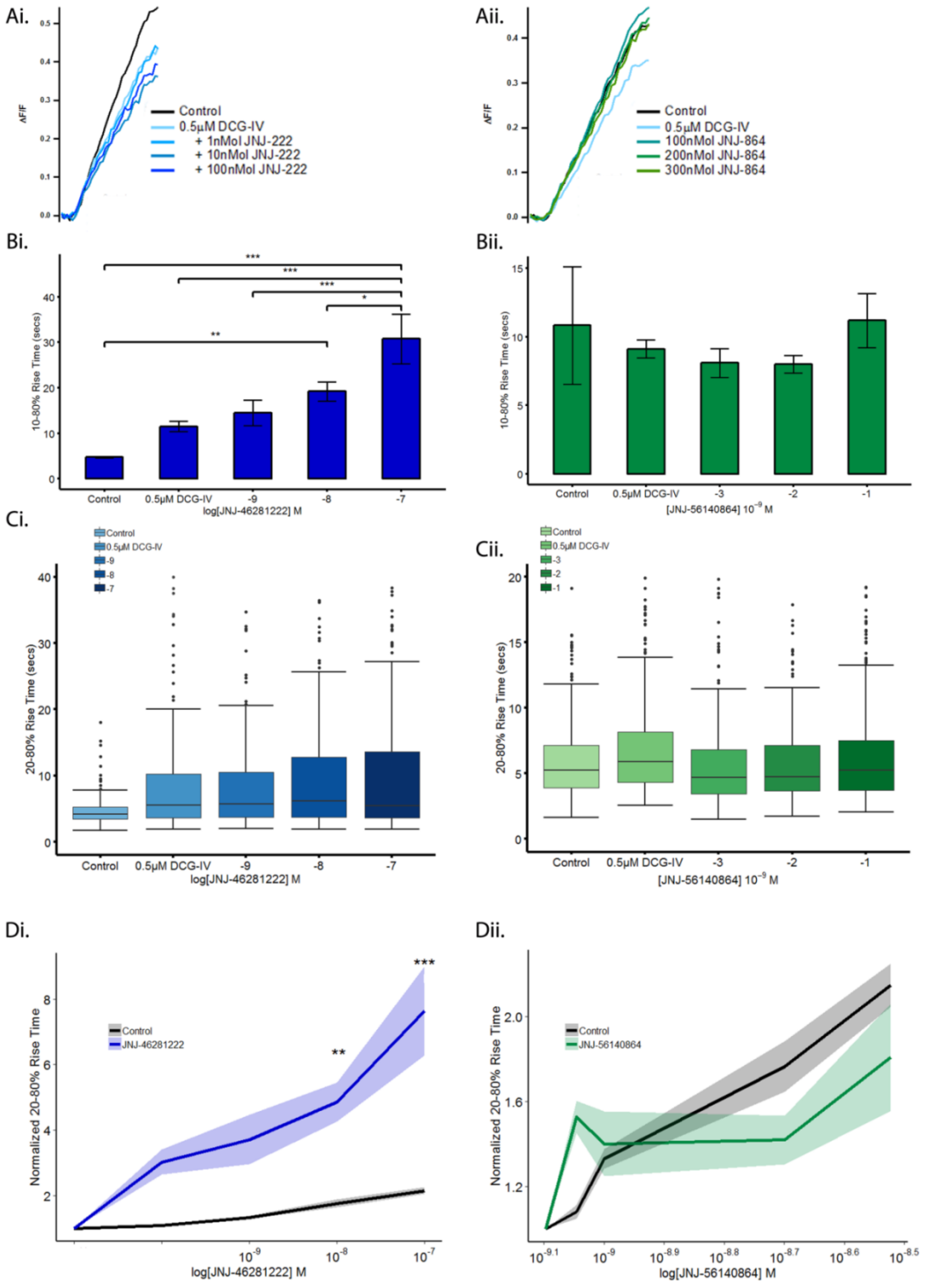

Figure 5.6 Characterizing the actions of mGluR2 allosteric modulators upon the kinetics of synaptic vesicle release A(i-ii) Average response profiles in response to increasing concentrations of mGluR2 allosteric modulators. B(i-ii). Bar plots representing the response amplitudes at each concentration assayed. C(i-ii). Boxplots showing the variation in kinetics over

the concentrations assayed. D(i). Comparison of the rate of exocytosis between JNJ-46281222 (mGluR2 PAM) and control (0.5µM DCG-IV) at each concentration assayed; p=0.00237 (10nMol) and p<0.001 (100nMol); Two-way ANOVA with Tukey's post-hoc comparisons; D(ii) Comparison of rate of exocytosis between JNJ-56140864 (mGluR2 NAM) treated and the control-treated cells at each time point assayed.

5.5. Exploring the synergistic effects of mGluR2 positive allosteric modulators (PAMS) and levetiracetam

As demonstrated by the data presented throughout this chapter, activation of the mGlu2 receptor attenuates glutamate release from the presynaptic terminal. Positive allosteric modulation, which does not directly activate the receptor yet exacerbates the agonist-mediated response, can be finely tuned by the abundance of the endogenous ligand, adjusting its actions accordingly. This makes positive allosteric modulators of mGluR2 attractive candidates for novel pharmacotherapies in the management of neurological diseases associated with excitotoxicity induced by excessive glutamate release.

A number of studies have evaluated mGluR2 PAMs as potential therapeutic agents in the management of neurological conditions (Johnson et al., 2003, Pinkerton et al., 2004, Layton et al., 2016, Lavreysen et al., 2015b), and it has been demonstrated that PAMs display anti-convulsant properties, blocking seizure onset in the 6Hz model of psychomotor seizures at 32mA and 44mA intensities. Recent work carried out *in vivo* by our industrial partner has revealed that co-administration of LEV and JNJ-46356479, a potent and selective mGluR2 PAM resulted in a significantly more potent effect than would be predicted for additive effects, and that plasma levels suggest that this synergism is not due to pharmacokinetic interactions (Metcalf et al., 2017). Therefore, the final objective of this chapter was to explore the effects of administering JNJ-46281222, an mGluR2 PAM, in combination with levetiracetam, specifically focusing on their actions upon vesicle recycling.

Having established in our previous work that turnover of the recycling pool is necessary for LEV to significantly modulate the presynaptic response, we employed a similar protocol for these experiments in which neurons were stimulated with 40APs at 20Hz to recruit the RRP at two minute intervals. Prior to the experiment, cultures were subjected to a single round of stimulation and imaging to pre-photobleach, and from which to create an unbiased ROI mask for subsequent analysis. The second round of stimulation/imaging took place in the absence of compound and

served as an internal control for synapse performance to counteract the heterogeneity across synapses when assessing compound effects. Following this, 10μM LEV and 1nmol JNJ-46281222 were added concurrently via the exchange of half the buffer volume (300μl), and after 2 minutes a 150AP, 20Hz stimulus given to recruit the recycling pool. In an attempt to minimize the effects of short-term plasticity induced by such a powerful stimulation, a six minute window was allowed to elapse before the next 40AP stimulus. A schematic of the protocol is seen in Fig 5.7.A.

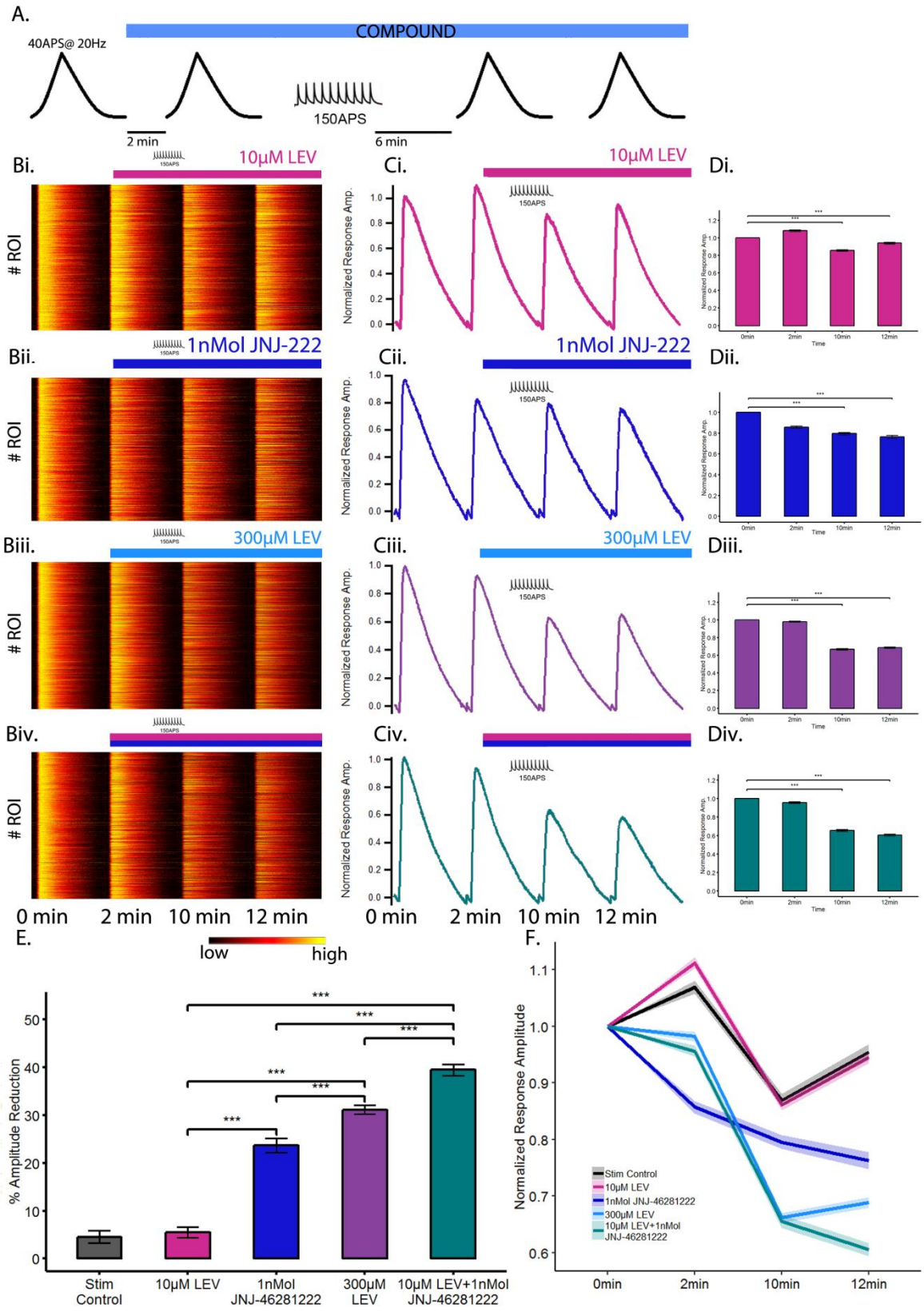

Fig.5.7. Exploring the synergistic depression of presynaptic response amplitude by mGluR2 positive allosteric modulation and LEV A) Schematic of protocol B.(i-iv). Heatplots illustrating

intensity of responses in each trial; intensity of the response is indicated via the scale shown in the calibration bar. C(i-iv). Normalized, averaged traces; traces were baseline subtracted and subsequently divided by the baseline fluorescence in order to generate baseline corrected (ΔF/F) traces. Traces from trials 2 onwards are shown normalized to the first response, pre-addition of compound D(i-iv). Bar plots representing the normalized response amplitudes ± SEM at each time point assayed. Values of average non-normalized peak amplitudes ± SEM (ΔF/F): (Di) 10μM LEV: 0 mins: 0.691 ± 0.008, 2 mins: 0.728 ± 0.010, 10 mins: 0.574 ± 0.008, 12 mins: 0.631 ± 0.010; (Dii) 1nMol JNJ- 46281222: 0mins: 0.543 ± 0.009, 2 mins: 0.451 ± 0.008, 10 mins: 0.420 ± 0.007, 12mins: 0.442 ± 0.008; (Diii) 300μM LEV 0 mins: 0.618 ± 0.006, 2 mins: 0.580 ± 0.006, 10 mins: 0.398 ± 0.006, 12 mins: 0.404 ± 0.006; (Div) 300μM LEV plus 1nMol JNJ-46281222: 0mins: 0.697 ± 0.009, 2 mins: 0.646 ± 0.008, 10 mins: 0.438 ± 0.008, 12 mins: 0.397 ± 0.007 E(ii) Comparison of response amplitudes across conditions at 12 min time point; 1nMol JNJ-46281222, 300μM LEV and 1nMol JNJ46281222 combined with 10μM LEV were significantly more potent inhibitors of presynaptic response amplitude than 10μM LEV given alone; $p<0.001$ in all instances, one-way ANOVA with Tukey's post-hoc comparisons. The combination of 1nMol JNJ-46281222 and 10μM LEV was also significantly more potent than either the 1nMol JNJ-46281222 or 300μM LEV; $p<0.001$ in both instances, one-way ANOVA with Tukey's post-hoc comparisons.

Of the compounds administered singularly, it is apparent that 300μM LEV is the most potent inhibitor of presynaptic release, depressing the response amplitude to a greater degree than either 10μM LEV or 1nMol JNJ-46281222 at the 10 and 12 minute time points; panels C and D (i-iii). Fig 5.7.E, which compares the response amplitudes at the 12 minute timepoint, reveals that the potencies of the singularly administered compounds ranks 10μM LEV (inactive) < 1nMol JNJ-46281222 < 300μM LEV. Both the JNJ-46281222 and the 300μM LEV were significantly more potent than the 10μM LEV ($p<0.001$ in both instances, one-way ANOVA with Tukey's post-hoc comparisons), which was not significantly different from the buffer control. N.B. At 12 minutes, apart from the 10μM LEV, all compounds were significantly different from the buffer at the $p < 0.001$ level (one-way ANOVA with Tukey's post-hoc comparisons); this is not shown on the graph to keep the presentation as clear as possible.

When looking at panels C(iv) and D(iv), which show the average trace and the normalized response amplitude of synapses co-treated with a sub-threshold dose of LEV (10μM) and 1nMol JNJ-46281222, the reduction in response amplitude at the 10 and 12 minute time points, post recruitment of the recycling-pool, is strikingly more pronounced than in neurons treated with either 10μM LEV or 1nMol JNJ-46281222 alone. In fact, the inhibition is more directly comparable to the effect seen with a 30-fold higher concentration of LEV (300μM). When this data is presented compositely (Fig 5.7.F), at the 10 minute time point it can be seen that the combination LEV-PAM therapy is equally as potent as 300μM LEV, and that by 12 minutes it is significantly more so ($p<0.001$), depressing the response by approximately 10% more. The results of the final time

point, presented in Figure 5.7.E., would suggest that an additive effect of 10μM LEV and 1nMol JNJ- 46281222 would result in <30% reduction in amplitude, however our results show that this combination treatment results in ~40% amplitude reduction, suggesting that a synergistic action is likely to be involved.

We next subsetted the data according to the criteria outlined in 5.3.1 and explored whether this synergistic effect extended to the release kinetics of the RRP. Figure 5.8 shows the effects that single administration of 300μM LEV, 10μM LEV and 1nMol JNJ-46281222 have upon exocytosis, compared with a combination of 10μM LEV and 1nMol JNJ-46281222 given concurrently. From the data presented here, it is clear that both levetiracetam and positive allosteric modulation of the mGlu2 receptor result in some slowing of RRP release, however positive allosteric modulation of the mGlu2 receptor results in an almost linear slowing of vesicle release (Fig 5.8.Bii), whereas the slowing elicited by levetiracetam requires turnover of the recycling pool and is only evident at the 10 and 12 minute time points, following the recruitment of the TRP with an 150AP stimulus. The response profiles depicted in 5.8.A(i-iii) clearly capture this effect, with increased exposure to either LEV or JNJ-46281222 resulting in a right-shifting of the response, indicative of slower release kinetics. However, from the response profiles detailed in Fig 5.8.Aiv and their mean 20-80% rise times, displayed in 5.8.B.iv, the increased modulatory action of release kinetics via co-administration of 10μM LEV and 1nMol JNJ-46281222 is evident.

Figure 5.8.D. displays the 20-80% rise time of the responses at the final time point normalized to the initial response, pre-compound. The order of potency is identical to that seen in the depression of the response amplitude; 10μM LEV < 1nMol JNJ-46281222< 300μM LEV < 10μM LEV + 1nMol JNJ-46281222. The combination of 10μM LEV and 1nMol JNJ-46281222 results in significantly more slowing of the release kinetics than any of the single therapeutic strategies ($p<0.001$ across all comparisons), and again this value is higher than would be expected for an additive effect, suggestive of synergistic action. Figure 5.8.E. is a graphical representation of the normalized 20-80% rise time at each of the time points assayed. Interestingly, synergistic action between the LEV and PAM is only evident following the150AP stimulation, which suggests that recycling pool turnover is still a requirement for the activation of LEV at the synapse, even when given in combination with compounds that do not require it.

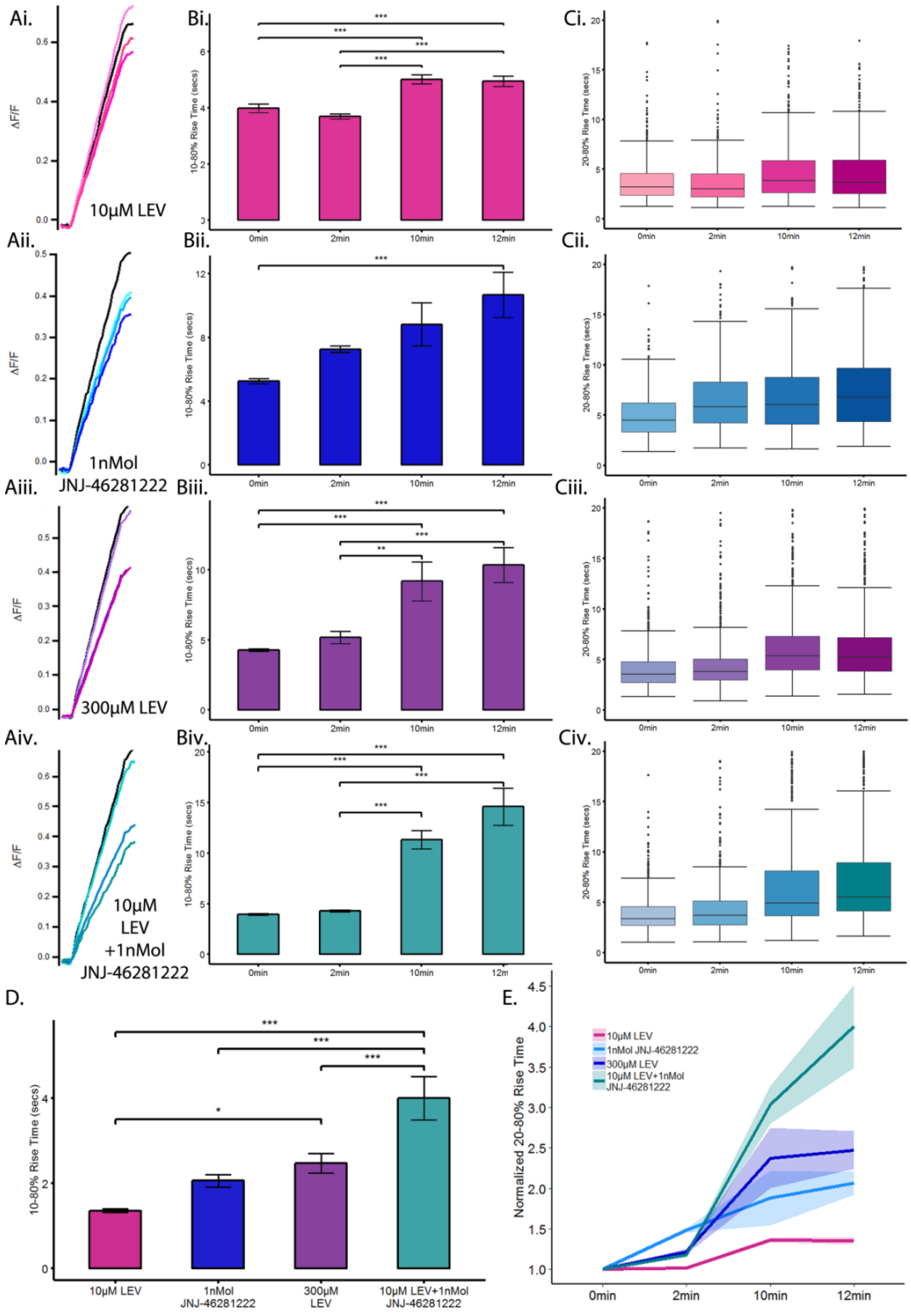

Fig. 5.8. Concurrent treatment with levetiracetam and positive modulators of mGluR2 results in slower release kinetics A(i-iv). Representation of profiles throughout the experiment. B.(i-iv). Barplots illustrating the changes in exocytotic rate across the experiment C(i-iv). Boxplots detailing the distribution of the exocytosis kinetics at each time point assayed. D. Comparison of

response amplitudes across conditions at 12 min time point. Synapses exposed to both JNJ-46281222 and 10μM LEV showed significant slowing in release kinetics when compared to either therapy alone or with 300μM LEV ($p<0.001$ in all instances). When compared with 10μM LEV, 300μM LEV significantly slows the rate of vesicle release; $p=0.00723$. F) Graphical comparison between the rates of exocytosis for each condition at each time point (Mean 20-80% rise ± SEM; standard error of measurement is indicated via shading.

5.6 Discussion

Through our work conducted on modulators of the mGlu2 receptor, we have identified two hallmarks of receptor activation at the presynaptic terminal, namely a reduction in synaptic vesicle release and the rate at which those vesicles are released. We have also demonstrated that combining a sub-threshold concentration of levetiracetam with a low concentration of JNJ-46281222, a PAM of mGluR2, results in synergistic inhibition of both the amplitude and release kinetics of vesicles. We have also provided validation that primary hippocampal cultures are an ideal model system in which to study the effects of these compounds, both alone and in combination.

Metabotropic glutamate receptors are a family of G-protein coupled receptors that control the activity of membrane enzymes and ion channels. Of this family, mGluR2 receptors are classified as Group II receptors. These are negatively coupled to adenylate cyclase (AC) and attenuate glutamate release through the down regulation of cAMP, leading to reduced phosphorylation of PKA (Conn and Pin, 1997). At the synapse, the presence of cAMP has been shown to play a critical role in the facilitation of synaptic transmission and the regulation of plasticity associated with learning and memory (Chavez-Noriega and Stevens, 1994, Chen and Regehr, 1997, Dixon and Atwood, 1989, Salin et al., 1996, Zhong and Wu, 1991).

In the synaptic vesicle cycle, successful fusion and release of vesicles governs the amplitude at which the terminal can respond. Therefore, in terms of vesicle recycling, the slowing of the rate at which vesicles undergo fusion and release is perhaps the more interesting characteristic of mGluR2 modulation as this is almost certainly the primary method by which response amplitude is mediated. In the results presented in section 5.3.1, we showed that DCG-IV, an agonist of mGluR2/3 decreases the rate of exocytosis in a concentration-dependent manner. As exocytosis is

tightly regulated by Ca^{2+}-influx at the presynaptic terminal, we examined the impact of DCG-IV upon Ca^{2+} dynamics at the presynaptic terminal using the optical reporter AAV6_syGCaMP6f (section 5.3.2). In the findings outlined here, we saw that the actions of DCG-IV on vesicle release were concentration-dependent whereas this was not evident in its action upon presynaptic Ca^{2+} influx (Fig 5.3.F), which led us to the conclusion that mGluR2/3 modulation probably acts, at least in part, downstream of Ca^{2+} influx, instead having direct impact upon exocytotic machinery. This conclusion is consistent with research by others in the field (Kamiya and Ozawa, 1999).

Experiments conducted with the mGluR2/3 agonist DCG-IV proved essential in identifying potential consequences of mGluR2 activation at the presynaptic terminal, which had not been previously characterized in electrophysiological imaging studies of primary hippocampal cultures. However due to DCG-IV's affinity for mGluR3, these experiments did not entitle us to claim the effects on vesicle release as attributes of mGluR2 modulation. Therefore, once we had established the actions of DCG-IV in our model system, we expanded our study to include highly specific allosteric modulators of the mGluR2 receptor, provided by our industrial partner.

The results presented in Figures 5.5 and 5.6 demonstrate that the amplitude of vesicle release and kinetics can be modulated in a concentration-dependent manner by specific mGluR2 allosteric modulators, indicative that these trademarks are idiosyncratic of mGluR2 modulation. At the synapse, release of neurotransmitter relies upon a series of protein interactions between synaptic vesicle membranes and the active zone, culminating in the fusion of the two membranes (Rothman, 1994, Bajjalieh and Scheller, 1995, Sudhof, 1995). This process is tightly regulated and is controlled by protein-machinery that remains highly conserved from yeast through to mammals (Bennett and Scheller, 1993, Ferro-Novick and Jahn, 1994). Of this machinery, SNARE-proteins play an essential role in exocytosis (Sudhof and Rizo, 2011), and have been shown *in vitro* to constitute the minimal complex required for successful fusion of the vesicle to the terminal membrane (Weber et al., 1998), albeit at a reduced rate than is observed *in vivo*. During exocytosis, three essential SNARE-proteins, synaptobrevin, syntaxin - 1 and SNAP-25 form a configuration that allows the 'zipping' together of the two membranes (Hanson et al., 1997, Lin and Scheller, 1997, Sutton et al., 1998). Finally, elevated Ca^{2+}, generated from action potential – driven depolarization-evoked opening of voltage-gated channels at the terminal, triggers an electrostatic or chemical change in the Ca^{2+} sensor, synaptotagmin, which completes the fusion reaction. Nevertheless, it is

apparent that the rapid, finely-tuned nature of exocytosis at small central synapses relies upon influence of more than these three essential factors.

Regulation of exocytosis by the cAMP-PKA signalling pathway has been demonstrated in a number of preparations, although the precise mechanisms are still unclear. To date, the PKA-mediated phosphorylation of cysteine string protein (CSP) and snapin are the only two exocytotic proteins that have been shown to undergo phosphorylation by PKA *in vitro* and *in vivo*, and to demonstrate that this phosphorylation has a marked effect on exocytosis (Evans et al., 2001, Chheda et al., 2001). Phosphorylation of CSP alters its interactions with syntaxin and synaptotagmin, whilst phosphorylation of snapin enhances its interactions with SNAP-25 and promotes the interaction of the SNARE-complex with synaptotagmin. Alternatively, PKA may impact upon the exocytotic machinery directly; evidence for this has been demonstrated by Trudeau et. al., who stimulated exocytosis in a Ca^{2+}-independent manner yet still found an increase in neurotransmitter release in response to PKA activation (Trudeau et al., 1996). Interestingly, these authors later show that PKA acts upon a Ca^{2+}-sensing step of exocytosis (Trudeau et al., 1998). From this, we interpret that mGluR2 modulation by the compounds tested in this chapter are most likely through PKA interaction with the exocytotic complex, although whether this is via direct inhibition of the complex itself or through secondary phosphorylation reactions of vesicular proteins is unclear.

As a final objective in this chapter, we evaluated the synergistic actions of LEV and mGluR2 PAMs at the presynaptic terminal. We revealed that levetiracetam and JNJ-46281222 act in a synergistic manner, resulting in greater attenuation and slowing of glutamate release than a relatively high concentration of LEV (300µM) given alone. Drug synergy is a highly pursued goal in combinational drug development (Fitzgerald et al., 2006), and extensive research has been done on the computer modelling of such interactions. In modelling such factors, network topology appears to govern the likelihood of a synergistic effect occurring, with synergism prevailing in drug combinations targeting closely connected targets (Yin et al., 2014). Therefore, it is likely that the pathways via which LEV and mGluR2 modulators act are closely linked. Interestingly, the amino-terminus of SV2A, which mediates its interactions with synaptotagmin, also contains substrate consensus sites of several protein kinases, including PKA. Therefore, this site could be a potential candidate in mediating the molecular interaction underlying the synergistic effect of mGluR2 modulators and LEV.

To conclude, we have identified that modulation of mGluR2 receptors at the presynaptic terminal results in slowed and attenuated glutamate release, and that this is unlikely to be due to a direct interaction with presynaptic Ca^{2+}- influx. We also showed that mGluR2 PAMs and the antiepileptic drug, levetiracetam produce a synergistic effect at the presynaptic terminal, which is likely to be beneficial in the treatment of multiple neurological disorders including epilepsy.

As a final caveat to the results presented in this chapter, it is worth noting that whilst the use of genetically targeted optical reporters guarantees a readout of mGluR2 modulation at the presynaptic terminal, mGluR2 expression itself is not confined to the presynaptic terminal (Neki et al., 1996). Therefore, we cannot be certain of whether the effects that we record at the presynaptic terminal are a result of pre- or postsynaptic mGluR2 activation, or a combination of both.

Chapter 6: Exploring the role of Tau on synaptic vesicle release, recycling and glutamate transmission

6.1. Introduction

Tau is a microtubule-associated-protein (MAP) that is widely implicated in a number of neurodegenerative diseases collectively known as the tauopathies, and its physiological role is to induce the formation and stabilization of microtubules via interactions with tublin (Bunker et al., 2004). There are three main models of aberrant tau protein expression which form the focus of this chapter: (1) a knockdown model; achieved via the use of an shRNA lentivirus; (2) overexpression of P301L tau; associated with familial frontal temporal lobe dementia (FTDP-17), and (3) overexpression of P301L tau in combination with $K18^{P301L}$-myc tagged fibrils; synthetic fibrils designed to mimic and promote the growth of neurofibrillary tangles (NFTs), which are a hallmark of Alzheimer's disease and other tauopathies. Primary hippocampal cultures cultivated from P0/P1 rats were used as the basis for each of the model systems.

Reduction of tau in primary neuronal cultures using anti-sense RNA has been demonstrated to suppress neuronal elongation (Caceres and Kosik, 1990), and primary hippocampal cultures generated from tau-deficient mice in some instances have been shown to have significant delays in maturation as quantified by the growth of axonal and neurite extensions (Dawson et al., 2001). *In vivo,* tau knockout models do not initially exhibit overt phenotypic alterations (Harada et al., 1994, Dawson et al., 2001, Tucker et al., 2001, Fujio et al., 2007) and only when aged do tau-deficient mice exhibit behavioural and motor impairments (Ikegami et al., 2000, Lei et al., 2012). These deficits have been associated with decreased numbers of tyrosine hydroxylase-positive neurons in the substantia nigra (SN) (Lei et al., 2012). Interestingly, reduction of this neuronal population has also been observed in a mouse model of FTDP-17 with Parkinsonism (Ittner et al., 2008), in which human tau carrying the FTDP-17 mutation K369I is overexpressed. Although tau knockout mice appear to develop motor impairments, suggesting that the loss of physiological tau function may contribute to the motor impairments evident in patients with tauopathy, in spatial

and memory tasks tau knockout mice do not appear compromised (Ikegami et al., 2000, Roberson et al., 2007, Dawson et al., 2010). It is already established that a loss of expression of long-term depression (LTD) is characteristic of tau deficiency, and is evident in both tau knockout mice and knockdown of tau in hippocampal slice cultures (Kimura et al., 2014), thus implicating modulation of neurotransmission is a likely target. Here we will build on the powerful methodological approaches that we have already established for assaying transmission and synaptic vesicle recycling (Chapters 3-5) to examine mechanistic principles of tau-associated modulation of presynaptic function.

As discussed in section 1.7.4, there is much debate as to whether the presence of aggregated tau in neurofibrillary tangles (NFTs) mediates toxicity or instead plays a neutral or protective role, and it is widely agreed that the oligomeric species is highly toxic (Spires-Jones et al., 2009). Therefore, to address the possible differences between soluble and aggregated tau in our experiments, we included two models in which the P301L mutation was expressed; one with $K18^{P301L}$-myc fibrils and one without. At a later date, we introduced a model of 1N4R WT-human tau (wt-Hu) overexpression, again achieved via infection with an adeno-associated virus. This model acted as a control for the pathogenic, P301L, tau overexpression, ensuring that any effects observed by inducing P301L expression where not inherent to all models of tau overexpression, including those overexpressing benign (wildtype) forms.

6.2. Validation of tauopathy models

Before embarking on imaging and electrophysiology, it was first important to confirm the validity of our tauopathic models. To do so, expression of P301L tau and $K18^{P301L}$ fibrils, or the knockdown of tau in primary hippocampal cultures was assessed via western blot and ICC at DIV 14; the earliest time point at which live-cell imaging was carried out. Preparation and maintenance of cultures from P0/P1 rat pups was identical to that described in the previous chapters, except at DIV 1, where cultures were treated with either a shRNA lentivirus for tau knockdown or AAV6-Tau(P301L) to induce overexpression of aberrant human tau. At DIV 3, $K18^{P301L}$ fibrils were seeded in selected cultures expressing the P301L mutation. N.B. For clarity fibrils are referred to as $K18^{P301L}$ and cultures treated with Tau(P301L) and $K18^{P301L}$ are referred to as $Tau(P301L)^{K18}$.

6.2.1. Lentiviral knockdown of tau in primary hippocampal cultures

As stated previously, the knockdown of tau was achieved via shRNA lentiviral infection. Following a sequence BLAST, TRNC000091298 shRNA lentivirus was selected for the total knockdown of tau upon the basis that its target sequence, ACAGGAAATGACGAGAAGAAA, resides within exon 9 of the *MAPT* gene, and thus is present all isoforms of tau, leading to the knockdown of both 3R and 4R variants. All shRNAs used in this body of work were cloned into a plKO.1 lentiviral vector. Further information about lentivirus production is given in the Chapter 2 (Methods). At DIV 1, cells were treated with either 10µl or 5µl of TRNC000091298, 10µl TRCN0000072256; a luciferase directed lentiviral shRNA or 10µl TRCN00000208001, containing the empty plKO vector. Neurons treated with either the luciferase directed shRNA or the empty plKO.1 vector provided negative controls, whilst neuronal lysate taken from cells cultured from a tau knockout mouse provided a positive control. Due to the lentiviral production being in-house, obtaining a titre was not possible. shRNA plasmids were originally obtained from Sigma Aldrich.

At DIV 14 cells were harvested for the detection of total tau using Western blotting. Briefly, cells were lysed with RIPA buffer supplemented with protease and phosphotase inhibitors, centrifuged at 14,000 rpm, 4°C and the supernatent transferred to fresh eppendorfs. Western blotting was carried out as described in section 2.3.1. To detect total tau levels, membranes were probed with an mTau5 primary antibody (Janssen Pharmaceutica). To provide quantification, membranes were stripped and probed for ß-actin. Image analysis was carried out using ImageJ.

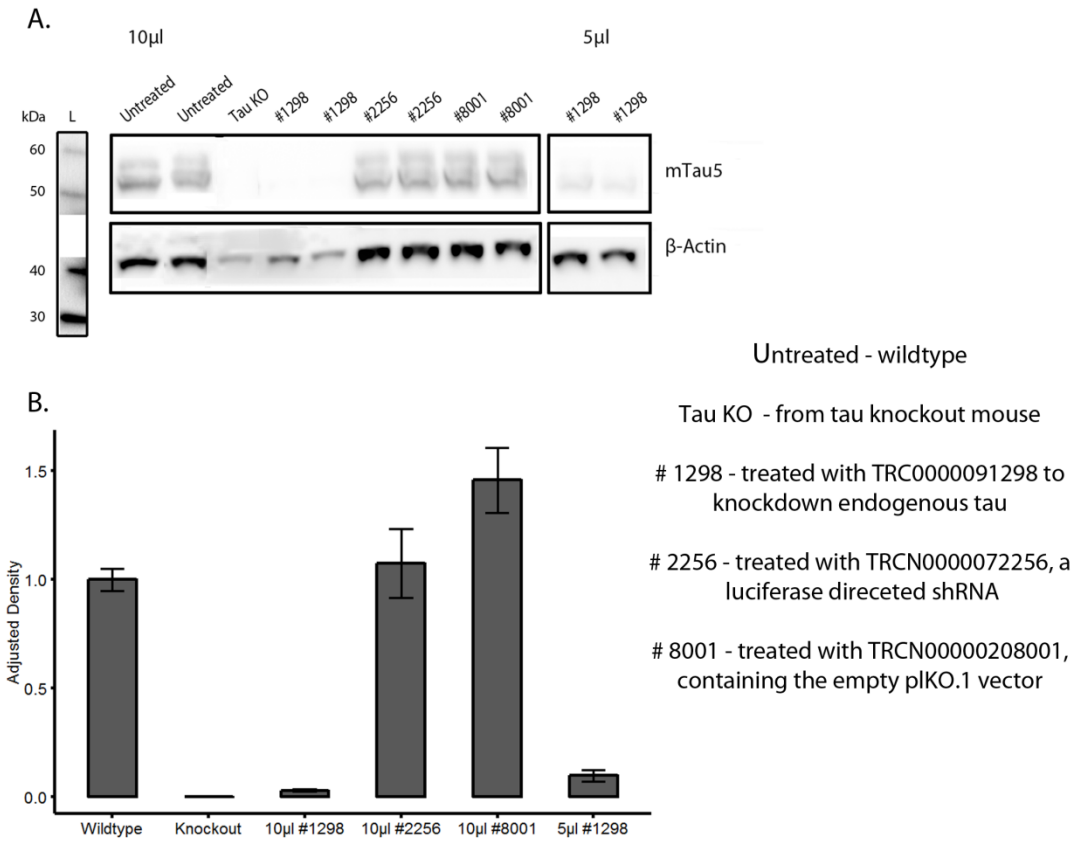

Figure 6.1. A) Validation of tau knockdown by TRC0000091298 A) Western blot probed with mTau5 for the dection of total murine tau (1:1000). 10µg protein was loaded per well. Blots were stipped and reprobed for β – actin (1:10,000). B) Adjusted density of tau expression in comparison with wildtype (untreated) cultures. Statistics were not possible as from a single experiment.

As seen in Figure 6.1.A, neurons cultured from a tau knockout mouse did not produce bands at either 51 or 55kDa, the molecular weights corresponding to 3R and 4R tau, verifying the specificity of the primary antibody. This is confirmed in the quantification in Fig. 6.1.B. Neurons treated with 10µl TRC0000091298 displayed approximately 3% of the signal compared with lysates taken from untreated wells, and those treated with 5µl TRC0000091298 approximately 10%. As expected, tau expression was not suppressed in neurons treated with the neagitve control viruses, TRCN0000072256 and TRCN00000208001. This confirmed that satisfactory knockdown of tau in primary rat hippocampal cultures could be achieved via the addition of 10µl TRC0000091298 shRNA lentivirus.

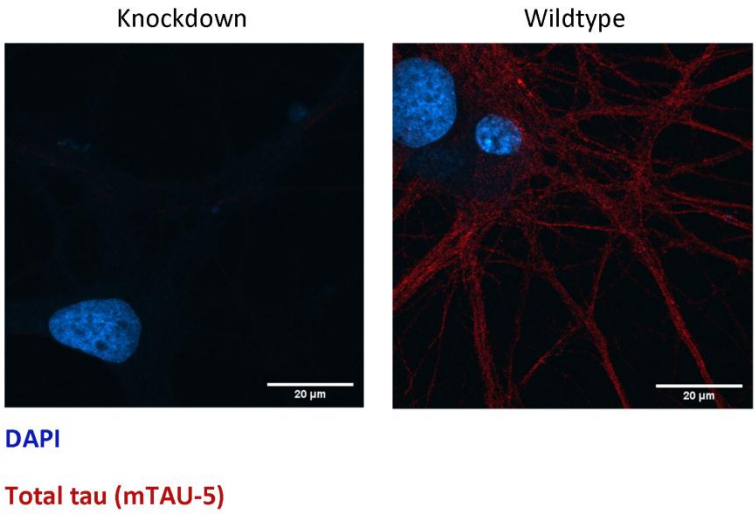

Figure 6.2. Knockdown of tau is verfied by immunocytochemistry. Knockdown of tau by 10µl TRC0000091298 was confirmed using immunofluorescent labelling. At DIV14, cells were probed for total tau expression using mTau-5 (1:100) antibody and an AlexaFluor-555 conjugated secondary antibody (1:1000).

6.2.2. Overexpression of P301L and K18^{P301L}-myc fibrils in primary hippocampal cultures

Overexpression of P301L mutated tau was achieved by infection of neurons with Tau(P301L) delivered via an adeno-associated virus at DIV 1 at an MOI of 100. P301L was cloned into an adeno-assosciated viral serotype-6 (AAV6) backbone containing terminal repeats. Woodchuck Hepatitus Virus (WHP) Posttranscriptional Regulatory element (WPRE), bGH-polyadenylation site, and expression were driven by the human synapsin-1 promotor. At DIV 3, recombinant synthetic fragments containing the four microtubule repeat binding domains (K18^{P301L}; residues Q244-E372 of the 1N4R human tau isoform) with a P301L mutation and C-terminal myc-tag were introduced to selected cultures. For *in vitro* fibril production, a solution comprising 40µM K18^{P301L}, 40µM low-molecular weight heparin (MW=3,000) and 2mM DTT in 100mM sodium acetate buffer (pH 7.0) was incubated at 37^{o}C for seven days. This was subsequently centrifuged at 100,000 x g for 1 hour at 4^{o}C and the pellet resuspended in the same volume of 100mM sodium acetate buffer. The K18^{P301L} fibrils were sonicated with 10x 1s pulses at 20% amplitude and stored in aliquots at -80^{o}C. Upon thawing, fibrils were further diluted in 100µM sodium acetate buffer (1:4) and re-sonicated, this solution was further diluted in culture medium and delivered to the cells at a final concentration of 2.5nmol.

Expression of P301L mutated human tau and $K18^{P301L}$-myc fibrils was detected at DIV 14 via Western blotting. Preparation of lysates and Western Blot protocol were identical to that described in 6.2.1, with the exception of the primary antibodies used: anti-AT8 (pSer202/Thr205), a monoclonal antibody was used at a dilution of 1:1000 for the detection of hyperphosphorylated tau (Vandermeeren et al., 1993), and mouse anti-HT7 was used for the detection of total human tau at a dilution of 1:2000 . Again, membranes were re-probed for ß-actin and quantification carried out using ImageJ.

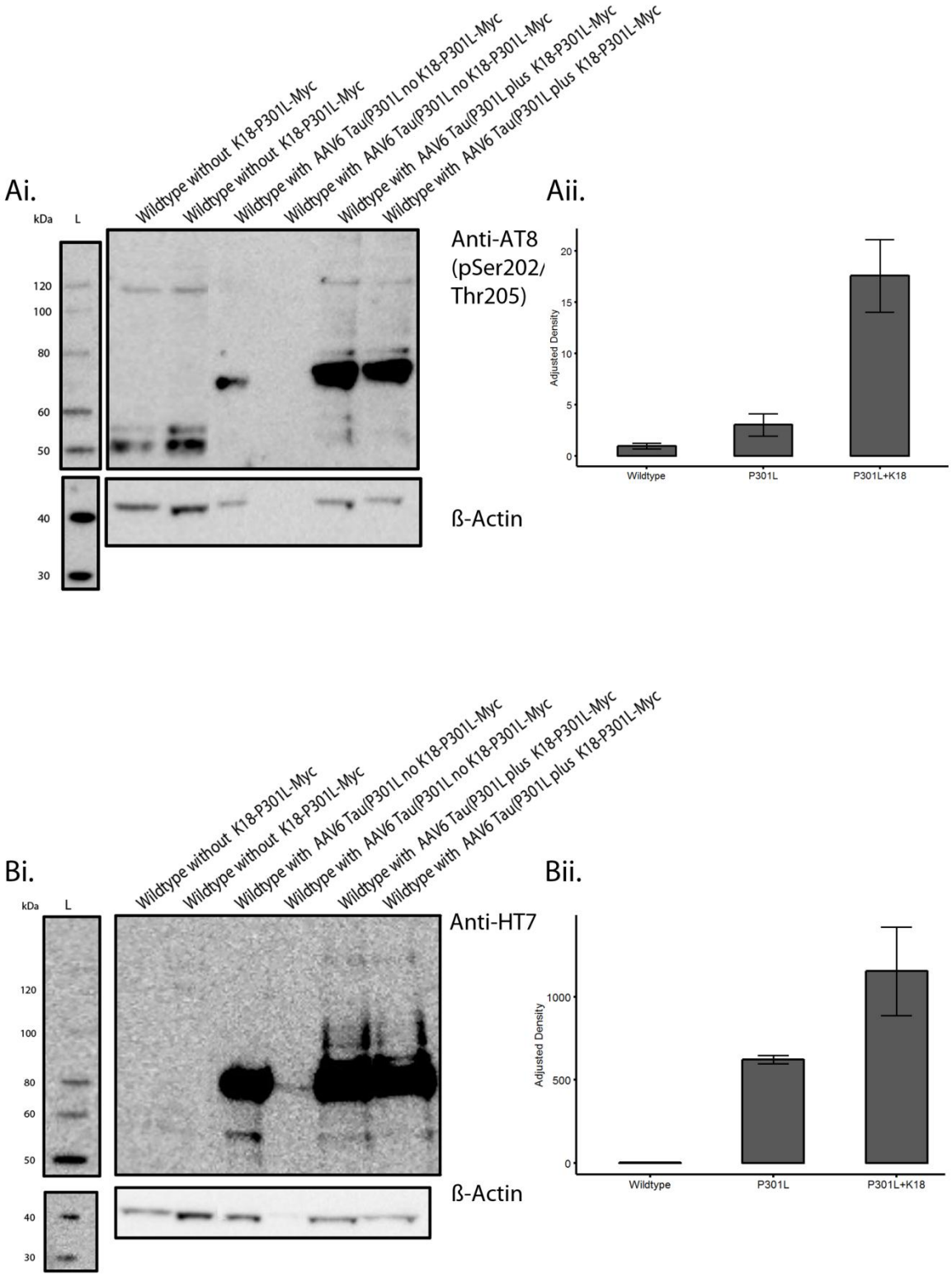

Figure 6.3. Validation of pathological tau expression Ai) Western blot probed for phosphorylated tau (AT-8; 1:1000) Aii) ß-actin quantification of blot shown in Ai. Bi) Western blot probed for

total human tau (HT-7; 1:2000) Bii) Quantification of the blot shown in Bi. NB. Statistical comparisons were not possible as both blots were from a single experiment.

In Fig 6.3.Ai, bands at approximately 68kDa demonstrate the presence of hyperphosphorylated human tau. In cells treated with both AAV6-Tau(P301L) and seeded with synthetic $K18^{P301L}$-myc fibrils, a secondary band (~79kDa) suggests the presence of an additional higher molecular weight hyperphosphorylated tau species , indicative of aggregation. Interestingly, in the untreated cells, some endogenous tau is present in its phosphorylated form (MW 51-55); however this is unsurprising as tau in rats tends to exist more frequently in phosphorylated forms than its human counterpart (Hanes et al., 2009). Quantification (Fig. 6.2.2.Aii) using a ß-actin standard revealed that the amount of phosphorylated tau in cells treated with AAV6-Tau(P301L) was approximately 3-fold that found in untreated cells, whereas in cells treated with both AAV6-Tau(P301L) and $K18^{P301L}$ the levels of phosphorylated tau were 17.5 fold that found in untreated cells.

A secondary western blot with anti-HT7 (Fig 6.2.2.Bi) confirmed that bands seen at 68-100kDa consist of purified human tau. Again, in cultures treated with AAV6-Tau(P301L) and seeded with $K18^{P301L}$-myc a band-shift can be seen (MW >79), which suggests aggregation. Human tau was not detected in untreated wells, and the relative densities of human tau in neurons treated with AAV6-Tau(P301L) alone and in cells treated with AAV6-Tau(P301L) with the subsequent addition of synthetic $K18^{P301L}$ fibrils are 621.6 and 1154.5 respectively in comparison with the untreated wildtype cultures (Fig 6.2.2.Bi).

Figure 6.4 shows the contrast in expression of phosphorylated tau in wildtype cultures and those treated with AAV6-Tau(P301L). Cultures were fixed at DIV 14 and probed with TAU5, for the detection of total tau (counter-probed using an AlexFluor-555 conjugated secondary antibody) and AT8, for the detection of tau phosphorylated at pSer202/Thr205 residues (counter-probed with an AlexaFluor-488 conjugated secondary antibody).

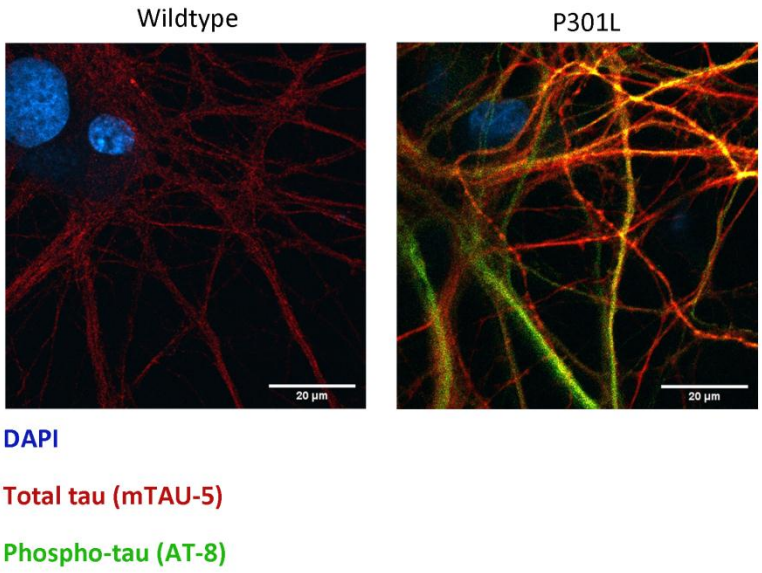

Figure 6.4. Presence of hyperphosphorylated tau is verfied by immunocytochemistry. Wildtype (left) and Tau(P301L) (right) were immunolabelled for total tau using Tau5 (1:200) and phosphorylated tau using AT-8 (1:500). DAPI was used as a nuclear counterstain

To confirm aggregation of $K18^{P301L}$ in our $Tau(P301L)^{K18}$ model we extracted soluble cytoplasmic proteins by fixing neurons in 4% PFA, 4% sucrose and 1% Triton X-100 (Volpicelli-Daley et al., 2014, Calafate et al., 2015b) and stained for insoluble tau with 15µM pFTAA in PBS for 30 minutes, after which ICC was carried out as described in section 2.3.3 of the Methods. pFTAA is a high affinity oligothiophene probe that detects filamentous tau *in vitro* and *in vivo* (Brelstaff et al., 2015). The results are shown in Figure 6.4.1. As expected, our fixation method completely removed the soluble tau fraction demonstrated by a lack of staining of phosphorylated tau in the P301L condition cf. Fig 6.4 where neurons were fixed under regular fixation conditions and neurons expressing P301L show high levels of staining for phosphorylated tau. Furthermore, neurons expressing both the P301L mutation and seeded with $K18^{P301L}$ fibrils showed high levels of pFTAA stained aggregates which co-localized with AT-8 staining, confirming our amyloid aggregates were comprised of phosphorylated tau. Wildtype neurons were not highly phosphorylated and seeding with $K18^{P301L}$ failed due to the lack of template and therefore showed no aggregation.

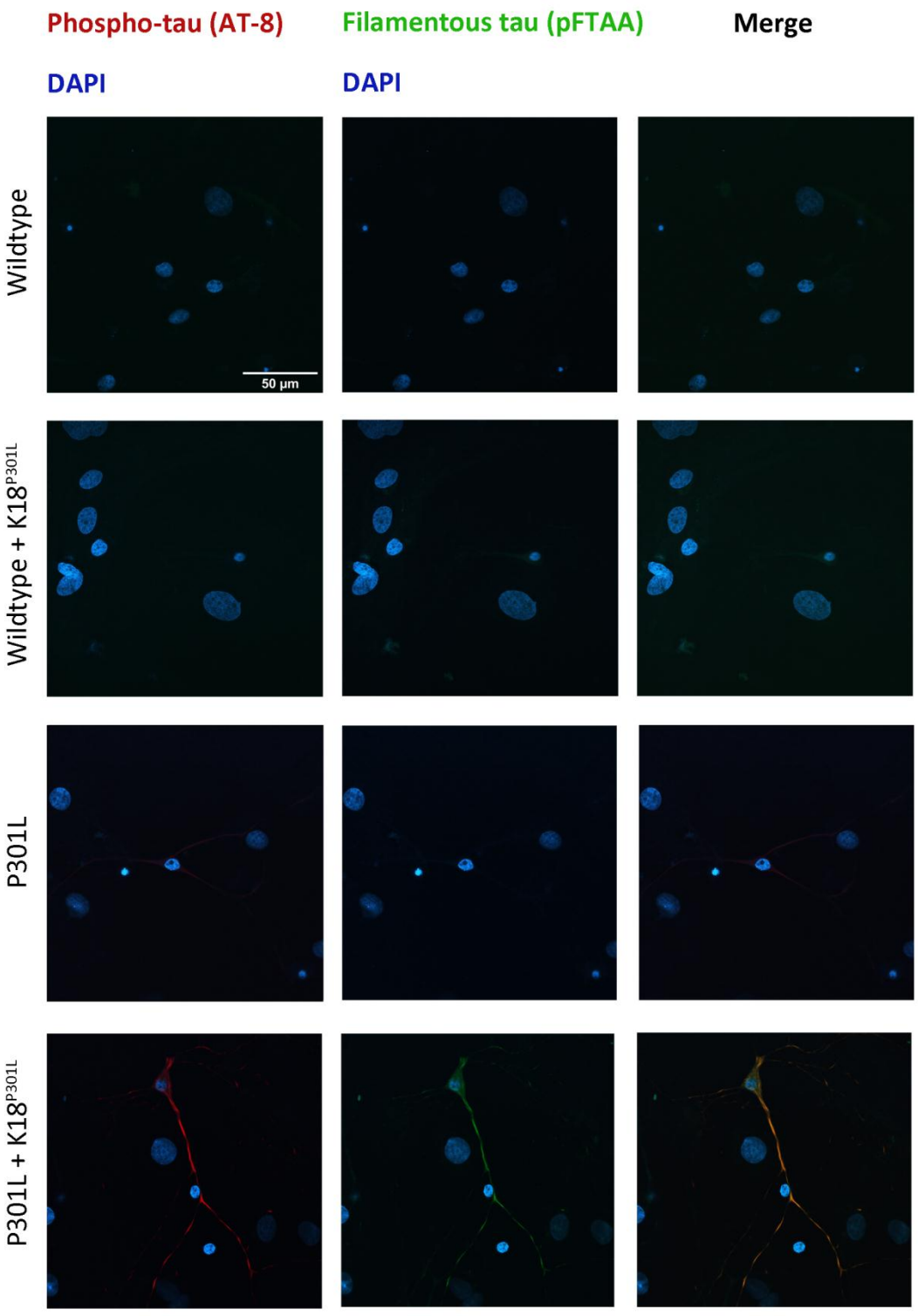

Fig 6.4.1 Confirmation of aggregation in Tau(P301L)K18- cultures using pFTAA. Neurons were immunolabelled for phosphorylated tau (AT-8; 1:500) and stained with pFTAA to detect aggregates. DAPI was used as a nuclear counterstain

6.2.3. Characterization of $K18^{P301L}$-myc fibrils

The majority of tauopathies result from sporadic mutation, however specific mutations within the *MAPT* gene, such as P301L, are the cause of several dominantly inherited FTD syndromes (Hutton et al., 1998). Expression of the P301L mutation has been shown to aggressively increase the propensity of tau to form amyloid; paracrystalline protein assemblies with a rich ß-sheet structure (Barghorn et al., 2000). Specific mutation-driven derivatives of tau have been shown to propagate *in vitro* and *in vivo* with high conformational fidelity, which gives rise to the classification of tau as 'prion-like' (Sanders et al., 2014). True prions are characterized by their ability to stably maintain specific, amyloidogenic conformations *in vivo*, with each distinctive structure resulting in a distinctive clinical pathology. Similarly, it has been demonstrated that different strains of tau carrying mutations associated with FTDP-17 result in uniquely presenting tauopathies, highlighting the relevance of structure to clinical presentation (Sanders et al., 2014, Kaufman et al., 2016, Narasimhan et al., 2017). Therefore, the aim of this section was to use biophysical techniques to provide structural characterization of the synthetic $K18^{P301L}$ fibrils used in this work. To do so we used Transmission electron microscopy (TEM), Circular dichroism (CD) and X-ray fibre diffraction (XRFD).

As mentioned previously, synthetic $K18^{P301L}$ fibrils were produced *in vitro* by incubating 40µM $K18^{P301L}$ peptide (*Tebu Bio)* with low molecular weight heparin (MW=3000) and 2mM DTT reducing agent in 100mM sodium acetate buffer (pH 7.0) at 37°C for 7 days. Following this, the solution underwent centrifugation at 100,000g (4°C) for 1 hour and the pellet resuspended in the same volume of 100mM sodium acetate buffer (pH 7.0). The $K18^{P301L}$ fibrils were sonicated with 10x 1s pulses at 20% amplitude and stored in aliquots at -80°C. Before adding the fibrils to primary neurons, they were thawed on ice, diluted to a concentration of 10µM, again using 100mM sodium acetate buffer (pH 7.0) and sonicated on ice for 20 minutes and further diluted in culture medium to 2.5nmol.

TEM was used to observe the morphology of $K18^{P301L}$ before and after the second sonication stages (Figure 6.5.Ai and ii). TEM grids were prepared by applying 4µl of peptide (concentration 10µM) to a Formvar grid and allowing two minutes for absorption before blotting dry, rinsing with miliQ-filtered water and negatively staining with 2% (w/v) uranyl acetate. Electron micrographs

shown in Figure 6.5 are the most representative of three independent sample preparations. Upon thawing and before sonication, $K18^{P301L}$ fibrils appear elongated and twisted (insert Fig 6.A.i), characteristic of paired helical filament formation. Aggregation of fibres is also evident. After twenty minutes of sonication (Fig 6.5.Aii), fibres are fragmented and are no longer found in large clumps. The electron micrograph taken post-sonication is representative of the state at which the fibrils are seeded into primary neuronal cultures pretreated with AAV6-Tau(P301L). Electron micrographs were obtained with the help of Saskia Pollock (Serpell / Staras lab, University of Sussex).

Confirmation that $K18^{P301L}$ fibrils have a secondary ß-sheet structure, inherent to all amyloid proteins, was carried out using CD and XRFD. To gain adequate signal, 40µM $K18^{P301L}$ was used in each preparation. The CD spectra obtained for $K18^{P301L}$ pre- and post-sonication is shown in Fig.6.5.B. $K18^{P301L}$ fibrils showed a strong ß-sheet signal (minima 218nm, maxima 195nm). The ß-sheet signal post-sonication is stronger than pre-sonication, which is likely due to an increased number of fibrils in solution after sonication. For XRFD, 10µl of peptide was suspended in between two wax-tipped borosilicate capillaries and incubated for 24 hours at room temperature in a parafilm – sealed petri dish to allow the formation of aligned fibres. Figure 6.5.C. shows the XRFD pattern generated from the $K18^{P301L}$ fibrils; $K18^{P301L}$ displays a cross-ß pattern, with a sharp reflection along the meridian at 4.7Å and a signal on the equator at 10Å. These signals, characteristic of a cross-β structure arise from hydrogen-bonded ß-strands that run perpendicular to the fibre axis to form ß-sheet ribbons that extend along the fibre axis (Morris and Serpell, 2012). Preparation of samples for CD and XRFD as well as data acquisition was carried out with the help of Youssra Al-Hilaly (Serpell lab, University of Sussex). In short, the three biophysical techniques confirmed that $K18^{P301L}$ forms filaments (TEM) with a β – rich conformation (CD) which gives the expected amyloid–like cross-β X-ray fibre diffraction pattern (Berriman et al., 2003).

Prior research has demonstrated that the successful seeding of tau fibrils is dependent on ß- sheet structure, whereby the propagation of fibrils is dependent upon a homotypic background conformation. The western blot included in Fig 6.5.D. demonstrates that this is also true for $K18^{P30L}$ fibrils. Here, treatment of cultures expressing only endogenous tau with $K18^{P30L}$fibrils i.e. a heterotypic background, does not result in successful seeding, resulting in an undetectable quantity of human tau in these cultures at DIV 14 (lane 3). This demonstrates the necessity of the P301L mutation to provide the correct scaffolding for the propagation of $K18^{P30L}$.

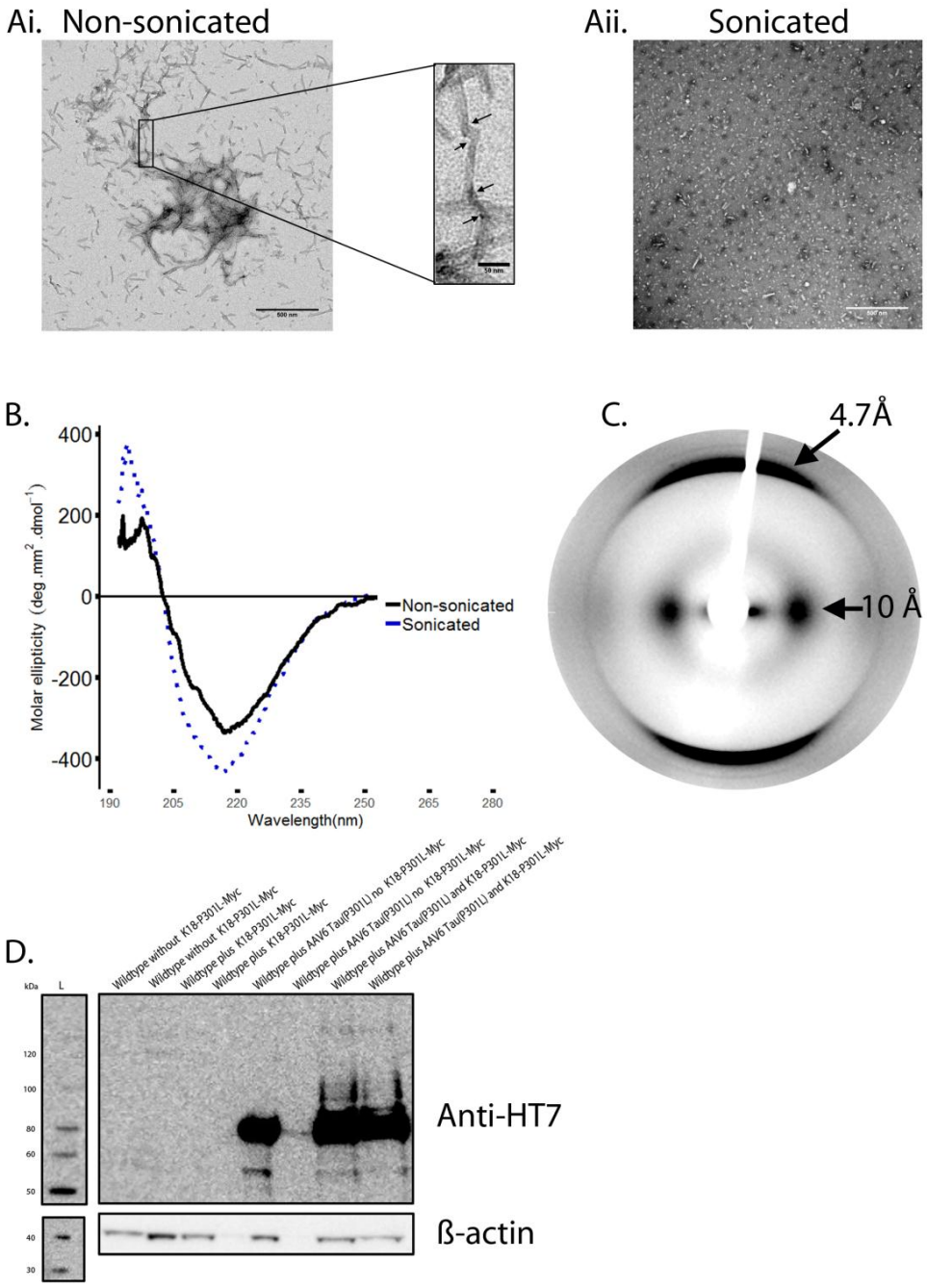

Fig 6.5 Structural characterization of K18^{P301L} fibrils. 10µM K18^{P30L} fibrils (Ai) were sonicated (Aii) and examined under TEM. B) CD spectra for 40µM of K18^{P30L}, sonicated and non-sonicated. Samples were prepared in 100mM sodium acetate buffer and measured in a 1mm pathlength cuvette and showed the expected signal at 218nm for β-strand conformation which was enhanced following sonication due to increased solubilization of protein in solution C) X-ray fibre diffraction pattern from aligned fibres formed by K18^{P30L} revealed characteristic cross-β diffraction signals at 4.7 Å and at 10 Å. D) Western blot demonstrating that K18^{P30L}cannot be

seeded in cultures not expressing the Tau(P301L) mutation. Total human tau was detected using HT-7 (1:2000).

6.3. Exploring the role of tau on synaptic vesicle release and recycling

Under regular physiological conditions, tau is found mainly concentrated in axons of neurons, where its role is the stabilization of microtubules. However, in cases of FTDP-17 pathology, such as conveyed by the P301L mutation, hyperphosphorylation of tau residues lower its binding affinity for microtubules (Wang and Mandelkow, 2016, Hong et al., 1998), resulting in its dissociation and mislocalization to presynaptic terminals and dendritic spines (Sahara et al., 2014, Hoover et al., 2010a). In *in vitro* synaptosome preparations, both wildtype and R406W tau (an alternative FTDP-17 pathogenic mutant) have been shown to bind synaptic vesicles. Nevertheless, mislocalization of tau to the presynaptic terminal *in vivo* is only present in FTDP-17 pathogenic mutants, making the binding of tau to synaptic vesicles under normal physiological circumstances unlikely (Zhou et al., 2017).

The ramifications of FTDP-17 pathology at the presynaptic terminal are relatively unexplored, whereas the mislocalization of tau to dendritic spines has been linked to abnormal trafficking of postsynaptic receptors (Hoover et al., 2010a, Ittner et al., 2010). At the fly neuromuscular junction (NMJ), *Drosophila melanogaster* expressing FTDP-associated mutations, including P301L, display significantly slower vesicle release and smaller recycling pools (Zhou et al., 2017). To build upon the research conducted at *dropsophila* NMJs, we wanted to explore the role of pathogenic tau upon synaptic vesicle recycling at small central synapses using rat primary hippocampal cultures.

Primary hippocampal cultures were prepared from P0/P1 rat pups and the various models created as described in section 6.2. Five models of differential tau expression were used: a knockdown model, created by lentiviral infection with 10µl TRC0000091298 at DIV 1; two models overexpressing the mutated P301L human tau delivered via an AAV6 vehicle, one seeded with $K18^{P301L}$ fibrils at DIV 3 and the other left unseeded, and a model overexpressing 1N4R wildtype human tau, again expressed via infection with AAV6 at DIV1. These were compared with untreated neurons expressing only endogenous rat tau. At DIV 7, all neurons were infected with AAV6-sypHy1x to allow the monitoring of synaptic vesicle dynamics. As in previous experiments, cultures were imaged at DIV 14 -21.

As a starting point for characterizing tau-related effects, we assayed the release and recycling of vesicles in each of our models in response to three different stimulation intensities; a 4AP stimulus to capture single fusion events, a 40AP stimulus to mobilize the RRP and a 1200AP stimulus to recruit the entire recycling pool. All were delivered at 20Hz. A schematic of the protocol is shown in Fig 6.6.A. Prior to data collection, responsive regions were detected and pre-photobleached by using a 40AP, 20Hz stimulus, followed by a 5 minute rest period before starting the 4AP stimulus. Two minutes were allowed to elapse between each round of stimulation. It is worth restating that we opted for a 4AP stimulus to examine quantal fusion events as the probability of release at hippocampal synapses has been estimated to be 0.22±0.03 (Branco et al., 2008), meaning that stimulation with a single action potential gives rise to a release event ~25% of the time. Therefore, by using a 4AP stimulation we increase the likelihood of capturing a single fusion event. Following data collection, experiments were analysed using custom written scripts in IgorPro.6. As it was unnecessary to compare the same synapses across each of the different stimuli, ROI detection was carried out for each of the individual image stacks so as to optimize the mask for that particular round of stimulation.

At 4APs, knockdown of endogenous tau has the most striking effect on response amplitude (Figures 6.6.Bi, Ci and Di), suggesting that endogenous wildtype tau may regulate quantal release events. Release events at synapses from knockdown cultures were significantly larger in comparison to wildtype, P301L-expressing, and WT-human tau expressing neurons ($p<0.001$ in all instances, one-way ANOVA). Interestingly, in comparison with the wildtype, the model expressing Tau(P301L) seeded with $K18^{P301L}$ also showed increased vesicle release upon 4AP stimulation, although the effect was more subtle, $p = 0.0104$ in comparison to the wildtype and $p = 0.00333$ in comparison overexpression of human tau (HT). Increased vesicle release in the knockdown was sustained during RRP recruitment; $p < 0.001$ in all comparisons, one-way ANOVA (Fig 6.6.Bii, Cii and Dii), Again, synapses in the $Tau(P301L)^{K18}$ model also showed an increased propensity for release ($p < 0.001$ in comparison to the wildtype, one-way ANOVA), and surprisingly so did synapses overexpressing wildtype human tau ($p < 0.01$ in comparison to the wildtype, one-way ANOVA). However, expression of the P301L mutation alone did not result in significant changes to RRP amplitude, suggesting that expression of P301L without $K18^{P301L}$ seeding does not affect either the size or the ability of this pool to release. However, the decay of this signal appears to be much faster (Fig 6.6.Bii), and therefore the kinetics of RRP release and retrieval are examined in the next section.

Figure 6.6.B(iii), C(iii) and D(iii) show that mobilization of the total recycling pool (1200APS at 20Hz) causes a strikingly different outcome to that observed at lower stimulation intensities. Under maximal stimulation, knockdown of tau results in the most significant impairment of TRP release ($p < 0.001$ in comparison to all other conditions, one-way ANOVA). Expression of P301L also results in highly compromised recycling pool (TRP) fusion ($p < 0.001$ in comparison with all other model systems, one-way ANOVA). Interestingly, in cultures expressing P301L and seeded with $K18^{P301L}$, this effect is ameliorated, with these cultures having a significantly larger TRP than their wildtype counterparts ($p < 0.001$, one-way ANOVA), as is also true in respect to the RRP. Neurons overexpressing wildtype human tau also had a significantly greater TRP release in comparison to the wildtype ($P < 0.001$, one-way ANOVA). Comparison of Figures 6.6.D(i-iii) highlights the changes in response distribution for each of the genotypes over each of the stimuli.

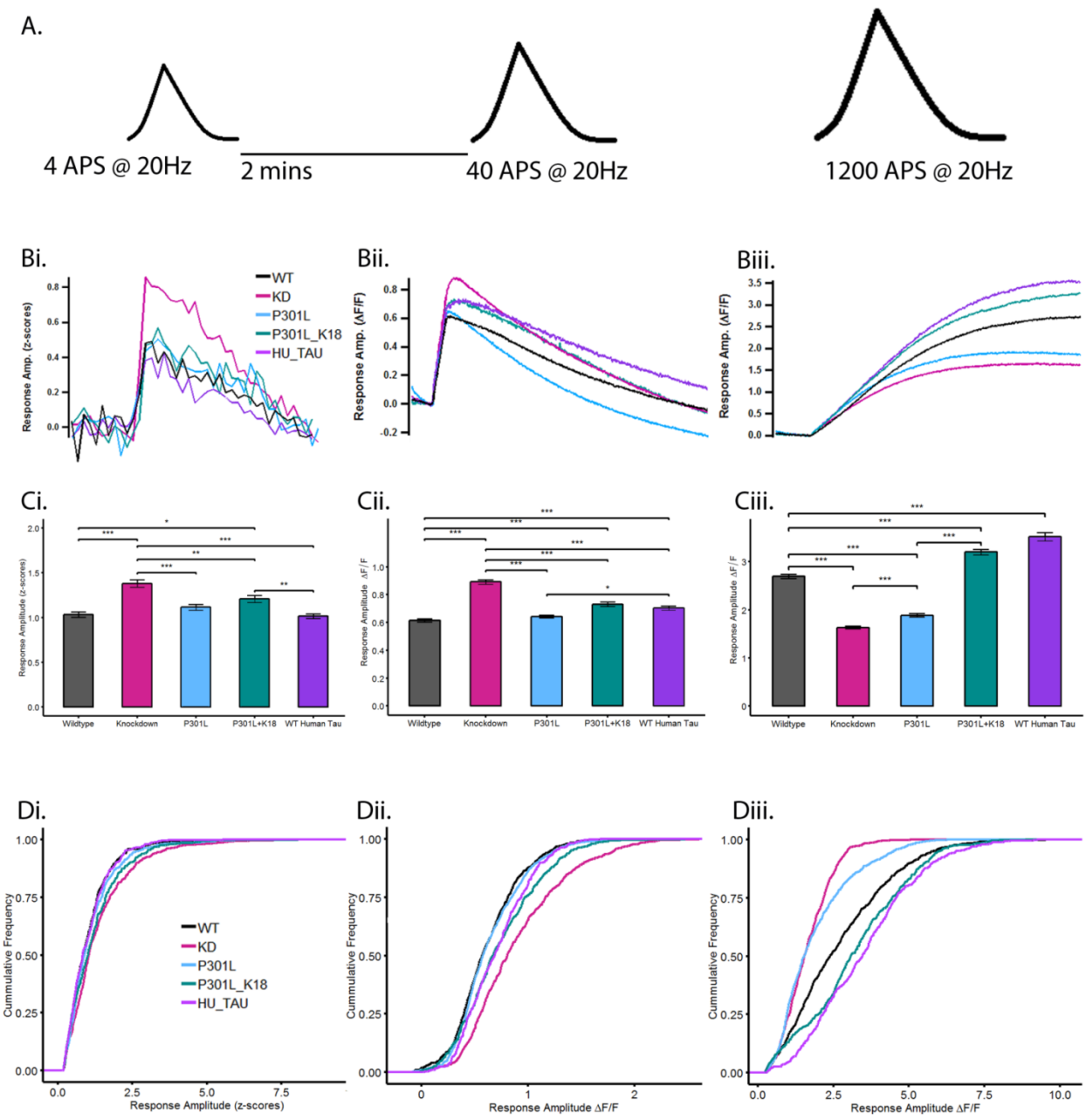

Figure 6.6. Modulation of quantal, RRP and total recycling pool release as a result of differential tau expression A) Schematic of protocol B) Traces of average responses recorded from synapses following i) 4AP, ii) 40AP and iii) 1200AP stimulation. All administered at 20Hz. C) Synaptic vesicle release as quantified using mean peak amplitude ± SEM following i) 4AP stimulation. Comparisons: WT vs KD; p<0.001, WT vs Tau(P301L)^{K18}; p=0.0104, KD vs Tau(P301L); p<0.001, KD vs Tau(P301L)^{K18}; p<0.001, KD vs WT human tau p<0.001, Tau(P301L)^{K18} vs WT human tau; p= 0.00333: One-way ANOVA with Tukey's post-hoc comparisons. Number of synapses: WT= 757, KD=971, Tau(P301L)= 762, Tau(P301L)^{K18} = 542, WT human tau = 737, all from a minimum of 4 coverslips. Ii) 40AP stimulation. Comparisons: WT vs KD; p<0.001, WT vs Tau(P301L)^{K18}; p<0.001, WT vs WT human tau; p<0.001, KD vs Tau(P301L); p<0.001, KD vs Tau(P301L)^{K18}; p<0.001, KD vs WT human tau; p<0.001, Tau(P301L) vs WT human tau; p= 0.0228: One-way ANOVA with

Tukey's post-hoc comparisons. Number of synapses: WT= 851, KD= 816, Tau(P301L)= 1079, Tau(P301L)^{K18} = 529, all from a minimum of 4 coverslips. iii) 1200APS. Comparisons: WT vs KD; p<0.001; WT vs Tau(P301L); p<0.001; WT vs Tau(P301L)^{K18}; p<0.001, WT vs WT human tau; p<0.001, KD vs Tau(P301L); p<0.001; KD vs Tau(P301L)^{K18}; p<0.001; KD vs WT human tau; p<0.001, Tau(P301L) vs Tau(P301L)^{K18}; p<0.001, Tau(P301L) vs WT human tau; p<0.001: one-way ANOVA. Number of synapses: WT = 1351, KD = 938; Tau(P301L) = 1097; Tau(P301L)^{K18} = 926, WT human tau = 622. All from a minimum of 4 coverslips. D. Cumulative frequency plots showing the distribution of response amplitudes to i) 4APs, ii) 40APS and iii) 1200APS.

6.3.1. The effect of tau on RRP kinetics

Using the same data as collected for section 6.2.1, we examined the effect of differential tau expression upon the recycling kinetics of the RRP, mobilized using a 40AP, 20Hz stimulus. This data is presented in Fig. 6.7. In Fig 6.7.Bi., the rate of exocytosis, as measured by linear regression of the 20-80% rise time, across each of the different tauopathic models is relatively similar, with the knockdown of endogenous tau causing exocytosis to be faster in comparison with the wildtype (p= 0.0403), and also faster in comparison with cultures overexpressing WT-human tau (p=0.0161). Figures Ci and Di reflect the similarity in distribution profiles of exocytotic rates across the different tau model systems.

Figure 6.7.Bii displays peak-normalized traces obtained from 40AP, 20Hz stimulation across each of the tau model systems, allowing easier visualization of differences in endocytosis. The rate of endocytosis was measured using single exponential fits of the signal decay. The most obvious effect of tau upon endocytosis can be seen in cultures expressing P301L but unseeded with K18^{P301L} fibrils, which undergo full endocytosis in 33.9 seconds, ~ 15 seconds faster than the wildtype cultures. Curiously, this acceleration is eradicated in the presence of K18^{P301L} fibrils, with neurons expressing the P301L mutation and K18^{P301L} fibrils actually completing endocytosis approximately 15 seconds slower than wildtype cultures. The differences in distribution of endocytosis kinetics, especially the marked difference between P301L and P301L^{K18} expressing neurons can be seen in figures 6.7.C.ii and Dii. Interestingly, Figure 6.7.C.ii highlights the extreme variability in endocytosis of Tau(P301L)^{K18} synapses, which may suggest that synapses in these cultures that are NFT bearing are recycling very slowly, yet those that are not tangle bearing are recycling very quickly, leading to a large IQR (shaded section of box). At the calyx of Held, timing of endocytosis following various stimulation intensities revealed differences in the retrieval time, depending on the action potential frequency and the number of vesicles released (Sun et al.,

2002). In our case, the amplitude of the fluorescence is representative of the number of vesicles released. Heterogeneity of release in experiments recruiting the RRP is discussed and shown in Chapter 4, Fig.4.2. Therefore, for a more detailed analysis, we separated the data into four groups based on the size of the response amplitude in order to study the extent of variability in endocytosis when the amplitude of exocytosis is constrained. This data is presented in Figures 6.7. and 6.8.

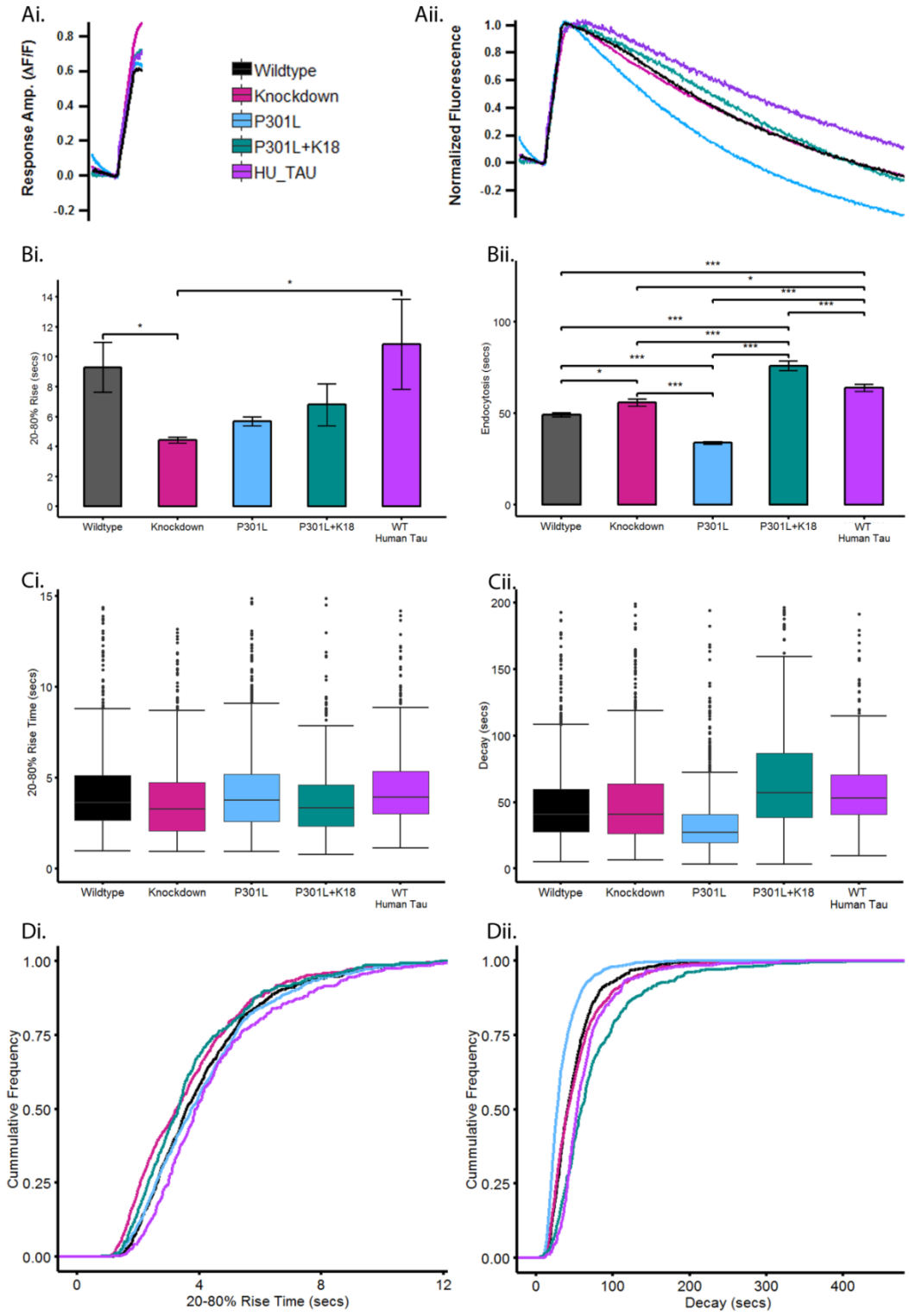

Figure 6.7. The effect of differential tau expression on release and endocytosis of the RRP A) Average traces showing i) exocytosis and ii) endocytosis. Traces are shown normalized to their peak amplitudes to simplify comparisons in signal decay. B) Mean± SEM of i) 20-80% rise, as measured by linear regression, representing exocytosis. Comparisons: WT vs KD; p = 0.0403, KD vs WT human tau; p = 0.0161: one-way ANOVA with Tukey's post hoc comparisons ii) endocytosis, as fitted by a single exponential. Values are 1/τ, giving time of decay in seconds.

Comparisons WT vs KD; p = 0.0134, WT vs Tau(P301L); p< 0.001; WT vs Tau(P301L)^{K18}, p<0.001l WT vs WT human tau; p<0.001, KD vs Tau(P301L); p<0.001, KD vs Tau(P301L)^{K18}; p< 0.001, KD vs WT human tau; p = 0.0117, Tau(P301L) vs Tau(P301L)^{K18}; p < 0.001, Tau(P301L) vs WT human tau; p < 0.001, Tau(P301L)^{K18} vs WT human tau; p < 0.001: one-way ANOVA with Tukey's post-hoc comparisons. Number of synapses: WT = 851, KD = 797, Tau(P301L) = 1057, Tau(P301L)^{K18} = 519, WT human tau = 458. All from a minimum of 4 coverslips C. Box and whisker plots showing the distributions of i) exocytosis kinetics and ii) endocytosis kinetics. Central divisions represent medians, shaded areas, the IQR and whiskers extend to 1.5x IQR. D. Cumulative frequency plots of i) exocytosis and ii) endocytosis kinetics.

In our dataset, we observed that the majority of synapses had response amplitudes that fell within a range of 1.5 ΔF/F units. Therefore, we grouped synapses which fell within the same quartiles; 'small response' synapses were regarded as those having amplitudes of less than 0.375 ΔF/F; 'medium response' synapses, 0.375 ≤ 0.75 ΔF/F; 'large response' synapses, 0.75 ≤ 1.125 ΔF/F, and 'very large response' synapses as those with response amplitudes in excess of 1.125 ΔF/F. Figure 6.8 displays peak-normalized traces of each of tau model system, subsetted by response amplitude and plotted against its wildtype counterpart. After subsetting, traces were again fitted with single exponential decay profiles to generate τ-coefficients and this data is presented in Fig 6.8.

Accelerated endocytosis in Tau(P301L) mutants is conserved across all synapses, independent of synapse size. One-way ANOVAs reveal that this difference in rate is highly significant; p < 0.001 in comparison to wildtype at small, medium and very large responding synapses, and p = 0.00357 at large response synapses. The box and whisker plots in Fig 6.9, panels Ai, Bi,Ci and Di demonstrate that the range of endocytic rates in P301L expressing neurons is reduced in P301L mutants, which might indicate that expression of this mutation reduces the variability in retrieval kinetics. Cumulative frequency plots, Figure 6.8, panels Aii, Bii, Cii and Dii, verify that the distribution in retrieval kinetics is left-shifted in P301L mutants revealing that a faster rate of endocytosis occurs across the synaptic population. In contrast, cultures expressing both the P301L tau mutation and K18^{P301L} fibrils showed slower retrieval kinetics than their wildtype counterparts, especially at large response and very large response synapses (p < 0.001 in both instances, one-way ANOVA). Overexpression of WT 1N4R human tau slowed endocytosis in synapses with small and medium responses compared with wildtype (p = 0.00560 and p = 0.00833 respectively, one-way ANOVA), however this effect was reduced at the level of large response synapses, p = 0.00288 and was not apparent in very large response synapses. Knockdown of tau mildly slowed endocytosis in large

response synapses ($p = 0.0108$) and very large response synapses ($p = 0.0399$) but did not appear to affect smaller response synapses.

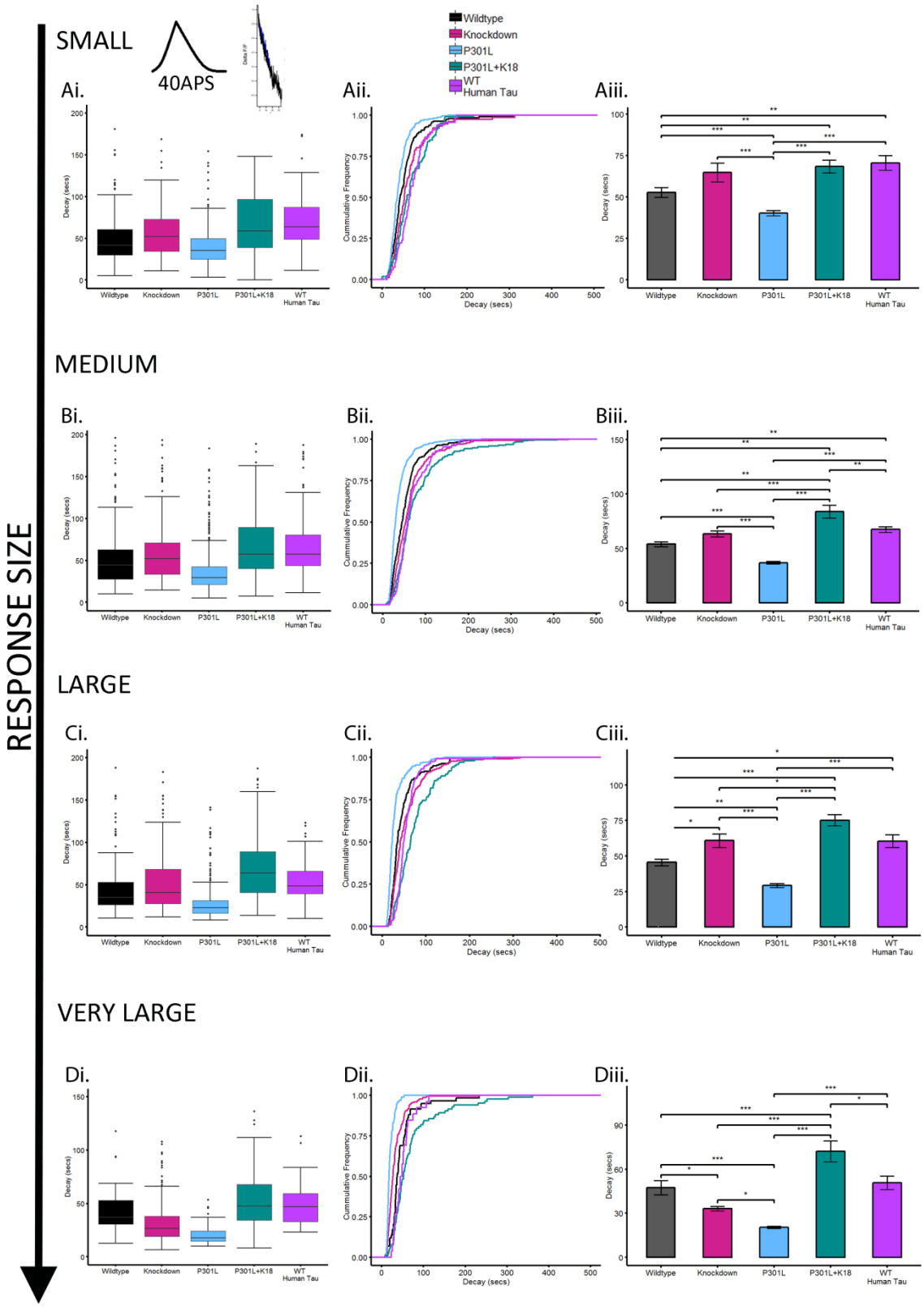

Figure 6.8. Kinetics of RRP retrieval when constrained to exocytosis A) Small synapses; peak amplitude <0.375 ΔF/F. Number of synapses: WT= 200, KD = 77, Tau(P301L) = 210, Tau(P301L)^{K19}

= 106, WT human tau = 70 i) Box and whisker plots show distribution of endocytic kinetics at small synapses. Central lines represent the median, shaded boxes, the IQR and whiskers extend to 1.5 x IQR ii) Cumulative frequency distribution of endocytosis kinetics of small synapses iii) Mean ± SEM of decay rates as fitted with a single exponential. Values shown are 1/τ, generating a time in seconds. Comparisons: WT vs Tau(P301L); p<0.001, WT vs Tau(P301L)^{K18}; p=0.00375, WT vs WT human tau; p = 0.00600, KD vs Tau(P301L); p < 0.001, Tau(P301L) vs Tau(P301L)^{K18}; p < 0.001, Tau(P301L) vs WT human tau; p < 0.001: one-way ANOVA with Tukey's post-hoc comparisons. B. Medium synapses: 0.0375≤ peak amplitude < 0.075 ΔF/F. Number of synapses: WT = 300, KD = 293 ,Tau(P301L) = 509, Tau(P301L)^{K18} = 192, WT human tau = 199 i) Box and whisker plots showing distributions of endocytic kinetics at medium synapses iii) Mean ± SEM of decay rates as fitted by a single exponential. Values shown are 1/τ, generating a time in seconds. Comparisons: WT vs Tau(P301L); p<0.001, WT vs Tau(P301L)^{K18}; p< 0.001, WT vs WT human tau; p = 0.00833, KD vs Tau(P301L); p < 0.001, KD vs Tau(P301L)^{K18}; p < 0.001, Tau(P301L) vs Tau(P301L)^{K18}; p < 0.001, Tau(P301L) vs WT human tau; p < 0.001, Tau(P301L)^{K18} vs WT human tau; p = 0.00488: one-way ANOVA with Tukey's post-hoc comparisons. C. Large synapses: 0.075 ≤ peak amplitude < 1.125 ΔF/F. Number of synapses: WT = 194, KD = 211, Tau(P301L) = 241, Tau(P301L)^{K18} = 192, WT human tau = 160 i) Box and whisker plots show distribution of endocytic kinetics at large synapses. ii) Cumulative frequency distribution of endocytosis kinetics at large synapses iii) Mean ± SEM of decay rates of large synapses as fitted with a single exponential. Values shown are 1/τ, generating a time in seconds. Comparisons: WT vs KD; p= 0.0108, WT vs Tau(P301L); p = 0.00357; WT vs Tau(P301L)^{K18}; p< 0.001, WT vs WT human tau; p = 0.0288, KD vs Tau(P301L); p < 0.001, KD vs Tau(P301L)^{K18}; p = 0.0495, Tau(P301L) vs Tau(P301L)^{K18}; p < 0.001, Tau(P301L) vs WT human tau; p< 0.001: one-way ANOVA with Tukey's post-hoc comparisons D) Very large synapses: 1.125ΔF ≤ peak amplitude. Number of synapses: WT= 58, KD = 216, Tau(P301L) = 94, Tau(P301L)^{K18} = 83, WT human tau = 26. i. Box and whisker plots show distribution of endocytic kinetics at very large synapses. Central division lines represent the median, shaded boxes, the IQR and whiskers extend to 1.5 x IQR ii) Cumulative frequency distribution of endocytosis kinetics at very large synapses iii) Mean ± SEM of decay rates as fitted with a single exponential. Values shown are 1/τ, generating a time in seconds. Comparisons: WT vs KD; p = 0.0399, WT vs Tau(P301L); p < 0.001, WT vs Tau(P301L)^{K18}, p < 0.001, KD vs Tau(P301L); p =0.0235, KD vs Tau(P301L)^{K18}; p < 0.001, Tau(P301L) vs Tau(P301L)^{K18}; p < 0.001, Tau(P301L) vs WT human tau; p< 0.001, Tau(P301L)^{K18} vs WT human tau; p = 0.0445: one-way ANOVA with Tukey's post-hoc comparisons.

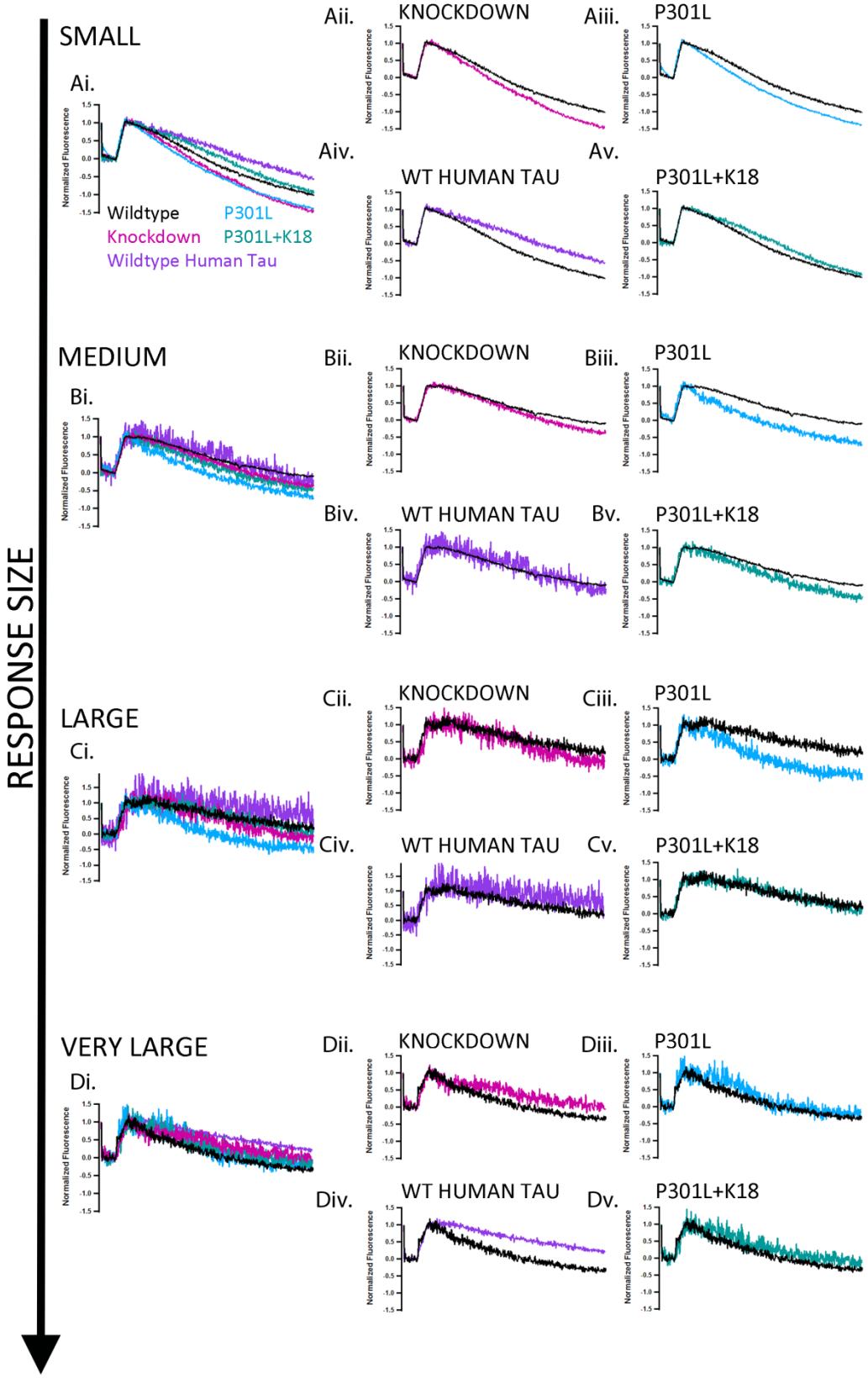

Figure 6.9. Comparisons of decay kinetics across all tau variants at each response size. Traces represent the average and are shown normalized to the peak to facilitate comparion of endocytosis. Each variant is shown plotted against the wildype, expressing only endogenous tau.

6.4. Understanding the role of tau on glutamate release at small central terminals

Neuronal network hyperexcitability is symptomatic of FTDP-17 mutation driven tauopathies and other neurodegenerative disorders including AD and schizophrenia (Lewerenz and Maher, 2015). When expressed in mice, P301L mutated tau results in increased glutamate release and impaired glutamate clearance in the hippocampus (Hunsberger et al., 2015). Using the optical reporter iGluSnFR, we sought to characterize the effects of differential tau expression upon glutamate release and clearance in primary hippocampal cultures.

Cultures were prepared from P0/P1 rats and the various tau expression models created as outlined previously in this chapter. Neurons were infected with AAV9-iGluSnFR (PennVector Core) at DIV 6/7 and imaged at DIV 14-21. For experimentation, coverslips were transferred to the custom built imaging chamber and maintained in 600µl EBS supplemented with 20µM AP-V and 50µM CNQX. Responsive regions were detected using a 40AP, 20Hz stimulus, following which 2 minutes were observed before starting the experiment. Neurons were stimulated with five successive rounds of 40AP stimuli (20Hz), with an inter-stimulus interval (ISI) of 5 seconds (Fig 6.10.A.). Successive stimulation, without adequate recovery time was employed to examine the role of tau in sustaining regular glutamate release during periods of high neuronal activity. Images were analysed using IgorPro.6. As iGluSnFR is a membrane bound construct, as opposed to sypHy or sy-GCaMP whose expression is localized to presynaptic terminals, detection of ROIs based upon pixel standard deviation was unsuitable. Therefore, we used a customized correlation algorithm in IgorPro, written by Professor Tom Baden. Firstly, the traces of all pixels in the field of view (FOV) were linearly correlated to the traces of every other pixel in the FOV. Neighbouring pixels with correlation coefficients (ρ) exceeding threshold correlation, $\rho_{Threshold}$ (> 0.2 in our experimental system) were then grouped into single ROIs. ROIs were grown until $\rho < \rho_{Threshold}$ in all neighbouring pixels, or the area of the ROI exceeded 10 pixels. An ROI mask was created based upon the first round of 40AP stimulation and used to analyse the subsequent trials.

Panels Bi, Ci, Di, Ei and Fi ion Figure 6.10 depict the average response profiles of synapses from each of the tau models. Across all trials, neurons expressing P301L pathogenic tau exhibited excessive glutamate release, significant at $P<0.001$ in comparison to all other groups at each round of stimulation (Fig 6.10.Bii, Cii, Dii, Eii and Fii). Glutamate release was quantified as the area under

the curve (AUC). Nevertheless, when comparing the average traces, it is evident that as stimulation progresses glutamate release in P301L expressing neurons becomes more similar to that of the wildtype (Fig 6.10.Biii cf. 6.10.Fiii), indicating that upon concurrent stimulation Tau(P301L) expressing neurons are able to regulate glutamate release to some extent. Intriguingly, seeding of Tau(P301L) expressing neurons with $K18^{P301L}$ fibrils seems to rescue this effect in the first four trials, and in terms of glutamate release these synapses do not seem to behave differently to synapses expressing endogenous tau (wildtype) during these rounds of stimulation. Only in the final trial do synapses expressing P301L+$K18^{P301L}$ exhibit attenuated glutamate release in comparison with the wildtype ($p=0.0256$). Knockdown of tau also has little effect on glutamate release until the final round of stimulation, where the mean amplitude of glutamate release is significantly lower than in the wildtype, $p = 0.0161$. Overexpression of 1N4R wildtype human tau (HU_TAU) does not cause any significant changes to the amplitude of glutamate release.

To explore whether or not differential tau protein expression influences the ability of neurons to adapt their release of glutamate upon successive stimulation without adequate recovery time, we normalized the amplitudes of trials 2-5 to the first peak. This data is shown in Fig 6.11. In wildtype synapses, attenuation of glutamate release happens relatively gradually, and glutamate release does not differ significantly between adjacent trials (Fig. 6.11.Ci). N.B. To avoid cluttering of the graph, only significance between neighbouring trials is displayed. The same is true of overexpression of WT human tau, where significant decreases in glutamate release can only be seen between the first and second trials ($p<0.001$) and fourth and fifth trials ($p = 0.0328$). In the tau knockdown and P301L and P301L+$K18^{P301L}$ expressing neurons, attenuation of glutamate release is more rapid and significant drops in response amplitude are seen in 92% of adjacent trials – see figure legend for detailed breakdown of results. Figure 6.11.E. compares the decrease in normalized response amplitude across all trials for each tau model and reveals that glutamate release is depressed to a similar extent in synapses expressing either wildtype or WT human tau, but is further supressed in tau knockdown, P301L and P301L+$K18^{P301L}$ models. Moreover, following the initial depression in response, glutamate release in neurons expressing endogenous or WT human tau appears to plateau whereas in tau knockdown, P301L and P301L+$K18^{P301L}$ cultures glutamate release is attenuated in an almost linear fashion. As a future direction it would be interesting to examine whether or not glutamate release in these synapses would eventually plateau or whether it would continue to decline linearly until synapse exhaustion.

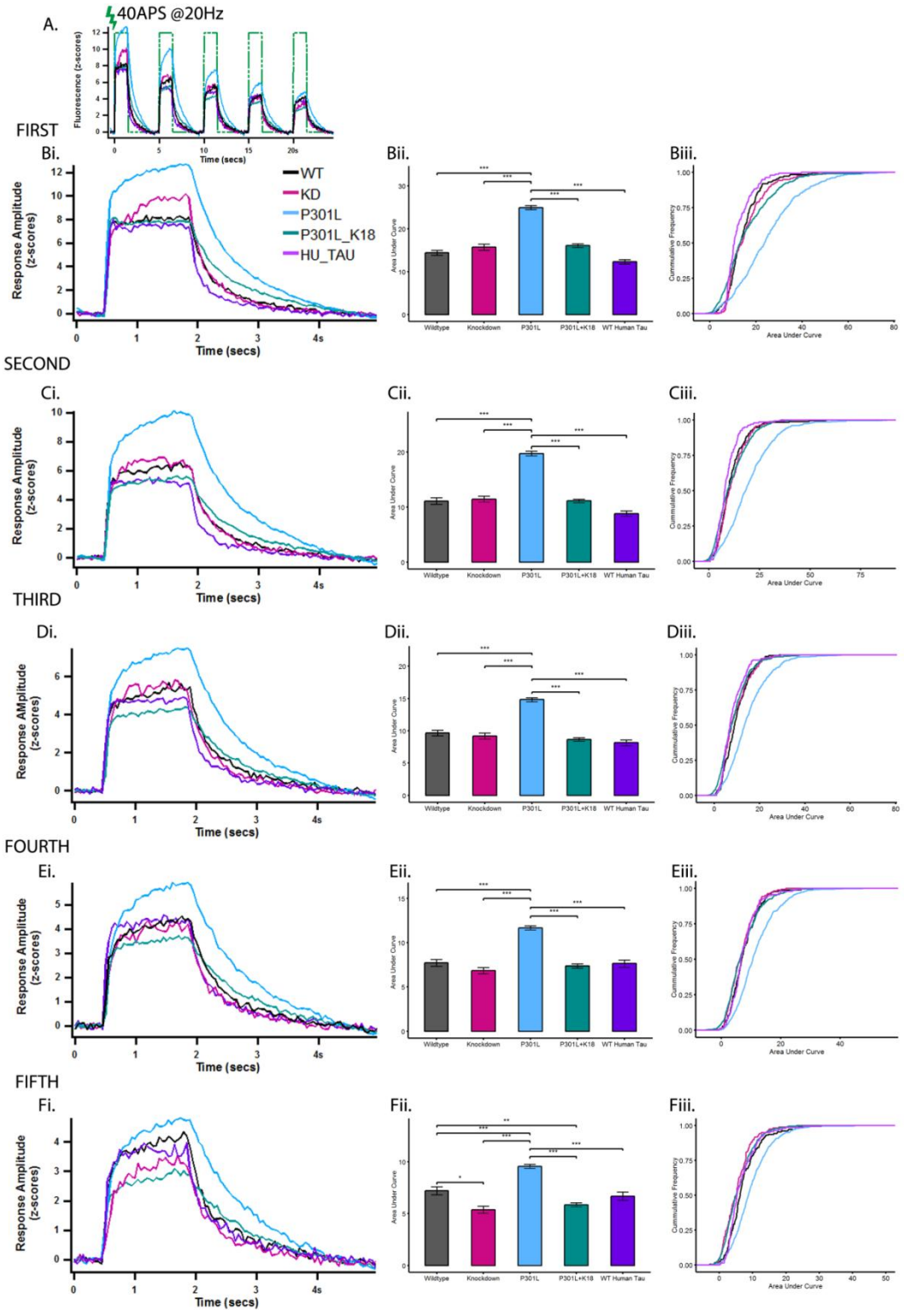

Figre 6.10. Comparison of glutamate release across all tau models upon repetitive stimulation with 40APs. Average traces generated per tau model, green lines indicate periods of stimulation with 40APS at 20Hz. Number of synapses: WT = 171, KD = 157, Tau(P301L) = 742, Tau(P301L)^{K18} = 654, WT human tau = 135 B-F(i) Average traces of response to first trial B-F(ii) Means ± SEM of

glutamate release, quantified as AUC. Bii) First trial: Tau(P301L) expressing neurons released significantly more than all other conditions; $p < 0.001$ in all instances Cii) Second trial: Tau(P301L) expressing neurons released significantly more than all other conditions; $p < 0.001$ in all instances Dii) Third trial: Tau(P301L) expressing neurons released significantly more than all other conditions; $p < 0.001$ in all instances Eii) Fourth trial: Tau(P301L) expressing neurons released significantly more than all other conditions; $p < 0.001$ in all instances Fii) Fifth Trial: Tau(P301L) expressing neurons released significantly more than all other conditions; $p < 0.001$ in all instances, WT vs KD; $p = 0.0161$, WT vs Tau(P301L)^{K18}; $p = 0.0256$, General linear model of repeated measures (GLM-RM) with Tukey's post-hoc comparisons. B-F(iii) Cumulative frequency distributions of glutamate release across all trials.

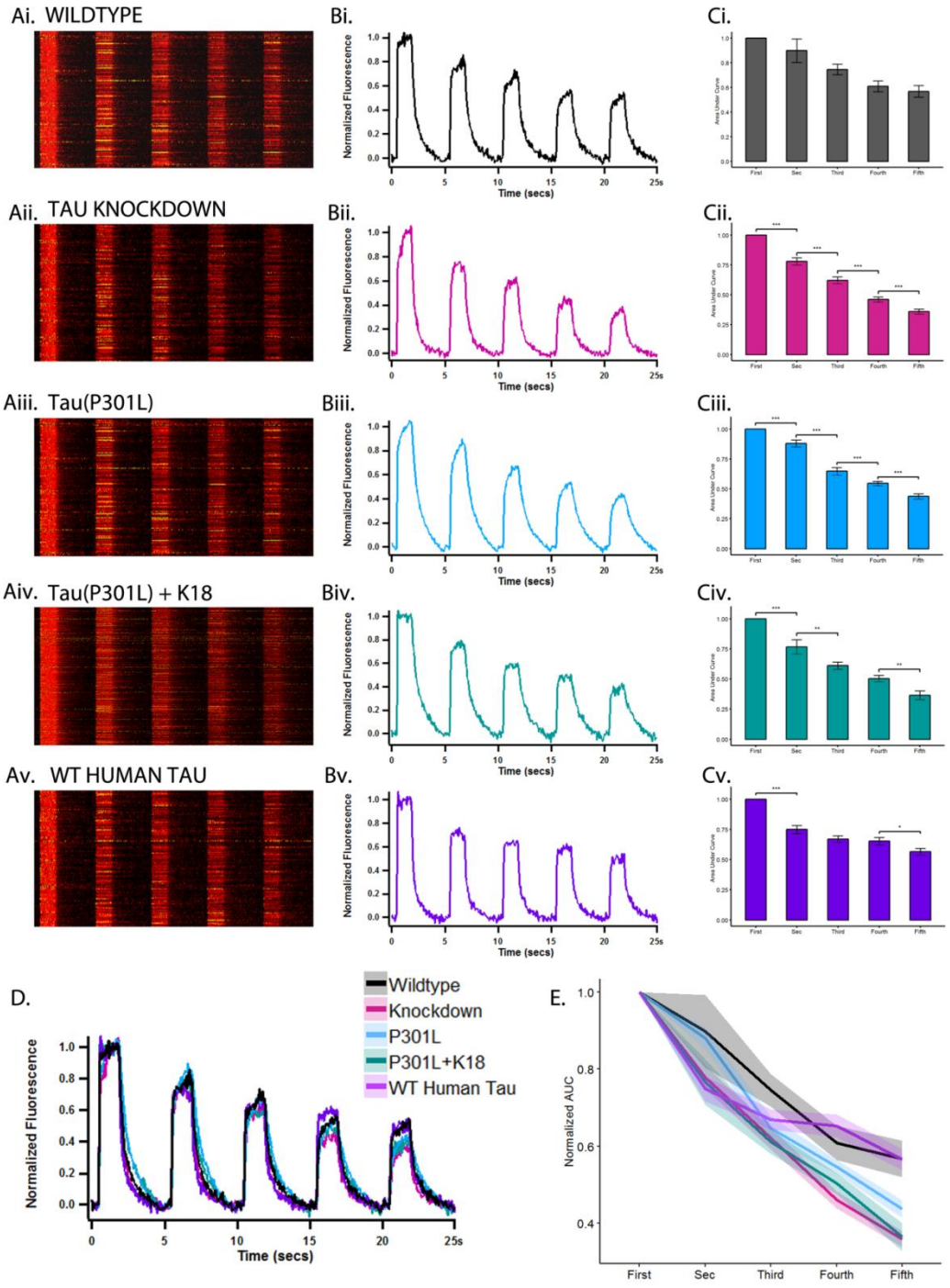

Figure 6.11 Depression of glutamate release at the synapse is enhanced in tau knockdown and neurons expressing Tau(P301L) and Tau(P301L)^{K18} Synapse numbers are the same as quoted for figure 6.10 A(i-v) Heatplots indicating response intensity, expressed normalized to the first peak B(i-v) Average of normalized traces per tau expression model C. Means ± SEM of normalized glutamate release, quantified as AUC. Statistics were generated using a general linear model of repeated measures with Tukey's post-hoc comparisons i) Wildtype ii) Tau knockdown: Comparisons; p< 0.001 in all instances iii) Tau(P301L): Comparisons; p< 0.001 in all instances iv) Tau(P301L)$^{K18+}$: Comparisons: First trial vs Second trial p < 0.001, Second trial vs Third trial; p = 0.00136, Fourth vs Fifth trials; p = 0.00594. v) WT human tau. Comparisons: First trial vs Second

trial; p < 0.001, Fourth vs Fifth trials; p = 0.0328. D) Composite showing normalized, average traces for each tau variant E. Rate of depression of glutamate release is not as pronounced in wildtype and WT human tau expressing cultures.

6.4.1. Glutamate clearance is impaired in neurons expressing P301L pathogenic tau

Impaired glutamate clearance as a result of neuronal dysfunction is implicated in a number of neurodegenerative diseases, including FTDP-17 driven tauopathies (Hunsberger et al., 2015). Under normal physiological conditions, glutamate levels in the synaptic cleft are tightly regulated as excess glutamatergic stimulation leads to neuronal excitotoxicity and eventually cell death. Here, we use iGluSnFR to monitor glutamate clearance in tau knockouts, overexpression of P301L with and without $K18^{P301L}$ fibrils, and overexpression of 1N4R wildtype human tau. Clearance in these culture systems is compared with glutamate clearance in untreated, wildtype neurons expressing solely endogenous rat tau. To examine glutamate clearance we used iGluSnFR, a rapid intensity-based fluorescent probe with excellent spatiotemporal dynamics. The use of iGluSnFR to quantify glutamate clearance at the synapse was first proposed by Parsons et. al., where it was applied in a mouse model of Huntingdon disease (Parsons et al., 2016).

Using the same dataset as presented in 6.4.1, the decay of fluorescent signal after a 40AP, 20Hz stimulation was fitted by a single exponential, generating a τ constant. Across trials 1-5, neurons expressing P301L alone and with $K18^{P301L}$ fibrils demonstrated impaired glutamate clearance (Figure 6.12.) ($p < 0.001$ in comparison with tau knockdown, overexpression of WT human tau and endogenous wildtype tau; two-way ANOVA). The inserts on panels Ai-Av. show peak normalized traces to simplify comparison of decay kinetics; these highlight the significant burden of P301L ± $K18^{P301L}$ in regards to glutamate clearance. The cumulative frequency plots (Fig 6.11.Ci-Cv) show that the distribution in glutamate clearance time is dramatically slowed across these neuronal populations in comparison with the knockdown, wildtype or wildtype human tau expression neurons. Notably, the range of clearance kinetics in Tau(P301) mutants with and without addition of $K18^{P301L}$ fibrils is much larger than in the other model systems (Fig 6.12.Ai-Av), reflected by the extended IQR in these plots. This suggests that in these cultures some neurons still retain regular physiological functions whilst others have been dramatically affected by the Tau(P301L) mutation. Interestingly, despite having vastly differences in glutamate release, in terms of glutamate clearance, Tau(P301L) cultures expressing fibrils behave similarly to those without fibrils.

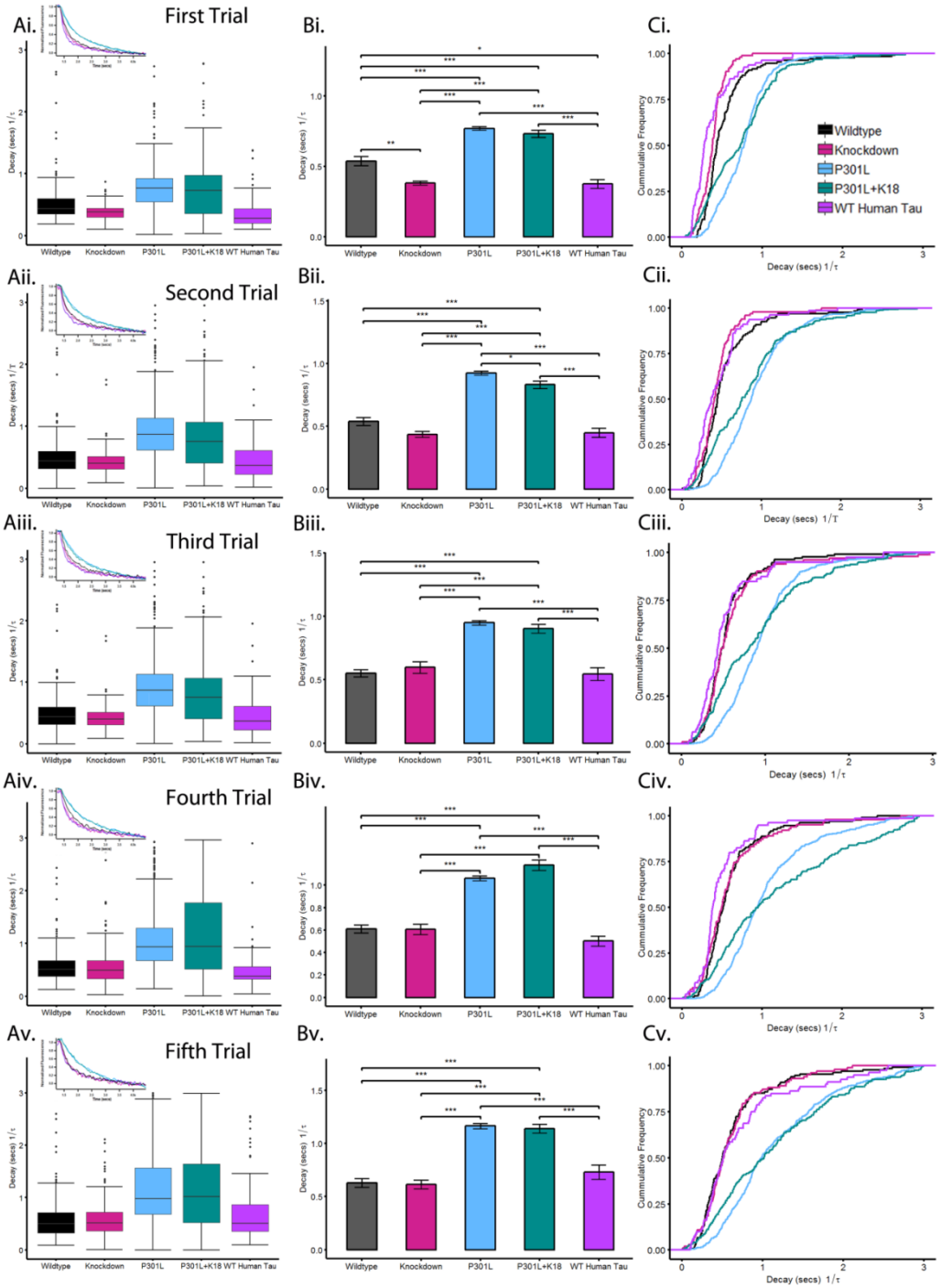

Figure 6.12. Clearance of glutamate is impaired in neurons expressing Tau(P301L) with and without the addition of $K18^{P301L}$ fibrils. Clearance of glutamate was quantified by fitting the decay of the iGluSnFR signal with a single exponential. Synapse numbers are as quoted for Fig 6.10. A(i-v). Distribution of clearance kinetics across all trials. Central shaded areas indicate the IQR; the division line, the median and the whiskers extend to 1.5 x IQR. Inserts show the decay of peak normalized traces. B. Means ±SEM of clearance kinetics. Statistics computed using GLM of repeated measures with Tukey's post-hoc comparisons i) First trial, comparisons; WT vs KD; p = 0.00757, WT vs Tau(P301L); p < 0.001, WT vs $Tau(P301L)^{K18}$; p < 0.001, WT vs WT human tau; p = 0.0118, KD vs Tau(P301L); p < 0.001, KD vs $Tau(P301L)^{K18}$;p < 0.001, Tau(P301L) vs WT human tau; p < 0.001, $Tau(P301L)^{K18}$; p< 0.001 ii) Second Trial, comparisons: WT vs Tau(P301L); p <

0.001, WT vs Tau(P301L)^{K18} ; p< 0.001, KD vs Tau(P301L); p < 0.001, KD vs Tau(P301L)^{K18} ; p < 0.001, Tau(P301L) vs Tau(P301L)^{K18}; p = 0.0164, Tau(P301L) vs WT human tau; p < 0.001, Tau(P301L)^{K18} vs Human tau, p < 0.001 iii) Third trial, comparisons: WT vs Tau(P301L); p < 0.001, WT vs Tau(P301L)^{K18} ; p< 0.001, KD vs Tau(P301L); p < 0.001, KD vs Tau(P301L)^{K18} ; p < 0.001, Tau(P301L) vs WT human tau; p < 0.001, Tau(P301L)^{K18} vs Human tau, p < 0.001 WT vs Tau(P301L); p < 0.001, WT vs Tau(P301L)^{K18} ; p< 0.001, KD vs Tau(P301L); p < 0.001, KD vs Tau(P301L)^{K18} ; p < 0.001, Tau(P301L) vs Tau(P301L)^{K18}; p = 0.0164, Tau(P301L) vs WT human tau; p < 0.001, Tau(P301L)^{K18} vs Human tau, p < 0.001 iv) Fourth trial, comparisons: WT vs Tau(P301L); p < 0.001, WT vs Tau(P301L)^{K18} ; p< 0.001, KD vs Tau(P301L); p < 0.001, KD vs Tau(P301L)^{K18} ; p < 0.001, Tau(P301L) vs WT human tau; p < 0.001, Tau(P301L)^{K18} vs Human tau, p < 0.001 WT vs Tau(P301L); p < 0.001, WT vs Tau(P301L)^{K18} ; p< 0.001, KD vs Tau(P301L); p < 0.001, KD vs Tau(P301L)^{K18} ; p < 0.001, Tau(P301L) vs WT human tau; p = 0.0164, Tau(P301L) vs WT human tau; p < 0.001, Tau(P301L)^{K18} vs Human tau, p < 0.001 v) Fifth trial, comparisons: : WT vs Tau(P301L); p < 0.001, WT vs Tau(P301L)^{K18} ; p< 0.001, KD vs Tau(P301L); p < 0.001, KD vs Tau(P301L)^{K18} ; p < 0.001, Tau(P301L) vs WT human tau; p < 0.001, Tau(P301L)^{K18} vs Human tau, p < 0.001 WT vs Tau(P301L); p < 0.001, WT vs Tau(P301L)^{K18} ; p< 0.001, KD vs Tau(P301L); p < 0.001, KD vs Tau(P301L)^{K18} ; p < 0.001, Tau(P301L) vs WT human tau; p < 0.001, Tau(P301L)^{K18} vs Human tau, p < 0.001 C(i-v) Cumulative frequency plots show distribution of glutamate clearance kinetics across all trials

6.5. Discussion

In Alzheimer's disease and other related tauopathies, hyperphosphorylated forms of microtubule-associated protein tau accumulate at the synapse and are thought to contribute to deficits in synaptic transmission and neurodegeneration. Under regular physiological conditions, tau binds and stabilizes microtubules in a manner that is tightly regulated by phosphorylation at serine and threonine residues (Buee et al., 2000, Lee et al., 2001).

In this chapter, we demonstrate that either knockdown of endogenous tau in a primary hippocampal culture system or overexpression of tau carrying the FTDP-17 mutation, P301L, result in a decrease in size of the total number of vesicles available for release at the synapse (Figure 6.3.Cii), recruited using a 1200AP stimulation at 20Hz. In addition to its microtubule-stabilizing properties, tau has also been implicated in the regulation of the actin cytoskeleton (Griffith and Pollard, 1982), and it has been shown that tau can mediate microtubule-actin co-alignment (Elie et al., 2015). At the synapse, actin exists in two states; monomeric G-actin, which is evenly distributed through axons and synaptic sites (Zhang and Benson, 2002), and filamentous actin (f-actin), which is proposed to surround and tether vesicle pools (Sankaranarayanan et al., 2003), (Shupliakov et al., 2002). Interestingly, elevated f-actin levels are found in P301L mouse models of FTDP-17 (Fulga et al., 2007) and the presence of Hirano bodies, actin-rich paracrystalline

inclusions, is found in brain histopathological samples of AD and related tauopathies (Spears et al., 2014). Therefore, we think that the expression of P301L pathogenic tau in our model system may cause restriction in synaptic vesicle mobility via enhanced f-actin crosslinking, rendering the synapse unable to recruit vesicles into the recycling pool during periods of high synaptic activity. Increased restriction of vesicles mobility as a result of increased actin polymerization has also been proposed in *Drosophila* (Zhou et al., 2017) The enhanced release of vesicles in tau knockdown cultures in response to 4AP and 40AP stimuli could also imply that, in the absence of tau, vesicles are less tightly associated with the actin cytoskeleton. The rationale as to why tau knockdown results in a reduced recycling pool is less clear but could arise from a compromised ability of microtubules to efficiently deliver the necessary components for vesicle recycling to the synapse during intense periods of activity.

In regards to the kinetics of synaptic vesicle recycling, expression of the Tau(P301L) mutation results in a significantly more rapid endocytosis. The P- L mutation in this model is located in the second microtubule binding domain, juxtaposed to the calmodulin binding domain, in such a position that it may effect calcium signal transduction (Padilla et al., 1990). Calcineurin is a Ca^{2+} / calmodulin dependent phosphatase, which has been demonstrated to accelerate endocytosis via the dephosphorylation of various endocytic proteins, including dynamin, amphiphysin or synaptojanin (Sun et al., 2010). Curiously, expression of Tau(P301L)^{K18} fibrils appears to ameliorate the effect of the Tau(P301L) mutation upon the release of the total recycling pool and endocytosis. Previous studies have proposed NFTs to have a role in neuroprotection, and suggest that that NFTs have the ability to absorb some of the toxic soluble tau species, hence defending against cell death and conserving the neuron for a greater length of time (Spires-Jones et al., 2009, de Calignon et al., 2012). In our system, it is possible that K18^{P301L} fibrils are creating these 'sinks', leading to a decreased association of the P301L mutated tau with either the cytoskeleton or other synaptic components.

Finally, we demonstrated that expressing Tau(P301L) and Tau(P301L)^{K18} in neurons resulted in increased glutamate release and impaired glutamate clearance. The exact mechanism by which P301L tau expression increases glutamate release in hippocampus is unknown, however increased VGLUT expression observed in TauP301L mice might explain the increase in glutamate release (Hunsberger et al., 2015). The number of VGLUT molecules is directly correlated with the number of glutamate molecules released by a single synaptic vesicle during exocytosis (Herzog et al., 2006,

Wilson et al., 2005), and overexpression of VGLUT results in increased glutamate release, leading to excitotoxic neurodegeneration (Daniels et al., 2011). Glutamate is generally thought to be cleared from the synaptic cleft by a family of Na^+-dependent transporters (Gegelashvili and Schousboe, 1997). Of these transporters, excitatory amino-acid transporter 2 (EAAT-2) is the most widely implicated in neurodegenerative disorders (Rothstein et al., 1993). Recently, EAAT-2 has been show to associate with phosphorylated tau and has been found in NFTs (Sasaki et al., 2009), strengthening the hypothesis that EAAT-2 expression is altered in tauopathies, therefore an important future direction of this work would be to examine changes in EAAT-2 expression and function in our model systems.

At this point, it is also worth highlighting the differential actions of $K18^{P301L}$ fibrils in the assays applied in this chapter. In terms of vesicle release, the addition of $K18^{P301L}$ seems to 'rescue' the effects of the P301L mutation, restoring the size of the recycling pool and reversing the acceleration in endocytosis. Nevertheless, both the P301L and $P301L^{K18}$ model systems exhibit enhanced glutamate release and slowed glutamate clearance kinetics and, here, the addition of $K18^{P301L}$ does not act as a 'rescue'. The reasons for this discrepancy in results is unclear without further experimentation, however it is perhaps indicative that there are several mechanisms of P301L – mediated toxicity at the synapse. As there is a lag time of a few days between the addition of P301L and the introduction of the $K18^{P301L}$ fibrils in our model system, one possible scenario is that soluble species of P301L have a more rapid effect on glutamate reuptake transporters than upon synaptic vesicle availability. Therefore the subsequent addition of fibrils is too late to reverse the damage upon glutamate reuptake transporters but in time to sequester enough of the toxic soluble species to prevent the association of Tau(P301L) with synaptic vesicles and its effects on vesicle release and retrieval. It must also be made clear that no definitive can be made without the addition of a wildtype control treated with $K18^{P30L}$ in imaging experiments. Due to the failure of $K18^{P301L}$ to seed on a wildtype background (Figs 6.4.1 and 6.5) and the time constraints of the project, this control was not included in the live –cell imaging experiments but should be included in future work to allow more substantial conclusions to be drawn.

From the data presented in this chapter, it can be concluded that *MAPT* P301L pathological tau has the ability to influence neurotransmitter release at the presynaptic terminal, as well as its reuptake. Whether or not P301L tau is present in a soluble or aggregated form seems to dramatically influence its effects on vesicle fusion and glutamate release, although has little

significance for glutamate clearance kinetics. Consistent with observation *in vivo,* knockdown of tau had fewer deleterious effects than the expression of pathogenic tau in primary hippocampal cultures.

Chapter 7: General Discussion

The objective of the work presented in this thesis was to characterize how modulation of key target substrates influences synaptic vesicle recycling and consequently transmission. Chemical synapses are the major junctions of information transfer and processing in the CNS. Therefore synaptic vesicles and presynaptically located receptors are attractive pharmacological targets, and understanding their modulation is key to the research and development of novel therapeutic strategies acting at the presynaptic terminal. Specifically, this work exploited optical approaches providing detailed mechanistic insight into events at individual synaptic terminals. Our findings concentrate on two systems: i) the action of the AED levetiracetam and novel allosteric modulators of mGluR2 and ii) differential expression of tau protein.

7.1. Pharmacological Modulation

Through exploiting a wide range of presynaptically targeted optical assays, we have built-up a unique and comprehensive overview of the direct actions of levetiracetam at the presynaptic terminal. Experiments and findings are summarised in Table 7.1. The development of a novel assay that combines sypHy1x, a targeted reporter of vesicle function, with an acute assay of LEV action, has allowed us to create an exclusively presynaptic readout that can be used to directly monitor vesicle dynamics in response to LEV intervention. This methodology stands apart from previous research in the field which relied upon long pre-incubation periods with LEV and postsynaptic readouts (Meehan et al., 2012, Garcia-Perez et al., 2015, Yang and Rothman, 2009).

Using this experimental technique, we show a clear relationship between synaptic activity and the efficacy of LEV. Using a 40AP, 20Hz protocol to recruit the RRP, we observed that LEV negatively impacts RRP release in a concentration-dependent manner, slowing its exocytosis and ultimately reducing the number of successful fusion events. However, in order to see a significant modulation in RRP size, neurons incubated with LEV had to first undergo a prior period of high neuronal activity, sufficient to turnover a large fraction of the recycling pool (150AP, 20Hz) (Fig 4.3). Without this high-intensity stimulation, even relatively high concentrations (300µM) of LEV do not have an effect (Fig 4.3). This is consistent with other research in the field that has shown that

suppression of spontaneous neuronal activity during LEV incubation occludes its effect (Meehan et al., 2012).

Effects of levetiracetam at the presynaptic terminal

Parameter Assayed	Experimental Readout	Observation
Activity Dependence	RRP release (40APs,20Hz) following a period of high intensity stimulation (150APs, 20Hz)	The ability of LEV to attenuate RRP release in a concentration-dependent manner is dependent on a period of high intensity stimulation sufficient to turnover a large portion of the recycling fraction of vesicles.
Exocytosis	Kinetics of RRP release as measured by 20-80% rise in fluorescent signal (40APs, 20Hz)	LEV slows the kinetics of RRP release in a concentration-dependent manner
Endocytosis	Kinetics of RRP retrieval measured by decay of fluorescent signal described by a single exponential fit (40APs, 20Hz)	LEV has no concentration-dependent impact on rate of endocytosis
Ca^{2+} dynamics	Presynaptic Ca^{2+} influx during RRP recruitment (40APs,20Hz)	LEV reduces Ca^{2+} influx in a non- concentration-dependent manner
Vesicle pool fractions	Alkaline trapping with v-TPase inhibitor - 40APs : RRP - 600APs: Recycling pool - NH_4Cl : Total pool	LEV reduces size of total vesicle pool
Release probability (*ρr)*	Probability of successful release during 10 rounds of stimulus evoking quantal events (10 x 4APs, 10Hz)	LEV increases *ρr*
Activity at low frequency	Vesicle release at low frequency stimulation (20APs, 2Hz)	LEV has no effect on vesicle release during low frequency activity

Table 7.1.

One possible explanation for our observations is that the binding site of LEV is located at an intravesicular portion of SV2A or at a region that is only accessible from the intravesicular side of the protein. In this model, increased levels of neuronal activity lead to an increased number of fusion events. This, in turn, increases the likelihood of LEV being taken-up into vesicles via endocytosis and enhances the probability of LEV binding to its target, SV2A. This is similar to the mechanism of action proposed for the clostridium toxins, Botulinum neurotoxin A (BoT.A) and tetanus neurotoxin, which enter vesicles by binding to SV2 inside the vesicle lumen (Dong et al., 2006, Yeh et al., 2010). These toxins completely block the release of neurotransmitter via cleavage of SNARE proteins (Schiavo et al., 1992, Blasi et al., 1993), rendering the vesicle unable to participate in future fusion events and leaving the toxin in the synaptic cleft to bind other active vesicles in subsequent rounds of neuronal firing. It is possible that LEV also has this additive mechanism of action, whereby the vesicles that do not contain LEV are more likely to participate in fusion and recycling, therefore taking up LEV themselves.

Vesicular entry is a simple and attractive model to explain why LEV preferentially targets hyperactive synapses. Nevertheless, our results demonstrate that Compound X, a derivative of LEV and an alternative modulator of SV2A function, does not require periods of intense activity in order to exert its actions. Moreover, its actions favour low frequency stimulation protocols (Fig 4.12) but are absent in high frequency stimulation protocols (Fig 4.3.1), which would seem to contradict the idea that modulators of SV2A rely upon vesicular entry to elicit their actions. Acceptance of vesicular entry as the putative model of LEV action has been cautioned by Löscher and other eminent researchers in the epilepsy field who rationalize that LEV would most likely reach its target through membrane diffusion given its pharmacokinetic profile (Loscher et al., 2016).

Considering our results, an alternative hypothesis may be that modulators of SV2A enter the presynaptic terminal via membrane diffusion but that they bind to SV2A in a manner that is dependent on the activity status of the neuron. The way in which neuronal activity alters SV2A ligand binding is unclear, however it is possible that activity-status could affect the conformational state of SV2A. In support of this hypothesis, two major conformational states of *SV2A* have been identified in mouse brain tissue; one with a pore-like opening towards the cytoplasm, and a second with a cleft-like opening towards the intravesicular space (Lynch et al., 2008). In addition, studies with an SV2A positive allosteric modulator (UCB1244283) have indicated that the SV2A

protein contains several interacting binding sites that are linked via the conformation of the protein, and that binding of levetiracetam and its derivative brivacetam recognize, induce or stabilize different conformations of the SV2A protein, providing rationale for their distinctive pharmacodynamic properties (Daniels et al., 2013). Therefore, this model could perhaps also explain why we observed a potentiation in release probability in LEV-treated neurons during rounds of low intensity stimulation (Fig 4.11).

Taken together, our results indicate that presynaptic activity is a key driver in selectively mediating the actions of SV2A modulators. Firstly, we have shown that LEV binding reduces the size of the readily releasable pool of vesicles and slows its release in an activity-dependent and concentration-dependent manner. This finding is consistent with a number of other groups who have estimated a reduction in RRP size based on postsynaptic measurements (Meehan et al., 2012, Yang et al., 2007), however it is the first time it has been conclusively demonstrated using a targeted optical reporter that directly assays vesicle release and recycling. Nonetheless, pinpointing whether it is vesicular entry or the conformational state of SV2A, or a different mechanism entirely, that mediates the effects of SV2A ligand binding is yet to be fully elucidated. Experimentally, answering this question poses several challenges as functional, fluorescently tagged derivatives of SV2A modulators do not yet exist, and nor is it possible to generate a crystal structure of SV2A in order to visualize the binding site under different stimulation paradigms.

Following the binding of LEV to SV2A, another important consideration is how LEV then mediates its antiepileptic effects. Although we are certain that SV2A is critical for normal synaptic function, its exact role is yet to be understood (Mendoza-Torreblanca et al., 2013). To date, SV2A has been proposed to have a number of different roles in the recycling of synaptic vesicles including Ca^{2+} - dependent exocytosis, neurotransmitter loading/ retention, vesicle priming and as transport of vesicle constituents (Rogawski et al., 2016). Therefore, unsurprisingly, our results suggest that LEV could be impacting at multiple stages of the vesicle cycle (Fig 7.1).

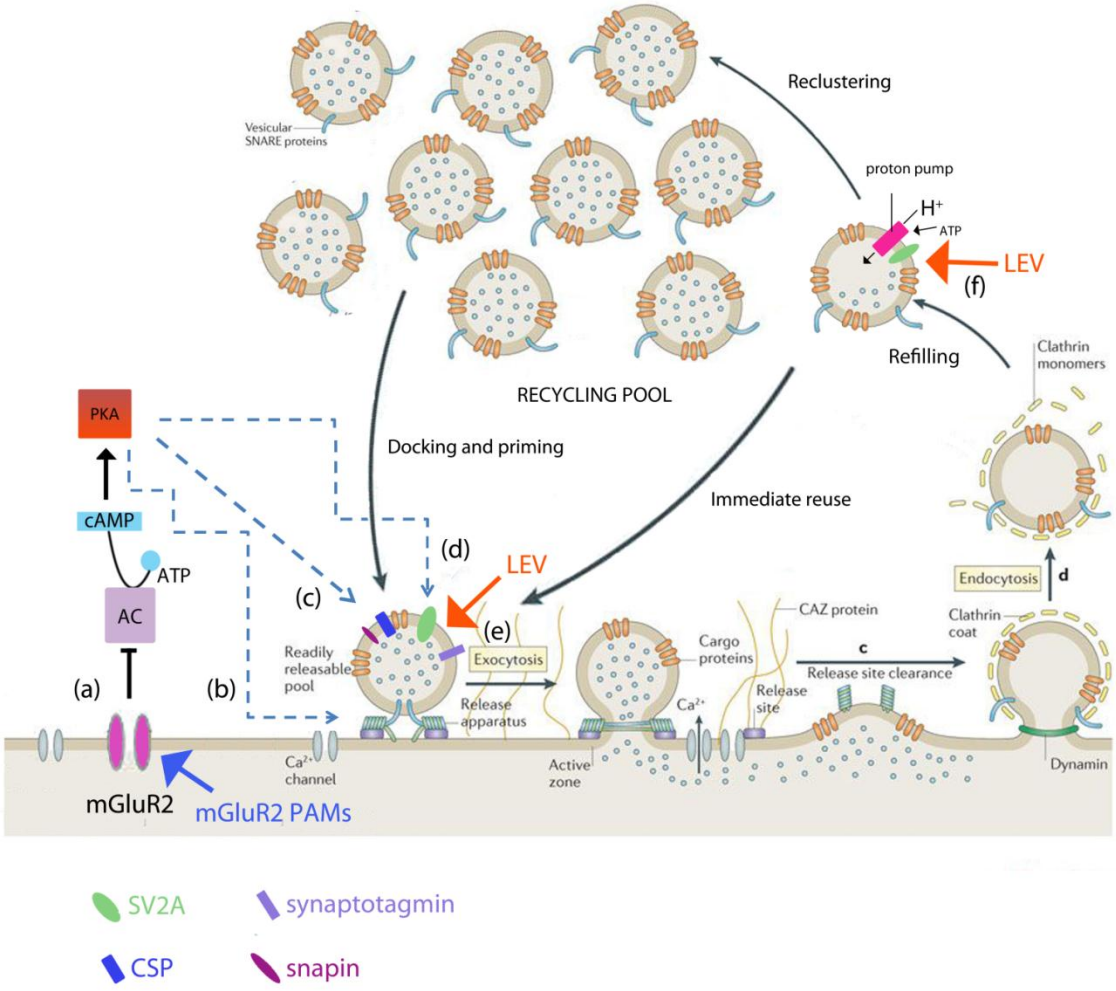

Figure 7.1 Potential targets for levetiracetam and mGluR2 modulation at the presynaptic terminal (a) cAMP-PKA signalling pathway. Modulation at mGluR2 by agonists/ PAMs results in decreased cAMP production and reduced PKA activation (b). Activated PKA may act directly on exocytotic machinery (c) Activated PKA phosphorylates synaptic vesicle proteins CSP and snapin, enhancing exocytosis (d) Activated PKA may directly phosphorylate SV2A (e) LEV acts on SV2A, potentially slowing exocytosis via interactions with synaptotagmin-1 (f) LEV acts on SV2A affecting the ability of the vesicle to refill/retain neurotransmitter.

In studies conducted in hippocampal cultures from SV2A knockout mice, the absence of SV2A results in a reduction in fusion competence and RRP size (Custer et al., 2006).) Interestingly, neurons overexpressing SV2A display also display a reduction in successful fusion events, a deficit that can be rescued with LEV administration (Nowack et al., 2011). This mirrors our results, where LEV increased ρ*r* following low intensity stimulation (Fig 4.11). Taken together, this data suggests that SV2A is an important player in the regulation of vesicle release, and it is likely that the binding of LEV and other SV2A ligands can positively or negatively influence vesicle fusion and exocytosis in a manner that is encoded by the levels of neuronal activity.

In our experiments, we show that DCG-IV; a direct mGluR2 agonist, and JNJ-46281222, an mGluR2 positive allosteric modulator (PAM) decrease RRP size and slow exocytosis in a concentration-dependent manner (Figs 5.5 and 5.6). This effect can be ameliorated by the introduction of JNJ-56140864, a negative mGluR2 modulator, verifying that this effect is most likely mediated via the mGluR2 pathway, rather than off-target interactions (Figs 5.5 and 5.6).

It has been demonstrated that compounds acting on mGlu2 receptors modulate exocytosis via the cAMP-PKA signalling pathway (Fig 7.1. pathway (a)) (Chavez-Noriega and Stevens, 1994, Schaffhauser et al., 2000), although whether or not PKA acts directly on exocytotic machinery (Fig 7.1, pathway (b)), or via secondary phosphorylation cascades (Fig 7.1, pathway (c)) remains to be revealed. Numerous phosphorylation targets of PKA have been identified, yet cysteine string protein (CSP) and snapin are the only two vesicular proteins that have been shown experimentally to undergo phosphorylation linked with a change in exocytosis (Evans et al., 2001, Chheda et al., 2001). In both circumstances, phosphorylation results in an alteration in protein interactions with the Ca^{2+} - sensor, synaptotagmin-1 (Fig 7.1 pathway (c)). Interestingly, synaptotagmin-1 is also a promising candidate in the mediation of exocytosis by SV2A. Disruption of synaptotagmin1 in mice results in a phenotype analogous to SV2A-mutants (Geppert et al., 1994). Moreover, a number of groups, including ours, have shown synaptotagmin-1 to co-precipitate with SV2A (Fig 4.X), suggesting close physiological interaction Furthermore, it has been shown that SV2A-synaptotagmin-1 interactions are dependent on SV2A phosphorylation (Pyle et al., 2000, Zhang et al., 2015) . SV2A--synaptotagmin-1 interactions are mediated by the amino-terminus of SV2A, which also contains substrate consensus sites of several protein kinases, including PKA (Pyle et al., 2000). Given that pharmacological synergism seems to be governed mainly by network topology,

with the probability of synergism prevailing in drug combinations directed towards closely connected targets (Yin et al., 2014), we believe that SV2A phosphorylation by PKA, or rather the lack of, may be a possible point of convergence of SV2A and mGluR2 modulators, giving rise to a synergistic effect (Fig 7.1, pathway (d)). Taking into consideration that SV2A conformation may be an important factor in determining the action of SV2A ligands, it is also possible that SV2A in its dephosphorylated state is stabilized in a conformation that favours binding of LEV, thus enhancing the likelihood of ligand binding.

Alkaline trapping experiments with sypHy and the v-ATPase bafilomycin revealed that LEV may also impact upon neurotransmitter filling/retention (Fig 7.1. pathway (f)). In the presence of LEV, we observed a reduction in the total pool of vesicles and a gradual but sustained increase in brightness of resting synaptic terminals compared with those in the control condition (Fig 4.9 and 4.10). Interestingly endocytosis, which is approximated as vesicle reacidification when using sypHy, remains unaffected by LEV, suggesting that LEV influences the ability of the vesicles to retain an acidic state, hence delayed alkalization and a gradual increase in brightness.

Although it is known that the reacidification of vesicles via the v-ATPase drives neurotransmitter loading, the precise way in which is coupled remains uncertain. Therefore, it is unclear whether the spontaneous alkalization that occurs in the presence of LEV could definitively affect neurotransmitter loading/retention. However, in isolated synaptic vesicle preparations, Budzinski et al. demonstrate that vesicles from SV2A knockouts do not exhibit a size increase when loaded with glutamate, suggesting that SV2A is required for successful neurotransmitter loading (Budzinski et al., 2009). It has also been put forward that SV2A provides a matrix that immobilises and regulates neurotransmitter release by electrostatic interaction with sugar moieties (Reigada et al., 2003). However, in circumstances where the neurotransmitter is negatively charged, as with glutamate, additional participation of a cation such as Ca^{2+} would be necessary (Mendoza-Torreblanca et al., 2013). In this model, interactions of SV2A sugar residues with other ions results in a scaffold that immobilizes the neurotransmitter, and conformational changes in SV2A allow the swelling of vesicles upon neurotransmitter loading. Therefore, it is possible that low SV2A levels or LEV treatment may result in low retention of neurotransmitter and reduced release capacity. As a future direction, it would be interesting to assay the levels of quantal release in the presence of LEV using an optical readout of glutamate release such as iGluSnFR.

At this stage, we cannot fully rule-out the possibility that a non-SV2A mediated effect of LEV could contribute to the effects that we observe. In particular, at therapeutically relevant concentrations, LEV has been reported to affect the inhibition of high-voltage gated (P/Q-type) Ca^{2+} - channels, the inhibition of AMPA currents, and the inhibition of Ca^{2+} from intracellular stores (Rogawski et al., 2016, Nagarkatti et al., 2008). Indeed, using our experimental system, we observed a reduction in presynaptic Ca^{2+}-influx the highest concentration that we assayed (300µM), which is consistent with the possible modulation of VDCCs or the modulation of Ca^{2+} release from intracellular stores. Nevertheless, we did not observe modulation at lower LEV concentrations. Although we cannot completely negate Ca^{2+} in considering the antiepileptic actions of LEV at the presynaptic terminal, our experiments provide strong evidence for an activity-dependent mechanism which has yet to have been reported in current available modulators of P/Q – type Ca^{2+}- channels (Mezler et al., 2012). Moreover, our experiments demonstrate that the impact of LEV on RRP release is concentration – dependent, whereas its impact on presynaptic Ca^{2+} is not (Fig 4.4), therefore suggesting that Ca^{2+} - channel blockage is not the primary mechanism through which LEV exerts its effects and is more likely to be a consequence of off – target interactions. At this point, it should be highlighted that, in order to maintain consistency between experiments conducted on vesicle release using sypHy and those carried out using syGCaMP6f, we assayed presynaptic Ca^{2+}- influx following a 40AP,20Hz stimulus, which is not an ideal stimulation range for the syGCaMP6f optical probe, entitling us to make comparisons between conditions but not to extrapolate information pertaining to actual Ca^{2+} concentrations. Finally, it has been shown that SV2A is the primary binding site for LEV (Lynch et al., 2004), and it is well established that an effect of LEV is occluded in SV2A knockout models (Kaminski et al., 2008, Kaminski et al., 2009, Garcia-Perez et al., 2015).

To conclude, we believe that LEV impacts vesicle recycling by multiple mechanisms, a view which is supported by evidence that SV2A has at least two mechanisms of action at the synapse (Nowack et al., 2010). Our results indicate that SV2A modulation is highly regulated by neuronal activity, which may arise either as consequence of the need of the ligand to enter the vesicle to bind SV2A or that the conformational state of SV2A is regulated by neuronal activity, thus favouring the binding of different ligands under different stimulation paradigms. We also demonstrate a synergistic effect of LEV and positive allosteric modulations of mGluR2, and suggest that a reduction in PKA-mediated phosphorylation may also contribute to stabilizing a particular conformation of SV2A, favouring the binding of LEV. Finally, we show that LEV may also inhibit the retention of neurotransmitter, compromising the ability of the vesicle to release.

7.2. Pathological Modulation

In addition to our studies on neuropharmacological agents, we explored the role of tau protein at the synapse. Specifically, we looked at the effects of knocking down endogenous tau, the overexpression of pathogenic tau and the role of fibrillary tangles on presynaptic neurotransmission.

Firstly, we showed that the size of the recycling fraction of vesicles is compromised in neurons overexpressing Tau(P301L) (Fig 6.6), a mutation in the *MAPT* gene associated with FTDP-17. Interestingly, elevated f-actin levels are found in P301L mouse models of FTDP-17 (Fulga et al., 2007) and Hirano bodies, actin-rich paracrystalline inclusions, are found in brain histopathological samples of AD and related tauopathies (Spears et al., 2014). Therefore, one possible interpretation of our findings is that expression of P301L may result in elevated levels of f-actin at the synapse, which in turn restricts the mobility of vesicles via its abundant crosslinking (Fig 7.2: P301L). This explanation is consistent with our observations that Tau(P3011L) did not have significant effects on quantal release or on release of the RRP, but only seemed to affect mobilization of the TRP. In support of this hypothesis, application of the actin depolymerizing drug, Latrunculin A has been shown to restore vesicle mobility and recycling pool size in Tau(P301L) *Drosophila* mutants (Zhou et al., 2017). Although predominantly thought of as a microtubule-stabilizing protein, the regulation of the actin cytoskeleton by tau has long been established (Griffith and Pollard, 1982), and it has been demonstrated that the presence of tau plays a key part in microtubule-actin co-alignment (Elie et al., 2015).

At the synapse, filamentous actin (f-actin) surrounds and tethers vesicle pools (Sankaranarayanan et al., 2003, Shupliakov et al., 2002), as is depicted in the wildtype synapse in Fig 7.2. Therefore, in synapses where tau expression has been knocked down using shRNA, we envisage vesicles having looser association with the actin cytoskeleton (Fig 7.2), resulting in an increased propensity of vesicles to undergo fusion following quantal and RRP recruiting stimuli (Fig 6.1). However, following a maximal stimulus to evoke turnover of the entire recycling pool (TRP), TRP capacity is revealed to be diminished (Fig 6.1), which we believe may arise from a compromised ability of

microtubules to deliver the necessary components for vesicle recycling during intense periods of synaptic activity, resulting in fewer vesicles available for recycling (Fig 7.2).

In addition to modulation of recycling pool size, we also demonstrate that Tau(P301L) expressing neurons exhibit faster rates of synaptic vesicle endocytosis than their wildtype counterparts following an RRP recruiting stimulus. Although the precise reason for this cannot be determined without further experimental evidence, it is possible that increased f-actin levels could also contribute to more efficient endocytosis. Recent evidence in the field indicates that the f-actin cytoskeleton interacts with clathrin mediated endocytosis (CME) in multiple ways. In yeast, protein dynamics at endocytic sites were analysed in cells expressing GFP-tagged endocytic proteins with genetic ablations (Kaksonen et al., 2005). Cells were challenged with Latrunculin A, an inhibitor of actin polymerization, and the disruption in the spatial organization of the different endocytic proteins examined. From the data compiled, the authors proposed a modular design of the endocytic protein machinery. According to this, there are four groups of proteins that cooperate to achieve an endocytic event: the 'coat', 'amphiphysin', 'WASP/myo' and the actin molecule. Components of the actin molecule require f-actin for their proper localization. The 'coat and 'amphiphysin' complexes are able to form without f-actin, but require the cytoskeleton for movement and disassembly, consistent with a role for f-actin in recruiting coat disassembly factors such as synaptojanin (Stefan et al., 2005), and the "WASP/Myo" module disassembles after f-actin polymerization has occurred. In mammalian model systems, Watanabe et al. have demonstrated a role for f-actin in ultrafast endocytosis; a form of endocytosis that is 200-fold faster than CME (Watanabe et al., 2013). Therefore, it is highly plausible that the increased polymerization of f-actin in Tau(P301L) mutants could result in faster endocytosis.

An alternative hypothesis as to why Tau(P301L) mutants exhibit faster RRP retrieval is that the P-L mutation is located in the second microtubule-binding domain, juxtaposed to the calmodulin binding domain in such a position that it may effect calcium signal transduction (Padilla et al., 1990). Calcineurin is a Ca^{2+} / calmodulin dependent phosphatase, which accelerates endocytosis via dephosphorylation of various endocytic proteins (Sun et al., 2010, Wu et al., 2014). It is worth noting that overexpression of wt-hTau slowed endocytic kinetics, therefore we assume that the overexpression of tau disrupts vesicle retrieval to some extent, however the accelerated endocytosis seen in Tau(P301L) neurons is mutation-specific. As a future direction, ultra-fast flash-

freeze electron microscopy would be a useful tool to further explore the roles of endogenous and pathogenic tau in endocytosis.

Notably, expression of $K18^{P301L}$ fibrils appears to rescue the effects of the Tau(P301L) mutation in our model system. NFTs have been suggested to have a role in neuroprotection, and it might be that that NFTs have the ability to absorb some of the toxic soluble tau species, hence defending against cell death and conserving the neuron for a greater length of time (Spires-Jones et al., 2009, de Calignon et al., 2012). In our system, it is possible that $K18^{P301L}$ fibrils are creating these 'sinks', leading to a decreased association of the P301L mutated tau with either the cytoskeleton or other synaptic components (Fig 7.2).

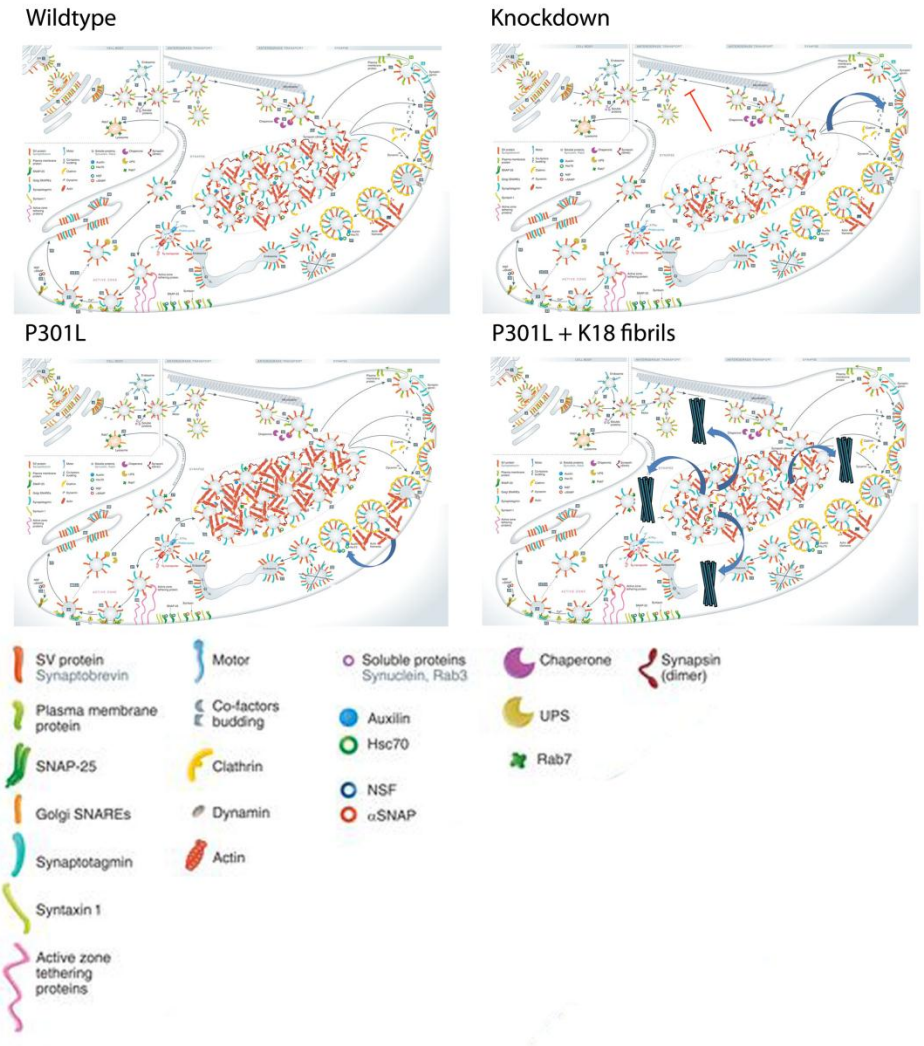

Figure 7.2. Interactions between tau and the actin cytoskeleton may modulate vesicle release and recycling Wildype synapse (top left): vesicles are tethered in pools by f-actin filaments.

Knockdown: Lack of tau leads to lack of association of vesicles with the actin cytoskeleton. This leads to an increased ρr following quantal and RRP recruiting stimuli. However, impairment in microtubule transport of vesicular components results in defective recycling pool replenishment and inability to sustain regular neurotransmission in periods of extensive activity. Tau(P301L): Presence of mutated tau leads to enhanced f-actin levels, resulting in the restriction of vesicle movement by extensive f-actin crosslinking. Rapid endocytosis may also arise as a result of increased f-actin or via other mechanisms. Tau(P301L)^{K18}: Presence of K18^{P301L} fibrils act as 'sinks' for aberrant tau, leading to the restoration of vesicle tethering and endocytosis.

Adapted from Haucke et. al, 2011

Finally, we demonstrated that primary hippocampal cultures expressing Tau(P301L) and Tau(P301L)^{K18} showed increased glutamate release and impaired glutamate clearance. Increased VGLUT expression has been observed in TauP301L mice, and we hypothesize that this could explain the increase in glutamate release seen in our experiments (Hunsberger et al., 2015). There is a tight correlation between the number of VGLUT molecules expressed and the number of glutamate molecules released by a single synaptic vesicle during exocytosis (Herzog et al., 2006, Wilson et al., 2005), and overexpression of VGLUT results in increased glutamate release, leading to excitotoxic neurodegeneration (Daniels et al., 2011). Vesicle release in Tau(P301L) mutants following an RRP-recruiting stimulus is not significantly different to wildtype (Fig 6.6), therefore we hypothesize that the excessive glutamate release is due to an aberration in neurotransmitter content, making increased expression of VGLUT1 a likely candidate. As LEV may compromise the ability of vesicles to retain neurotransmitter (Fig 7.1), as a future direction it would be interesting to ascertain if LEV treatment could ameliorate the excessive glutamate transmission see in Tau(P301L) overexpression. As a further caveat to the work carried out with iGluSnFR in this body of work, it should be noted that as we were using a stimulus of >10Hz, the temporal resolution of iGluSnFR did not allow resolution of the peaks of individual release events and therefore we were only entitled to allow to make relative comparisons in terms of glutamate release, not extrapolate actual values

7.3 Concluding Statement

In this body of work, we have defined and characterized the effects of pharmacological and pathological manipulation at the level of single synaptic terminals. In terms of synaptic vesicle recycling, we have identified various hallmarks of SV2A and mGluR2 modulation, as well as the role of endogenous tau and the ramifications of overexpressing FTDP-17 pathogenic tau. Now that we have started to piece together mechanisms for the actions of levetiracetam and allosteric

modulation of mGluR2 at the presynaptic terminal in physiologically normal synapses, we can begin to translate this information into pathogenic models. Given that we have identified several disruptions in synaptic vesicle release and retrieval in hippocampal cultures expressing Tau(P301L), we believe that further research into targeted manipulation of the synaptic vesicle cycle could be key in informing further therapeutic strategies for tauopathies and possibly other neurological disorders.

References

2006. *In:* BROMFIELD, E. B., CAVAZOS, J. E. & SIRVEN, J. I. (eds.) *An Introduction to Epilepsy.* West Hartford (CT).

ABDERRAHMANI, A., NIEDERHAUSER, G., PLAISANCE, V., ROEHRICH, M. E., LENAIN, V., COPPOLA, T., REGAZZI, R. & WAEBER, G. 2004. Complexin I regulates glucose-induced secretion in pancreatic beta-cells. *J Cell Sci,* 117**,** 2239-47.

ABE, T., SUGIHARA, H., NAWA, H., SHIGEMOTO, R., MIZUNO, N. & NAKANISHI, S. 1992. Molecular characterization of a novel metabotropic glutamate receptor mGluR5 coupled to inositol phosphate/Ca2+ signal transduction. *J Biol Chem,* 267**,** 13361-8.

AIHARA, Y., MASHIMA, H., ONDA, H., HISANO, S., KASUYA, H., HORI, T., YAMADA, S., TOMURA, H., YAMADA, Y., INOUE, I., KOJIMA, I. & TAKEDA, J. 2000. Molecular cloning of a novel brain-type Na(+)-dependent inorganic phosphate cotransporter. *J Neurochem,* 74**,** 2622-5.

ALABI, A. A. & TSIEN, R. W. Synaptic vesicle pools and dynamics. *Cold Spring Harb Perspect Biol,* 4**,** a013680.

ALABI, A. A. & TSIEN, R. W. 2012. Synaptic vesicle pools and dynamics. *Cold Spring Harb Perspect Biol,* 4**,** a013680.

ALABI, A. A. & TSIEN, R. W. 2013. Perspectives on kiss-and-run: role in exocytosis, endocytosis, and neurotransmission. *Annu Rev Physiol,* 75**,** 393-422.

ANDERL, J. L., REDPATH, S. & BALL, A. J. 2009. A neuronal and astrocyte co-culture assay for high content analysis of neurotoxicity. *J Vis Exp*.

ANDORFER, C., ACKER, C. M., KRESS, Y., HOF, P. R., DUFF, K. & DAVIES, P. 2005. Cell-cycle reentry and cell death in transgenic mice expressing nonmutant human tau isoforms. *J Neurosci,* 25**,** 5446-54.

ANWYL, R. 1999. Metabotropic glutamate receptors: electrophysiological properties and role in plasticity. *Brain Res Brain Res Rev,* 29**,** 83-120.

ARAVANIS, A. M., PYLE, J. L., HARATA, N. C. & TSIEN, R. W. 2003. Imaging single synaptic vesicles undergoing repeated fusion events: kissing, running, and kissing again. *Neuropharmacology,* 45**,** 797-813.

ARENDT, T., STIELER, J., STRIJKSTRA, A. M., HUT, R. A., RUDIGER, J., VAN DER ZEE, E. A., HARKANY, T., HOLZER, M. & HARTIG, W. 2003. Reversible paired helical filament-like phosphorylation of tau is an adaptive process associated with neuronal plasticity in hibernating animals. *J Neurosci,* 23**,** 6972-81.

ARMATO, U., CHIARINI, A., CHAKRAVARTHY, B., CHIOFFI, F., PACCHIANA, R., COLARUSSO, E., WHITFIELD, J. F. & DAL PRA, I. 2013. Calcium-sensing receptor antagonist (calcilytic) NPS 2143 specifically blocks the increased secretion of endogenous Abeta42 prompted by exogenous fibrillary or soluble Abeta25-35 in human cortical astrocytes and neurons-therapeutic relevance to Alzheimer's disease. *Biochim Biophys Acta,* 1832**,** 1634-52.

ATTWELL, D. & LAUGHLIN, S. B. 2001. An energy budget for signaling in the grey matter of the brain. *J Cereb Blood Flow Metab,* 21**,** 1133-45.

BAAS, P. W. & QIANG, L. 2005. Neuronal microtubules: when the MAP is the roadblock. *Trends in Cell Biology,* 15**,** 183-187.

BAJJALIEH, S. M., FRANTZ, G. D., WEIMANN, J. M., MCCONNELL, S. K. & SCHELLER, R. H. 1994. Differential expression of synaptic vesicle protein 2 (SV2) isoforms. *J Neurosci,* 14**,** 5223-35.

BAJJALIEH, S. M., PETERSON, K., SHINGHAL, R. & SCHELLER, R. H. 1992. SV2, a brain synaptic vesicle protein homologous to bacterial transporters. *Science,* 257**,** 1271-3.

BAJJALIEH, S. M. & SCHELLER, R. H. 1995. The biochemistry of neurotransmitter secretion. *J Biol Chem,* 270**,** 1971-4.

BALAJI, J. & RYAN, T. A. 2007. Single-vesicle imaging reveals that synaptic vesicle exocytosis and endocytosis are coupled by a single stochastic mode. *Proc Natl Acad Sci U S A,* 104**,** 20576-81.

BANKER, G. A. & COWAN, W. M. 1977. Rat hippocampal neurons in dispersed cell culture. *Brain Res,* 126**,** 397-42.

BARTHOLOME, O., VAN DEN ACKERVEKEN, P., SANCHEZ GIL, J., DE LA BRASSINNE BONARDEAUX, O., LEPRINCE, P., FRANZEN, R. & ROGISTER, B. 2017. Puzzling Out Synaptic Vesicle 2 Family Members Functions. *Front Mol Neurosci,* 10**,** 148.

BEGCEVIC, I., KOSANAM, H., MARTINEZ-MORILLO, E., DIMITROMANOLAKIS, A., DIAMANDIS, P., KUZMANOV, U., HAZRATI, L. N. & DIAMANDIS, E. P. 2013. Semiquantitative proteomic analysis of human hippocampal tissues from Alzheimer's disease and age-matched control brains. *Clin Proteomics,* 10**,** 5.

BELLOCCHIO, E. E., HU, H., POHORILLE, A., CHAN, J., PICKEL, V. M. & EDWARDS, R. H. 1998. The localization of the brain-specific inorganic phosphate transporter suggests a specific presynaptic role in glutamatergic transmission. *J Neurosci,* 18**,** 8648-59.

BELLOCCHIO, E. E., REIMER, R. J., FREMEAU, R. T., JR. & EDWARDS, R. H. 2000. Uptake of glutamate into synaptic vesicles by an inorganic phosphate transporter. *Science,* 289**,** 957-60.

BENNETT, M. K. & SCHELLER, R. H. 1993. The molecular machinery for secretion is conserved from yeast to neurons. *Proc Natl Acad Sci U S A,* 90**,** 2559-63.

BERRIMAN, J., SERPELL, L. C., OBERG, K. A., FINK, A. L., GOEDERT, M. & CROWTHER, R. A. 2003. Tau filaments from human brain and from in vitro assembly of recombinant protein show cross-beta structure. *Proc Natl Acad Sci U S A,* 100**,** 9034-8.

BERTRAM, L., LANGE, C., MULLIN, K., PARKINSON, M., HSIAO, M., HOGAN, M. F., SCHJEIDE, B. M., HOOLI, B., DIVITO, J., IONITA, I., JIANG, H., LAIRD, N., MOSCARILLO, T., OHLSEN, K. L., ELLIOTT, K., WANG, X., HU-LINCE, D., RYDER, M., MURPHY, A., WAGNER, S. L., BLACKER, D., BECKER, K. D. & TANZI, R. E. 2008. Genome-wide association analysis reveals putative Alzheimer's disease susceptibility loci in addition to APOE. *Am J Hum Genet,* 83**,** 623-32.

BETZ, W. J. & BEWICK, G. S. 1992. Optical analysis of synaptic vesicle recycling at the frog neuromuscular junction. *Science,* 255**,** 200-3.

BETZ, W. J., MAO, F. & SMITH, C. B. 1996. Imaging exocytosis and endocytosis. *Curr Opin Neurobiol,* 6**,** 365-71.

BLASI, J., CHAPMAN, E. R., LINK, E., BINZ, T., YAMASAKI, S., DE CAMILLI, P., SUDHOF, T. C., NIEMANN, H. & JAHN, R. 1993. Botulinum neurotoxin A selectively cleaves the synaptic protein SNAP-25. *Nature,* 365**,** 160-3.

BORGES, C. F. Q. D. O. 2017. *Assaying synaptic function using genetically- encoded optical reporters in the context of Alzheimer's disease.* Masters, Universidade de Coimbra.

BRAAK, H. & BRAAK, E. 1991. Neuropathological stageing of Alzheimer-related changes. *Acta Neuropathol,* 82**,** 239-59.

BRAGINA, L., FATTORINI, G., GIOVEDI, S., MELONE, M., BOSCO, F., BENFENATI, F. & CONTI, F. 2011. Analysis of Synaptotagmin, SV2, and Rab3 Expression in Cortical Glutamatergic and GABAergic Axon Terminals. *Front Cell Neurosci,* 5**,** 32.

BRANCO, T., MARRA, V. & STARAS, K. 2010. Examining size-strength relationships at hippocampal synapses using an ultrastructural measurement of synaptic release probability. *J Struct Biol,* 172**,** 203-10.

BRANCO, T. & STARAS, K. 2009. The probability of neurotransmitter release: variability and feedback control at single synapses. *Nat Rev Neurosci,* 10**,** 373-83.

BRANCO, T., STARAS, K., DARCY, K. J. & GODA, Y. 2008. Local dendritic activity sets release probability at hippocampal synapses. *Neuron,* 59**,** 475-85.

BRELSTAFF, J., SPILLANTINI, M. G. & TOLKOVSKY, A. M. 2015. pFTAA: a high affinity oligothiophene probe that detects filamentous tau in vivo and in cultured neurons. *Neural Regen Res,* 10**,** 1746-7.

BUCKLEY, K. & KELLY, R. B. 1985. Identification of a transmembrane glycoprotein specific for secretory vesicles of neural and endocrine cells. *J Cell Biol,* 100**,** 1284-94.

BUDZINSKI, K. L., ALLEN, R. W., FUJIMOTO, B. S., KENSEL-HAMMES, P., BELNAP, D. M., BAJJALIEH, S. M. & CHIU, D. T. 2009. Large structural change in isolated synaptic vesicles upon loading with neurotransmitter. *Biophys J,* 97**,** 2577-84.

BUEE, L., BUSSIERE, T., BUEE-SCHERRER, V., DELACOURTE, A. & HOF, P. R. 2000. Tau protein isoforms, phosphorylation and role in neurodegenerative disorders. *Brain Res Brain Res Rev,* 33**,** 95-130.

BUNKER, J. M., WILSON, L., JORDAN, M. A. & FEINSTEIN, S. C. 2004. Modulation of microtubule dynamics by tau in living cells: implications for development and neurodegeneration. *Mol Biol Cell,* 15**,** 2720-8.

BURGALOSSI, A., JUNG, S., MEYER, G., JOCKUSCH, W. J., JAHN, O., TASCHENBERGER, H., O'CONNOR, V. M., NISHIKI, T., TAKAHASHI, M., BROSE, N. & RHEE, J. S. 2010. SNARE protein recycling by alphaSNAP and betaSNAP supports synaptic vesicle priming. *Neuron,* 68**,** 473-87.

BURGER, P. M., MEHL, E., CAMERON, P. L., MAYCOX, P. R., BAUMERT, M., LOTTSPEICH, F., DE CAMILLI, P. & JAHN, R. 1989. Synaptic vesicles immunoisolated from rat cerebral cortex contain high levels of glutamate. *Neuron,* 3**,** 715-20.

BURGER, W. & BURGE, M. 2008. *Digital image processing : an algorithmic introduction using Java,* New York, Springer.

CACERES, A. & KOSIK, K. S. 1990. Inhibition of neurite polarity by tau antisense oligonucleotides in primary cerebellar neurons. *Nature,* 343**,** 461-3.

CALAFATE, S., BUIST, A., MISKIEWICZ, K., VIJAYAN, V., DANEELS, G., DE STROOPER, B., DE WIT, J., VERSTREKEN, P. & MOECHARS, D. 2015a. Synaptic Contacts Enhance Cell-to-Cell Tau Pathology Propagation. *Cell Reports,* 11**,** 1176-1183.

CALAFATE, S., BUIST, A., MISKIEWICZ, K., VIJAYAN, V., DANEELS, G., DE STROOPER, B., DE WIT, J., VERSTREKEN, P. & MOECHARS, D. 2015b. Synaptic Contacts Enhance Cell-to-Cell Tau Pathology Propagation. *Cell Rep,* 11**,** 1176-83.

CALLAHAN, L. M. & COLEMAN, P. D. 1995. Neurons bearing neurofibrillary tangles are responsible for selected synaptic deficits in Alzheimer's disease. *Neurobiol Aging,* 16**,** 311-4.

CALLAHAN, L. M., VAULES, W. A. & COLEMAN, P. D. 1999. Quantitative decrease in synaptophysin message expression and increase in cathepsin D message expression in Alzheimer disease neurons containing neurofibrillary tangles. *J Neuropathol Exp Neurol,* 58**,** 275-87.

CARTMELL, J. & SCHOEPP, D. D. 2000. Regulation of neurotransmitter release by metabotropic glutamate receptors. *J Neurochem,* 75**,** 889-907.

CATTERALL, W. A. 1998. Structure and function of neuronal Ca2+ channels and their role in neurotransmitter release. *Cell Calcium,* 24**,** 307-23.

CECCARELLI, B., HURLBUT, W. P. & MAURO, A. 1973. Turnover of transmitter and synaptic vesicles at the frog neuromuscular junction. *J Cell Biol,* 57**,** 499-524.

CHAKROBORTY, S. & STUTZMANN, G. E. 2014. Calcium channelopathies and Alzheimer's disease: insight into therapeutic success and failures. *Eur J Pharmacol,* 739**,** 83-95.

CHAMBERLAIN, L. H. & BURGOYNE, R. D. 1998. Cysteine string protein functions directly in regulated exocytosis. *Mol Biol Cell,* 9**,** 2259-67.

CHANG, W. P. & SUDHOF, T. C. 2009. SV2 renders primed synaptic vesicles competent for Ca2+ -induced exocytosis. *J Neurosci,* 29**,** 883-97.

CHAUDHRY, F. A., REIMER, R. J., BELLOCCHIO, E. E., DANBOLT, N. C., OSEN, K. K., EDWARDS, R. H. & STORM-MATHISEN, J. 1998. The vesicular GABA transporter, VGAT, localizes to synaptic vesicles in sets of glycinergic as well as GABAergic neurons. *J Neurosci,* 18**,** 9733-50.

CHAVEZ-NORIEGA, L. E. & STEVENS, C. F. 1994. Increased transmitter release at excitatory synapses produced by direct activation of adenylate cyclase in rat hippocampal slices. *J Neurosci,* 14**,** 310-7.

CHEN, C. & REGEHR, W. G. 1997. The mechanism of cAMP-mediated enhancement at a cerebellar synapse. *J Neurosci,* 17**,** 8687-94.

CHEN, T. W., WARDILL, T. J., SUN, Y., PULVER, S. R., RENNINGER, S. L., BAOHAN, A., SCHREITER, E. R., KERR, R. A., ORGER, M. B., JAYARAMAN, V., LOOGER, L. L., SVOBODA, K. & KIM, D. S. 2013. Ultrasensitive fluorescent proteins for imaging neuronal activity. *Nature,* 499**,** 295-300.

CHEN, X., BARG, S. & ALMERS, W. 2008. Release of the styryl dyes from single synaptic vesicles in hippocampal neurons. *J Neurosci,* 28**,** 1894-903.

CHHEDA, M. G., ASHERY, U., THAKUR, P., RETTIG, J. & SHENG, Z. H. 2001. Phosphorylation of Snapin by PKA modulates its interaction with the SNARE complex. *Nat Cell Biol,* 3**,** 331-8.

CLAYTON, E. L. & COUSIN, M. A. 2009. The molecular physiology of activity-dependent bulk endocytosis of synaptic vesicles. *J Neurochem,* 111**,** 901-14.

COCHILLA, A. J., ANGLESON, J. K. & BETZ, W. J. 1999. Monitoring secretory membrane with FM1-43 fluorescence. *Annu Rev Neurosci,* 22**,** 1-10.

COLE, A. A., CHEN, X. & REESE, T. S. 2016. A Network of Three Types of Filaments Organizes Synaptic Vesicles for Storage, Mobilization, and Docking. *J Neurosci,* 36**,** 3222-30.

CONN, P. J., CHRISTOPOULOS, A. & LINDSLEY, C. W. 2009. Allosteric modulators of GPCRs: a novel approach for the treatment of CNS disorders. *Nat Rev Drug Discov,* 8**,** 41-54.

CONN, P. J. & JONES, C. K. 2009. Promise of mGluR2/3 activators in psychiatry. *Neuropsychopharmacology,* 34**,** 248-9.

CONN, P. J. & PIN, J. P. 1997. Pharmacology and functions of metabotropic glutamate receptors. *Annu Rev Pharmacol Toxicol,* 37**,** 205-37.

COSTA, C., MARTELLA, G., PICCONI, B., PROSPERETTI, C., PISANI, A., DI FILIPPO, M., PISANI, F., BERNARDI, G. & CALABRESI, P. 2006. Multiple mechanisms underlying the neuroprotective effects of antiepileptic drugs against in vitro ischemia. *Stroke,* 37**,** 1319-26.

CREVECOEUR, J., FOERCH, P., DOUPAGNE, M., THIELEN, C., VANDENPLAS, C., MOONEN, G., DEPREZ, M. & ROGISTER, B. 2013. Expression of SV2 isoforms during rodent brain development. *BMC Neurosci,* 14**,** 87.

CRIMINS, J. L., ROCHER, A. B., PETERS, A., SHULTZ, P., LEWIS, J. & LUEBKE, J. I. 2011. Homeostatic responses by surviving cortical pyramidal cells in neurodegenerative tauopathy. *Acta Neuropathol,* 122**,** 551-64.

CROWDER, K. M., GUNTHER, J. M., JONES, T. A., HALE, B. D., ZHANG, H. Z., PETERSON, M. R., SCHELLER, R. H., CHAVKIN, C. & BAJJALIEH, S. M. 1999. Abnormal neurotransmission in mice lacking synaptic vesicle protein 2A (SV2A). *Proc Natl Acad Sci U S A,* 96**,** 15268-73.

CUSTER, K. L., AUSTIN, N. S., SULLIVAN, J. M. & BAJJALIEH, S. M. 2006. Synaptic vesicle protein 2 enhances release probability at quiescent synapses. *J Neurosci,* 26**,** 1303-13.

DANIELS, R. W., MILLER, B. R. & DIANTONIO, A. 2011. Increased vesicular glutamate transporter expression causes excitotoxic neurodegeneration. *Neurobiol Dis,* 41**,** 415-20.

DANIELS, V., WOOD, M., LECLERCQ, K., KAMINSKI, R. M. & GILLARD, M. 2013. Modulation of the conformational state of the SV2A protein by an allosteric mechanism as evidenced by ligand binding assays. *Br J Pharmacol,* 169**,** 1091-101.

DARDOU, D., DASSESSE, D., CUVELIER, L., DEPREZ, T., DE RYCK, M. & SCHIFFMANN, S. N. 2011. Distribution of SV2C mRNA and protein expression in the mouse brain with a particular emphasis on the basal ganglia system. *Brain Res,* 1367**,** 130-45.

DARSTEIN, M., PETRALIA, R. S., SWANSON, G. T., WENTHOLD, R. J. & HEINEMANN, S. F. 2003. Distribution of kainate receptor subunits at hippocampal mossy fiber synapses. *J Neurosci,* 23**,** 8013-9.

DAWSON, H. N., CANTILLANA, V., JANSEN, M., WANG, H., VITEK, M. P., WILCOCK, D. M., LYNCH, J. R. & LASKOWITZ, D. T. 2010. Loss of tau elicits axonal degeneration in a mouse model of Alzheimer's disease. *Neuroscience,* 169**,** 516-31.

DAWSON, H. N., FERREIRA, A., EYSTER, M. V., GHOSHAL, N., BINDER, L. I. & VITEK, M. P. 2001. Inhibition of neuronal maturation in primary hippocampal neurons from tau deficient mice. *J Cell Sci,* 114**,** 1179-87.

DE CALIGNON, A., POLYDORO, M., SUAREZ-CALVET, M., WILLIAM, C., ADAMOWICZ, D. H., KOPEIKINA, K. J., PITSTICK, R., SAHARA, N., ASHE, K. H., CARLSON, G. A., SPIRES-JONES, T. L. & HYMAN, B. T. 2012. Propagation of tau pathology in a model of early Alzheimer's disease. *Neuron,* 73**,** 685-97.

DE ROBERTIS, E. D. & BENNETT, H. S. 1955. Some features of the submicroscopic morphology of synapses in frog and earthworm. *J Biophys Biochem Cytol,* 1**,** 47-58.

DECKER, J. M., KRUGER, L., SYDOW, A., ZHAO, S., FROTSCHER, M., MANDELKOW, E. & MANDELKOW, E. M. 2015. Pro-aggregant Tau impairs mossy fiber plasticity due to structural changes and Ca(++) dysregulation. *Acta Neuropathol Commun,* 3**,** 23.

DEL CASTILLO, J. & KATZ, B. 1954. Quantal components of the end-plate potential. *J Physiol,* 124**,** 560-73.

DENKER, A., KROHNERT, K., BUCKERS, J., NEHER, E. & RIZZOLI, S. O. 2011. The reserve pool of synaptic vesicles acts as a buffer for proteins involved in synaptic vesicle recycling. *Proc Natl Acad Sci U S A,* 108**,** 17183-8.

DENKER, A. & RIZZOLI, S. O. Synaptic vesicle pools: an update. *Front Synaptic Neurosci,* 2**,** 135.

DIRIL, M. K., WIENISCH, M., JUNG, N., KLINGAUF, J. & HAUCKE, V. 2006. Stonin 2 is an AP-2-dependent endocytic sorting adaptor for synaptotagmin internalization and recycling. *Dev Cell,* 10**,** 233-44.

DITTMAN, J. & RYAN, T. A. 2009. Molecular circuitry of endocytosis at nerve terminals. *Annu Rev Cell Dev Biol,* 25**,** 133-60.

DIXIT, R., ROSS, J. L., GOLDMAN, Y. E. & HOLZBAUR, E. L. 2008. Differential regulation of dynein and kinesin motor proteins by tau. *Science,* 319**,** 1086-9.

DIXON, D. & ATWOOD, H. L. 1989. Adenylate cyclase system is essential for long-term facilitation at the crayfish neuromuscular junction. *J Neurosci,* 9**,** 4246-52.

DOBRUNZ, L. E. 2002. Release probability is regulated by the size of the readily releasable vesicle pool at excitatory synapses in hippocampus. *Int J Dev Neurosci,* 20**,** 225-36.

DOBRUNZ, L. E. & STEVENS, C. F. 1997. Heterogeneity of release probability, facilitation, and depletion at central synapses. *Neuron,* 18**,** 995-1008.

DOHENY, H. C., RATNARAJ, N., WHITTINGTON, M. A., JEFFERYS, J. G. & PATSALOS, P. N. 1999. Blood and cerebrospinal fluid pharmacokinetics of the novel anticonvulsant levetiracetam (ucb L059) in the rat. *Epilepsy Res,* 34**,** 161-8.

DONG, M., YEH, F., TEPP, W. H., DEAN, C., JOHNSON, E. A., JANZ, R. & CHAPMAN, E. R. 2006. SV2 is the protein receptor for botulinum neurotoxin A. *Science,* 312**,** 592-6.

DOORNBOS, M. L., PEREZ-BENITO, L., TRESADERN, G., MULDER-KRIEGER, T., BIESMANS, I., TRABANCO, A. A., CID, J. M., LAVREYSEN, H., AP, I. J. & HEITMAN, L. H. 2016. Molecular mechanism of positive allosteric modulation of the metabotropic glutamate receptor 2 by JNJ-46281222. *Br J Pharmacol,* 173**,** 588-600.

DOROSTKAR, M. M., DREOSTI, E., ODERMATT, B. & LAGNADO, L. 2010. Computational processing of optical measurements of neuronal and synaptic activity in networks. *J Neurosci Methods,* 188**,** 141-50.

DREOSTI, E. & LAGNADO, L. 2011. Optical reporters of synaptic activity in neural circuits. *Exp Physiol,* 96**,** 4-12.

DREOSTI, E., ODERMATT, B., DOROSTKAR, M. M. & LAGNADO, L. 2009. A genetically encoded reporter of synaptic activity in vivo. *Nat Methods,* 6**,** 883-9.

DUBEY, M., CHAUDHURY, P., KABIRU, H. & SHEA, T. B. 2008. Tau inhibits anterograde axonal transport and perturbs stability in growing axonal neurites in part by displacing kinesin cargo: Neurofilaments attenuate tau-mediated neurite instability. *Cell Motility and the Cytoskeleton,* 65**,** 89-99.

DUMANCHIN, C., CAMUZAT, A., CAMPION, D., VERPILLAT, P., HANNEQUIN, D., DUBOIS, B., SAUGIER-VEBER, P., MARTIN, C., PENET, C., CHARBONNIER, F., AGID, Y., FREBOURG, T. & BRICE, A. 1998. Segregation of a missense mutation in the microtubule-associated protein tau gene with familial frontotemporal dementia and parkinsonism. *Hum Mol Genet,* 7**,** 1825-9.

DUVOISIN, R. M., ZHANG, C. & RAMONELL, K. 1995. A novel metabotropic glutamate receptor expressed in the retina and olfactory bulb. *J Neurosci,* 15**,** 3075-83.

EBNETH, A., GODEMANN, R., STAMER, K., ILLENBERGER, S., TRINCZEK, B., MANDELKOW, E. M. & MANDELKOW, E. 1998. Overexpression of tau protein inhibits kinesin-dependent trafficking of vesicles, mitochondria, and endoplasmic reticulum: Implications for Alzheimer's disease. *Journal of Cell Biology,* 143**,** 777-794.

EDELSTEIN, A. D., TSUCHIDA, M. A., AMODAJ, N., PINKARD, H., VALE, R. D. & STUURMAN, N. Advanced methods of microscope control using muManager software. *J Biol Methods,* 1.

EGGERMANN, E., BUCURENCIU, I., GOSWAMI, S. P. & JONAS, P. 2011. Nanodomain coupling between Ca(2)(+) channels and sensors of exocytosis at fast mammalian synapses. *Nat Rev Neurosci,* 13**,** 7-21.

ELIE, A., PREZEL, E., GUERIN, C., DENARIER, E., RAMIREZ-RIOS, S., SERRE, L., ANDRIEUX, A., FOUREST-LIEUVIN, A., BLANCHOIN, L. & ARNAL, I. 2015. Tau co-organizes dynamic microtubule and actin networks. *Sci Rep,* 5**,** 9964.

ELLIS, E. L. & DELBRUCK, M. 1939. The Growth of Bacteriophage. *J Gen Physiol,* 22**,** 365-84.

ENGQVIST-GOLDSTEIN, A. E. & DRUBIN, D. G. 2003. Actin assembly and endocytosis: from yeast to mammals. *Annu Rev Cell Dev Biol,* 19**,** 287-332.

EVANS, G. J., WILKINSON, M. C., GRAHAM, M. E., TURNER, K. M., CHAMBERLAIN, L. H., BURGOYNE, R. D. & MORGAN, A. 2001. Phosphorylation of cysteine string protein by protein kinase A. Implications for the modulation of exocytosis. *J Biol Chem,* 276**,** 47877-85.

FARINHA, A., LAVREYSEN, H., PEETERS, L., RUSSO, B., MASURE, S., TRABANCO, A. A., CID, J. & TRESADERN, G. 2015. Molecular determinants of positive allosteric modulation of the human metabotropic glutamate receptor 2. *Br J Pharmacol,* 172**,** 2383-96.

FATT, P. & KATZ, B. 1952. Spontaneous subthreshold activity at motor nerve endings. *J Physiol,* 117**,** 109-28.

FENSTER, S. D., KESSELS, M. M., QUALMANN, B., CHUNG, W. J., NASH, J., GUNDELFINGER, E. D. & GARNER, C. C. 2003. Interactions between Piccolo and the actin/dynamin-binding protein Abp1 link vesicle endocytosis to presynaptic active zones. *J Biol Chem,* 278**,** 20268-77.

FERNANDEZ-ALFONSO, T. & RYAN, T. A. 2004. The kinetics of synaptic vesicle pool depletion at CNS synaptic terminals. *Neuron,* 41**,** 943-53.

FERNANDEZ-ALFONSO, T. & RYAN, T. A. 2008. A heterogeneous "resting" pool of synaptic vesicles that is dynamically interchanged across boutons in mammalian CNS synapses. *Brain Cell Biol,* 36**,** 87-100.

FERNANDEZ-BUSNADIEGO, R., ZUBER, B., MAURER, U. E., CYRKLAFF, M., BAUMEISTER, W. & LUCIC, V. 2010. Quantitative analysis of the native presynaptic cytomatrix by cryoelectron tomography. *J Cell Biol,* 188**,** 145-56.

FERNANDEZ-CHACON, R., WOLFEL, M., NISHIMUNE, H., TABARES, L., SCHMITZ, F., CASTELLANO-MUNOZ, M., ROSENMUND, C., MONTESINOS, M. L., SANES, J. R., SCHNEGGENBURGER, R. & SUDHOF, T. C. 2004. The synaptic vesicle protein CSP alpha prevents presynaptic degeneration. *Neuron,* 42**,** 237-51.

FERRAGUTI, F. & SHIGEMOTO, R. 2006. Metabotropic glutamate receptors. *Cell Tissue Res,* 326**,** 483-504.

FERRO-NOVICK, S. & JAHN, R. 1994. Vesicle fusion from yeast to man. *Nature,* 370**,** 191-3.

FESCE, R., GROHOVAZ, F., VALTORTA, F. & MELDOLESI, J. 1994. Neurotransmitter release: fusion or 'kiss-and-run'? *Trends Cell Biol,* 4**,** 1-4.

FITZGERALD, J. B., SCHOEBERL, B., NIELSEN, U. B. & SORGER, P. K. 2006. Systems biology and combination therapy in the quest for clinical efficacy. *Nat Chem Biol,* 2**,** 458-66.

FOWLER, M. W. & STARAS, K. 2015. Synaptic vesicle pools: Principles, properties and limitations. *Exp Cell Res,* 335**,** 150-6.

FOX, L. M., WILLIAM, C. M., ADAMOWICZ, D. H., PITSTICK, R., CARLSON, G. A., SPIRES-JONES, T. L. & HYMAN, B. T. 2011. Soluble tau species, not neurofibrillary aggregates, disrupt neural system integration in a tau transgenic model. *J Neuropathol Exp Neurol,* 70**,** 588-95.

FRANKE, K., BERENS, P., SCHUBERT, T., BETHGE, M., EULER, T. & BADEN, T. 2017. Inhibition decorrelates visual feature representations in the inner retina. *Nature,* 542**,** 439-444.

FREDJ, N. B. & BURRONE, J. 2009. A resting pool of vesicles is responsible for spontaneous vesicle fusion at the synapse. *Nat Neurosci,* 12**,** 751-8.

FREMEAU, R. T., JR., VOGLMAIER, S., SEAL, R. P. & EDWARDS, R. H. 2004. VGLUTs define subsets of excitatory neurons and suggest novel roles for glutamate. *Trends Neurosci,* 27**,** 98-103.

FROST, A., UNGER, V. M. & DE CAMILLI, P. 2009. The BAR domain superfamily: membrane-molding macromolecules. *Cell,* 137**,** 191-6.

FUJIO, K., SATO, M., UEMURA, T., SATO, T., SATO-HARADA, R. & HARADA, A. 2007. 14-3-3 proteins and protein phosphatases are not reduced in tau-deficient mice. *Neuroreport,* 18**,** 1049-52.

FULGA, T. A., ELSON-SCHWAB, I., KHURANA, V., STEINHILB, M. L., SPIRES, T. L., HYMAN, B. T. & FEANY, M. B. 2007. Abnormal bundling and accumulation of F-actin mediates tau-induced neuronal degeneration in vivo. *Nat Cell Biol,* 9**,** 139-48.

GANDHI, S. P. & STEVENS, C. F. 2003. Three modes of synaptic vesicular recycling revealed by single-vesicle imaging. *Nature,* 423**,** 607-13.

GARCIA-PEREZ, E., MAHFOOZ, K., COVITA, J., ZANDUETA, A. & WESSELING, J. F. 2015. Levetiracetam accelerates the onset of supply rate depression in synaptic vesicle trafficking. *Epilepsia,* 56**,** 535-45.

GEE, K. R., BROWN, K. A., CHEN, W. N., BISHOP-STEWART, J., GRAY, D. & JOHNSON, I. 2000. Chemical and physiological characterization of fluo-4 Ca(2+)-indicator dyes. *Cell Calcium,* 27**,** 97-106.

GEGELASHVILI, G. & SCHOUSBOE, A. 1997. High affinity glutamate transporters: regulation of expression and activity. *Mol Pharmacol,* 52**,** 6-15.

GEORGE, S. R., O'DOWD, B. F. & LEE, S. P. 2002. G-protein-coupled receptor oligomerization and its potential for drug discovery. *Nat Rev Drug Discov,* 1**,** 808-20.

GEPPERT, M., GODA, Y., HAMMER, R. E., LI, C., ROSAHL, T. W., STEVENS, C. F. & SUDHOF, T. C. 1994. Synaptotagmin I: a major Ca2+ sensor for transmitter release at a central synapse. *Cell,* 79**,** 717-27.

GIANNAKOPOULOS, P., HERRMANN, F. R., BUSSIERE, T., BOURAS, C., KOVARI, E., PERL, D. P., MORRISON, J. H., GOLD, G. & HOF, P. R. 2003. Tangle and neuron numbers, but not amyloid load, predict cognitive status in Alzheimer's disease. *Neurology,* 60**,** 1495-500.

GIBSON, G. E. & PETERSON, C. 1987. Calcium and the aging nervous system. *Neurobiol Aging,* 8**,** 329-43.

GITLER, D., CHENG, Q., GREENGARD, P. & AUGUSTINE, G. J. 2008. Synapsin IIa controls the reserve pool of glutamatergic synaptic vesicles. *J Neurosci,* 28**,** 10835-43.

GOMEZ-ISLA, T., HOLLISTER, R., WEST, H., MUI, S., GROWDON, J. H., PETERSEN, R. C., PARISI, J. E. & HYMAN, B. T. 1997. Neuronal loss correlates with but exceeds neurofibrillary tangles in Alzheimer's disease. *Ann Neurol,* 41**,** 17-24.

GOMEZ-ISLA, T., SPIRES, T., DE CALIGNON, A. & HYMAN, B. T. 2008. Neuropathology of Alzheimer's disease. *Handb Clin Neurol,* 89**,** 233-43.

GONZALEZ-MAESO, J., ANG, R. L., YUEN, T., CHAN, P., WEISSTAUB, N. V., LOPEZ-GIMENEZ, J. F., ZHOU, M., OKAWA, Y., CALLADO, L. F., MILLIGAN, G., GINGRICH, J. A., FILIZOLA, M., MEANA, J. J. & SEALFON, S. C. 2008. Identification of a serotonin/glutamate receptor complex implicated in psychosis. *Nature,* 452**,** 93-7.

GORSKY, M. K., BURNOUF, S., SOFOLA-ADESAKIN, O., DOLS, J., AUGUSTIN, H., WEIGELT, C. M., GRONKE, S. & PARTRIDGE, L. 2017. Pseudo-acetylation of multiple sites on human Tau proteins alters Tau phosphorylation and microtubule binding, and ameliorates amyloid beta toxicity. *Sci Rep,* 7**,** 9984.

GOWER, A. J., NOYER, M., VERLOES, R., GOBERT, J. & WULFERT, E. 1992. ucb L059, a novel anti-convulsant drug: pharmacological profile in animals. *Eur J Pharmacol,* 222**,** 193-203.

GRANSETH, B. & LAGNADO, L. 2008. The role of endocytosis in regulating the strength of hippocampal synapses. *J Physiol,* 586**,** 5969-82.

GRANSETH, B., ODERMATT, B., ROYLE, S. J. & LAGNADO, L. 2006. Clathrin-mediated endocytosis is the dominant mechanism of vesicle retrieval at hippocampal synapses. *Neuron,* 51**,** 773-86.

GRIFFITH, L. M. & POLLARD, T. D. 1982. The interaction of actin filaments with microtubules and microtubule-associated proteins. *J Biol Chem,* 257**,** 9143-51.

GROEMER, T. W. & KLINGAUF, J. 2007. Synaptic vesicles recycling spontaneously and during activity belong to the same vesicle pool. *Nat Neurosci,* 10**,** 145-7.

GRONBORG, M., PAVLOS, N. J., BRUNK, I., CHUA, J. J., MUNSTER-WANDOWSKI, A., RIEDEL, D., AHNERT-HILGER, G., URLAUB, H. & JAHN, R. 2010. Quantitative comparison of glutamatergic and GABAergic synaptic vesicles unveils selectivity for few proteins including MAL2, a novel synaptic vesicle protein. *J Neurosci,* 30**,** 2-12.

GULYAS, A. I., MEGIAS, M., EMRI, Z. & FREUND, T. F. 1999. Total number and ratio of excitatory and inhibitory synapses converging onto single interneurons of different types in the CA1 area of the rat hippocampus. *J Neurosci,* 19**,** 10082-97.

HANES, J., ZILKA, N., BARTKOVA, M., CALETKOVA, M., DOBROTA, D. & NOVAK, M. 2009. Rat tau proteome consists of six tau isoforms: implication for animal models of human tauopathies. *J Neurochem,* 108**,** 1167-76.

HANGER, D. P., SEEREERAM, A. & NOBLE, W. 2009. Mediators of tau phosphorylation in the pathogenesis of Alzheimer's disease. *Expert Rev Neurother,* 9**,** 1647-66.

HANSON, P. I., HEUSER, J. E. & JAHN, R. 1997. Neurotransmitter release - four years of SNARE complexes. *Curr Opin Neurobiol,* 7**,** 310-5.

HARADA, A., OGUCHI, K., OKABE, S., KUNO, J., TERADA, S., OHSHIMA, T., SATO-YOSHITAKE, R., TAKEI, Y., NODA, T. & HIROKAWA, N. 1994. Altered microtubule organization in small-calibre axons of mice lacking tau protein. *Nature,* 369**,** 488-91.

HARATA, N., RYAN, T. A., SMITH, S. J., BUCHANAN, J. & TSIEN, R. W. 2001. Visualizing recycling synaptic vesicles in hippocampal neurons by FM 1-43 photoconversion. *Proc Natl Acad Sci U S A,* 98**,** 12748-53.

HARATA, N. C., ARAVANIS, A. M. & TSIEN, R. W. 2006. Kiss-and-run and full-collapse fusion as modes of exo-endocytosis in neurosecretion. *J Neurochem,* 97**,** 1546-70.

HARDY, J. & SELKOE, D. J. 2002. The amyloid hypothesis of Alzheimer's disease: progress and problems on the road to therapeutics. *Science,* 297**,** 353-6.

HARRIS, K. M. & SULTAN, P. 1995. Variation in the number, location and size of synaptic vesicles provides an anatomical basis for the nonuniform probability of release at hippocampal CA1 synapses. *Neuropharmacology,* 34**,** 1387-95.

HAUCKE, V., NEHER, E. & SIGRIST, S. J. 2011. Protein scaffolds in the coupling of synaptic exocytosis and endocytosis. *Nat Rev Neurosci,* 12**,** 127-38.

HAYASHI, Y., MOMIYAMA, A., TAKAHASHI, T., OHISHI, H., OGAWA-MEGURO, R., SHIGEMOTO, R., MIZUNO, N. & NAKANISHI, S. 1993. Role of a metabotropic glutamate receptor in synaptic modulation in the accessory olfactory bulb. *Nature,* 366**,** 687-90.

HAYASHI, Y., TANABE, Y., ARAMORI, I., MASU, M., SHIMAMOTO, K., OHFUNE, Y. & NAKANISHI, S. 1992. Agonist analysis of 2-(carboxycyclopropyl)glycine isomers for cloned metabotropic glutamate receptor subtypes expressed in Chinese hamster ovary cells. *Br J Pharmacol,* 107**,** 539-43.

HEIDELBERGER, R., STERLING, P. & MATTHEWS, G. 2002. Roles of ATP in depletion and replenishment of the releasable pool of synaptic vesicles. *J Neurophysiol,* 88**,** 98-106.

HELASSA, N., DURST, C. D., COATES, C., KERRUTH, S., ARIF, U., SCHULZE, C., WIEGERT, J. S., GEEVES, M., OERTNER, T. G. & TOROK, K. 2018. Ultrafast glutamate sensors resolve high-frequency release at Schaffer collateral synapses. *Proc Natl Acad Sci U S A,* 115**,** 5594-5599.

HELASSA, N., PODOR, B., FINE, A. & TOROK, K. 2016. Design and mechanistic insight into ultrafast calcium indicators for monitoring intracellular calcium dynamics. *Sci Rep,* 6**,** 38276.

HELASSA, N., ZHANG, X. H., CONTE, I., SCARINGI, J., ESPOSITO, E., BRADLEY, J., CARTER, T., OGDEN, D., MORAD, M. & TOROK, K. 2015. Fast-Response Calmodulin-Based Fluorescent Indicators Reveal Rapid Intracellular Calcium Dynamics. *Sci Rep,* 5**,** 15978.

HERZOG, E., NADRIGNY, F., SILM, K., BIESEMANN, C., HELLING, I., BERSOT, T., STEFFENS, H., SCHWARTZMANN, R., NAGERL, U. V., EL MESTIKAWY, S., RHEE, J., KIRCHHOFF, F. & BROSE, N. 2011. In vivo imaging of intersynaptic vesicle exchange using VGLUT1 Venus knock-in mice. *J Neurosci,* 31**,** 15544-59.

HERZOG, E., TAKAMORI, S., JAHN, R., BROSE, N. & WOJCIK, S. M. 2006. Synaptic and vesicular co-localization of the glutamate transporters VGLUT1 and VGLUT2 in the mouse hippocampus. *J Neurochem,* 99**,** 1011-8.

HEUSER, J. E. & REESE, T. S. 1973. Evidence for recycling of synaptic vesicle membrane during transmitter release at the frog neuromuscular junction. *J Cell Biol,* 57**,** 315-44.

HOLDERITH, N., LORINCZ, A., KATONA, G., ROZSA, B., KULIK, A., WATANABE, M. & NUSSER, Z. 2012. Release probability of hippocampal glutamatergic terminals scales with the size of the active zone. *Nat Neurosci,* 15**,** 988-97.

HONG, M., ZHUKAREVA, V., VOGELSBERG-RAGAGLIA, V., WSZOLEK, Z., REED, L., MILLER, B. I., GESCHWIND, D. H., BIRD, T. D., MCKEEL, D., GOATE, A., MORRIS, J. C., WILHELMSEN, K. C., SCHELLENBERG, G. D., TROJANOWSKI, J. Q. & LEE, V. M. 1998. Mutation-specific functional impairments in distinct tau isoforms of hereditary FTDP-17. *Science,* 282**,** 1914-7.

HOOVER, B. R., REED, M. N., SU, J., PENROD, R. D., KOTILINEK, L. A., GRANT, M. K., PITSTICK, R., CARLSON, G. A., LANIER, L. M., YUAN, L. L., ASHE, K. H. & LIAO, D. 2010a. Tau mislocalization to dendritic spines mediates synaptic dysfunction independently of neurodegeneration. *Neuron,* 68**,** 1067-81.

HOOVER, B. R., REED, M. N., SU, J. J., PENROD, R. D., KOTILINEK, L. A., GRANT, M. K., PITSTICK, R., CARLSON, G. A., LANIER, L. M., YUAN, L. L., ASHE, K. H. & LIAO, D. Z. 2010b. Tau Mislocalization to Dendritic Spines Mediates Synaptic Dysfunction Independently of Neurodegeneration. *Neuron,* 68**,** 1067-1081.

HOPF, F. W., WATERS, J., MEHTA, S. & SMITH, S. J. 2002. Stability and plasticity of developing synapses in hippocampal neuronal cultures. *J Neurosci,* 22**,** 775-81.

HOSOI, N., HOLT, M. & SAKABA, T. 2009. Calcium dependence of exo- and endocytotic coupling at a glutamatergic synapse. *Neuron,* 63**,** 216-29.

HUANG, Y. & MUCKE, L. 2012. Alzheimer mechanisms and therapeutic strategies. *Cell,* 148**,** 1204-22.

HUNSBERGER, H. C., RUDY, C. C., BATTEN, S. R., GERHARDT, G. A. & REED, M. N. 2015. P301L tau expression affects glutamate release and clearance in the hippocampal trisynaptic pathway. *J Neurochem,* 132**,** 169-82.

HUTTNER, W. B., SCHIEBLER, W., GREENGARD, P. & DE CAMILLI, P. 1983. Synapsin I (protein I), a nerve terminal-specific phosphoprotein. III. Its association with synaptic vesicles studied in a highly purified synaptic vesicle preparation. *J Cell Biol,* 96**,** 1374-88.

HUTTON, M., LENDON, C. L., RIZZU, P., BAKER, M., FROELICH, S., HOULDEN, H., PICKERING-BROWN, S., CHAKRAVERTY, S., ISAACS, A., GROVER, A., HACKETT, J., ADAMSON, J., LINCOLN, S., DICKSON, D., DAVIES, P., PETERSEN, R. C., STEVENS, M., DE GRAAFF, E., WAUTERS, E., VAN BAREN, J., HILLEBRAND, M., JOOSSE, M., KWON, J. M., NOWOTNY, P., CHE, L. K., NORTON, J., MORRIS, J. C., REED, L. A., TROJANOWSKI, J., BASUN, H., LANNFELT, L., NEYSTAT, M., FAHN, S., DARK, F., TANNENBERG, T., DODD, P. R., HAYWARD, N., KWOK, J. B., SCHOFIELD, P. R., ANDREADIS, A., SNOWDEN, J., CRAUFURD, D., NEARY, D., OWEN, F., OOSTRA, B. A., HARDY, J., GOATE, A., VAN SWIETEN, J., MANN, D., LYNCH, T. & HEUTINK, P. 1998. Association of missense and 5'-splice-site mutations in tau with the inherited dementia FTDP-17. *Nature,* 393**,** 702-5.

HYMAN, B. T. 2011. Amyloid-dependent and amyloid-independent stages of Alzheimer disease. *Arch Neurol,* 68**,** 1062-4.

IKEDA, K. & BEKKERS, J. M. 2009. Counting the number of releasable synaptic vesicles in a presynaptic terminal. *Proc Natl Acad Sci U S A,* 106**,** 2945-50.

IKEGAMI, S., HARADA, A. & HIROKAWA, N. 2000. Muscle weakness, hyperactivity, and impairment in fear conditioning in tau-deficient mice. *Neurosci Lett,* 279**,** 129-32.

IQBAL, K., LIU, F., GONG, C. X., ALONSO ADEL, C. & GRUNDKE-IQBAL, I. 2009. Mechanisms of tau-induced neurodegeneration. *Acta Neuropathol,* 118**,** 53-69.

ITAKURA, M., MISAWA, H., SEKIGUCHI, M., TAKAHASHI, S. & TAKAHASHI, M. 1999. Transfection analysis of functional roles of complexin I and II in the exocytosis of two different types of secretory vesicles. *Biochem Biophys Res Commun,* 265**,** 691-6.

ITO, I., FUTAI, K., KATAGIRI, H., WATANABE, M., SAKIMURA, K., MISHINA, M. & SUGIYAMA, H. 1997. Synapse-selective impairment of NMDA receptor functions in mice lacking NMDA receptor epsilon 1 or epsilon 2 subunit. *J Physiol,* 500 (Pt 2)**,** 401-8.

ITTNER, L. M., FATH, T., KE, Y. D., BI, M., VAN EERSEL, J., LI, K. M., GUNNING, P. & GOTZ, J. 2008. Parkinsonism and impaired axonal transport in a mouse model of frontotemporal dementia. *Proc Natl Acad Sci U S A,* 105**,** 15997-6002.

ITTNER, L. M., KE, Y. D., DELERUE, F., BI, M., GLADBACH, A., VAN EERSEL, J., WOLFING, H., CHIENG, B. C., CHRISTIE, M. J., NAPIER, I. A., ECKERT, A., STAUFENBIEL, M., HARDEMAN, E. & GOTZ, J. 2010. Dendritic function of tau mediates amyloid-beta toxicity in Alzheimer's disease mouse models. *Cell,* 142**,** 387-97.

IVANNIKOV, M. V., SUGIMORI, M. & LLINAS, R. R. 2013. Synaptic vesicle exocytosis in hippocampal synaptosomes correlates directly with total mitochondrial volume. *J Mol Neurosci,* 49**,** 223-30.

IVERSEN, L., MULVIHILL, E., HALDEMAN, B., DIEMER, N. H., KAISER, F., SHEARDOWN, M. & KRISTENSEN, P. 1994. Changes in metabotropic glutamate receptor mRNA levels following global ischemia: increase of a putative presynaptic subtype (mGluR4) in highly vulnerable rat brain areas. *J Neurochem,* 63**,** 625-33.

JAFFE, D. B. & CARNEVALE, N. T. 1999. Passive normalization of synaptic integration influenced by dendritic architecture. *J Neurophysiol,* 82**,** 3268-85.

JANSSENS, N. & LESAGE, A. S. 2001. Glutamate receptor subunit expression in primary neuronal and secondary glial cultures. *J Neurochem,* 77**,** 1457-74.

JANZ, R., GODA, Y., GEPPERT, M., MISSLER, M. & SUDHOF, T. C. 1999. SV2A and SV2B function as redundant Ca2+ regulators in neurotransmitter release. *Neuron,* 24**,** 1003-16.

JOHNSON, M. P., BAEZ, M., JAGDMANN, G. E., JR., BRITTON, T. C., LARGE, T. H., CALLAGARO, D. O., TIZZANO, J. P., MONN, J. A. & SCHOEPP, D. D. 2003. Discovery of allosteric potentiators for the metabotropic glutamate 2 receptor: synthesis and subtype selectivity of N-(4-(2-methoxyphenoxy)phenyl)-N-(2,2,2- trifluoroethylsulfonyl)pyrid-3-ylmethylamine. *J Med Chem,* 46**,** 3189-92.

JOLY, C., GOMEZA, J., BRABET, I., CURRY, K., BOCKAERT, J. & PIN, J. P. 1995. Molecular, functional, and pharmacological characterization of the metabotropic glutamate receptor type 5 splice variants: comparison with mGluR1. *J Neurosci,* 15**,** 3970-81.

JUN, K., PIEDRAS-RENTERIA, E. S., SMITH, S. M., WHEELER, D. B., LEE, S. B., LEE, T. G., CHIN, H., ADAMS, M. E., SCHELLER, R. H., TSIEN, R. W. & SHIN, H. S. 1999. Ablation of P/Q-type Ca(2+) channel currents, altered synaptic transmission, and progressive ataxia in mice lacking the alpha(1A)-subunit. *Proc Natl Acad Sci U S A,* 96**,** 15245-50.

KAECH, S. & BANKER, G. 2006. Culturing hippocampal neurons. *Nat Protoc,* 1**,** 2406-15.

KAESER, P. S., DENG, L., FAN, M. & SUDHOF, T. C. 2012. RIM genes differentially contribute to organizing presynaptic release sites. *Proc Natl Acad Sci U S A,* 109**,** 11830-5.

KAESER, P. S., DENG, L., WANG, Y., DULUBOVA, I., LIU, X., RIZO, J. & SUDHOF, T. C. 2011. RIM proteins tether Ca2+ channels to presynaptic active zones via a direct PDZ-domain interaction. *Cell,* 144**,** 282-95.

KAKSONEN, M., TORET, C. P. & DRUBIN, D. G. 2005. A modular design for the clathrin- and actin-mediated endocytosis machinery. *Cell,* 123**,** 305-20.

KAMINSKI, R. M., GILLARD, M., LECLERCQ, K., HANON, E., LORENT, G., DASSESSE, D., MATAGNE, A. & KLITGAARD, H. 2009. Proepileptic phenotype of SV2A-deficient mice is associated with reduced anticonvulsant efficacy of levetiracetam. *Epilepsia,* 50**,** 1729-40.

KAMINSKI, R. M., MATAGNE, A., LECLERCQ, K., GILLARD, M., MICHEL, P., KENDA, B., TALAGA, P. & KLITGAARD, H. 2008. SV2A protein is a broad-spectrum anticonvulsant target: functional

correlation between protein binding and seizure protection in models of both partial and generalized epilepsy. *Neuropharmacology,* 54**,** 715-20.

KAMIYA, H. & OZAWA, S. 1999. Dual mechanism for presynaptic modulation by axonal metabotropic glutamate receptor at the mouse mossy fibre-CA3 synapse. *J Physiol,* 518 (Pt 2)**,** 497-506.

KARUNANITHI, S., MARIN, L., WONG, K. & ATWOOD, H. L. 2002. Quantal size and variation determined by vesicle size in normal and mutant Drosophila glutamatergic synapses. *J Neurosci,* 22**,** 10267-76.

KASPROWICZ, J., KUENEN, S., MISKIEWICZ, K., HABETS, R. L., SMITZ, L. & VERSTREKEN, P. 2008. Inactivation of clathrin heavy chain inhibits synaptic recycling but allows bulk membrane uptake. *J Cell Biol,* 182**,** 1007-16.

KATSUSE, O., LIN, W. L., LEWIS, J., HUTTON, M. L. & DICKSON, D. W. 2006. Neurofibrillary tangle-related synaptic alterations of spinal motor neurons of P301L tau transgenic mice. *Neurosci Lett,* 409**,** 95-9.

KATZ, B. & MILEDI, R. 1967. Ionic requirements of synaptic transmitter release. *Nature,* 215**,** 651.

KAUFMAN, S. K., SANDERS, D. W., THOMAS, T. L., RUCHINSKAS, A. J., VAQUER-ALICEA, J., SHARMA, A. M., MILLER, T. M. & DIAMOND, M. I. 2016. Tau Prion Strains Dictate Patterns of Cell Pathology, Progression Rate, and Regional Vulnerability In Vivo. *Neuron,* 92**,** 796-812.

KAVALALI, E. T. 2015. The mechanisms and functions of spontaneous neurotransmitter release. *Nat Rev Neurosci,* 16**,** 5-16.

KHACHATURIAN, Z. S. 1987. Hypothesis on the regulation of cytosol calcium concentration and the aging brain. *Neurobiol Aging,* 8**,** 345-6.

KIM, S. H. & RYAN, T. A. 2009. Synaptic vesicle recycling at CNS snapses without AP-2. *J Neurosci,* 29**,** 3865-74.

KIM, S. H. & RYAN, T. A. 2010. CDK5 serves as a major control point in neurotransmitter release. *Neuron,* 67**,** 797-809.

KIMURA, T., WHITCOMB, D. J., JO, J., REGAN, P., PIERS, T., HEO, S., BROWN, C., HASHIKAWA, T., MURAYAMA, M., SEOK, H., SOTIROPOULOS, I., KIM, E., COLLINGRIDGE, G. L., TAKASHIMA, A. & CHO, K. 2014. Microtubule-associated protein tau is essential for long-term depression in the hippocampus. *Philos Trans R Soc Lond B Biol Sci,* 369**,** 20130144.

KLITGAARD, H., MATAGNE, A., GOBERT, J. & WULFERT, E. 1998. Evidence for a unique profile of levetiracetam in rodent models of seizures and epilepsy. *Eur J Pharmacol,* 353**,** 191-206.

KONONENKO, N. L. & HAUCKE, V. 2015. Molecular mechanisms of presynaptic membrane retrieval and synaptic vesicle reformation. *Neuron,* 85**,** 484-96.

KONONENKO, N. L., PUCHKOV, D., CLASSEN, G. A., WALTER, A. M., PECHSTEIN, A., SAWADE, L., KAEMPF, N., TRIMBUCH, T., LORENZ, D., ROSENMUND, C., MARITZEN, T. & HAUCKE, V. 2014. Clathrin/AP-2 mediate synaptic vesicle reformation from endosome-like vacuoles but are not essential for membrane retrieval at central synapses. *Neuron,* 82**,** 981-8.

KOPEIKINA, K. J., CARLSON, G. A., PITSTICK, R., LUDVIGSON, A. E., PETERS, A., LUEBKE, J. I., KOFFIE, R. M., FROSCH, M. P., HYMAN, B. T. & SPIRES-JONES, T. L. 2011. Tau accumulation causes mitochondrial distribution deficits in neurons in a mouse model of tauopathy and in human Alzheimer's disease brain. *Am J Pathol,* 179**,** 2071-82.

KULIK, A., VIDA, I., LUJAN, R., HAAS, C. A., LOPEZ-BENDITO, G., SHIGEMOTO, R. & FROTSCHER, M. 2003. Subcellular localization of metabotropic GABA(B) receptor subunits GABA(B1a/b) and GABA(B2) in the rat hippocampus. *J Neurosci,* 23**,** 11026-35.

LAFERLA, F. M. 2002. Calcium dyshomeostasis and intracellular signalling in Alzheimer's disease. *Nat Rev Neurosci,* 3**,** 862-72.

LANDFIELD, P. W. 1987. 'Increased calcium-current' hypothesis of brain aging. *Neurobiol Aging,* 8**,** 346-7.

LASAGNA-REEVES, C. A., CASTILLO-CARRANZA, D. L., SENGUPTA, U., CLOS, A. L., JACKSON, G. R. & KAYED, R. 2011. Tau oligomers impair memory and induce synaptic and mitochondrial dysfunction in wild-type mice. *Molecular Neurodegeneration,* 6.

LAURIE, D. J., BODDEKE, H. W., HILTSCHER, R. & SOMMER, B. 1996. HmGlu1d, a novel splice variant of the human type I metabotropic glutamate receptor. *Eur J Pharmacol,* 296**,** R1-R3.

LAVREYSEN, H., AHNAOU, A., DRINKENBURG, W., LANGLOIS, X., MACKIE, C., PYPE, S., LUTJENS, R., LE POUL, E., TRABANCO, A. A. & NUNEZ, J. M. 2015a. Pharmacological and pharmacokinetic properties of JNJ-40411813, a positive allosteric modulator of the mGlu2 receptor. *Pharmacol Res Perspect,* 3**,** e00096.

LAVREYSEN, H., LANGLOIS, X., DONCK, L. V., NUNEZ, J. M., PYPE, S., LUTJENS, R. & MEGENS, A. 2015b. Preclinical evaluation of the antipsychotic potential of the mGlu2-positive allosteric modulator JNJ-40411813. *Pharmacol Res Perspect,* 3**,** e00097.

LAYTON, M. E., REIF, A. J., HARTINGH, T. J., RODZINAK, K., DUDKIN, V., WANG, C., ARRINGTON, K., KELLY, M. J., 3RD, GARBACCIO, R. M., O'BRIEN, J. A., MAGLIARO, B. C., USLANER, J. M., HUSZAR, S. L., FILLGROVE, K. L., TANG, C., KUO, Y. & JACOBSON, M. A. 2016. Discovery of 5-aryl-1,3-dihydro-2H-imidazo[4,5-b]pyridin-2-ones as positive allosteric modulators of metabotropic glutamate subtype-2 (mGlu2) receptors with efficacy in a preclinical model of psychosis. *Bioorg Med Chem Lett,* 26**,** 1260-4.

LEE, C. W. & PENG, H. B. 2008. The function of mitochondria in presynaptic development at the neuromuscular junction. *Mol Biol Cell,* 19**,** 150-8.

LEE, C. Y., CHEN, C. C. & LIOU, H. H. 2009a. Levetiracetam inhibits glutamate transmission through presynaptic P/Q-type calcium channels on the granule cells of the dentate gyrus. *Br J Pharmacol,* 158**,** 1753-62.

LEE, H. G., PERRY, G., MOREIRA, P. I., GARRETT, M. R., LIU, Q., ZHU, X., TAKEDA, A., NUNOMURA, A. & SMITH, M. A. 2005. Tau phosphorylation in Alzheimer's disease: pathogen or protector? *Trends Mol Med,* 11**,** 164-9.

LEE, H. G., ZHU, X., CASADESUS, G., PALLAS, M., CAMINS, A., O'NEILL, M. J., NAKANISHI, S., PERRY, G. & SMITH, M. A. 2009b. The effect of mGluR2 activation on signal transduction pathways and neuronal cell survival. *Brain Res,* 1249**,** 244-50.

LEE, V. M., GOEDERT, M. & TROJANOWSKI, J. Q. 2001. Neurodegenerative tauopathies. *Annu Rev Neurosci,* 24**,** 1121-59.

LEI, P., AYTON, S., FINKELSTEIN, D. I., SPOERRI, L., CICCOTOSTO, G. D., WRIGHT, D. K., WONG, B. X., ADLARD, P. A., CHERNY, R. A., LAM, L. Q., ROBERTS, B. R., VOLITAKIS, I., EGAN, G. F., MCLEAN, C. A., CAPPAI, R., DUCE, J. A. & BUSH, A. I. 2012. Tau deficiency induces parkinsonism with dementia by impairing APP-mediated iron export. *Nat Med,* 18**,** 291-5.

LEWERENZ, J. & MAHER, P. 2015. Chronic Glutamate Toxicity in Neurodegenerative Diseases-What is the Evidence? *Front Neurosci,* 9**,** 469.

LI, H., FOSS, S. M., DOBRYY, Y. L., PARK, C. K., HIRES, S. A., SHANER, N. C., TSIEN, R. Y., OSBORNE, L. C. & VOGLMAIER, S. M. 2011. Concurrent imaging of synaptic vesicle recycling and calcium dynamics. *Front Mol Neurosci,* 4**,** 34.

LI, Y. C. & KAVALALI, E. T. 2017. Synaptic Vesicle-Recycling Machinery Components as Potential Therapeutic Targets. *Pharmacol Rev,* 69**,** 141-160.

LI, Z., BURRONE, J., TYLER, W. J., HARTMAN, K. N., ALBEANU, D. F. & MURTHY, V. N. 2005. Synaptic vesicle recycling studied in transgenic mice expressing synaptopHluorin. *Proc Natl Acad Sci U S A,* 102**,** 6131-6.

LIN, R. C. & SCHELLER, R. H. 1997. Structural organization of the synaptic exocytosis core complex. *Neuron,* 19**,** 1087-94.

LIU, G. & TSIEN, R. W. 1995. Synaptic transmission at single visualized hippocampal boutons. *Neuropharmacology,* 34**,** 1407-21.

LIU, J., GUO, T., WU, J., BAI, X., ZHOU, Q. & SUI, S. F. 2007. Overexpression of complexin in PC12 cells inhibits exocytosis by preventing SNARE complex recycling. *Biochemistry (Mosc),* 72**,** 439-44.

LOSCHER, W., GILLARD, M., SANDS, Z. A., KAMINSKI, R. M. & KLITGAARD, H. 2016. Synaptic Vesicle Glycoprotein 2A Ligands in the Treatment of Epilepsy and Beyond. *CNS Drugs,* 30**,** 1055-1077.

LOSCHER, W. & HONACK, D. 1993. Profile of ucb L059, a novel anticonvulsant drug, in models of partial and generalized epilepsy in mice and rats. *Eur J Pharmacol,* 232**,** 147-58.

LOSCHER, W. & SCHMIDT, D. 2011. Modern antiepileptic drug development has failed to deliver: ways out of the current dilemma. *Epilepsia,* 52**,** 657-78.

LUKYANETZ, E. A., SHKRYL, V. M. & KOSTYUK, P. G. 2002. Selective blockade of N-type calcium channels by levetiracetam. *Epilepsia,* 43**,** 9-18.

LYNCH, B. A., LAMBENG, N., NOCKA, K., KENSEL-HAMMES, P., BAJJALIEH, S. M., MATAGNE, A. & FUKS, B. 2004. The synaptic vesicle protein SV2A is the binding site for the antiepileptic drug levetiracetam. *Proc Natl Acad Sci U S A,* 101**,** 9861-6.

LYNCH, B. A., MATAGNE, A., BRANNSTROM, A., VON EULER, A., JANSSON, M., HAUZENBERGER, E. & SODERHALL, J. A. 2008. Visualization of SV2A conformations in situ by the use of Protein Tomography. *Biochem Biophys Res Commun,* 375**,** 491-5.

LYNCH, J. M., TATE, S. K., KINIRONS, P., WEALE, M. E., CAVALLERI, G. L., DEPONDT, C., MURPHY, K., O'ROURKE, D., DOHERTY, C. P., SHIANNA, K. V., WOOD, N. W., SANDER, J. W., DELANTY, N., GOLDSTEIN, D. B. & SISODIYA, S. M. 2009. No major role of common SV2A variation for predisposition or levetiracetam response in epilepsy. *Epilepsy Res,* 83**,** 44-51.

MANDELKOW, E. M., BIERNAT, J., STAMER, K., TRINCZEK, B. & MANDELKOW, E. 2001. The dual role of tau in cell polarisation and organelle trafficking. *Neuroscientific Basis of Dementia***,** 101-111.

MANDELKOW, E. M., STAMER, K., VOGEL, R., THIES, E. & MANDELKOW, E. 2003. Clogging of axons by tau, inhibition of axonal traffic and starvation of synapses. *Neurobiol Aging,* 24**,** 1079-85.

MARRA, V., BURDEN, J. J., THORPE, J. R., SMITH, I. T., SMITH, S. L., HAUSSER, M., BRANCO, T. & STARAS, K. 2012. A preferentially segregated recycling vesicle pool of limited size supports neurotransmission in native central synapses. *Neuron,* 76**,** 579-89.

MARVIN, J. S., BORGHUIS, B. G., TIAN, L., CICHON, J., HARNETT, M. T., AKERBOOM, J., GORDUS, A., RENNINGER, S. L., CHEN, T. W., BARGMANN, C. I., ORGER, M. B., SCHREITER, E. R., DEMB, J. B., GAN, W. B., HIRES, S. A. & LOOGER, L. L. 2013. An optimized fluorescent probe for visualizing glutamate neurotransmission. *Nat Methods,* 10**,** 162-70.

MATZ, J., GILYAN, A., KOLAR, A., MCCARVILL, T. & KRUEGER, S. R. 2010. Rapid structural alterations of the active zone lead to sustained changes in neurotransmitter release. *Proc Natl Acad Sci U S A,* 107**,** 8836-41.

MCINTIRE, S. L., REIMER, R. J., SCHUSKE, K., EDWARDS, R. H. & JORGENSEN, E. M. 1997. Identification and characterization of the vesicular GABA transporter. *Nature,* 389**,** 870-6.

MCMAHON, H. T. & BOUCROT, E. 2011. Molecular mechanism and physiological functions of clathrin-mediated endocytosis. *Nat Rev Mol Cell Biol,* 12**,** 517-33.

MCOMISH, C. E., DEMIREVA, E. Y. & GINGRICH, J. A. 2016. Developmental expression of mGlu2 and mGlu3 in the mouse brain. *Gene Expr Patterns,* 22**,** 46-53.

MEEHAN, A. L., YANG, X., YUAN, L. L. & ROTHMAN, S. M. 2012. Levetiracetam has an activity-dependent effect on inhibitory transmission. *Epilepsia,* 53**,** 469-76.

MENDOZA-TORREBLANCA, J. G., VANOYE-CARLO, A., PHILLIPS-FARFAN, B. V., CARMONA-APARICIO, L. & GOMEZ-LIRA, G. 2013. Synaptic vesicle protein 2A: basic facts and role in synaptic function. *Eur J Neurosci,* 38**,** 3529-39.

MERRIFIELD, C. J., PERRAIS, D. & ZENISEK, D. 2005. Coupling between clathrin-coated-pit invagination, cortactin recruitment, and membrane scission observed in live cells. *Cell,* 121**,** 593-606.

METCALF, C. S., KLEIN, B. D., SMITH, M. D., PRUESS, T., CEUSTERS, M., LAVREYSEN, H., PYPE, S., VAN OSSELAER, N., TWYMAN, R. & WHITE, H. S. 2017. Efficacy of mGlu2 -positive allosteric modulators alone and in combination with levetiracetam in the mouse 6 Hz model of psychomotor seizures. *Epilepsia,* 58**,** 484-493.

MEZLER, M., HERMANN, D., SWENSEN, A. M., DRAGUHN, A., TERSTAPPEN, G. C., GROSS, G., SCHOEMAKER, H., FREIBERG, G., PRATT, S., GOPALAKRISHNAN, S. M. & NIMMRICH, V. 2012. Development and validation of a fluorescence-based HTS assay for the identification of P/Q-type calcium channel blockers. *Comb Chem High Throughput Screen,* 15**,** 372-85.

MIESENBOCK, G., DE ANGELIS, D. A. & ROTHMAN, J. E. 1998. Visualizing secretion and synaptic transmission with pH-sensitive green fluorescent proteins. *Nature,* 394**,** 192-5.

MIETELSKA-POROWSKA, A., WASIK, U., GORAS, M., FILIPEK, A. & NIEWIADOMSKA, G. 2014. Tau protein modifications and interactions: their role in function and dysfunction. *Int J Mol Sci,* 15**,** 4671-713.

MILOSEVIC, I., GIOVEDI, S., LOU, X., RAIMONDI, A., COLLESI, C., SHEN, H., PARADISE, S., O'TOOLE, E., FERGUSON, S., CREMONA, O. & DE CAMILLI, P. 2011. Recruitment of endophilin to clathrin-coated pit necks is required for efficient vesicle uncoating after fission. *Neuron,* 72**,** 587-601.

MINAKAMI, R., KATSUKI, F., YAMAMOTO, T., NAKAMURA, K. & SUGIYAMA, H. 1994. Molecular cloning and the functional expression of two isoforms of human metabotropic glutamate receptor subtype 5. *Biochem Biophys Res Commun,* 199**,** 1136-43.

MOGHADDAM, B. 2004. Targeting metabotropic glutamate receptors for treatment of the cognitive symptoms of schizophrenia. *Psychopharmacology (Berl),* 174**,** 39-44.

MORFINI, G. A., BURNS, M., BINDER, L. I., KANAAN, N. M., LAPOINTE, N., BOSCO, D. A., BROWN, R. H., JR., BROWN, H., TIWARI, A., HAYWARD, L., EDGAR, J., NAVE, K. A., GARBERRN, J., ATAGI, Y., SONG, Y., PIGINO, G. & BRADY, S. T. 2009. Axonal transport defects in neurodegenerative diseases. *J Neurosci,* 29**,** 12776-86.

MORRIS, K. L. & SERPELL, L. C. 2012. X-ray fibre diffraction studies of amyloid fibrils. *Methods Mol Biol,* 849**,** 121-35.

MURTHY, V. N. & DE CAMILLI, P. 2003. Cell biology of the presynaptic terminal. *Annu Rev Neurosci,* 26**,** 701-28.

MURTHY, V. N., SCHIKORSKI, T., STEVENS, C. F. & ZHU, Y. 2001. Inactivity produces increases in neurotransmitter release and synapse size. *Neuron,* 32**,** 673-82.

MURTHY, V. N., SEJNOWSKI, T. J. & STEVENS, C. F. 1997. Heterogeneous release properties of visualized individual hippocampal synapses. *Neuron,* 18**,** 599-612.

MURTHY, V. N. & STEVENS, C. F. 1998. Synaptic vesicles retain their identity through the endocytic cycle. *Nature,* 392**,** 497-501.

NAGARKATTI, N., DESHPANDE, L. S. & DELORENZO, R. J. 2008. Levetiracetam inhibits both ryanodine and IP3 receptor activated calcium induced calcium release in hippocampal neurons in culture. *Neurosci Lett,* 436**,** 289-93.

NAKAI, J., OHKURA, M. & IMOTO, K. 2001. A high signal-to-noise Ca(2+) probe composed of a single green fluorescent protein. *Nat Biotechnol,* 19**,** 137-41.

NAKAJIMA, Y., IWAKABE, H., AKAZAWA, C., NAWA, H., SHIGEMOTO, R., MIZUNO, N. & NAKANISHI, S. 1993. Molecular characterization of a novel retinal metabotropic glutamate receptor mGluR6 with a high agonist selectivity for L-2-amino-4-phosphonobutyrate. *J Biol Chem,* 268**,** 11868-73.

NAKANISHI, S. 1992. Molecular diversity of glutamate receptors and implications for brain function. *Science,* 258**,** 597-603.

NARASIMHAN, S., GUO, J. L., CHANGOLKAR, L., STIEBER, A., MCBRIDE, J. D., SILVA, L. V., HE, Z., ZHANG, B., GATHAGAN, R. J., TROJANOWSKI, J. Q. & LEE, V. M. Y. 2017. Pathological Tau Strains from Human Brains Recapitulate the Diversity of Tauopathies in Nontransgenic Mouse Brain. *J Neurosci,* 37**,** 11406-11423.

NEHER, E. & SAKABA, T. 2008. Multiple roles of calcium ions in the regulation of neurotransmitter release. *Neuron,* 59**,** 861-72.

NEKI, A., OHISHI, H., KANEKO, T., SHIGEMOTO, R., NAKANISHI, S. & MIZUNO, N. 1996. Pre- and postsynaptic localization of a metabotropic glutamate receptor, mGluR2, in the rat brain: an immunohistochemical study with a monoclonal antibody. *Neurosci Lett,* 202**,** 197-200.

NICHOLLS, R. E., ZHANG, X. L., BAILEY, C. P., CONKLIN, B. R., KANDEL, E. R. & STANTON, P. K. 2006. mGluR2 acts through inhibitory Galpha subunits to regulate transmission and long-term plasticity at hippocampal mossy fiber-CA3 synapses. *Proc Natl Acad Sci U S A,* 103**,** 6380-5.

NISWENDER, C. M. & CONN, P. J. 2010. Metabotropic glutamate receptors: physiology, pharmacology, and disease. *Annu Rev Pharmacol Toxicol,* 50**,** 295-322.

NOWACK, A., MALARKEY, E. B., YAO, J., BLECKERT, A., HILL, J. & BAJJALIEH, S. M. 2011. Levetiracetam reverses synaptic deficits produced by overexpression of SV2A. *PLoS One,* 6**,** e29560.

NOWACK, A., YAO, J., CUSTER, K. L. & BAJJALIEH, S. M. 2010. SV2 regulates neurotransmitter release via multiple mechanisms. *Am J Physiol Cell Physiol,* 299**,** C960-7.

O'ROURKE, N. A., WEILER, N. C., MICHEVA, K. D. & SMITH, S. J. 2012. Deep molecular diversity of mammalian synapses: why it matters and how to measure it. *Nat Rev Neurosci,* 13**,** 365-79.

OHISHI, H., SHIGEMOTO, R., NAKANISHI, S. & MIZUNO, N. 1993. Distribution of the messenger RNA for a metabotropic glutamate receptor, mGluR2, in the central nervous system of the rat. *Neuroscience,* 53**,** 1009-18.

OKAMOTO, N., HORI, S., AKAZAWA, C., HAYASHI, Y., SHIGEMOTO, R., MIZUNO, N. & NAKANISHI, S. 1994. Molecular characterization of a new metabotropic glutamate receptor mGluR7 coupled to inhibitory cyclic AMP signal transduction. *J Biol Chem,* 269**,** 1231-6.

ORENBUCH, A., SHALEV, L., MARRA, V., SINAI, I., LAVY, Y., KAHN, J., BURDEN, J. J., STARAS, K. & GITLER, D. 2012. Synapsin selectively controls the mobility of resting pool vesicles at hippocampal terminals. *J Neurosci,* 32**,** 3969-80.

PADILLA, R., MACCIONI, R. B. & AVILA, J. 1990. Calmodulin binds to a tubulin binding site of the microtubule-associated protein tau. *Mol Cell Biochem,* 97**,** 35-41.

PANDA, D., SAMUEL, J. C., MASSIE, M., FEINSTEIN, S. C. & WILSON, L. 2003. Differential regulation of microtubule dynamics by three- and four-repeat tau: implications for the onset of neurodegenerative disease. *Proc Natl Acad Sci U S A,* 100**,** 9548-53.

PARK, H., LI, Y. & TSIEN, R. W. 2012. Influence of synaptic vesicle position on release probability and exocytotic fusion mode. *Science,* 335**,** 1362-6.

PARMENTIER, M. L., PIN, J. P., BOCKAERT, J. & GRAU, Y. 1996. Cloning and functional expression of a Drosophila metabotropic glutamate receptor expressed in the embryonic CNS. *J Neurosci,* 16**,** 6687-94.

PARSONS, M. P., VANNI, M. P., WOODARD, C. L., KANG, R., MURPHY, T. H. & RAYMOND, L. A. 2016. Real-time imaging of glutamate clearance reveals normal striatal uptake in Huntington disease mouse models. *Nat Commun,* 7**,** 11251.

PIN, J. P., WAEBER, C., PREZEAU, L., BOCKAERT, J. & HEINEMANN, S. F. 1992. Alternative splicing generates metabotropic glutamate receptors inducing different patterns of calcium release in Xenopus oocytes. *Proc Natl Acad Sci U S A,* 89**,** 10331-5.

PINHEIRO, P. S. & MULLE, C. 2008. Presynaptic glutamate receptors: physiological functions and mechanisms of action. *Nat Rev Neurosci,* 9**,** 423-36.

PINKERTON, A. B., VERNIER, J. M., SCHAFFHAUSER, H., ROWE, B. A., CAMPBELL, U. C., RODRIGUEZ, D. E., LORRAIN, D. S., BACCEI, C. S., DAGGETT, L. P. & BRISTOW, L. J. 2004. Phenyl-tetrazolyl acetophenones: discovery of positive allosteric potentiatiors for the metabotropic glutamate 2 receptor. *J Med Chem,* 47**,** 4595-9.

PISANI, A., BONSI, P., MARTELLA, G., DE PERSIS, C., COSTA, C., PISANI, F., BERNARDI, G. & CALABRESI, P. 2004. Intracellular calcium increase in epileptiform activity: modulation by levetiracetam and lamotrigine. *Epilepsia,* 45**,** 719-28.

POLYDORO, M., ACKER, C. M., DUFF, K., CASTILLO, P. E. & DAVIES, P. 2009. Age-dependent impairment of cognitive and synaptic function in the htau mouse model of tau pathology. *J Neurosci,* 29**,** 10741-9.

POPUGAEVA, E. & BEZPROZVANNY, I. 2013. Role of endoplasmic reticulum Ca2+ signaling in the pathogenesis of Alzheimer disease. *Front Mol Neurosci,* 6**,** 29.

PRINCE, M., WIMO, A., GEURCHET, M., ALI, G.-C., WU, Y.-T., PRINA, M. & INTERNATIONAL, A. S. D. 2015. World Alzheimer Report 2015: The Global Impact of Dementia: An analysis of prevelence, incidence, cost and trends. London.

PUTNAM, T. J. & MERRITT, H. H. 1937. Experimental Determination of the Anticonvulsant Properties of Some Phenyl Derivatives. *Science,* 85**,** 525-6.

PYLE, R. A., SCHIVELL, A. E., HIDAKA, H. & BAJJALIEH, S. M. 2000. Phosphorylation of synaptic vesicle protein 2 modulates binding to synaptotagmin. *J Biol Chem,* 275**,** 17195-200.

QU, L., AKBERGENOVA, Y., HU, Y. & SCHIKORSKI, T. 2009. Synapse-to-synapse variation in mean synaptic vesicle size and its relationship with synaptic morphology and function. *J Comp Neurol,* 514**,** 343-52.

RAJAKULENDRAN, S., GRAVES, T. D., LABRUM, R. W., KOTZADIMITRIOU, D., EUNSON, L., DAVIS, M. B., DAVIES, R., WOOD, N. W., KULLMANN, D. M., HANNA, M. G. & SCHORGE, S. 2010. Genetic and functional characterisation of the P/Q calcium channel in episodic ataxia with epilepsy. *J Physiol,* 588**,** 1905-13.

RATNAYAKA, A., MARRA, V., BUSH, D., BURDEN, J. J., BRANCO, T. & STARAS, K. 2012. Recruitment of resting vesicles into recycling pools supports NMDA receptor-dependent synaptic potentiation in cultured hippocampal neurons. *J Physiol,* 590**,** 1585-97.

REGEHR, W. G. 2012. Short-term presynaptic plasticity. *Cold Spring Harb Perspect Biol,* 4**,** a005702.

REIGADA, D., DIEZ-PEREZ, I., GOROSTIZA, P., VERDAGUER, A., GOMEZ DE ARANDA, I., PINEDA, O., VILARRASA, J., MARSAL, J., BLASI, J., ALEU, J. & SOLSONA, C. 2003. Control of neurotransmitter release by an internal gel matrix in synaptic vesicles. *Proc Natl Acad Sci U S A,* 100**,** 3485-90.

REY, S. A., SMITH, C. A., FOWLER, M. W., CRAWFORD, F., BURDEN, J. J. & STARAS, K. 2015. Ultrastructural and functional fate of recycled vesicles in hippocampal synapses. *Nat Commun,* 6**,** 8043.

RICHARDS, D. A. 2010. Regulation of exocytic mode in hippocampal neurons by intra-bouton calcium concentration. *J Physiol,* 588**,** 4927-36.
RICKMAN, C., HU, K., CARROLL, J. & DAVLETOV, B. 2005. Self-assembly of SNARE fusion proteins into star-shaped oligomers. *Biochem J,* 388**,** 75-9.
RIZZOLI, S. O. 2014. Synaptic vesicle recycling: steps and principles. *EMBO J,* 33**,** 788-822.
RIZZOLI, S. O. & BETZ, W. J. 2005. Synaptic vesicle pools. *Nat Rev Neurosci,* 6**,** 57-69.
ROBERSON, E. D., HALABISKY, B., YOO, J. W., YAO, J., CHIN, J., YAN, F., WU, T., HAMTO, P., DEVIDZE, N., YU, G. Q., PALOP, J. J., NOEBELS, J. L. & MUCKE, L. 2011. Amyloid-beta/Fyn-induced synaptic, network, and cognitive impairments depend on tau levels in multiple mouse models of Alzheimer's disease. *J Neurosci,* 31**,** 700-11.
ROBERSON, E. D., SCEARCE-LEVIE, K., PALOP, J. J., YAN, F., CHENG, I. H., WU, T., GERSTEIN, H., YU, G. Q. & MUCKE, L. 2007. Reducing endogenous tau ameliorates amyloid beta-induced deficits in an Alzheimer's disease mouse model. *Science,* 316**,** 750-4.
ROCHER, A. B., CRIMINS, J. L., AMATRUDO, J. M., KINSON, M. S., TODD-BROWN, M. A., LEWIS, J. & LUEBKE, J. I. 2010. Structural and functional changes in tau mutant mice neurons are not linked to the presence of NFTs. *Exp Neurol,* 223**,** 385-93.
ROGAWSKI, M. A., LOSCHER, W. & RHO, J. M. 2016. Mechanisms of Action of Antiseizure Drugs and the Ketogenic Diet. *Cold Spring Harb Perspect Med,* 6.
ROHDE, J., KIRSCHSTEIN, T., WILKARS, W., MULLER, L., TOKAY, T., PORATH, K., BENDER, R. A. & KOHLING, R. 2012. Upregulation of presynaptic mGluR2, but not mGluR3 in the epileptic medial perforant path. *Neuropharmacology,* 62**,** 1867-73.
ROSENMUND, C. & STEVENS, C. F. 1996. Definition of the readily releasable pool of vesicles at hippocampal synapses. *Neuron,* 16**,** 1197-207.
ROTHMAN, J. E. 1994. Mechanisms of intracellular protein transport. *Nature,* 372**,** 55-63.
ROTHSTEIN, J. D., JIN, L., DYKES-HOBERG, M. & KUNCL, R. W. 1993. Chronic inhibition of glutamate uptake produces a model of slow neurotoxicity. *Proc Natl Acad Sci U S A,* 90**,** 6591-5.
ROUX, A., UYHAZI, K., FROST, A. & DE CAMILLI, P. 2006. GTP-dependent twisting of dynamin implicates constriction and tension in membrane fission. *Nature,* 441**,** 528-31.
ROYO, N. C., VANDENBERGHE, L. H., MA, J. Y., HAUSPURG, A., YU, L., MARONSKI, M., JOHNSTON, J., DICHTER, M. A., WILSON, J. M. & WATSON, D. J. 2008. Specific AAV serotypes stably transduce primary hippocampal and cortical cultures with high efficiency and low toxicity. *Brain Res,* 1190**,** 15-22.
SAGNE, C., EL MESTIKAWY, S., ISAMBERT, M. F., HAMON, M., HENRY, J. P., GIROS, B. & GASNIER, B. 1997. Cloning of a functional vesicular GABA and glycine transporter by screening of genome databases. *FEBS Lett,* 417**,** 177-83.
SAHARA, N., MURAYAMA, M., HIGUCHI, M., SUHARA, T. & TAKASHIMA, A. 2014. Biochemical Distribution of Tau Protein in Synaptosomal Fraction of Transgenic Mice Expressing Human P301L Tau. *Front Neurol,* 5**,** 26.
SALIN, P. A., MALENKA, R. C. & NICOLL, R. A. 1996. Cyclic AMP mediates a presynaptic form of LTP at cerebellar parallel fiber synapses. *Neuron,* 16**,** 797-803.
SANDERS, D. W., KAUFMAN, S. K., DEVOS, S. L., SHARMA, A. M., MIRBAHA, H., LI, A., BARKER, S. J., FOLEY, A. C., THORPE, J. R., SERPELL, L. C., MILLER, T. M., GRINBERG, L. T., SEELEY, W. W. & DIAMOND, M. I. 2014. Distinct tau prion strains propagate in cells and mice and define different tauopathies. *Neuron,* 82**,** 1271-88.
SANKARANARAYANAN, S., ATLURI, P. P. & RYAN, T. A. 2003. Actin has a molecular scaffolding, not propulsive, role in presynaptic function. *Nat Neurosci,* 6**,** 127-35.
SANKARANARAYANAN, S. & RYAN, T. A. 2001. Calcium accelerates endocytosis of vSNAREs at hippocampal synapses. *Nat Neurosci,* 4**,** 129-36.

SANTACRUZ, K., LEWIS, J., SPIRES, T., PAULSON, J., KOTILINEK, L., INGELSSON, M., GUIMARAES, A., DETURE, M., RAMSDEN, M., MCGOWAN, E., FORSTER, C., YUE, M., ORNE, J., JANUS, C., MARIASH, A., KUSKOWSKI, M., HYMAN, B., HUTTON, M. & ASHE, K. H. 2005. Tau suppression in a neurodegenerative mouse model improves memory function. *Science,* 309**,** 476-81.

SANTOS, M. S., PARK, C. K., FOSS, S. M., LI, H. & VOGLMAIER, S. M. 2013. Sorting of the vesicular GABA transporter to functional vesicle pools by an atypical dileucine-like motif. *J Neurosci,* 33**,** 10634-46.

SARA, Y., VIRMANI, T., DEAK, F., LIU, X. & KAVALALI, E. T. 2005. An isolated pool of vesicles recycles at rest and drives spontaneous neurotransmission. *Neuron,* 45**,** 563-73.

SASAKI, K., SHIMURA, H., ITAYA, M., TANAKA, R., MORI, H., MIZUNO, Y., KOSIK, K. S., TANAKA, S. & HATTORI, N. 2009. Excitatory amino acid transporter 2 associates with phosphorylated tau and is localized in neurofibrillary tangles of tauopathic brains. *FEBS Lett,* 583**,** 2194-200.

SAUGSTAD, J. A., KINZIE, J. M., MULVIHILL, E. R., SEGERSON, T. P. & WESTBROOK, G. L. 1994. Cloning and expression of a new member of the L-2-amino-4-phosphonobutyric acid-sensitive class of metabotropic glutamate receptors. *Mol Pharmacol,* 45**,** 367-72.

SCHAFER, M. K., VAROQUI, H., DEFAMIE, N., WEIHE, E. & ERICKSON, J. D. 2002. Molecular cloning and functional identification of mouse vesicular glutamate transporter 3 and its expression in subsets of novel excitatory neurons. *J Biol Chem,* 277**,** 50734-48.

SCHAFFHAUSER, H., CAI, Z., HUBALEK, F., MACEK, T. A., POHL, J., MURPHY, T. J. & CONN, P. J. 2000. cAMP-dependent protein kinase inhibits mGluR2 coupling to G-proteins by direct receptor phosphorylation. *J Neurosci,* 20**,** 5663-70.

SCHIAVO, G., BENFENATI, F., POULAIN, B., ROSSETTO, O., POLVERINO DE LAURETO, P., DASGUPTA, B. R. & MONTECUCCO, C. 1992. Tetanus and botulinum-B neurotoxins block neurotransmitter release by proteolytic cleavage of synaptobrevin. *Nature,* 359**,** 832-5.

SCHIKORSKI, T. & STEVENS, C. F. 1997. Quantitative ultrastructural analysis of hippocampal excitatory synapses. *J Neurosci,* 17**,** 5858-67.

SCHOEPP, D. D., JANE, D. E. & MONN, J. A. 1999. Pharmacological agents acting at subtypes of metabotropic glutamate receptors. *Neuropharmacology,* 38**,** 1431-76.

SCHUSKE, K. R., RICHMOND, J. E., MATTHIES, D. S., DAVIS, W. S., RUNZ, S., RUBE, D. A., VAN DER BLIEK, A. M. & JORGENSEN, E. M. 2003. Endophilin is required for synaptic vesicle endocytosis by localizing synaptojanin. *Neuron,* 40**,** 749-62.

SCHWEIZER, F. E., MYERS, K. M. & CAPUTO, A. 2012. In the zone: presynaptic function at high res. *Nat Neurosci,* 15**,** 928-9.

SCRANTON, T. W., IWATA, M. & CARLSON, S. S. 1993. The SV2 protein of synaptic vesicles is a keratan sulfate proteoglycan. *J Neurochem,* 61**,** 29-44.

SHELDON, A. L. & ROBINSON, M. B. 2007. The role of glutamate transporters in neurodegenerative diseases and potential opportunities for intervention. *Neurochem Int,* 51**,** 333-55.

SHUPLIAKOV, O., BLOOM, O., GUSTAFSSON, J. S., KJAERULFF, O., LOW, P., TOMILIN, N., PIERIBONE, V. A., GREENGARD, P. & BRODIN, L. 2002. Impaired recycling of synaptic vesicles after acute perturbation of the presynaptic actin cytoskeleton. *Proc Natl Acad Sci U S A,* 99**,** 14476-81.

SIKSOU, L., ROSTAING, P., LECHAIRE, J. P., BOUDIER, T., OHTSUKA, T., FEJTOVA, A., KAO, H. T., GREENGARD, P., GUNDELFINGER, E. D., TRILLER, A. & MARTY, S. 2007. Three-dimensional architecture of presynaptic terminal cytomatrix. *J Neurosci,* 27**,** 6868-77.

SJOSTRAND, F. S. 1953. The ultrastructure of the innersegments of the retinal rods of the guinea pig eye as revealed by electron microscopy. *J Cell Physiol,* 42**,** 45-70.

SLADECZEK, F., PIN, J. P., RECASENS, M., BOCKAERT, J. & WEISS, S. 1985. Glutamate stimulates inositol phosphate formation in striatal neurones. *Nature,* 317**,** 717-9.
SMITH, M. A., CASADESUS, G., JOSEPH, J. A. & PERRY, G. 2002. Amyloid-beta and tau serve antioxidant functions in the aging and Alzheimer brain. *Free Radic Biol Med,* 33**,** 1194-9.
SMITH, S. M., RENDEN, R. & VON GERSDORFF, H. 2008. Synaptic vesicle endocytosis: fast and slow modes of membrane retrieval. *Trends Neurosci,* 31**,** 559-68.
SPEARS, W., FURGERSON, M., SWEETNAM, J. M., EVANS, P., GEARING, M., FECHHEIMER, M. & FURUKAWA, R. 2014. Hirano bodies differentially modulate cell death induced by tau and the amyloid precursor protein intracellular domain. *BMC Neurosci,* 15**,** 74.
SPIRES-JONES, T. L., STOOTHOFF, W. H., DE CALIGNON, A., JONES, P. B. & HYMAN, B. T. 2009. Tau pathophysiology in neurodegeneration: a tangled issue. *Trends Neurosci,* 32**,** 150-9.
STADTFELD, M., VARAS, F. & GRAF, T. 2005. Fluorescent protein-cell labeling and its application in time-lapse analysis of hematopoietic differentiation. *Methods Mol Med,* 105**,** 395-412.
STAFSTROM, C. E. 2012. "Please release me, let me go"-changes in presynaptic release following status epilepticus. *Epilepsy Curr,* 12**,** 170-1.
STARAS, K., BRANCO, T., BURDEN, J. J., POZO, K., DARCY, K., MARRA, V., RATNAYAKA, A. & GODA, Y. 2010. A vesicle superpool spans multiple presynaptic terminals in hippocampal neurons. *Neuron,* 66**,** 37-44.
STEFAN, C. J., PADILLA, S. M., AUDHYA, A. & EMR, S. D. 2005. The phosphoinositide phosphatase Sjl2 is recruited to cortical actin patches in the control of vesicle formation and fission during endocytosis. *Mol Cell Biol,* 25**,** 2910-23.
STUTZMANN, G. E., SMITH, I., CACCAMO, A., ODDO, S., LAFERLA, F. M. & PARKER, I. 2006. Enhanced ryanodine receptor recruitment contributes to Ca2+ disruptions in young, adult, and aged Alzheimer's disease mice. *J Neurosci,* 26**,** 5180-9.
SUDHOF, T. C. 1995. The synaptic vesicle cycle: a cascade of protein-protein interactions. *Nature,* 375**,** 645-53.
SUDHOF, T. C. 2004. The synaptic vesicle cycle. *Annu Rev Neurosci,* 27**,** 509-47.
SUDHOF, T. C. 2012. The presynaptic active zone. *Neuron,* 75**,** 11-25.
SUDHOF, T. C. 2013. Neurotransmitter release: the last millisecond in the life of a synaptic vesicle. *Neuron,* 80**,** 675-90.
SUDHOF, T. C. & RIZO, J. 2011. Synaptic vesicle exocytosis. *Cold Spring Harb Perspect Biol,* 3.
SUGIYAMA, H., ITO, I. & HIRONO, C. 1987. A new type of glutamate receptor linked to inositol phospholipid metabolism. *Nature,* 325**,** 531-3.
SUN, J. Y., WU, X. S. & WU, L. G. 2002. Single and multiple vesicle fusion induce different rates of endocytosis at a central synapse. *Nature,* 417**,** 555-9.
SUN, T., QIAO, H., PAN, P. Y., CHEN, Y. & SHENG, Z. H. 2013. Motile axonal mitochondria contribute to the variability of presynaptic strength. *Cell Rep,* 4**,** 413-9.
SUN, T., WU, X. S., XU, J., MCNEIL, B. D., PANG, Z. P., YANG, W., BAI, L., QADRI, S., MOLKENTIN, J. D., YUE, D. T. & WU, L. G. 2010. The role of calcium/calmodulin-activated calcineurin in rapid and slow endocytosis at central synapses. *J Neurosci,* 30**,** 11838-47.
SUTTON, R. B., FASSHAUER, D., JAHN, R. & BRUNGER, A. T. 1998. Crystal structure of a SNARE complex involved in synaptic exocytosis at 2.4 A resolution. *Nature,* 395**,** 347-53.
SWINYARD, E. A. 1949. Laboratory assay of clinically effective antiepileptic drugs. *J Am Pharm Assoc Am Pharm Assoc,* 38**,** 201-4.
SWINYARD, E. A., BROWN, W. C. & GOODMAN, L. S. 1952. Comparative assays of antiepileptic drugs in mice and rats. *J Pharmacol Exp Ther,* 106**,** 319-30.
TAKAMORI, S., MALHERBE, P., BROGER, C. & JAHN, R. 2002. Molecular cloning and functional characterization of human vesicular glutamate transporter 3. *EMBO Rep,* 3**,** 798-803.

TAKAMORI, S., RHEE, J. S., ROSENMUND, C. & JAHN, R. 2000. Identification of a vesicular glutamate transporter that defines a glutamatergic phenotype in neurons. *Nature,* 407**,** 189-94.

TAKAMORI, S., RHEE, J. S., ROSENMUND, C. & JAHN, R. 2001. Identification of differentiation-associated brain-specific phosphate transporter as a second vesicular glutamate transporter (VGLUT2). *J Neurosci,* 21**,** RC182.

TAKASHIMA, A. 2008. Hyperphosphorylated tau is a cause of neuronal dysfunction in tauopathy. *Journal of Alzheimers Disease,* 14**,** 371-375.

TANABE, Y., MASU, M., ISHII, T., SHIGEMOTO, R. & NAKANISHI, S. 1992. A family of metabotropic glutamate receptors. *Neuron,* 8**,** 169-79.

TANABE, Y., NOMURA, A., MASU, M., SHIGEMOTO, R., MIZUNO, N. & NAKANISHI, S. 1993. Signal transduction, pharmacological properties, and expression patterns of two rat metabotropic glutamate receptors, mGluR3 and mGluR4. *J Neurosci,* 13**,** 1372-8.

TASCHENBERGER, H., WOEHLER, A. & NEHER, E. 2016. Superpriming of synaptic vesicles as a common basis for intersynapse variability and modulation of synaptic strength. *Proc Natl Acad Sci U S A,* 113**,** E4548-57.

THEVENAZ, P., RUTTIMANN, U. E. & UNSER, M. 1998. A pyramid approach to subpixel registration based on intensity. *IEEE Trans Image Process,* 7**,** 27-41.

THIES, E. & MANDELKOW, E. 2007. Missorting of Tau in neurons causes degeneration of synapses that can be rescued by the kinase MARK2/Par-1 (vol 27, pg 2896, 2007). *Journal of Neuroscience,* 27.

TRABANCO, A. A., CID, J. M., LAVREYSEN, H., MACDONALD, G. J. & TRESADERN, G. 2011. Progress in the developement of positive allosteric modulators of the metabotropic glutamate receptor 2. *Curr Med Chem,* 18**,** 47-68.

TRIMBUCH, T. & ROSENMUND, C. 2016. Should I stop or should I go? The role of complexin in neurotransmitter release. *Nat Rev Neurosci,* 17**,** 118-25.

TRUCKENBRODT, S. & RIZZOLI, S. O. 2014. Spontaneous vesicle recycling in the synaptic bouton. *Front Cell Neurosci,* 8**,** 409.

TRUDEAU, L. E., EMERY, D. G. & HAYDON, P. G. 1996. Direct modulation of the secretory machinery underlies PKA-dependent synaptic facilitation in hippocampal neurons. *Neuron,* 17**,** 789-97.

TRUDEAU, L. E., FANG, Y. & HAYDON, P. G. 1998. Modulation of an early step in the secretory machinery in hippocampal nerve terminals. *Proc Natl Acad Sci U S A,* 95**,** 7163-8.

TUCKER, K. L., MEYER, M. & BARDE, Y. A. 2001. Neurotrophins are required for nerve growth during development. *Nat Neurosci,* 4**,** 29-37.

UM, J. W., KAUFMAN, A. C., KOSTYLEV, M., HEISS, J. K., STAGI, M., TAKAHASHI, H., KERRISK, M. E., VORTMEYER, A., WISNIEWSKI, T., KOLESKE, A. J., GUNTHER, E. C., NYGAARD, H. B. & STRITTMATTER, S. M. 2013. Metabotropic glutamate receptor 5 is a coreceptor for Alzheimer abeta oligomer bound to cellular prion protein. *Neuron,* 79**,** 887-902.

VAN DER JEUGD, A., AHMED, T., BURNOUF, S., BELARBI, K., HAMDAME, M., GROSJEAN, M. E., HUMEZ, S., BALSCHUN, D., BLUM, D., BUEE, L. & D'HOOGE, R. 2011. Hippocampal tauopathy in tau transgenic mice coincides with impaired hippocampus-dependent learning and memory, and attenuated late-phase long-term depression of synaptic transmission. *Neurobiol Learn Mem,* 95**,** 296-304.

VANDERMEEREN, M., MERCKEN, M., VANMECHELEN, E., SIX, J., VAN DE VOORDE, A., MARTIN, J. J. & CRAS, P. 1993. Detection of tau proteins in normal and Alzheimer's disease cerebrospinal fluid with a sensitive sandwich enzyme-linked immunosorbent assay. *J Neurochem,* 61**,** 1828-34.

VAROQUI, H., SCHAFER, M. K., ZHU, H., WEIHE, E. & ERICKSON, J. D. 2002. Identification of the differentiation-associated Na+/PI transporter as a novel vesicular glutamate transporter expressed in a distinct set of glutamatergic synapses. *J Neurosci,* 22**,** 142-55.

VENKATESAN, K., ALIX, P., MARQUET, A., DOUPAGNE, M., NIESPODZIANY, I., ROGISTER, B. & SEUTIN, V. 2012. Altered balance between excitatory and inhibitory inputs onto CA1 pyramidal neurons from SV2A-deficient but not SV2B-deficient mice. *J Neurosci Res,* 90**,** 2317-27.

VERSTREKEN, P., LY, C. V., VENKEN, K. J., KOH, T. W., ZHOU, Y. & BELLEN, H. J. 2005. Synaptic mitochondria are critical for mobilization of reserve pool vesicles at Drosophila neuromuscular junctions. *Neuron,* 47**,** 365-78.

VOGLMAIER, S. M., KAM, K., YANG, H., FORTIN, D. L., HUA, Z., NICOLL, R. A. & EDWARDS, R. H. 2006. Distinct endocytic pathways control the rate and extent of synaptic vesicle protein recycling. *Neuron,* 51**,** 71-84.

VOLPICELLI-DALEY, L. A., GAMBLE, K. L., SCHULTHEISS, C. E., RIDDLE, D. M., WEST, A. B. & LEE, V. M. 2014. Formation of alpha-synuclein Lewy neurite-like aggregates in axons impedes the transport of distinct endosomes. *Mol Biol Cell,* 25**,** 4010-23.

WADEL, K., NEHER, E. & SAKABA, T. 2007. The coupling between synaptic vesicles and Ca2+ channels determines fast neurotransmitter release. *Neuron,* 53**,** 563-75.

WANG, C., WANG, Y., HU, M., CHAI, Z., WU, Q., HUANG, R., HAN, W., ZHANG, C. X. & ZHOU, Z. 2016. Synaptotagmin-11 inhibits clathrin-mediated and bulk endocytosis. *EMBO Rep,* 17**,** 47-63.

WANG, J. Z., XIA, Y. Y., GRUNDKE-IQBAL, I. & IQBAL, K. 2013. Abnormal hyperphosphorylation of tau: sites, regulation, and molecular mechanism of neurofibrillary degeneration. *J Alzheimers Dis,* 33 Suppl 1**,** S123-39.

WANG, Y. & MANDELKOW, E. 2016. Tau in physiology and pathology. *Nat Rev Neurosci,* 17**,** 5-21.

WATAKABE, A., OHTSUKA, M., KINOSHITA, M., TAKAJI, M., ISA, K., MIZUKAMI, H., OZAWA, K., ISA, T. & YAMAMORI, T. 2015. Comparative analyses of adeno-associated viral vector serotypes 1, 2, 5, 8 and 9 in marmoset, mouse and macaque cerebral cortex. *Neurosci Res,* 93**,** 144-57.

WATANABE, S., ROST, B. R., CAMACHO-PEREZ, M., DAVIS, M. W., SOHL-KIELCZYNSKI, B., ROSENMUND, C. & JORGENSEN, E. M. 2013. Ultrafast endocytosis at mouse hippocampal synapses. *Nature,* 504**,** 242-247.

WATANABE, S., TRIMBUCH, T., CAMACHO-PEREZ, M., ROST, B. R., BROKOWSKI, B., SOHL-KIELCZYNSKI, B., FELIES, A., DAVIS, M. W., ROSENMUND, C. & JORGENSEN, E. M. 2014. Clathrin regenerates synaptic vesicles from endosomes. *Nature,* 515**,** 228-33.

WEBER, T., ZEMELMAN, B. V., MCNEW, J. A., WESTERMANN, B., GMACHL, M., PARLATI, F., SOLLNER, T. H. & ROTHMAN, J. E. 1998. SNAREpins: minimal machinery for membrane fusion. *Cell,* 92**,** 759-72.

WELZEL, O., HENKEL, A. W., STROEBEL, A. M., JUNG, J., TISCHBIREK, C. H., EBERT, K., KORNHUBER, J., RIZZOLI, S. O. & GROEMER, T. W. 2011. Systematic heterogeneity of fractional vesicle pool sizes and release rates of hippocampal synapses. *Biophys J,* 100**,** 593-601.

WHITE, H. S., SMITH-YOCKMAN, M., SRIVASTAVA, A. & WILCOX, K. 2006. Therapeutic assays for the identification and characterization of antiepileptic and antiepileptogenic drugs. *In:* PITKÄNEN, A., SCHWARTZKROIN, P. A. & MOSHÉ, S. L. (eds.) *Models of seizures and epilepsy.* Amsterdam: Elsevier.

WILHELM, B. G., GROEMER, T. W. & RIZZOLI, S. O. 2010. The same synaptic vesicles drive active and spontaneous release. *Nat Neurosci,* 13**,** 1454-6.

WILSON, N. R., KANG, J., HUESKE, E. V., LEUNG, T., VAROQUI, H., MURNICK, J. G., ERICKSON, J. D. & LIU, G. 2005. Presynaptic regulation of quantal size by the vesicular glutamate transporter VGLUT1. *J Neurosci,* 25**,** 6221-34.

WOJCIK, S. M., RHEE, J. S., HERZOG, E., SIGLER, A., JAHN, R., TAKAMORI, S., BROSE, N. & ROSENMUND, C. 2004. An essential role for vesicular glutamate transporter 1 (VGLUT1) in postnatal development and control of quantal size. *Proc Natl Acad Sci U S A,* 101**,** 7158-63.

WU, B., YAMAGUCHI, H., LAI, F. A. & SHEN, J. 2013. Presenilins regulate calcium homeostasis and presynaptic function via ryanodine receptors in hippocampal neurons. *Proc Natl Acad Sci U S A,* 110**,** 15091-6.

WU, X. S., ZHANG, Z., ZHAO, W. D., WANG, D., LUO, F. & WU, L. G. 2014. Calcineurin is universally involved in vesicle endocytosis at neuronal and nonneuronal secretory cells. *Cell Rep,* 7**,** 982-8.

XI, Z. X., RAMAMOORTHY, S., BAKER, D. A., SHEN, H., SAMUVEL, D. J. & KALIVAS, P. W. 2002. Modulation of group II metabotropic glutamate receptor signaling by chronic cocaine. *J Pharmacol Exp Ther,* 303**,** 608-15.

XIA, Z., DUDEK, H., MIRANTI, C. K. & GREENBERG, M. E. 1996. Calcium influx via the NMDA receptor induces immediate early gene transcription by a MAP kinase/ERK-dependent mechanism. *J Neurosci,* 16**,** 5425-36.

XU, J., MCNEIL, B., WU, W., NEES, D., BAI, L. & WU, L. G. 2008. GTP-independent rapid and slow endocytosis at a central synapse. *Nat Neurosci,* 11**,** 45-53.

XU, T. & BAJJALIEH, S. M. 2001. SV2 modulates the size of the readily releasable pool of secretory vesicles. *Nat Cell Biol,* 3**,** 691-8.

XUE, M., REIM, K., CHEN, X., CHAO, H. T., DENG, H., RIZO, J., BROSE, N. & ROSENMUND, C. 2007. Distinct domains of complexin I differentially regulate neurotransmitter release. *Nat Struct Mol Biol,* 14**,** 949-58.

YANG, X. F. & ROTHMAN, S. M. 2009. Levetiracetam has a time- and stimulation-dependent effect on synaptic transmission. *Seizure,* 18**,** 615-9.

YANG, X. F., WEISENFELD, A. & ROTHMAN, S. M. 2007. Prolonged exposure to levetiracetam reveals a presynaptic effect on neurotransmission. *Epilepsia,* 48**,** 1861-9.

YAO, J., NOWACK, A., KENSEL-HAMMES, P., GARDNER, R. G. & BAJJALIEH, S. M. 2010. Cotrafficking of SV2 and synaptotagmin at the synapse. *J Neurosci,* 30**,** 5569-78.

YARAR, D., WATERMAN-STORER, C. M. & SCHMID, S. L. 2005. A dynamic actin cytoskeleton functions at multiple stages of clathrin-mediated endocytosis. *Mol Biol Cell,* 16**,** 964-75.

YEH, F. L., DONG, M., YAO, J., TEPP, W. H., LIN, G., JOHNSON, E. A. & CHAPMAN, E. R. 2010. SV2 mediates entry of tetanus neurotoxin into central neurons. *PLoS Pathog,* 6**,** e1001207.

YIN, N., MA, W., PEI, J., OUYANG, Q., TANG, C. & LAI, L. 2014. Synergistic and antagonistic drug combinations depend on network topology. *PLoS One,* 9**,** e93960.

YU, J. T., CHANG, R. C. C. & TAN, L. 2009. Calcium dysregulation in Alzheimer's disease: From mechanisms to therapeutic opportunities. *Progress in Neurobiology,* 89**,** 240-255.

YU, W., POLEPALLI, J., WAGH, D., RAJADAS, J., MALENKA, R. & LU, B. 2012. A critical role for the PAR-1/MARK-tau axis in mediating the toxic effects of Abeta on synapses and dendritic spines. *Hum Mol Genet,* 21**,** 1384-90.

ZAKHARENKO, S. S., ZABLOW, L. & SIEGELBAUM, S. A. 2002. Altered presynaptic vesicle release and cycling during mGluR-dependent LTD. *Neuron,* 35**,** 1099-110.

ZANDER, J. F., MUNSTER-WANDOWSKI, A., BRUNK, I., PAHNER, I., GOMEZ-LIRA, G., HEINEMANN, U., GUTIERREZ, R., LAUBE, G. & AHNERT-HILGER, G. 2010. Synaptic and vesicular coexistence of VGLUT and VGAT in selected excitatory and inhibitory synapses. *J Neurosci,* 30**,** 7634-45.

ZHANG, H., SUN, S., HERREMAN, A., DE STROOPER, B. & BEZPROZVANNY, I. 2010. Role of presenilins in neuronal calcium homeostasis. *J Neurosci,* 30**,** 8566-80.

ZHANG, N., GORDON, S. L., FRITSCH, M. J., ESOOF, N., CAMPBELL, D. G., GOURLAY, R., VELUPILLAI, S., MACARTNEY, T., PEGGIE, M., VAN AALTEN, D. M., COUSIN, M. A. & ALESSI, D. R. 2015. Phosphorylation of synaptic vesicle protein 2A at Thr84 by casein kinase 1 family kinases controls the specific retrieval of synaptotagmin-1. *J Neurosci,* 35**,** 2492-507.

ZHANG, Q., LI, Y. & TSIEN, R. W. 2009a. The dynamic control of kiss-and-run and vesicular reuse probed with single nanoparticles. *Science,* 323**,** 1448-53.

ZHANG, Q., LI, Y. & TSIEN, R. W. 2009b. Response to Comment on "The Dynamic Control of Kiss-And-Run and Vesicular Reuse Probed with Single Nanoparticles". *Science,* 325**,** 1499-1499.

ZHANG, W. & BENSON, D. L. 2002. Developmentally regulated changes in cellular compartmentation and synaptic distribution of actin in hippocampal neurons. *J Neurosci Res,* 69**,** 427-36.

ZHONG, Y. & WU, C. F. 1991. Altered synaptic plasticity in Drosophila memory mutants with a defective cyclic AMP cascade. *Science,* 251**,** 198-201.

ZHOU, L., MCINNES, J., WIERDA, K., HOLT, M., HERRMANN, A. G., JACKSON, R. J., WANG, Y. C., SWERTS, J., BEYENS, J., MISKIEWICZ, K., VILAIN, S., DEWACHTER, I., MOECHARS, D., DE STROOPER, B., SPIRES-JONES, T. L., DE WIT, J. & VERSTREKEN, P. 2017. Tau association with synaptic vesicles causes presynaptic dysfunction. *Nat Commun,* 8**,** 15295.

ZHU, Y., XU, J. & HEINEMANN, S. F. 2009. Two pathways of synaptic vesicle retrieval revealed by single-vesicle imaging. *Neuron,* 61**,** 397-411.